Developing stem-cell containing organoids as a pre-clinical model for colorectal cancer therapeutics

Luned Marged Badder

A thesis presented for the award of *Doctor of Philosophy (Ph.D)*

Cardiff School of Biosciences
European Cancer Stem Cell Research Institute

2013 – 2017

Declaration

This work has not been submitted in substance for any other degree or award at this or any other university or place of learning, nor is being submitted concurrently in candidature for any degree or other award.

Signed ……………………………………… (candidate)   Date …………………………

STATEMENT 1

This thesis is being submitted in partial fulfilment of the requirements for the degree of PhD.

Signed ……………………………………… (candidate)   Date …………………………

STATEMENT 2

This thesis is the result of my own independent work/investigation, except where otherwise stated. Other sources are acknowledged by explicit references. The views expressed are my own.

Signed ……………………………………… (candidate)   Date …………………………

STATEMENT 3

I hereby give consent for my thesis, if accepted, to be available online in the University's Open Access repository and for inter-library loan, and for the title and summary to be made available to outside organisations.

Signed ……………………………………… (candidate)   Date …………………………

STATEMENT 4: PREVIOUSLY APPROVED BAR ON ACCESS

I hereby give consent for my thesis, if accepted, to be available online in the University's Open Access repository and for inter-library loans **after expiry of a bar on access previously approved by the Academic Standards & Quality Committee.**

Signed ……………………………………… (candidate)   Date …………………………

Acknowledgements

First and foremost, my sincerest thanks go to three supervisors on this project. Firstly to Professor Alan Clarke, whom sadly passed away before the completion of my Ph.D, for providing scientific wisdom and exciting discussions that paved the way for the future of this project. Also to Dr Paul Shaw for providing me with an opportunity to pursue this research, as well as his support and enthusiasm throughout. I am also indebted to Professor Trevor Dale for providing scientific guidance whilst encouraging my independence as a researcher in equal measures. I am also grateful to patients, members of the Wales Cancer Bank, University Hospital Wales Colorectal surgical team and the Histopathology unit who made the project possible by providing us with consented samples and clinical information. I would like to thank Cancer Research Wales for funding this studentship.

To all members of the Dale lab, Clarke lab, and 3rd floor East of Biosciences, I wish to extend a thank you for making my Ph.D experience an enjoyable one. In particular to Drs Mairi Thomas and Anika Offergeld, for their continued friendship and lab-based support. I wish to thank Dr Andrew Hollins for his involvement in the organoid workflow, assistance and encouragement throughout, as well as Dr Kenneth Ewan who conducted critical experiments within this thesis. A number of people have contributed technically to this work; I am particularly grateful to Kate Densley and Jennifer Shone, two project student's who's hard work helped produce some elements of Chapters 4 and 5, respectively; members of the Bioimaging research hub for confcal and histological imaging support; as well as the 'Data Clinic' team for their patient efforts with statistical analysis. Further afield, I extend my appreciative thanks to Drs Leo Price, Bram Herpers and Kuan Yan (OcellO,Leiden) for their phenotypic screening support and hours of discussion, aswell as Dr. Dirk Wienke and team in Merck Serono (Darmstadt, Germany), to whom I thank equally.

Table of contents

List of Figures

List of Tables

Abbreviations and Definitions

Symbols

°C	Degrees Celsius
Δ	Delta
µg	Micrograms
µl	Microlitres
µm	Micrometre
µM	Micromolar

A

AKT	Protein Kinase B
APC	Adenomatous Polyposis Coli
ATM	Ataxia-telangiectasia mutated
Ascl2:	Achaete Scute like 2
ATP	Adenoise triphosphate
ATR	ataxia–telangiectasia and Rad3 related
AXIN1/2	Axis inhibitor protein 1/2

B

BMP	Bone Morphogenic Protein
BSA	Bovine Serum Albumin

C

CBC	Crypt Base Columnar cell
cDNA	complimentary deoxyribonucleic acid
Chk1/2	checkpoint kinase 1/2
CI	Combination Index
CRC	colorectal cancer
CRISPR	Clustered regularly interspaced short palindromic repeats
CSC	cancer stem cell
C_T	Cycle Time

D

DDR	DNA damage response
dH_2O	deionised water
DNase	deoxyribonuclease
Dkk1	Dickkopf1
DMEM /F12	Dulbecco's Modified Eagle Medium, nutrient mixture F12
DMSO	Dimethyl sulfoxide
DNA	Deoxyribonucleic Acid
DNAse	Dioxyribonuclease
Dsh	Dishevelled

E

ECM	Extracellular Matrix
EC_{50}	(Half maximal) Effective concentration
EDTA	Ethylenediaminetetraacetic acid
EGF	Epidermal Growth Factor
EGFR	Epidermal Growth Factor Receptor
EPCAM	Epithelial Cell Adhesion Molecule
Erk	extracellular regulated Map kinase
EM	emission
EX	excitation
EtOH	Ethanol

F

FAC(S)	Fluorescence-activated cell sorting
FBS	Foetal Bovine Serum
FAP	Familial adenomatous polyposis
Fzd	Frizzled

G

g   Gram
GEMM   Genetically Engineered Mouse
         Model
GFP   Green Fluorescent Protein
GSK3   Glycogen Synthase Kinase 3
GRB2   Growth Factor Receptor
         Binding protein 2
GTPase   Guanosin-5'-
         triphosphate binding proteins

H

H&E   Hematoxylin & Eosin

I

IC_{50} (Half maximal) Inhibitory
         concentration
IF   Immunofluorescence
IHC   Immunohistochemistry
iPSC   induced Pluripotent Stem Cell
ISC   Intestinal Stem Cell

K

KRAS   Kirsten Rat Sarcoma viral
         oncogene homolog
Krt20   Cytokeratin 20

L

L   Litre
LEF   Lymphoid Enhance-Binding
Factor 1
Lgr4/5/6   Leucine-rich repeat
         containing G protein coupled
         receptor 4/5/6
LRP   Low desnity lipoprotein
         receptor-related protein

M

M   Molar/moles

mAb   Monoclonal Antibody
MAPK   Mitogen activated Protein
         Kinase
Mek   Mitogen activated protein
         kinase
mCRC   metastatic Colorectal cancer
mg   Miligram
ml   Mililitre
mM   Milimolar
mRNA   Messenger Ribonucleic Acid
MSI   Microsatellite instability
mTORC2   mechanistic target of
         rapamycin complex 2
MTT   3-(4,5-dimethylthiazol-2-yl)
                2,5-diphenyltetrazolium
                bromide
Muc2   Mucin 2

N

n   number
NGS   Next Generation Sequencing
NICD   Notch intracellular Domain
nM   Nanomolar
Nog   Noggin
NOD/SCID   Non-obese
                diabetic/severe
                combined immune
                deficiency
NSAID(s)   Non steroidal anti-
                inflamattory drug(s)

O

OGT   Oxford Gene Technologies
o/n   Overnight

P

PBS   Phosphate Buffered Saline
PCA   Principle Component Analysis
PCR   Polymerase chain reaction
PDK1   phosphoinositide-depdenet
         protein kinase 1
PDTX/PDX   Patient derived Tumour
                Xenograft
PFA   Paraformaldehyde

PI3K   Phosphoinositide 3-kinases
PIP_2 Phosphatidylinositol 4,5 bisphosphate
PIP_3 Phosphatidylinositol 3,4,5-triphosphate
PTEN   phosphatase and TENsin homolog deleted on chromosome 10

Q

qRT-PCR : Quantiative Reverse Transcription Polymerase Chain Reaction

R

RNA   Ribonucleic acid
Rnf43   ring finger 43
ROCK   Rho-associated protein kinase
Rpm   Revolutions per minute
Rspo1   R-spondin 1
RT   Room Temperature

S

SD   Standard Deviation
shRNA   Short hairpin RNA
SoC   Standard of care
SOS   Sevenless homolog
SEM   Standard error of the mean

T

TA   Transit amplifying
Taq   DNA polymerase from *Thermus aquaticus*
TCF   T-cell-specific transcription factor
TGF   Transforming Growth Factor
TNKS   Tankyrases
TNKSI   Tankyrase(s) inhibitor
TNM   Tumour, Node, Metastasis
TRITC   Tetramethylrhodamine

W

Wnt   Wingless
WT   Wild type

Z

Znrf3   Zinc and Ring finger 3

123

2D   Two dimensional
3D   Three Dimensional
5-FU   5'- Fluouracil

Abstract

Colorectal cancer (CRC) is the second most common cause of cancer related deaths in the UK. Whilst identification of molecular events that contribute to the initiation and progression of CRC have facilitated the development of predictive biomarker-driven therapeutics, their success in the clinic has been restricted by the lack of anticipated responses. Furthermore, not all genetic signatures of a tumour have been linked to related drug targets, highlighting the need for novel development of compounds and better therapeutic rationales for the treatment of patient subsets. The limited success of targeted therapies, both within the clinic and drug discovery pipeline, has been attributed to a lack of effective preclinical models that are capable of capturing the complexity of deregulated signalling networks. The development of functional readouts that better represent tumour complexity, is therefore imperative to confirm the effects of hypothesis-driven therapeutics.

This thesis therefore aimed to investigate whether 3D CRC organoids , which show a degree of greater complexity compared to preceding *in vitro* models, could be applied as suitable readouts for stratified medicine programmes and novel compounds within the drug discovery setting. To achieve this, a panel of 3D patient-derived CRC organoids cultures were generated. Suitable methodologies were established to facilitate organoids towards quantifiable, robust assay formats. This platform enabled the study of organoids within an *in vitro* clinical trial setting, based upon treatments administered within the ongoing FOCUS 4 stratified medicine trial, exploring organoids' capacity to predict responses to targeted therapeutics. Organoids were differentially sensitive to therapies, irrespective of their genotypic background. It will be interesting to see whether prediction-response correlations observed in this study are typical of those seen in patients and whether functional readouts will be required to support stratified medicine approaches. Quantitative image-based analysis was also found to identify signatures of organoid responses against novel Wnt signalling inhibitors, suggesting that organoids may constitute a

platform that can be used to study the effects of targeting a prospective cancer stem cell (CSC) population. Taken together, the findings in this thesis highlight the utility of patient derived organoid models as a functional model to evaluate novel therapeutic strategies, potentially generating clinically relevant hypotheses.

1. Introduction

1.1 Anatomy and function of the intestine

The mammalian lower gastrointestinal tract is comprised of both the small and large intestine. The small intestine emerges from the pyloric sphincter of the stomach and is divided into the duodenum, jejunum and ileum. This tube-like structure is composed of a range of cell types, which facilitate some key roles including enzymatic digestion and absorption of nutrients. The large intestine extends from the caecum, through the ascending colon, transverse colon, descending colon, sigmoid colon, to the rectum, which then opens to the anus. The large intestine mainly functions in maintaining fluid and electrolyte balance by absorption of water from food material. It also is the primary site for degradation of complex carbohydrates and nutrients by the gut microbiota. The intestine is highly plastic, undergoing continuous self-renewal to facilitate its functions within such a harsh environment. The luminal surface of the large intestine is composed of a single epithelial cell layer that invaginates into the underlying submucosa, forming crypt structures. Beneath the epithelial sheet are stromal fibroblasts and a surrounding vasculature. The smooth muscle layer resides further below and is responsible for generating the peristaltic movement required to move food through the intestine.

1.2 Intestinal epithelium homeostasis

1.2.1 Cell compartments within the large intestine

At a cellular level, the large intestine is composed of a main epithelial cell layer, which form the basis of individual crypt structures. At the base of the colonic crypt reside a progeny of multipotent stem cells capable of differentiating into multiple epithelial lineages including enterocytes, endocrine cells and goblet cells (Pinto and Clevers 2005; Ashley 2013a; Barker 2014a). As cells from the base of the crypt

1

migrate towards the lumen of the intestine, they undergo differentiation into distinct cell progenies, which perform critical functions involved in intestinal homeostasis. Cells continue to migrate until they are eventually shed into the lumen at the apex of the crypt, resulting in a process that rapidly regenerates the colonic epithelium, depicted in Figure 1.1(Barker 2014). The population of intestinal stem cells (ISCs) at the base of the crypts facilitate a continual turnover of cells, generating daughter cells capable of differentiating into any of the epithelial lineages within the intestine. Differentiated cells have several functions within the intestine. The absorptive enterocytes align each individual crypt and are critical for nutrient uptake as food moves through the intestinal tube. Goblet cells, identified through their expression of Mucin 2, provide lubrication to lesser the impact of mechanical stress from peristalsis of food through the gut. Furthermore, endocrine cells play a role secreting various hormones that maintain gut homeostasis (Pinto and Clevers 2005). The entire intestinal epithelium is renewed between every 3-5 days and is tightly regulated to maintain tissue homeostasis.
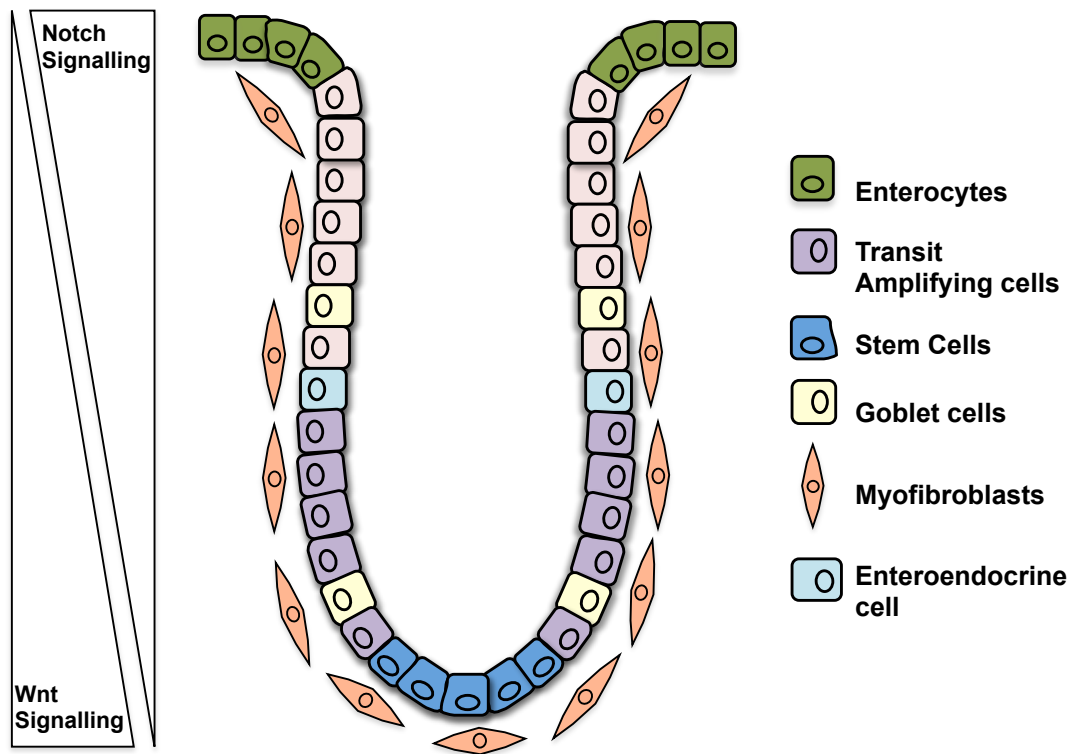
Figure 1.1 Schematic of a single crypt within the large intestine

Schematic diagram a single colonic crypt showing the range of cell types. The base of the crypt is composed of a stem cell niche, whereby stem cells are able to self renew and differentiate into various lineages whilst migrating to the tip of the crypt. Crypt proliferation is generally maintained by high levels of Wnt Signalling, and cell differentiation occurs primarily due to increased levels of Notch signalling when closest to the lumen.

1.2.2   Colorectal stem cell maintenance

The adult stem cells are defined as a population of pluripotent cells capable of self-renewal and differentiation that carry out functions of vital importance for tissue homeostasis and maintenance (Ashley 2013a). Within the intestine, the rapid renewal of the tissue occurs as a result of continual migration of intestinal stem cells towards the intestinal lumen along the crypt-villus axis (Fre *et al.* 2005).
As such, a number of protective mechanisms are in place to prevent neoplastic growth within a rapidly renewing environment. Such mechanisms include the induction of quiescence to repair damaged DNA of rapidly proliferating cells, and the ability to undergo programmed cell death by apoptosis to maintain stem cell integrity (Blanpain *et al* 2011; Barker 2014a).

The foundation of the current understanding of intestinal stem cells is based upon studies in the murine small intestine, which can also be applied to the colonic epithelium in humans. Early studies demonstrated that the self-renewing component of the intestine is located at the base of the crypt, in the '+4 region' suggesting that the migration of epithelial cells towards the intestinal lumen originated from the crypt (Pinto and Clevers 2005). This evidence was furthered using DNA labelling of stem cells using ^{3}[H]-thymidine, whilst labelling newly synthesised DNA strands with a different marker (bromodeoxyuridine), enabling a segregation of the two markers to further study stem cell dynamics. Recent evidence suggests that stem cell identity within the intestine is more plastic than previously thought, with the possibility that crypt based columnar cells (CBC) can function as stem cells (Barker 2014a). It has therefore been postulated that the crypt base contains both active cells (The CBC cells) as well as more quiescent stem cells (+4 cells) that function as a reserve in response to injury (Barker 2014a). Subsequently, a number of markers have been postulated as possible indicators of intestinal stem cells. Lineage tracing experiments have demonstrated that leucine rich repeat containing G protein coupled receptor 5(Lgr5)+ cells in the crypt had the capacity to

form all different epithelial lineages over a 2 month period in the mouse (Barker *et al.* 2007a), as well as within *in vitro* experiments (Sato *et al.* 2009) (discussed further in section 1.8). Furthermore, engraftments of single Lgr5+ cells have been shown to successfully repair the colonic epithelium (Yui *et al.* 2012). Analysis of gene expression profiles of intestinal epithelial cells expressing high and low levels of Lgr5 has further identified markers such as *Ascl2,* a Wnt signalling target (van der Flier *et al.* 2009). Subsequent studies have concluded that *Ascl2* , alongside ß-catenin/Tcf, is able to activate genes related to cell stemness, and thus initiate transcription that is responsive to Wnt signalling (Schuijers *et al.* 2015).

1.2.3   Signalling pathways implicated within intestinal homeostasis

A range of intricate networks, which interplay to control cellular proliferation, migration, and apoptosis, closely regulate the overall structure and function of the dynamic intestinal tissue. This is mediated by a gradient of signalling pathways that control gene expression to control the fate of a well-defined epithelial hierarchy and maintain stem cell homeostasis, some of which are discussed here.

1.2.3.1   Wnt signalling pathway

The canonical (ß-catenin dependent) Wnt signalling pathway plays a major role during mammalian development, mediating effects on an array of target genes involved in proliferation, cell adhesion and migration.

In the absence of a Wnt ligand, the canonical Wnt signalling pathway remains in an 'off-state' whereby cytoplasmic β- catenin is marked by a destruction complex composed of multiple proteins, including axis inhibitor (Axin) scaffolding protein, the tumour suppressor Adenomatous polyposis coli (APC), and the serine/threonine kinases CK1 and Glycogen Synthase Kinase-3 (GSK3). The destruction complex acts to phosphorylate ß-catenin on serine and threonine residues leading to ubiquitination and protesomal degradation. Activation of canonical Wnt signalling, as a result of Wnt ligand binding to Frizzled and lipoprotein receptor-related protein 5/6 (LRP5/6) co-receptors, mediates the interaction between Dishevelled (Dsh) and Axin at the

cell surface, preventing the formation of the ß-catenin destruction complex. Consequently, free pools of cytoplasmic β-catenin accumulate and translocate to the nucleus (Kim *et al.* 2008) subsequently displacing Groucho, a transcriptional repressor, and binds to T-cell specific transcription factor of Lymphoid enhancer-binding factor 1 (TCF/LEF) family of transcription factors, facilitating the transcription of Wnt target genes (Barker 2014a). Wnt signalling is further potentiated by the R(oof plate specific)-spondin protein family, which, upon binding with their receptor leucine-rich G protein coupled receptor 4/5/6 (LGR4/5/6) or Lgr5 receptor, active in adult stem cells in the base of crypts, enhance the Wnt ligand signal. This effect is mediated by the inhibition of zinc and ring finger 3 (Znrf3) and ring finger 43 (Rnf43) transmembrane ubiquitin ligases, which target Fzd/Lrp receptors for degradation (Barker *et al.* 2013; Koo *et al.* 2012; de Lau *et al.* 2011a). The R-spondins therefore elicit their effect by inhibiting the removal of Fzd and Lrp receptors from the cell surface, thus mediating β-catenin stabilization (de Lau *et al.* 2014) As a result, this amplifies the Wnt responses (Barker *et al.* 2013), enhancing gene transcription. A number of Wnt target genes are associated with cell proliferation, migration and adhesion and include, but are not restricted to, *c-myc*, *Cyclin D1*, *CD44* and *Axin 2* (Krausova and Korinek 2014)*.

Wnt signalling (Figure 1.2) has a diverse role throughout development and homeostasis and is therefore tightly regulated at variety of stages to maintain physiology. At a cellular level, downregulation of Wnt signalling can occur through multiple feedback loops which, upon ß-catenin transcription, mediate the upregulation of Axin2 to re-establish the formation of the ß-catenin destruction complex. Furthermore, the destruction complex is also directly regulated as required; Axin , for example, is one of the concentration-limiting components of the destruction complex and is in turn tightly regulated by tankyrases 1/2, members of the poly ADP ribosylation enzymes family that attenuate Wnt signalling by mediating Axin stabilisation (Wu *et al.* 2016; de Sousa and Vermeulen 2016; de Sousa *et al.* 2011).

In the intestine, Wnt signalling has long been recognised as a master regulator of the turnover of stem cell generation (Schuijers and Clevers 2012; Pinto and Clevers 2005) and has been shown to be a key mediator of proliferation and intestinal homeostasis. Within the intestinal crypt, a gradient of expression of Wnt agonists and antagonists mediate tight regulation of this pathway, with highest relative Wnt levels prominent in the base of crypts (Schuijers and Clevers 2012). A number of studies have demonstrated the implications of Wnt signalling in crypt development and function. Firstly, conditional homozygous deletion of ß-catenin in the intestine has been shown to result in an increase in apoptotic events and crypt ablation in a transgenic mouse line (Ireland *et al.* 2004). In concordance with this, Fevr *et al* demonstrated that ß-catenin loss results in a rapid absence of proliferating cells, a loss of crypt formation, and strikingly, an induction of terminal differentiation in ISCs (Fevr *et al.* 2007). Furthermore, overexpression of *DIckkopf1* (Dkk1), a Wnt antagonist, causes progressive degeneration of crypt architectures (Kuhnert *et al.* 2004), and alters crypt-villus structure within small intestine of mice (Pinto *et al.* 2003). Conversely, injection of human R-spondin 1 (hRSpo1) has been shown to result in an aberrant activation of the Wnt pathway, and an overall increase in the number of Lgr5+ stem cells in mice (Kim *et al.* 2005). Taken together, such studies emphasise the importance of the Wnt signalling network in the ISC compartment, and in maintenance of homeostasis.
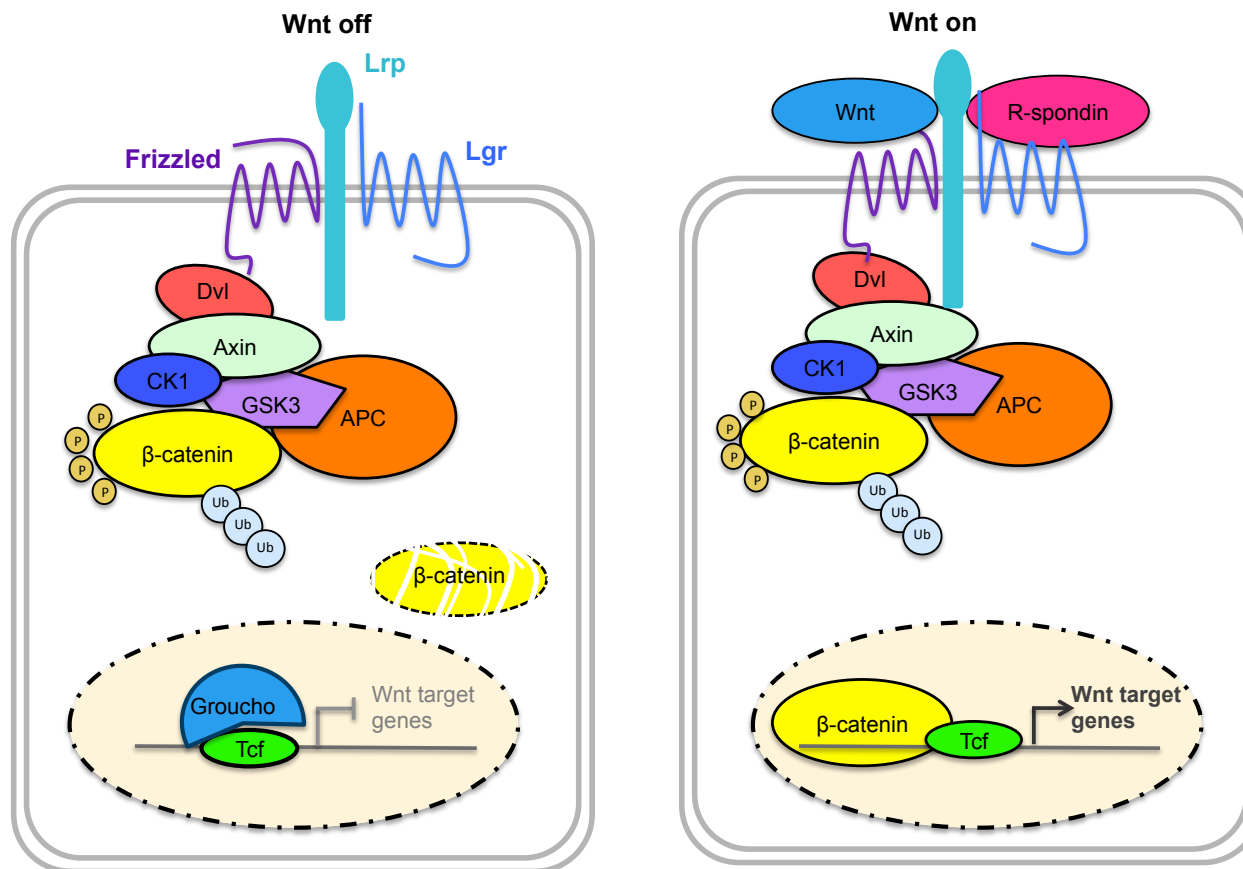
Figure 1.2 The Canonical Wnt signalling pathway

The Wnt signalling pathway is typically represented in a 'off' and 'on' state. In the absence of Wnt ligand, a destruction complex formed of multiple proteins including Axin and APC, glycogen synthase kinase 3 and casein kinase 1, all of which mediate the degradation of ß-catenin by ubiquitination, preventing translocation into the nucleus. In the presence of Wnt ligand, the destruction complex is recruited to the receptor-ligand complex, enabling the accumulation of ß-catenin within the cytoplasm. This in turn mediates downstream activation of target gene expression.

1.2.3.2 The Notch signalling pathway

Notch signalling is activated in response to cell-cell contact; an extracellular domain binds to a Jagged or Delta ligands that reside on a opposing cell surfaces, as depicted in Figure 1.3. The interaction of Notch ligands with the Notch receptor induces proteolytic cleavage at the extracellular domain, mediated by the tumour necrosis factor-α-converting enzyme (TACE). Following this interaction, the transmembrane receptor domain of Notch (NICD) is cleaved by a presenilin-γ secretase complex, which mediates the translocation of the intracellular receptor domain to the nucleus (Qiao and Wong 2009). Notch signalling effectors regulate the transcription factor CSL that control gene expression of Notch target genes. Target genes of Notch signalling have various functions such as cell proliferation and differentiation (Badalà *et al.* 2011)

Notch signalling plays a pivotal role in the coordination of differentiation events within intestinal epithelial cells, and is therefore critical in maintaining intestinal development and homeostasis, and equally a role in the transformation of epithelial cells towards a more malignant phenotype (Ashley 2013a). Both Notch1 and Jagged-1 are expressed at high levels in transit amplifying cells of the colon (Badalà *et al.* 2011). The loss of notch signalling in mouse intestinal stem cells promotes the differentiation of stem cells towards a goblet or enteroendocrine cell lineages (van Es *et al.* 2010) as opposed to absorptive cells. Conversely, induced Notch signalling activation has been shown to reduce differentiation and increase proliferation of progenitor cells (Fre *et al.* 2005). Using inducible tissue-specific Notch-mutant mice, studies have further demonstrated the role of Notch signalling in crypt differentiation and proliferation, whereby loss of Notch receptors result in loss of cell cycle progression of crypt progenitor cells (Riccio *et al.* 2008) . Culture of intestinal stem cells has also demonstrated that extracellular application of Notch ligands to culture conditions directs stem cells towards a more differentiated phenotype (Yin *et al.* 2013). Some studies have also highlighted the interplay

between Notch and Wnt signalling within the intestine, particularly in the ISC population. Recently, it has been shown, by utility of Notch blocking antibodies, that Notch signalling has the ability to diminish outputs of Wnt signalling, thus also contributing to stem cell activity (Tian *et al.* 2015).

1.2.3.3 TGFβ / BMP signalling pathway

The Transforming Growth Factor Beta (TGFβ) family of proteins are involved in an array of cell signalling events. Upon ligand binding to membrane-bound receptors (Type I and Type II) the type II receptor dimerises with type I, and then phosphorylates the cytoplasmic domain of type I. This phosphorylated domain in turn recruits Smad2/Smad3 cytosolic proteins and mediates their phosphorylation. The Bone Morphogenic Protein (BMP) signalling pathway forms a large subgroup of the TGFβ family, and typically results in the recruitment and phosphorylation of Smad1, Smad 5 and Smad 8 (Yeung *et al.* 2011). The dissociation and activation of recruited Smads enable a complex formation with Smad 4. This in turn mediates the translocation of the complex to the nucleus, enabling the interaction with co-activators and co-repressors of transcription, enabling the expression of TGFβ related genes upon binding, as represented in Figure 1.3. Target genes are involved in the inhibition of growth and proliferation, highlighting a definitive role in the intestine (Ashley 2013b).

BMP signalling is predominantly active at the surface of the colon lumen as opposed to the stem cell rich compartments at the base of crypts. The BMP pathway has a definitive role in the establishment of the crypt axis in the intestine as well as maintaining the proliferative environment to restrict intestinal hyperproliferation. Mechanistically, the direct inhibition of Wnt-driven ß-catenin dependent signalling by functional BMP signalling ensures the terminal differentiation of intestinal cell lineages, particularly the maturation of secretory lineages (Auclair *et al.* 2007). Inhibition of BMP signalling, using agents such has Noggin has previously been shown to result in the formation of ectopic crypts (Batts *et al.* 2006). BMP inhibition has also been linked to an expanding stem and progenitor cell population in the

intestine, eventually resulting in intestinal polyposis (He *et al.* 2004). An interplay between BMP and Wnt signalling has also been postulated, with some studies having shown that Wnt signalling is suppressed by BMP to further control self renewal of ISCs (Yeung *et al.* 2011; He *et al.* 2004). Recent *in vitro* studies with Lgr5+ ISCs cultured with BMP showed an overall suppression in a stem cell marker signature, suggesting that functional BMP signalling limit self-renewal of a pool of stem cells in the crypt, and in turn prevents hyperproliferation (Qi *et al.* 2017).
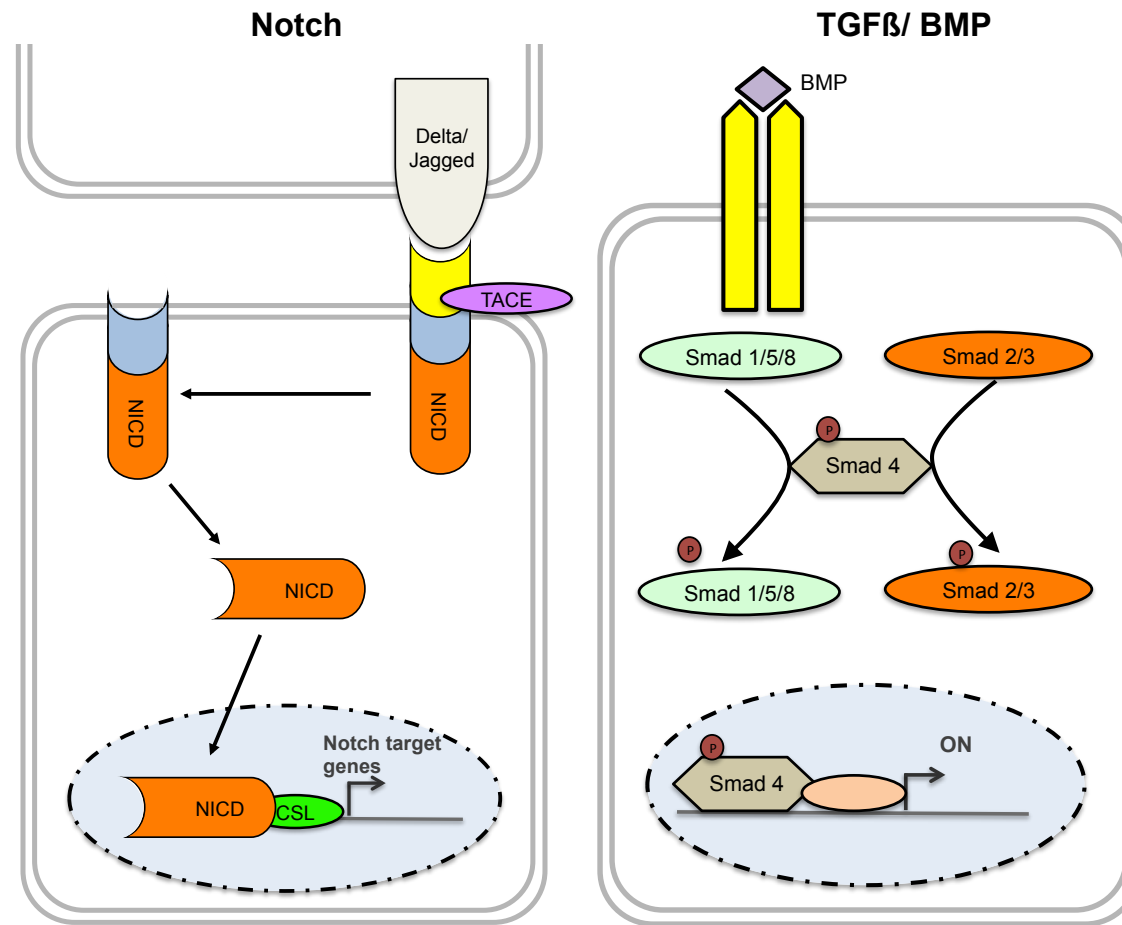
Figure 1.3 Schematic of Notch and TGFß/BMP Signaling

Homeostasis of the large intestine relies on Notch and TGFß/BMP signalling, which play a role in the expression of genes associated with specific functions such as proliferation and differentiation.

1.2.3.4 Mitogen-Activated Protein Kinase Pathways (MAPK/ERK) signalling pathway

The canonical MAPK/ERK pathway, as depicted in Figure 1.4, is activated by receptor tyrosine kinases, such as EGFR, that mediate a downstream signalling cascade (Burotto *et al.* 2015). Upon stimulation, downstream RAS proteins, including HRAS, NRAS and KRAS, are localised to the membrane, which in turn triggers the growth-factor receptor binding protein 2 (GRB2), activating Sevenless homolog (SOS), both of which mediate the activation of RAS. RAS proteins belong to a family of guanosine-5'-triphosphate binding proteins (GTPases) and are thus activated by dissociation of guanosine diphosphate to guanosine triphosphate-bound RAS (Santarpia *et al.* 2012). This mediates a number of downstream effects, including recruitment of RAF protein isoforms (ARAF,BRAF and CRAF) to the cell membrane, and activation of function (Dhillon *et al.* 2007). RAF in turn activates Mitogen activated kinase 1/2 (Mek 1/2) which then activate extracellular signal-related kinase 1/2 (ERK 1/2). Upon activation, ERK1/ERK2 phosphorylate a number of cellular and nuclear substrates whereby cell cycle regulators are targeted; including cyclin D, as well as target genes involved in apoptosis including *Bim* (Mebratu and Tesfaigzi 2009) which mediate a broad range of cellular responses such stimulation of proliferation, differentiation survival and apoptosis (Santarpia *et al.* 2012; Burotto *et al.* 2015).
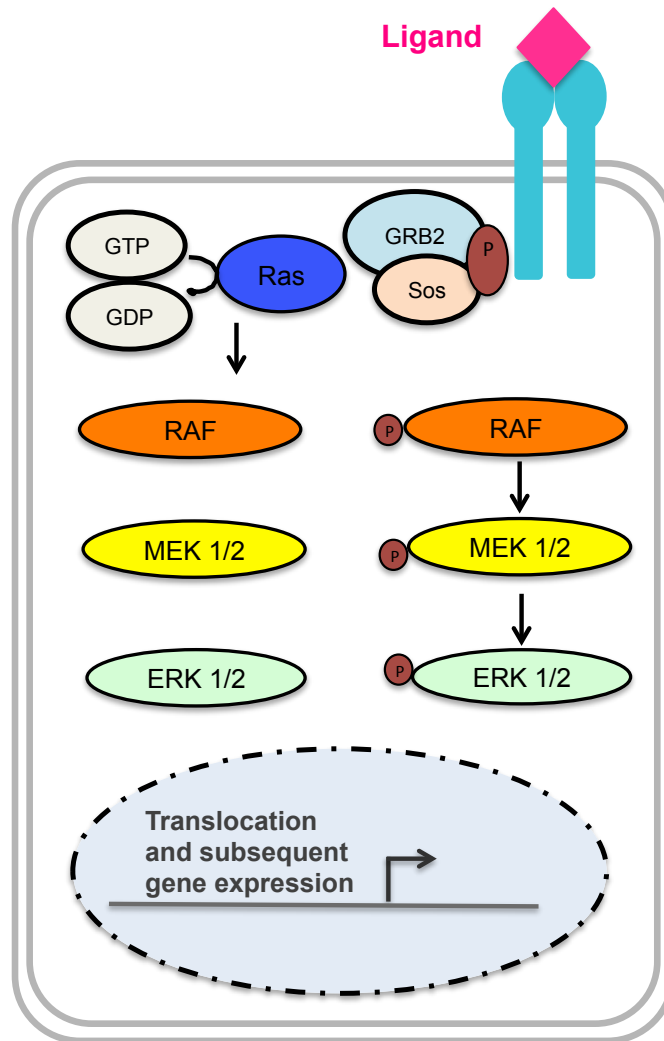
Figure 1.4 Schematic of EGFR/RAF/MEK/ERK signalling

Activation of receptor Tyrosine Kinases (RTKs) such as EGFR lead to recruitment of GRB2, and SOS, the guanine nucleotide exchange factor. This in turn activates Ras, mediating the phosphorylation and activation of Raf. This initiates the phosphorylation of MEK1/2, with subsequently phosphorylates ERK 1/2. Activated ERK1/2 is translocated to the nucleus, which leads to the activation of transcription factors involved in cell cycle regulation, proliferation and cell survival.

1.2.3.5   Phosphoinositide 3-kinases (PI3Ks) Signalling

Phosphoinositide 3-kinases (PI3Ks) are a family of lipid kinases composed of regulatory subunits and a catalytic subunit, which exist in several isoforms and are tightly regulated in the normal cell (Engelman 2009). PI3K activation occurs as a result of receptor tyrosine kinases, G-protein coupled receptors and interaction with Ras (Zhao and Vogt 2008).

Once activated, PI3Ks initiate the phosphorylation of the 3' hydroxyl group of phosphatidylinositol 4,5 bisphosphate (PIP$_2$) to phosphatidylinositol 3,4,5-triphosphate (PIP$_3$) on the plasma membrane. Signalling can be terminated at this point by the phosphatase PTEN (phosphatase and TENsin homolog deleted on chromosome 10), which facilitates the hydrolysis of PIP$_3$ to PiP$_2$ (Zhao and Vogt 2008). Upon accumulation of PIP$_3$, AKT is recruited to the membrane, whereby phosphoinositide-dependent protein kinase 1 (PDK1) phosphorylates within the activation loop of AKT (threonine 308), and mechanistic target of rapamycin complex 2 (mTORC2) phosphorylates a hydrophobic motif of AKT (serine 473) facilitating AKT activation. Following activation, AKT mediates the phosphorylation of several proteins, which, in turn regulate several cell processes including proliferation, cell survival and protein synthesis (Engelman 2009).

1.3   Colorectal cancer

Colorectal cancer is the third most common cancer, and the second most common cause of cancer related deaths in the UK (CRUK, 2014). The incidence of CRC is particularly high due to the challenging environment of the tissue. The high rate of cell division required to facilitate the rapid turnover of cells within the crypts provide a potential source of DNA replication errors, making oncogenic transformations more likely (Ashley *et al.* 2013). Furthermore, colorectal tissue is directly exposed to carcinogens from ingested food, and thus provides multiple factors for carcinogenic occurrences to take place.

CRC is classically divided into sporadic and hereditary conditions. Sporadic CRC development has been proposed as a process whereby modulation in the aforementioned signalling pathways, as well as accumulative genetic abnormalities in oncogenes or tumour suppressor genes, can drive the transition from normal epithelial tissue to a benign adenoma, to a carcinoma which has the potential to metastasise into other tissues within the body (Gervaz *et al.* 2004; Smith *et al.* 2002), with proposed mechanisms discussed in section 1.3.2. The incidence of sporadic bowel cancer is largely attributed to external factors, such as diet, smoking and increased alcohol consumption, with recent studies also investigating the role of the gut microbiota in the initiation and possible influence on carcinogenic processes (Drewes *et al.* 2016).

Hereditary conditions have also been found to contribute to the incidence of CRC, namely through familial adenomatous polyposis (FAP), a hereditary condition which leads to the development of polyps with potential to form benign lesions and adenocarcinomas (Bodmer *et al.* 1987).

1.3.1   TNM and Dukes staging of colorectal cancer

Histopathological assessment of patient tumour samples enables disease staging, ideally from surgical resection specimens according to the Tumour Node Metastasis (TNM) system. This is a revised modification of the previously established Dukes' staging and is of prognostic significance, as highlighted in Figure 1.5 and Table 1.1 (Greene 2004). This enables an assessment of degree of the degree of invasion of a primary tumour, as designated by Tumour T stage T1-T4, a pathological assessment of tumour cell presence in regional lymph nodes (N stage N0-2), and finally, a classification for metastases distant from the primary malignancy 'M' 'M' (x,0,1) to indicate local or further metastasis.
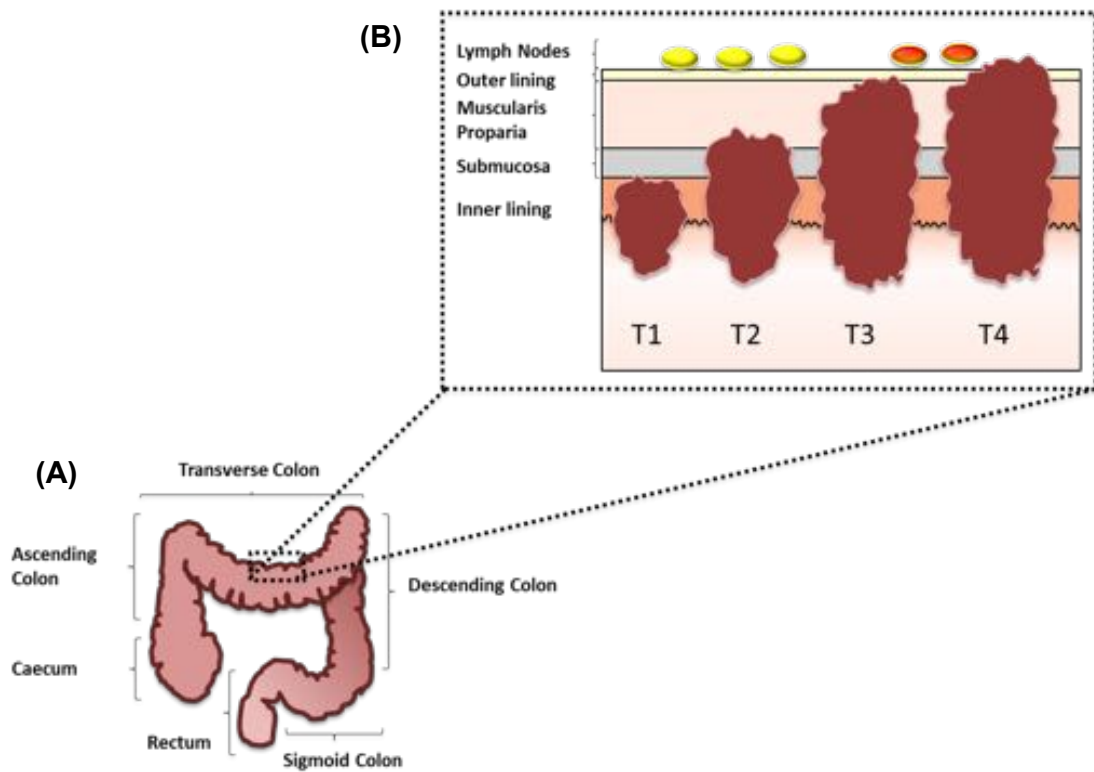
Figure 1.5 Gross anatomy of the large intestine showing representative grading for tumour invasion.

(A) Gross anatomy of the large intestine, from the caecum to the rectum. Surgically resected specimens from the Wales Cancer Bank come from throughout this region. (**B**) Diagram representing 'TNM' staging of colorectal cancer; early stages show tumour invasion into the inner lining of the colon, whilst later stages show invasion which can spread to adjacent lymph nodes and potentially metastasise into other regions of the body.

Table 1.1 TNM/ Dukes' classification of colorectal cancer.

Table describing tumour stages for classification of disease progression.

	TNM Classification	Dukes' Classification
Stage 0	Carcinoma in situ	
Stage I	Tumour invasion of the submucosa of the bowel only (T1, N0, M0)	A
	Tumour invasion of the muscle layer of the bowel wall, muscularis propria (T2, N0,M0)	B1
Stage II	Tumour invasion, into the outer lining of the bowel wall (T3, N0, M0)	B2
	Tumour invaded through the outer lining of the bowel wall (T4, N0, M0)	B2
Stage III	1-3 lymph nodes contain cancer cells (T1-2, N1, M0)	C1
	4 or more lymph nodes containing cancer cells (T1-2, N2, M0)	C1
	1-3 lymph nodes contain cancer cells (T3-4, N1, M0)	C2
	4 or more lymph nodes containing cancer cells (T3-4, N2, M0)	C2
Stage IV	Known metastasis in the patient (T1-4, N1-2, M1)	D

1.3.2 The genetic progression of colorectal cancer development

Given the intricate plethora of aforementioned signalling pathways involved in maintaining intestinal homeostasis, it is unsurprising that modulation of such pathways as a result of mutations in key tumour suppressors and oncogenes have the potential to initiate and drive CRC progression. The understanding of molecular events that are key to tumour initiation and progression not only underpin the understanding of tumourigenesis, but are also of vital relevance to the development of novel targeted therapies.

Sporadic CRC development has been proposed as a process whereby modulation in homeostatic signalling pathways, as well as accumulative genetic abnormalities in oncogenes or tumour suppressor genes, drive the transition from normal epithelial tissue to a benign adenoma, to a carcinoma which has the potential to metastasise into other tissues, as depicted in Figure 1.6 (Gervaz et al. 2004; Smith et al. 2002). The development of CRC has long been established as a multi-step process, whereby mutations are acquired and accumulated, driving tumour progression from a dysplastic epithelium, to benign adenoma and adenocarcinoma, which then has the potential to metastasise into other tissues. This 'classic' genetic model of CRC progression was proposed over 20 years ago in a landmark study by Fearon and Vogelstein, where they carried out a comprehensive analysis of histopathological and genetic data in late stage tumours compared to early stage tumours to understand mutations that initiate and play a role in CRC development (Fearon and Vogelstein 1990). It was observed that many genetic alterations occurred at a higher frequency in late stage tumours. The authors hypothesised that the adenomatous polyposis coli (*APC*) gene was the initiating mutation in the formation of benign lesions, leading the acquisition of activating mutations in kirsten rat sarcoma viral oncogene homolog (*KRAS*), allelic loss of 18q locus and *p53* loss, all of which were critical drivers of tumour progression due to genetically unstable cells (Fearon and Vogelstein 1990; Pinto and Clevers 2005; Gervaz *et al.* 2004). Despite such

alterations having been observed in the advanced tumours, this work came with the caveat that such specific genetic alterations were not observed in all tumours and that it was more likely that the accumulative mutations, rather than their order of acquisition lead to advanced tumour formation (Fearon and Vogelstein 1990). Further to these remarks, Smith et al (Smith *et al.* 2002) noted that mutations in all genes *APC, KRAS* and *P53* occurred in only 6.6% of tumours of a cohort of over 100 CRC patients, suggesting that alternative genetic pathways occur in CRC progression.

The loss of the tumour suppressor *APC* is well established as a key driver for CRC progression. An activating mutation in *APC* was firstly associated with patients suffering from familial adenomatous polyposis (FAP), a hereditary condition which leads to multiple polyp development (Bodmer *et al.* 1987). Both germline and somatic *APC* mutations result in aberrant signalling which allow the formation of benign lesions, which can potentially initiate tumour progression. APC regulates the degradation of β-catenin and is hence a critical component of the Wnt-signalling cascade. Mutations therefore result in a constitutive activation of canonical Wnt signalling which causes an activation of transcription of downstream signals, primarily involved in enhanced cell proliferation. Inactivation of *APC* in the murine intestinal epithelium has previously been implicated in a rapid relocalisation of ß-catenin to the nucleus in histological samples, suggestive of Wnt signalling induction, resulting in cellular changes such as an expansion of a progenitor cell population in the crypt and a failure of cells to migrate and differentiate (Sansom *et al.* 2004).

Activating mutations in *RAS* often follows in colorectal cancer progression. Early studies that grouped adenomas according to volume noted that mutations in *KRAS* or *NRAS* were prevalent in larger adenomas (Vogelstein *et al.* 1988) suggesting that *RAS* mutations facilitate tumour progression towards malignancy. DNA sequencing studies have further confirmed the role of mutated *RAS* in colorectal cancer, particularly *KRAS* activating mutations, which constitute approximately 40% of colorectal cancers, the majority in codon 12 (Cancer Genome Atlas Network 2012). As discussed further in section 1.5, KRAS is a downstream mediator of the MAP/ERK pathway, constituting a role in a major signalling cascade that is integrated with

multiple pathways, and thus constitutes a large role in control of cell proliferation and cell survival.

The transition from adenoma to carcinoma is further driven by loss of the long arm of chromosome 18, then the tumour suppressor p53, which, in the normal cell mediates cell cycle suppression or induces apoptosis in response to stress or damage (Colussi *et al.* 2013) . The later stages of colorectal tumourigenesis are frequently classified by p53 loss of function, and approximately 75% of CRC contain p53 mutations (Cancer Genome Atlas Network 2012). Such mutations result in the stimulation of high proliferative activity due to failed function in cell cycle control. Frequently, a molecular event which co-occurs is the LOH of chromosome 18q, where the genes Smad2, Smad4 and DCC are located (Colussi *et al.* 2013).

A comparison of normal and tumour tissue by deep sequencing has further emphasised the complexity of events that drive the formation of colorectal tumourigenesis, by demonstrating the plethora of genes involved in tumour progression (Wood *et al.* 2007; Cancer Genome Atlas Network 2012). It has been noted in such studies that other changes are likely to occur during this classic progression model, and further studies have demonstrated the implication of an array of signalling cascades that also influence CRC progression, including the PI3K pathway, further discussed in section 1.2.3.5. The recent 'Big Bang' theory, postulates that tumour growth results from the expansion of an initial population of cells containing mutations such as *APC* and *KRAS*, with heterogeneous subclones continuously accumulating within the tumour, resulting in intratumoral heterogeneity (Sottoriva *et al.* 2015). Such studies highlight the complex genomic landscape of CRC, which ultimately plays a role in explaining the difficulty in identifying therapeutics for CRC.

Normal Epithelium　　**Early adenoma**　　**Late adenoma**　　**Carcinoma**

APC
loss

KRAS
activation

P53
loss

Genomic Instability
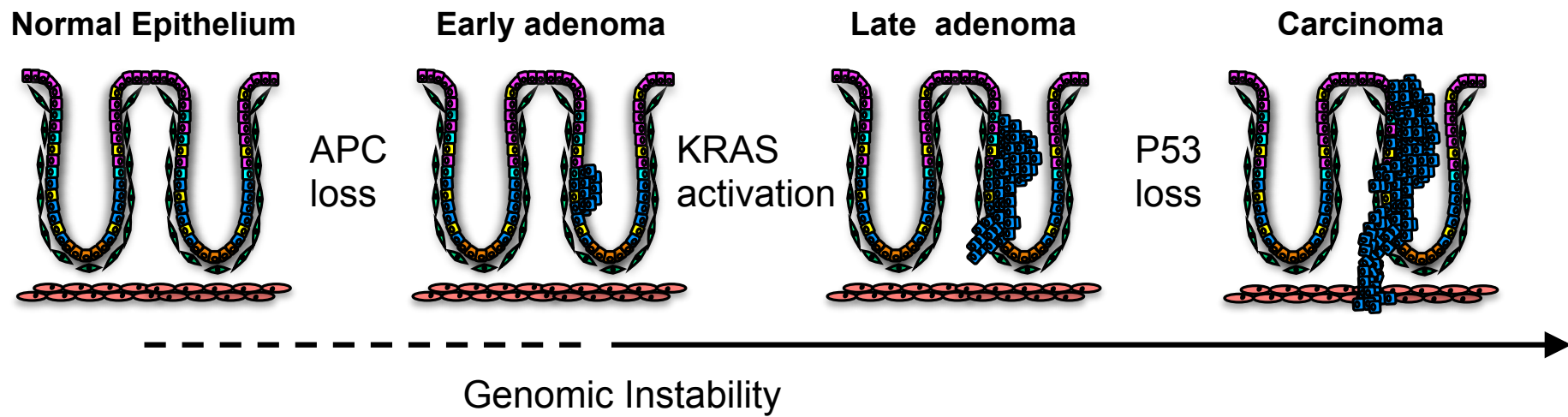
Figure 1.6 Schematic of tumour initiation and progression in the intestine.

Classical model of tumour progression proposed by Fearon and Volgstein, depicting accumulating mutations that lead to the transition of the normal epithelium to carcinoma formation.

1.4   Current therapeutic strategies for CRC

Therapeutic strategies for CRC primarily involve surgical resection of both tumour and metastasis, in conjunction with radiotherapy and/or chemotherapy in the neoadjuvant (prior surgery) setting to shrink the tumour, or in the adjuvant setting (following surgery). For rectal cancer patients specifically, the administration of chemotherapy alongside radiotherapy is frequently used as a therapeutic strategy.

5-Fluoruracil (5-FU) was introduced as a chemotherapeutic agent over 40 years ago and has remained the most widely used treatment regimen for CRC. 5-FU, when metabolised to 5-fluoro-2'-deoxyuridylate, acts as an irreversible thymidylate synthase inhibitor, disrupting DNA and RNA synthesis leading to the initiation of apoptosis and cell death (Gill *et al.* 2003). As a monotherapy, 5-FU or in recent advances Capecitabine, a pro-drug equivalent, is associated with an improved disease free median survival (Longley *et al.* 2003) rate in approximately 10-15% of patients. 5-FU is frequently used in combination to overcome these limited response rates. Leucovorin, a folinic acid that mechanistically stabilises bonds formed by thymidylate synthase and a metabolite of fluorouracil, has been shown to improve survival compared to 5-FU alone (12 months versus 7 months) (Poon *et al.* 1991)and in prospective studies the addition to Leucovorin to a chemotherapeutic regime conferred response rates of 23% (Gill *et al.* 2003).

Further advances have been made to improve the therapeutic repertoire of CRC treatment, including the generation of oxaliplatin, which induces cross-linking of DNA, impairing DNA synthesis and cell replication (Longley *et al.* 2003). Although somewhat active as a single agent, oxaliplatin in combination with 5-FU and levouricin, has been shown to yield response rates of 20% in refractory disease (Andre *et al.* 1998). Similarly, irinotecan, a topoisomerase 1 inhibitor, has been reported to improve median survival in patients receiving 5-FU/Leucovorin/Irinotecan compared to 5-FU/ Leucovorin alone, as well as higher response rates in 387 patients within the randomised trial (Douillard *et al.* 2000;

Goldberg *et al.* 2005). Varying combinations of fluorouracil, irinotecan and oxaliplatin are now well established in the clinic, dependent on CRC tumour stages, and have been found to increase median survival (Goldberg *et al.* 2005).

However, despite the substantial improvement made to CRC treatment over the past decade, chemotherapeutics are toxic and combination chemotherapeutics show increased toxicities, such that treatment regimes are generally limited by the damage inflicted on healthy tissues. Clinical trials, such as the Medical Research Council (MRC) COIN trial, have reported some reduction in toxic effects when chemotherapeutics are administered intermittently as opposed to continuous pre-defined intervals which are regular in the clinic. However, such regimens have failed to significantly improve overall survival in advanced CRC (Adams *et al.* 2011) . Another consideration for the continued use of chemotherapeutic agents is their strong association with tumour resistance, which ultimately leads to patient relapse and tumour progression. Studies investigating treatments in the adjuvant setting have thus far reported limited benefits of combinations at more advances stages of CRC; the MOSAIC trial for Stage III CRC patients, for example, showed that Leucovorin, oxaliplatin and 5-FU combination increased disease free survival at 3 years by only 7%, compared to 5-FU and leucovorin alone (Binefa *et al.* 2014). The advances in chemotherapeutic therapies in the curative setting therefore need to be improved.

The advances in the understanding of CRC and biomarkers of tumour types have moved treatment towards more targeted therapy to improve survival. The epidermal growth factor (EGFR) for example, is a receptor tyrosine kinase that is an emerging prognostic biomarker for CRC following identification of EGFR amplification across CRC patient samples (Resnick *et al.* 2004; Spano *et al.* 2005). Cetuximab and Panitumumab are two anti-EGFR monoclonal antibody therapies that inhibit the EGFR transmembrane glycoprotein, inhibiting downstream signalling. Both agents have been approved in the clinical setting, with the exception of *KRAS* mutant patients, which fail to respond to EGFR inhibitor therapy (Roock *et al.* 2010). As shown in Figure 1.4, the EGFR ligand lies upstream of RAS; a mutation in *KRAS*

could thus override any inhibition of upstream targets and maintain downstream signaling. Despite vast advances in the understanding of CRC biology, treatment remains largely palliative and is limited in overall impact upon long-term survival. Studies are still underway to improve survival long-term by investigating targeted therapies, as well as scheduling chemotherapeutic regimens appropriately.

1.5 Deregulated pathways in CRC development and associated targeted therapies for a biomarker-driven clinical trial.

1.5.1 FOCUS 4 clinical trial as a molecularly stratified clinical trial

The MRC/NIHR, alongside Cancer Research UK (CRUK) have funded a NCRI CRC Clinical Studies Group development, FOCUS 4 (registered ISRCT90061546) as a drive to investigate biomarker-selected therapies in CRC. This UK-wide clinical trial is a molecularly stratified, multi-arm programme (**Figure 1.7**) that aims to address the relation between tumour biomarker profiles and selective therapeutic intervention to improve progression free survival in CRC.

As depicted in **Figure 1.7**, this trial aims to classify patients with progressed or inoperable metastatic CRC according to the molecular background of their tumour, and treat accordingly. Following 16 weeks of palliative chemotherapy, and fulfilment of eligibility criteria, patients will be categorised into sub-groups (treatment 'arms') according to the molecular make-up of their tumour. Patients will be randomized to receive treatment or placebo and their progression free response to treatment will be tested. The panel of molecular markers under investigation are based on biomarkers that have been previously identified or hypothesised to elicit predictable responses to targeted therapies, particularly from previous data collected from the MRC COntinuous or INtermittent (COIN) trial, and will be discussed in turn. The adaptive design of the trial enables progressive changes to be incorporated during the course of the trial as a result of novel biomarker identification, novel treatments, or the identification of trial arms better fitted with alternative treatments. Given the complex mutation spectrum in CRC, it would be a fair assumption that patients could

harbour a number of the main molecular mutations and thus be categorised into several arms. Treatments are therefore tiered based on a hierarchy (arms left to right) according to the strength of prognostic effect and targets of agents used (Professor Tim Maughan, personal communication). The trial version as depicted below will be discussed in the context of this thesis (as discussed with members of FOCUS 4 team and recent publications (Richman *et al.* 2015).
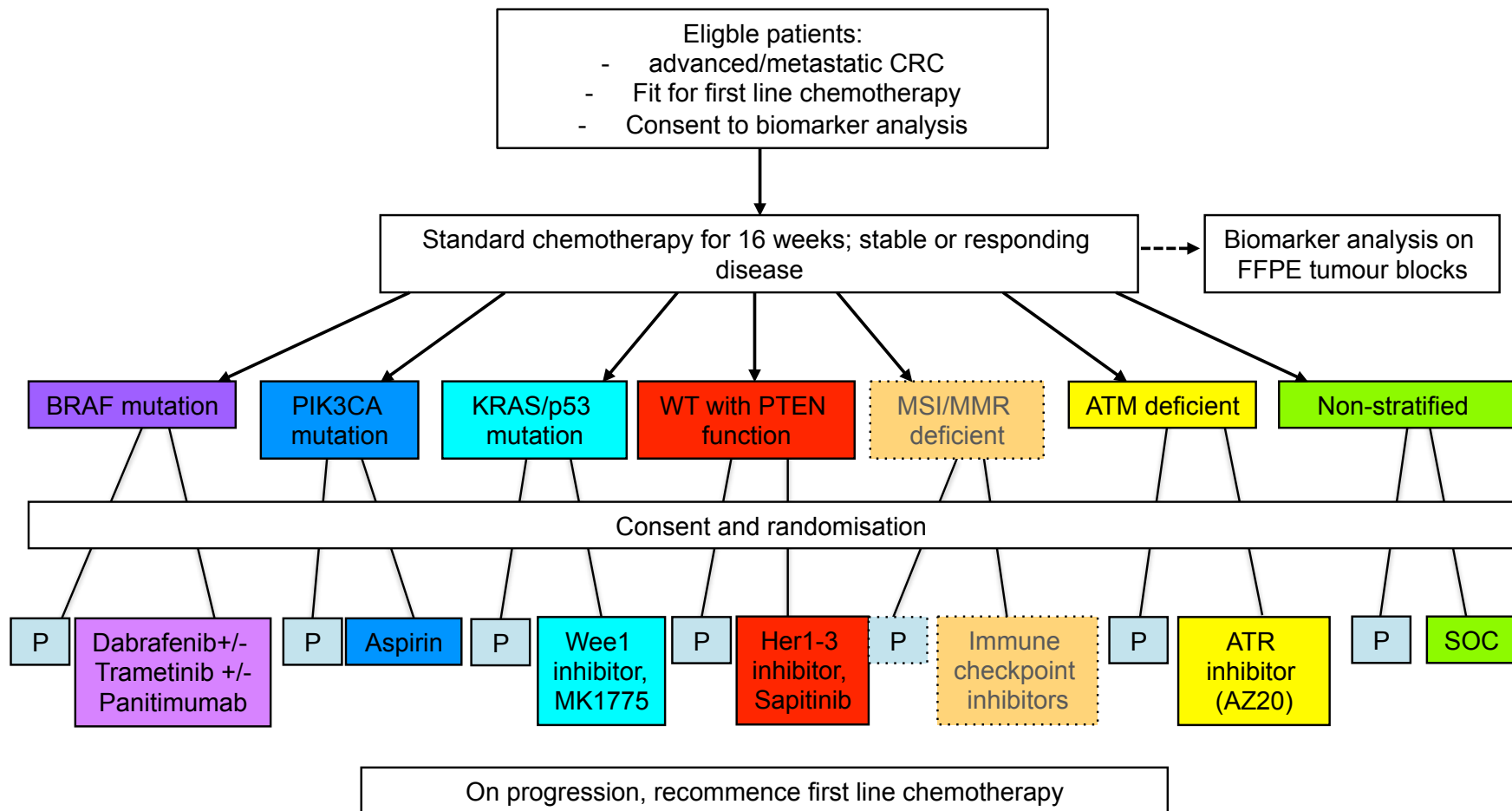
Figure 1.7 Outline of the MRC FOCUS 4 clinical trial.

Patients with metastatic CRC, fit for first line chemotherapy will undergo biomarker analysis, and will be stratified on the basis of the molecular profile of their tumour and treated accordingly, adapted from FOCUS 4 master protocol. The MSI/MMR deficient arm (dotted) is beyond the scope of this thesis and is for reference only.

1.5.2 Targeting the Mitogen-Activated Protein Kinase Pathways (MAPK/ERK) pathway

Mutations in numerous components within the MAPK/ERK signaling cascade (previously discussed in intestinal homeostasis in section 1.2.3.4) result in altered gene expression and constitutive activation in MAPK/ERK signaling activity, and have been shown to be involved in CRC tumour progression. *KRAS* mutations are found in approximately 40% of CRCs (Cancer Genome Atlas Network 2012), with the majority of such activating mutations occurring at codon 12. MAPK signaling is also aberrantly activated in CRCs following oncogenic mutations in *BRAF,* and lead to a constitutive activation of BRAF kinase activation, resulting in the phosphorylation and activation of MEK 1/2 (Santarpia *et al.* 2012) and therefore sustained MAPK activity. *BRAF* mutations are found in approximately 8-12% of CRCs, and occur mostly at the V600 domain whereby a single amino acid is substituted to glutamic acid (V600E), resulting in a constitutive kinase activity (Corcoran 2015). Importantly, KRAS and BRAF activating mutations are mutually exclusive, and thus act as key negative predictors for response against monoclonal antibodies against EGFR, such as cetuximab. Therapies that target the MAPK pathway have therefore been generated in a strategy to target RAS and RAF protein, and more recently, MEK as a downstream target of both.

At the receptor tyrosine kinase level, the MAPK ERK pathway can be activated by EGFR activity, and aberrantly activated by EGFR gene overexpression, amplification as a result of activating mutations as observed in CRCs (Santarpia *et al.* 2012; Burotto *et al.* 2015). Monoclonal antibodies (mAbs) which have been directed against the extracellular domain of EGFR have been developed, and have shown effectiveness in CRC with amplification of EGFR-mediated signalling. Panitumumab is a mAb developed for use in metastatic CRC and has an overall overall 8% response rate, with improved toxicities compared to mAbs such as cetuximab (Roberts and Der 2007; Gibson *et al.* 2006). In addition to EGFR inhibition, selective BRAF inhibitors have been developed, such as vemurafenib and Dabrafenib and have proved to yield

high response rates in BRAF-mutant melanoma patients (Ahronian *et al.* 2015). However, pre-clinical studies have reported that CRC patients harbouring the same mutation do not necessarily respond to direct inhibition of BRAF, indicating that this strategy fails to sufficiently inhibit MAPK signaling. Studies have suggested that negative feedback loops, driven by EGFR-mediated reactivation, compensate for RAF inhibition in *BRAF-* mutant CRC cells, resulting in feedback reactivation of MAPK signaling (Corcoran *et al.* 2012; Prahallad *et al.* 2012). Some evidence has also suggested that BRAF mutant CRCs express high levels of total EGFR compared to melanomas bearing the same mutation, suggesting that EGFR-dependent resistance would be more prominent within BRAF-mutant CRCs (Corcoran 2015; Corcoran *et al.* 2012). Furthermore, inhibition of downstream targets such as MEK1/2 have been shown suppress activation of ERK and thus improve overall targeted inhibition of the MAPK pathway, inducing an improved outcome in numerous xenograft models of pancreas, breast and colon, (Roberts and Der 2007; Davies *et al.* 2007). However, targeting downstream KRAS or BRAF activity using MEK1/2 inhibitors in colorectal cancer cells has highlighted some instances of acquired resistance to therapy, in which KRAS or BRAF activity are amplified as a result of treatment (Little *et al.* 2014).

In order to suppress feedback reactivation of MAPK signaling cascade and overcome acquired resistance, it has been hypothesized that sustained inhibition of a combination of components within the pathway could be an alternative approach to therapy. Combinations of RAF/MEK or EGFR/RAF inhibition have thus been introduced in clinical trials and have recently showing some response rates (Corcoran *et al.* 2015), with newer trials introducing triple combination therapy against EGFR, RAF and MEK . Within the FOCUS 4 clinical trial a treatment regimen of an anti EGFR antibody (Panitumumab), alongside BRAF inhibitor (Dabrafenib) will be tested for efficacy and progression free survival with and without a MEK 1/2 inhibitor (Trametinib) in patients harboring BRAF V600E mutations (*BRAF* mutation arm).

1.5.3 Phosphoinositide 3-kinase (PI3K pathway)

Deregulation of the numerous components within the PI3K cascade is associated with many malignancies, and further findings in the literature support the involvement of aberrant PI3K signalling in tumour progression (Samuels and Velculescu 2004; Engelman 2009a). The *PIK3CA* gene encodes the p110α catalytic subunit of PI3K, and mutations occur at a frequency of approximately 15% of CRCs (Cancer Genome Atlas Network 2012). Further studies have identified that 80% of mutations within *PIK3CA* are frequently found within conserved hotspots in the helical (exon 9) and kinase (exon 20) domain of the protein, resulting in a constitutive activation of the PI3K-AKT pathway that regulates proliferation, apoptosis and metabolism (Samuels *et al.* 2004; Samuels and Velculescu 2004). Further studies have found that disruption of helical or kinase domain of two colorectal cancer cell lines resulted in activation of the AKT pathway, and highlighted the role of PIK3CA in attenuating apoptotic events (Samuels *et al.* 2005).

Currently, compounds that directly target elements of PI3K signalling are being introduced in clinical trial. BEZ235 (Novartis), for example, is a dual PI3K/ mTOR inhibitor that has demonstrated promising results in tumour xenografts and GEMMs (Maira *et al.* 2008; Raja *et al.* 2015) . Given the complex network involved for PI3K signalling, it is worth noting that the complex landscape of mutations in CRC could provide a mechanism of resistance against PI3K targeted therapies, whereby mutations or amplifications in downstream or linked pathway components could induce compensatory effects of inhibition (Liu *et al.* 2009). Emerging data from retrospective studies have thus far shown beneficial effects of aspirin administration in patients harbouring mutations in exon 9 and 20 of PIK3CA, improving overall mortality compared to placebo (Liao *et al.* 2012). *In vitro* studies have somewhat confirmed that *PIK3CA* mutations play a role in aspirin sensitivity; a recent study demonstrated that aspirin activity was exacerbated in CRC cell lines with *PIK3CA* mutations (Zumwalt *et al.* 2017) The precise mechanisms involved are thus far unknown, and are therefore under exploration in the FOCUS 4 clinical trial, whereby

PIK3CA mutant patients will receive aspirin following standard of care treatment (Figure 1.7).

1.5.4   Agents targeting the DNA damage response pathway

The DNA damage response (DDR) consists of a plethora of complex signalling events which facilitate transient cell cycle arrest, DNA repair or apoptosis, in order to maintain the genomic integrity of cells (Khalil *et al.* 2012).

Ataxia-telangiectasia mutated (ATM) and ataxia–telangiectasia and Rad3 related (ATR) are central kinases that are activated as a result of replicative stress induced by double strand breaks in DNA or stalled replications forks. Upon activation of DNA damage, ATM directly stabilises the tumour suppressor p53, or indirectly via the downstream mediator checkpoint kinase 2 (Chk2). As a result of p53 activation, the gene expression of cell cycle checkpoint activators, such as p21, or genes involved in apoptosis are induced. This ultimately initiates G1/S phases of the cell cycle checkpoint to initiate cell cycle arrest, DNA repair and henceforth cell survival (Weber and Ryan 2015a). ATR monitors replication fork progression and is a principal component of the G2/M cell cycle. ATR mediates downstream effects via checkpoint kinase 1 (Chk1), which subsequently facilitates the degradation of Cdc25c, and activation of Wee1 kinase activity. As a result, the phosphorylation and inactivation of the Cdk2-cyclin B complex results in cell-cycle arrest, preventing entry into mitosis. This mechanism enables the suppression of DNA replication progression, allowing time to identify the source and resolve replicative stress (Matheson *et al.* 2016).

The deregulation of the G1 checkpoint is a characteristic of many cancer types, and ultimately impairs DNA damage repair prior to replication, resulting in the accumulation of mutations during DNA synthesis. However, the G2/M checkpoint is retained in cancer cells. Damage present at G2/M leads to cell cycle arrest such that cancer cells are able to repair DNA defects that would otherwise lead to catastrophic changes that drive apoptosis (Khalil *et al.* 2012). Theoretically, the selective ablation

of tumour cells can be achieved by G2/M checkpoint inhibition, since normal cells with functional checkpoints would be unaffected. The abrogation of the G2/M checkpoint has therefore been exploited as a potential therapeutic option to target tumour cells carrying specific defects in DNA repair or damage, driving cells to undergo mitosis, and essentially cell death by mitotic catastrophe (Matheson *et al.* 2016).

Pre-clinical studies have shown promise in targeting components of the DDR pathway that would induce cell death selectively in tumour cells. Wee1 is expressed in many tumour types, including colorectal cancer, with a recent study identifying Wee1 expression in the nuclei of 89% patient histological samples (Egeland *et al.* 2016), and current studies underway to establish clinical significance. *In vitro* studies have demonstrated the efficacy of a potent and selective Wee1 inhibitor, MK-1775 in inducing DNA damage in G2/M and S-phase cells (Guertin *et al.* 2013), as well as enhancing cytotoxic effects in colon cancer cell lines treated with a standard of care treatment, 5-FU. A similar therapeutic strategy is targeting ATR; cancers with pre-existing ATM loss would theoretically respond to ATR inhibition as both cell cycle checkpoints would be abrogated, impacting downstream signalling pathways such as checkpoint kinases, and lead to cell death.

Many studies have revealed that inhibition of ATR increases the sensitivity of cancer cells to replication stress, thus inducing cell death and inhibiting tumour growth. A compound developed by Aztrazeneca, AZD6738, an analogue of AZ20, with improved solubility, has been demonstrated to induce substantial effects *in vivo* (Weber and Ryan 2015b) whereby established human LoVo colorectal adenocarcinoma xenografts dosed with ATR inhibitor showed a substantial reduction in tumour volume (Foote *et al.* 2013). Within the FOCUS 4 clinical trial, targeting the DDR pathway will be an approach within two treatment arms. Firstly, patients harbouring ATM loss, as established from immunohistochemistry (IHC) will be treated with AZD6738 (ATR inhibitor). Wee1 inhibitors will be administered to patients harbouring KRAS/p53 mutations to further establish links between Wee1 inhibitions as a therapeutic strategy for RAS mutant patients (Figure 1.8). Within the

FOCUS 4 trial, it is hypothesised that treatment with Wee1 inhibitor will induce synthetic lethality in RAS/p53 mutant tumours due to the defective G1 checkpoint in cells, and increased replication stress (FOCUS4-C Protocol, 2017). p53 is a key regulator of the G1 checkpoint and thus p53 deficient cells are more likely to be susceptible to treatment targeting the G2 checkpoint. The rationale for targeting mutant RAS is also based on studies which have demonstrated the role of Ras in mitotic progression, that could be exploited for synthetic lethality as a therapeutic treatment (Luo *et al.* 2009; FOCUS4-C 2017) .
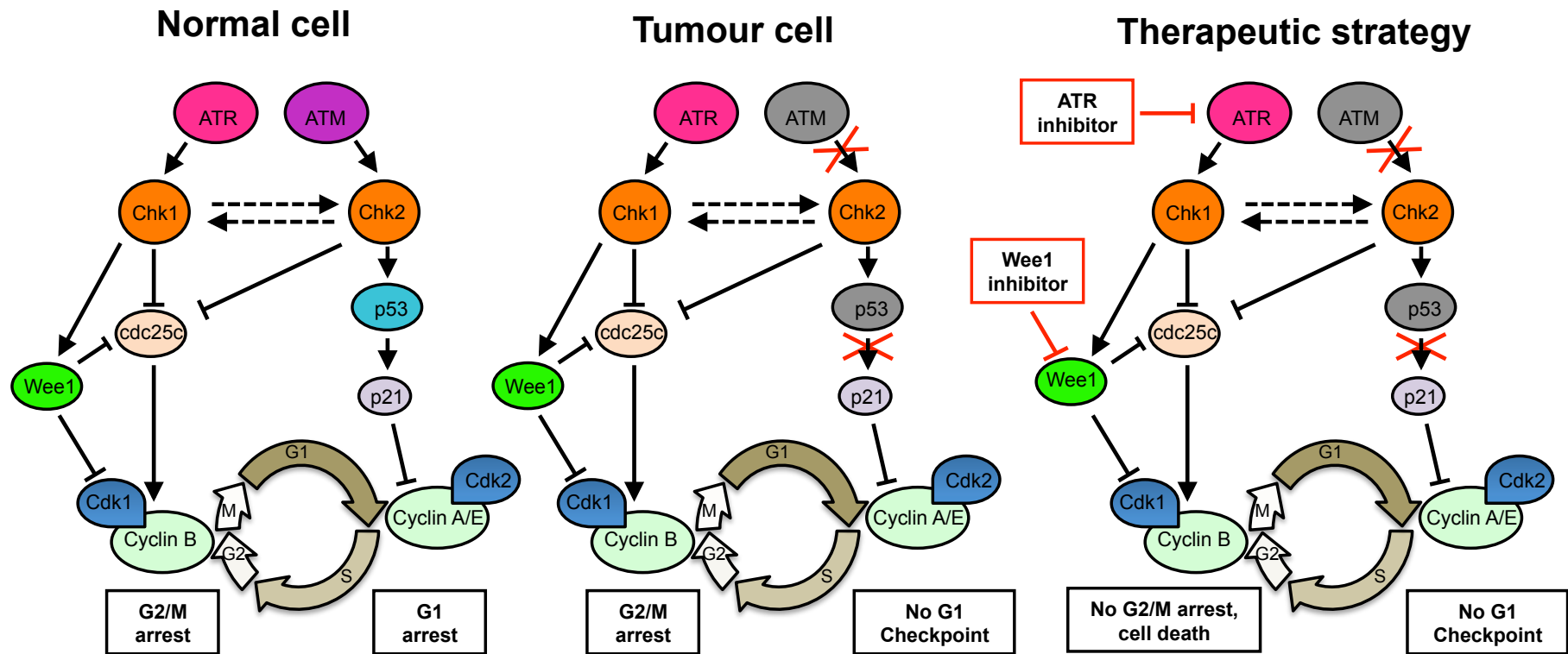
Figure 1.8 Schematic of DNA damage response pathway

Representation of DNA damage response in normal, tumour cells, and as a therapeutic strategy to induce synthetic lethality.

1.5.5   Tumour heterogeneity and patient stratification for treatment

Despite extensive therapeutic strategies implemented to target tumour development, a major reason for a lack of response in drug trials is as a result of inter- and intra- patient heterogeneity *de novo* and acquired by tumours. CRC overall is a very heterogeneous disease, occurring between tumour types as well as within a tumour mass. Studies by the Cancer Genome Atlas Network, for example, successfully performed a genome-scale analysis of over 200 different CRC samples (Cancer Genome Atlas Network 2012), with integrative analysis highlighting markers for more aggressive carcinomas. Evidence of correlation between gene expression signatures and treatments effective against tumour growth are slowly mounting. For example, *KRAS*-mutant CRCs have been shown to have limited responses to EGFR-targeting antibodies, due to downstream signalling with limits the effects of EGFR inhibition (Linardou *et al.* 2008). This has been further highlighted in a consortium of patient-derived CRC xenografts (Julien *et al.* 2012a). Studies of various molecular subtypes *in vitro* have been associated with differential responses to chemotherapeutics (Sadanandam *et al.* 2013).

The recognition of intra-tumour heterogeneity as a hallmark of CRC has resulted in a paradigm shift in clinical implications, with growing emphasis upon stratifying patients according to the molecular signature of a tumour, that ultimately defines and appropriate therapeutic strategy and suitability to a particular anti-cancer agent (Gervaz et al. 2004). It is becoming increasingly evident that biomarkers that predict patient response to treatment will be required for drugs to go into late stage clinical trials (Puig *et al.* 2013). However, genomic-focused precision oncology has also been recognised as a limited platform to predict the outcomes of complex biological signaling. The presence or absence of genetic drivers often underestimates the activity of corresponding biological pathways (Daniela *et al.*,2017) and are potentially unable to represent signalling feedback controls, cross-talk with other pathways, as well as tissue-dependent differences. Given that biomarkers are present within a dynamic signalling network, a more comprehensive approach to

elucidate mechanisms are required (Alizadeh *et al*., 2015). Many studies characterizing the genomic, epigenomic, proteomic and transcriptomic profiles of tumours are becoming more prevalent in the literature. Linking different model platforms is therefore critical to ascertain a more comprehensive approach to overcome challenges of tumour heterogeneity (Daniela *et al*.,2017).

1.6   Novel targeted therapies for colorectal cancer

1.6.1   Cancer stem cells

Similarly to the normal colonic epithelium, colorectal tumours are composed of a heterogeneous population of cells which exhibit various levels of differentiation and self-renewal capacities, shown at both histological and molecular levels (Vermeulen *et al.* 2008). The cancer stem cell (CSC) hypothesis maintains that, similar to tissue-specific stem cells that regulate normal tissue homeostasis, a sub-population of clonogenic cancer cells with stem cell-like characteristics are capable of self-renewal and multi-lineage differentiation, enabling tumour propagation and expansion. An increasing body of evidence supports the CSC hypothesis, following observations that only a sub-population of genetically identical cancer cells (termed tumour-initiating cells) have the capacity to form tumours when transplanted into immune deficient mice (O'Brien *et al.* 2007), implying that not all cell types are able to regenerate another tumour bulk. Considerable efforts to experimentally identify CSC populations have gained momentum in the literature.

One of the most prominent candidates as a colorectal cancer stem cell marker is CD133. CD133+ cells were firstly shown to enrich for tumour-initiating cells in comparison to CD133- cells when incorporated into a mouse transplantation assay (O'Brien *et al.* 2007; Lugli *et al.* 2010). Vermeulen *et al* suggested that CSCs are characterised by multiple markers that are co-expressed on cells with the tumour-initiating capacity. Using single cell cloning experiments, they demonstrated that 1/16 CD133+ cells had the capacity to produce a colony, compared to 1/250 CD133-negative cells. An improved colony formation capacity was found when cells

expressed both CD133 and CD24, suggesting a single marker does not necessarily represent a cancer stem cell (Vermeulen *et al.* 2008). Further to this, dissociation of CRC tumour samples from both patient and established xenograft to single cell suspension and analysis by flow cytometry enabled cell sorting determined by specific surface markers. It was shown that successful engraftment was dependent on a population of cells expressing high levels of CD44 and epithelial cell adhesion molecule (EpCAM). Lgr5 and CD24 have since been identified as markers expressed within ISC, which were overexpressed in colorectal cancers (Barker *et al.* 2007b; Vermeulen *et al.* 2008). It is worth noting however that a number of caveats are still raised in the literature when using such experimentation models. Firstly, dissociation and culture of tumour cells in itself may alter cell surface marker expression, and must therefore be interpreted with caution as a representation of the *in vivo* situation (Clevers 2011) . Furthermore, xenotransplantation assays, despite being a current gold standard for cancer stem cell identification, is not necessarily pathophysiologically relevant to tumour growth. Such assays, despite being carried out *in vivo*, are unlikely to wholly represent cells due to an alteration in their environment and potential lack in appropriate growth factors. Results may therefore be an artefact of enhanced selection of a subpopulation of cells and not necessarily a true representation of a CSC population (Visvader and Lindeman 2008).

Taking such caveats into account, and given the lack of the unequivocal identity of the cell-of-origin of cancer within the literature, there has been a drive in recent years to further apply novel techniques to expand current understanding following identification of markers (de Sousa *et al.* 2011). Conditional transgenic techniques in mice have enabled specific deletion in stem cells, such as *APC* deletion within Lgr5+ of CD133+ stem cells in the intestine, which enabled Wnt pathway activation. This in turn enhanced intestinal transformation and tumour propagation, which was not mirrored by the same deletion in progenitor or differentiated cells (Barker *et al.* 2009). Moreover, using fluorescent 'confetti' reporter alleles for lineage tracing in mouse models of tumourigenesis, it has been demonstrated that Lgr5+ cells marked a subpopulation of intestinal adenoma cells capable of propagating adenomas

composed of cells organised in a hierarchy, containing Lgr5+ positive cells as well as different cell types (Snippert *et al.* 2014).

Under the assumption that a population of slowly dividing CSCs maintains tumour growth, from a clinical perspective, successful ablation of a tumour would require the removal of this cell population, as depicted in Figure 1.9. Chemotherapeutic agents that target rapidly dividing cells, in theory, are therefore more likely to induce cytotoxic effects upon bulk tumour cells, enabling slowly dividing CSCs to repopulate the tumour and confer relapse potential. Studies have identified a correlation between recurrent colorectal tumours and a high level of stem cell marker expression (Merlos-Suárez *et al.* 2011). CSC-mediated resistance has also been increasingly evident in the literature, with many studies identifying CSC specific resistance mechanisms such as DNA damage repair and acquisition of drug transporters to efflux a cytotoxic agent from the cell (Visvader and Lindeman 2008).

Targeting CSCs is therefore becoming an attractive target for treatment, however, it presents difficulties: markers that exclusively identify CSCs remain to be ascertained, and their overlap with ISC markers could present as damage to normal tissue (Zeilstra *et al.* 2008). However, the very fact that ISC and CSCs from the same tissue of origin are highly interlinked in terms of molecular signals provides prospective targets for therapy. Pathways that maintain ISC populations, such as the Wnt signalling cascade, are frequently activated in CSCs originating from the same tissue, and Wnt activity has been shown to define colonic CSCs *in vitro* (Vermeulen *et al.* 2010). Hence, alteration of Wnt signalling dynamics is an attractive therapeutic target to eliminate a prospective CSC population in CRC.
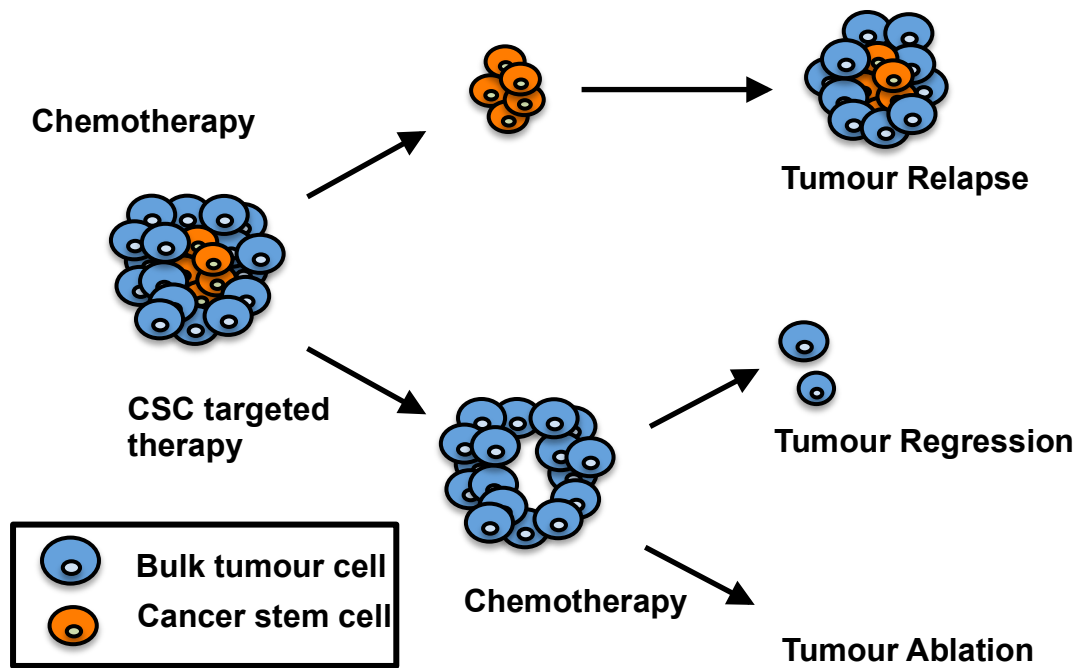
Figure 1.9 The Cancer stem cell hypothesis

Targeting Cancer stem cells (CSCs) is becoming an attractive therapeutic strategy. Cancer stem cells could potentially repopulate a tumour, therefore targeting cancer stem cells could ablate tumour cells.

1.6.2 Targeting the Wnt signalling pathway as a therapeutic strategy for CRC

Aberrant Wnt signalling is strongly associated with both sporadic and hereditary forms of CRC initiation and development. Wnt signalling is best regarded as a whole network as opposed to a strict linear cascade, and due to such complexity, alterations within multiple components of the pathway can modulate Wnt signalling. In a recent study whereby a sample of patient tumours were sequenced, it was found that 93% contained Wnt signalling pathway alterations, with a high frequency harbouring mutations in the genes *APC* and *CTNNB1* (ß-catenin encoding). Despite the subsequent accumulation of multiple mutations that further drive CRC progression, Wnt activation maintenance appears to be a continued requirement for cell survival. Inducible short hairpin RNA (shRNA)- mediated silencing and reactivation of *APC* within transgenic mice was recently shown to reverse intestinal hyperproliferation, even in the presence of *KRAS* and *p53* mutations, suggesting that *APC* loss has a role in tumour maintenance (Dow *et al.* 2015; de Sousa and Vermeulen 2016).

Furthermore, the role of Wnt signalling and maintenance of CSCs in the intestine is becoming more apparent in the literature, with a growing number of studies supporting the notion that CRC cells with stem-like features are characterised by high Wnt activity (de Sousa and Vermeulen 2016). Using a Wnt reporter construct in human CRC cell lines, Vermeulen *et al.* demonstrated that Wnt signalling activity not only marks a hierarchical subset of colon cancer cells with stem-like characteristics, but is a target pathway for further modulation by secreted factors within the microenvironment, suggesting that CSCs retain some levels of plasticity (Vermeulen *et al.* 2010; de Sousa and Vermeulen 2016).

Inhibition of the Wnt signalling pathway has therefore been postulated as a prospective therapeutic strategy. The diversity of the Wnt pathway mutation

spectrum means that aberrant Wnt activation is not necessarily confined to a single mutation, making it difficult to bypass multiple components of the pathway that can compensate for inhibitory effects. Although mutations may be distinct, they ultimately lead to ß-catenin led transcription of key Wnt related genes (de Sousa and Vermeulen 2016) and thus intervention can occur at multiple levels.

Efforts have therefore been made in recent years to target Wnt signalling at the various levels within the pathway; from the Wnt ligand, to downstream proteins that influence Wnt-related gene expression (Novellasdemunt *et al.* 2015). One such class of components that have shown promise as a valid inhibitor of the Wnt signalling cascade are inhibitors of tankyrases 1 (TNKS1) and/or TNKS2 activity, which have been shown modulate the concentration-limiting component of the ß-catenin destruction complex, Axin. The TNKS inhibitor XAV939, originally reported by Huang et al, was shown to inhibit ß-catenin mediated transcription (Huang *et al.* 2009) and has been further shown to promote Axin stability, inhibiting Wnt signalling in a ß-catenin dependent manner in APC-mutant CRC cell lines (Wu *et al.* 2016). Reduced growth is accompanied by reduced stemness and induced differentiation, further highlighting the importance of Wnt signalling in CSCs. Multiple analogues of tankyrase inhibitors have since been reported in the literature; JW55, HW67, JW64, G007-LK and G244-LM and have reported to reduce the growth of *APC* mutant CRC tissue in xenograft models (Waaler *et al.,* 2012; Lau *et al.* 2013).

Given that the Wnt signalling cascade has a critical role in homeostasis of multiple organ systems, not limited to the intestine, side effects may be anticipated. Tankyrase inhibitors administered to mice have also been reported to induce epithelial degeneration and inflammation; however, such side effects were reversible, highlighting the key balance of Wnt signalling activity (Zhong *et al.* 2015). Targeting such a crucial signalling cascade therefore requires the identification of context-specific therapeutic windows that ensure minimal side effects while maximising on-target activity. Furthermore, the transition of such compounds to the clinic, relies on extensive pre-clinical studies within relevant models to investigate the effects.

1.7 Pre-clinical models of CRC for translational research

1.7.1 *In vivo* models: Mouse- and Patient Derived Xenografts

Pre-clinical studies using xenograft models have successfully overcome some limitations presented by cell lines, providing an approach to study tumour development and interactions with surrounding environment *in vivo*. Immuno-deficient mice that are injected subcutaneously with culture-adapted tumour cell lines successfully generate tumours and have been of therapeutic value. However, studies have also demonstrated that xenografts rarely exhibit clinically relevant drug profiles with patients with pathologically equivalent tumour and hence do not correlate with Phase II clinical trial outcomes (Voskoglou-nomikos et al. 2003).

Patient derived tumour xenografts (PDTXs) are generated by the implantation of resected human tumour material into immuno-compromised mice, and have proved to show clinical relevance to primary tumours. A recent study demonstrated the potential of PDTXs as a valid preclinical model of CRC, as patients were treated according to successful drug responses of their xenograft counterparts. A close correlation was found between drug screens on mice and clinical patient outcome, in terms of drug resistance and sensitivity (Hidalgo *et al.* 2011). Furthermore, PDTXs have also shown promise to retain tumour heterogeneity of human colorectal cancer within molecular studies, as well as general histopathological features (Julien *et al.* 2012b). The translational relevance of PDTX models have recently been studied in the context of targeted therapies, whereby a comparison between molecular data gathered from PDTX models and those previously published for patient tumours in the Cancer Genome Atlas Study showed a similar trend in genomic alteration frequencies as well as generating responses to cetuximab (EGFR inhibitor) representative of clinical data from patients which responses observed in KRAS wild type models only (Nunes *et al.* 2015; Bertotti *et al.* 2016).

Despite emerging evidence that PDTXs have the potential to serve as relevant modes that more closely resemble the original tumour in comparison to established cell lines, multiple caveats need to be considered (Siolas and Hannon 2013).

Firstly, on a practical level, establishment of PDTX models can vary from one tumour to the next, with variable rates of engraftment, ranging from a latency period of 2 to 12 months until a tumour is established (Siolas and Hannon 2013), if at all, which could pose a problem in the development of avatar models that are designed to mimic patient responses. Furthermore, the need for rigorous preclinical testing involves a high number of mice usage and associated costs, which in turn limits large scale studies such as multiple drug combinations. Recent attempts have been made towards moving PDTX models towards a high-throughput screening platform. Gao et al (2015) reported the generation of 1000 extensively characterised PDTX models from a range of different cancer types and subsequently showed a relevant clinical translation, performing a 'one animal per model treatment' approach (Gao *et al.* 2015). However, given that the genomic landscape is more representative at a population level as opposed to a personalized medicine setting, this approach has limitations in sufficiently representing individual tumour heterogeneity (Gao *et al.* 2015).

As well as logistical problems, the host mice need to be immunocompromised to circumvent xenograft rejection, resulting in a loss of interaction between tumour and immunological component. Not only does this hamper examining the stromal effects upon a given tumour interactions (Sachs and Clevers 2014), but also excludes assessment of immunotherapeutic agents on a given PDTX model. In terms of high throughput screening, despite the relevance of PDTX to patient tumours, such models are not yet able to replace pre clinical data from *in vitro* studies (Sachs and Clevers 2014). Alternative strategies would therefore need to be explored to relieve experimental burden, such as the use of *in vitro* models to carry out large scale pharmacogenomics screens (Byrne *et al.* 2017).

1.7.2   2D Culture of primary tumour material

The culture of primary material from the large intestine has proved challenging due to the finite lifespan of colonic epithelial cells; cell viability is often compromised as isolated primary cells frequently undergo apoptosis as a result of separation from respective connective tissue and transfer to plastic (Hofmann *et al.* 2007). Studies have shown that growth of primary cells from intact crypts and grown on extracellular-matrix coated dishes is limited to 24 hours in culture (Wilhelm et al. 2012). An approach which has been favoured is the short term culture of tumour sections, such as those described by Centenera et al. 2012, showing the *ex vivo* culture of human primary prostate tissue which can be implemented into short term assessments of drug sensitivities (Centenera *et al.* 2012). However, primary 2D cultures ultimately fail to accurately resemble tissue-specific features such as cell differentiation, gene expression and cell-to-cell contact that result in a limited life span.

Some recent approaches have investigated the isolation of stem-like cells from primary tissues, whereby cultures were propagated from primary tumour material in suspension, and then transferred to an extracellular matrix substitute (Matrigel). Only in the presence of matrigel were the cells able to differentiate (Ashley *et al.* 2014). However, despite positively expressing markers relevant to CRCs, a large proportion of isolated cells were necrotic, containing a number of cystic structures that were unviable after extensive expansion. Continuous cultures within these systems are therefore yet to show suitability towards long-term studies. (Ashley *et al.* 2014).

1.7.3   Generation and culture of cell lines in 2D and 3D

The applications of cell-based assays using 2D immortalised clonal cell lines have been a mainstay of biological investigation of many cancers, including CRC. Immortalised 2D cell lines are traditionally grown in a monolayer of homogeneous cells, whereby mainly proliferating cells stretch to adhere to a flat surface. Overall,

such cultures are relatively easy to propagate and maintain in culture. Furthermore, the array of cancer cell lines available not only constitutes a resource that is useful to both delineate molecular mechanisms involved in tumourigenesis and drug screening, but have also shown partial representation of genetic backgrounds of primary tissue enabling screening on multiple cell types (Mouradov *et al.* 2014). Next generation sequencing methods have enabled extensive genomic, epigenetic and transcriptomic characterisation of a library of cancer cell lines, thus providing a useful resource for biological and therapeutic readouts (Garnett and Mcdermott 2014).

Nonetheless, it has long been recognised that 2D cell lines are unable to faithfully recapitulate specific aspects of cancer biology and therefore not necessarily a fully relevant model system for CRC. Of the 10% of compounds that enter clinical development based on pre-clinical studies in 2D cell lines and subsequent testing in animals, a huge contribution of drugs fail at later phases and this is largely attributed to pre-clinical testing, whereby 2D cell lines do not reflect clinical efficacy (Breslin and O'Driscoll 2013; Edmondson *et al.* 2014). Findings from 2D culture conditions of cell lines therefore have a limited translation to expected outcomes *in vivo*, and could not only generate false positive results that generate little therapeutic benefit for patients (Crockford *et al.* 2013) but also miss potential promising candidates in drug screenings.

The disparity between cell lines in 2D and counterpart tumours a due to a number of factors. Firstly, the monolayer culture of clonal cells fails to represent the tumour environment, such that oxygen and nutrients perfuse equally, which fails to capture cellular reprogramming typically observed within subpopulations of tumour cells to enhance an either hypoxic or aerobic metabolic profile (Hanahan and Weinberg 2011). Morphologically, cells grown in this way are also unable to establish cell-to-cell contacts, and thus critical cell signalling elements of a tumour. A representation of the heterogeneous nature of CRC is also compromised in such cultures. The generation of cell lines from solid tumours rarely generates a high yield of viable cells as they often fail to adapt to the *in vitro* environment, and as a result become mostly

clonal, and potentially lose the ability to differentiate into different cell types (Sachs and Clevers 2014; Hongisto *et al.* 2013). As 2D cell lines only represent a subtype of cells, this would result in some bias and not necessarily a full representation of how the tumour bulk would respond to treatment. A large number of cell lines would therefore be required to capture the genetic diversity of a single tumour.

In order to translate *in vitro* CRC studies towards a more relevant *in vivo* tumour situation, attempts to transition 2D cell lines to a 3D system have been reported in the literature. These include suspended cell aggregates or 3D spheroids embedded within a matrix such as laminin-rich matrigel, to promote relevant cell signalling and tissue architecture. Such structures have demonstrated that distinct spheroid morphologies are cell line dependent. A study by Luca et al demonstrated that culturing an array of 2D CRC cell lines influenced morphology of spheroids, that did not necessarily correlate with migratory or proliferative capacity (Luca *et al.* 2013). Some CRC lines have been shown to form grape-like clusters in culture, whereas others have the capacity to form polarised cells surrounding a central lumen representative of the intestinal *in vivo* architecture. Such structures have the capacity to differentiate into enterocyte, enteroendocrine and goblet cell lineages expressing limited intestinal differentiation markers such as Villin and stem cell markers such as CD44 (Yeung *et al.* 2010). However, given that only a subset of cell lines can form such structures, there are limitations as to how many different tumour types this could indeed resemble.

Interestingly, an overall differential response between drug sensitivities and gene expression of the same lines grown in 2D and 3D have been reported in the literature (Karlsson *et al.* 2012; Luca *et al.* 2013). For both drug discovery, and biomarker driven therapeutic pre-clinical studies, 2D cell lines have classically been utilised to facilitate high throughput drug assays due to their ease of expansion maintenance in culture. The definitive *in vitro* model would ideally combine features from such systems to fully recapitulate patient tumours; to maintain tissue specific structure whilst maintaining relevant cell signalling, have the capacity to retain

several cell lineages as well retaining relevance in large scale studies for preclinical data acquisition.

1.8 Organoid culture as a pre-clinical model system

1.8.1 Development of the organoid model

Attempts to further translate *in vivo* biology to 3D *in vitro* culture from primary material have widely been reported in the literature over a number of decades, following observations that 2D cell lines are a less than ideal surrogate to study tissue-specific systems. The use of floating collagen gels and hanging drop cell culture methods to facilitate 3D structure formation, to name a few examples, have aimed to develop models more representative of the *in vivo* situation, in the form of general 'organoid' systems, with the most recent advances and new definitions within the field discussed here.

An organoid, at simplest, is defined as a structure resembling the organ from which it is derived. More specifically, an organoid is considered as a structure grown in 3D, originating from stem cells, which consist of organ-specific cell types that self-organize and are capable of continuous expansion *in vitro* (Simian and Bissell 2016; Clevers 2016). The earliest attempts at culturing intestinal organoids from primary material were presented by Evans et al (1992) where they described the generation and growth of 3D organoids from rat intestinal tissue (Evans *et al.* 1992). Despite providing a system that was more functionally capable of resembling the intestine compared to immortalised cell lines, the transient nature of the Intestinal stem cells resulted in cultures failing to survive beyond 1 month. The stem-cell containing organoid culture system was defined in a landmark study by Toshiro Sato and Hans Clevers (2009), whereby a robust methodology was revealed to develop organoids that not only recapitulated murine intestinal crypt physiology, but promoted the successful expansion of a stem cell compartment, including Lgr5+ stem cells, propagating their renewal and long term culture (Sato *et al.* 2009). Stem-cell containing organoids differ hugely from their equivalent predecessors cultured from primary material. Firstly, on a cellular level, they are composed of both stem cells,

derived from the tissue of origin that facilitate long term culture, as well as the capacity to differentiate into several epithelial lineages, capable of recapitulating relevant cell signalling (Yin *et al.* 2013). Structurally, stem-cell containing organoids contain cells in an organ-specific architecture, encompassing physiological characteristics, such as intestinal organoids that contain crypt-like structures surrounding a central 'lumen'with appropriate cell polarity. Such spatial organisation of cell surface receptors engaged in interactions with surrounding cells in turn influence signal transduction from neighbouring cells, influencing overall cell behaviour (Edmondson *et al.* 2014).

The sustainable growth of such structures without a stroma were established in the form of a 3D matrigel-based laminin-rich model to support growth of intestinal crypts or FAC-sorted Lgr5+ intestinal epithelium stem cells, and intricate growth conditions to mimic the environment of the intestinal epithelium (Sato *et al.* 2009). The manipulation of highly conserved signalling pathways, implicated in regulating the hierarchy of intestinal cell renewal in the intestine, by addition of relevant growth factor supplements within culture media was found to be critical to support organoid propagation and proliferation. The control of the Wnt signalling, a key component in the maintenance of crypt proliferation and maintenance of the intestinal stem cell niche (Pinto *et al.* 2003; Kuhnert *et al.* 2004) was found to be pivotal in maintaining intestinal organoid self-renewal (Sato *et al.* 2009; Ootani *et al.* 2009). The addition of R-spondin within growth media further potentiated the activation of the Wnt signalling pathway within cells, recapitulating conditions found within the intestinal stem cell niche. Wnt signalling activation was further found to be critical for organoid generation and proliferation in a concentration-dependent manner (de Lau et al. 2011; Sato et al. 2009). The inhibition of transforming growth factor- β (TGF-β) and BMP signalling, previously implicated in expansion of crypt numbers (Haramis *et al.* 2004), by exogenous addition of Noggin in media, as well as the inclusion of epidermal growth factor (EGF) for proliferation enhancement were also found to be minimum additional components required to sustain long-term culture of crypts (Sato *et al.* 2009).Further studies have demonstrated that addition of components that manipulate Notch signalling can specifically induce the

differentiation of intestinal stem cells into several different epithelial cell lineages, including enterocytes and goblet cells. Subsequent studies have identified small molecules to manipulate the differentiation capacity and lineages of intestinal cells within organoids, further emphasising the importance of the organoid environment for sustained growth (Yin *et al.* 2013).

These conditions were further adapted to culture material from the human colon, as well as colorectal adenoma and adenocarcinoma tissue from patient biopsies (Sato *et al.* 2011a). These CRC organoids were shown to grow as complex irregular structures, and consisted of endocrine, goblet cells and highly proliferative cell types (Sato *et al.* 2011a). More recent studies have demonstrated an improved genotypic resemblance and stability within organoids which are thought to further contribute to represent patient populations (Fujii *et al.* 2016a).

Organoids are a promising model to further study aspects of both normal and tumour biology compared to previous *in vitro* systems, and have thus far demonstrated a number of applications from different tissues such as liver, pancreas, prostate under defined culture conditions for each tissue. An advantage of organoids is the ability to produce organoids derived from patient material, either from resected surgical tumours, or from induced pluripotent stem cells (iPSCs) (Watson *et al.* 2014). Overall, the utilities of such a culture system are extensive; from assessing individual cell populations and interactions implicated within tumour development, to their capacity to be utilised for large-scale drug screens.

1.8.2 Translational relevance of organoids for CRC therapy; analysis of 2D lines versus 3D models

Despite the advances of large scale i*n vitro* assays as a tool to assess efficacies of new compounds in drug discovery, as well as establishing therapeutic effects of biomarker-driven therapies in patients, biologically relevant results require a platform that will reflect cell responses *in vivo* (Edmondson *et al.* 2014). The advantages of 3D organoid culture in terms of representative tumour heterogeneity,

spatial cell organisation, and retention of a complement of stem and differentiated cell types to facilitate long term culture, hold promise to bridge the gap between current *in vitro* studies and *in vivo* data for oncological drug screens, as shown in Figure 1.10. However, given the numerous aspects of cell biology that advanced 3D organoid cultures can retain in comparison to preceding 2D systems, there is a requirement for suitable techniques that are capable of analysis and quantification of relevant features within complex structures. A number of novel methodologies, some of which have been adapted from utility in 2D cell lines, have become more apparent in the literature to facilitate the transition of organoids to a more high throughput platform (Li *et al.* 2015; Di, Klop, Rogkoti, Devedec, Water van de, *et al.* 2014; Edmondson *et al.* 2014).

 The use of metabolic assays as a quantifiable readout of drug-induced effects in the form of fluorescent or luminescent based measurements have been well established for 2D systems, and have been somewhat adapted further for utility in 3D cultures. Quantifiable assays such as 3-(4,5-dimethylthiazol-2-yl)-2,5-diphenyltetrazolium bromide (MTT) staining, whereby MTT is converted to a measurable form in the presence of viable cells and subsequently quantified by absorbance measurements, have been utilised in mouse organoids to assess drug-induced toxicity (Grabinger *et al.* 2014). However, as measurements of MTT absorbance relies on lysis of cells in DMSO to solubilize formazan crystals, an additional step to solubilise matrigel was required to facilitate measurements. Whilst this demonstrated a successful application of MTT in this format, such adjustments are not necessarily compatible for high throughput measurements (Young and Reed 2016).

Commercially available end point assays have also been utilised to test drug responses within 3D systems, such as the luciferase based Cell-Titer Glo assay (Promega), an end-point assay that quantifies relative ATP levels within samples. In a recent study, this assay was utilised to assess the effects of a titration of a panel of 83 compounds upon a biobank of patient-derived organoids (Wetering *et al.*, 2015). Whilst responses were relatively reproducible, assay noise was observed in some individual experiments, most likely as a result of variability in organoid numbers and

sizes between and across assays. Quantifiable detection of compounds with subtler effects, other than cytotoxicity, was also found to be more challenging in terms of generating reproducible readouts. Such studies also highlight the need for standardised protocols for the effective scale-up of organoids), enabling them to be generated from little resected patient material to facilitate a rapid transition to reproducible, robust and more high throughput assay formats. Furthermore, there is a need to determine the relevance of organoids to reflect patient responses.

The structural organisation and cellular composition of organoids, whilst improving biological relevance compared to 2D cell lines, introduces many challenges for their use in image analysis methods to facilitate robust and sensitive detection measurements(Edmondson *et al.* 2014). Assessing changes in cellular morphology using light microscopy, facilitates basic morphometric measurements such as overall number of structures and diameters, at multiple points in culture, is frequently limited to one plane of view, restricting quantifiable parameters (Grabinger *et al.* 2014). In recent years, a paradigm shift in 3D tumour models has pushed technologies towards more sophisticated phenotypic screening methods compatible with high throughput technology (Li *et al.* 2016; Sandercock *et al.* 2015), incorporating appropriate immunofluorescent staining protocols for confocal imaging, as well as analysis software capable of measuring numerous morphometric parameters of 3D structures, to further capture subtle effects of drug-induced phenotypes (Sandercock *et al.* 2015; Di *et al.* 2014).

The structural and biological complexity of 3D organoids compared to preceding *in vitro* models therefore introduces many challenges for their use in large-scale screens, where reproducible, robust and sensitive detection methods are critical. Before organoids can therefore be established as a sufficient model system, there is a need to explore their relevance to current clinical applications as well as novel drug discovery.
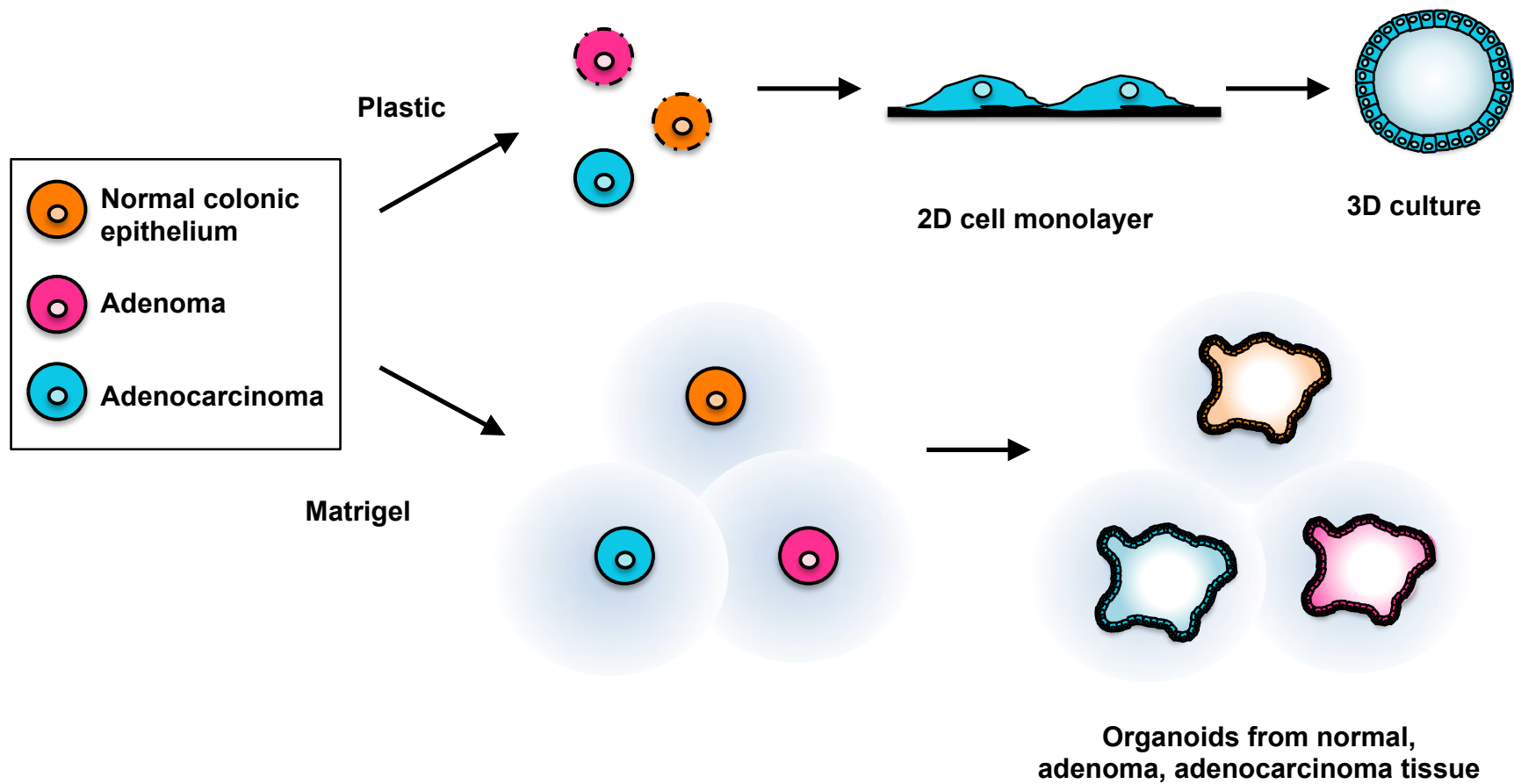
Figure 1.10 2D versus 3D culture from normal, adenoma and adenocarcinoma cells.

For 2D cell line culture, cells often undergo many changes to adapt to proliferating on plastic. Growing cells in the 3D environment that is more physiologically relevant enables long term culture of normal, adenoma and adenocarcinoma cells from the intestine. *Image adapted from Sachs and Clevers (2014).*

1.9   Project aims and objectives

The understanding of complex mutational landscapes that confer drug sensitivity is fundamental to identify suitable therapeutic agents for CRC patients. However, the identification of biomarker-driven therapeutics based upon genomic analyses of a tumour does not necessarily correlate with an inhibitory effect upon tumour growth, and thus lacks predictive power in the clinic. An understanding of the functionality of genomic alterations and their influence upon treatment responses remains limited due to a lack of preclinical models that can fully recapitulate tumour responses to therapy. The need for such a model system is therefore imperative to understand mechanistic effects of biomarker-driven treatments in patients, as well as to indicate potential novel targets for the treatment of CRC. Consequently, the overarching aim of this thesis is to assess whether patient derived CRC organoids are suitable models, capable of generating functional readouts for precision oncology as well as the drug discovery pipeline. To address this, the results chapters presented herein are comprised of three distinct aims.

The first aim of this thesis, discussed in Chapter 3, was to develop and optimise suitable methodologies to facilitate the expansion of novel CRC patient-derived organoids, representative of clinically relevant tumour subtypes, towards a functional, robust and reproducible assay system that could be exploited for subsequent studies.

This thesis also aimed to evaluate the efficacy of organoids as a functional readout for biomarker-driven therapies in the context of a clinical trial for CRC, to explore their potential as matched models of patient responses to therapy. To address this, organoids were used within a purely *"in vitro* clinical trial"* setting, whereby drug sensitivity profiles of a cohort of organoids were generated to mirror compounds administered to patients within the stratified arms of the FOCUS 4 clinical trial.

The final key objective of this thesis was to ascertain the role of organoids as a suitable pre-clinical model system within the drug discovery pipeline. To facilitate this, novel Wnt signalling inhibitors (Merck Serono) were utilised to evaluate treatment-specific responses of organoids and potential effects on prospective CSC populations, enhancing the premise of organoids as tools to study effects of therapeutic agents that target complex signalling networks.

2 Materials and Methods

2.1 Processing of Primary material

2.1.1 Human Tissue

All samples from our full patient cohort were provided by the Wales Cancer Bank (WCB, University Hospital of Wales) with informed consent. All patient derived material was treated in concordance with the Human Tissue Act (HTA), and any patient derived samples provided remain anonymous. All samples provided from patient material were assigned a number ('isolation x') for our internal records, and could be traced to an I.D number from the WCB. Any waste material generated as part of the isolation process was disposed of in compliance with the HTA.

2.1.2 Processing of human material

Following surgical resection, a sample each of tumour and surrounding healthy tissue of approximately 30mm -150mm in diameter of the colonic epithelium were obtained and stored at 4°C in Hibernate A (Invitrogen) prior to processing. Samples were stored for minimal time, typically between 1 and 12 hours, and only isolated if stored within optimal conditions (i.e stored in Hibernate A medium). Isolation of both normal crypts, and tumour cell fragments were performed in parallel. In some cases within our subset, a 'methylene blue' stain was applied to our samples prior to histopathological inspection.

2.1.2.1 Dissection of intestinal epithelium

Human tissue was processed as described by Sato *et al* (2011). Briefly, carcinoma samples were placed within storage media within a petri dish and dissected to remove connective tissue, then further dissected into pieces approximately 2mm in diameter.

2.1.2.2 Enzymatic digestion and chelation

Following dissection, tumour tissue was placed in respective 50ml falcon tubes and subjected to multiple washes in Phosphate Buffered Saline (PBS, Invitrogen) at room temperature until their surrounding suspension solution was clear. Following washes, pieces of carcinoma epithelium were incubated in enzyme digestion buffer (DMEM containing 2.5% Foetal Bovine Serum (FBS), 1% Penicillin/Streptomycin ,125µg/ml Dispase (all Invitrogen),1mg/ml Collagenase from *Clostridium histolyticum* (Sigma))at 37°C for 30 minutes. After incubation, enzyme digestion buffer was removed, and tissue was triturated in PBS at room temperature to remove fragments of cells. Supernatants generated in processing both normal and carcinoma tissue were collected into 50ml Falcon tubes coated with FBS. The process was repeated approximately three times to isolate all cell fragments from tissue.

2.1.2.3 Isolation of tumour cells

Following trituration and isolation of cells, supernatants collected intestinal were centrifuged at 4°C for 5 minutes at 800 RPM. After removal of supernatants, the pellets were resuspended in basal '3+' media (Advanced DMEM F12 (Invitrogen) with 1% GlutaMAX (Invitrogen), 1% HEPES buffer solution (Invitrogen) and 1% Penicillin/ Streptomycin) and then filtered (70 µm) to separate cell clusters. Isolated carcinoma fragments from colonic epithelium were then counted and resuspended in desired volume of growth factor reduced Matrigel (BD Biosciences) to contain approximately 1000 fragments per 50µl of Matrigel. 50µl droplets of Matrigel was then seeded onto pre-incubated 24 well plates (Nunc) and then incubated at 37°C to allow full polymerisation

2.2 Tumour organoid culture

2.2.1 Generation of 3D organoids

Culture conditions previously reported by Sato et al., (2011)were applied to cell fragments in polymerized matrigel. A previous study by Sato et al. (2009) reportedly screened multiple growth factors and hormones to determine the essential requirements of efficient plating of murine-derived organoids, then furthermore for

human colonic organoids. Organoids required various growth factors to enhance proliferation. In addition to 3+ basal media, B27 (1X ,Invitrogen) , N2 (1X, Invitrogen), N-acetylcysteine (1mM, Sigma) were added. Advanced Wnt3a condition media (40%) secreted from LWnt3a cells was found to be a necessary requirement to maintain proliferation, in addition to conditioned R-spondin (10%). A panel of growth factors including Epidermal Growth Factor (50ng/ml,Peprotech), Noggin (100ng/ml, Peprotech) were found to be essential for maintenance of culture. Nicotinamide (10mM, Sigma) was also used to maintain expansion in culture. 2 small molecule modulators of mitogen-activated protein kinases , A83-01 (0.5µM, Tocris) and SB202190 (10µM, Sigma) improved expansion of crypts. This 'Full' media was added to organoids derived from healthy colonic epithelium.

For the propagation of carcinoma organoids, it was found that organoids had an enhanced survival rate when culture in two different media types (Table 2.1);

(i)   7+ Media: 3+ media with B27 (1X ,Invitrogen) , N2 (1X, Invitrogen), N-acetylcysteine (1mM, Sigma) and Fungizone were added

(ii)   'Full' Media, as described as above

The Rho-associated protein kinase (ROCK) inhibitor Y-27632 (10 µM, R&D) was included in both Full and 7+ plus media conditions for the first 5 days in culture, and for the first 3 days after organoid passage.

Table 2.1 Table denoting components required for 7+ and Full media conditions.

Asterisk (*) denotes components that are withdrawn from media; fungizone was applied on organoids between 0-6 weeks following culture to limit infections. Y-27632 ROCK inhibitor was applied for first 5 days following isolation. Underlined components are requirements for 3+ basal media. Further details are included in the Appendix.

Component	Target/ purpose	3+ Media	7+ Media	Full Media
ADV-DMEM/F12		1X	1X	1X
Penicillin/Streptocymcin		100 U/ml	100 U/ml	100 U/ml
HEPES (1M)		10mM	10mM	10mM
GlutaMAX (100X)		2mM	2mM	2mM
N2 (100X)			1X	1X
B27 (50X)			1X	1X
N-acetylcysteine	Anti-oxidant		1mM	1mM
Epidermal Growth Factor (EGF)	Epidermal Growth Factor Receptor			50ng/ml
Mouse recombinant Noggin	TGF-ß modulator			100ng/ml
A-83-01	Alk4/5/7 inhibitor			500µM
SB202190	P38/MAP kinase inhibitor			10µM
Wnt3A conditioned medium	Wnt signalling activator			40% (v/v)
R-spondin conditioned medium	Wnt signalling enhancing			10% (v/v)
Fungizone*	Anti-fungal agent		2µl/ml	2µl/ml
Y-27632*	ROCK inhibitor		10µM	10µM

2.2.2 Routine organoid culture maintenance

2.2.2.1 Organoid passage

Organoids were passaged as whole colonies, at a split ratio between 1:2-1:8 approximately every two weeks, or as required. Culture medium was removed from wells and replaced with fresh basal medium. Organoids embedded within matrigel were lifted from wells in media and centrifuged at 40g for approximately 5 minutes. Organoids were triturated (physically sheared) using a P200 pipette tip, and washed in fresh media to remove residual matrigel. Fragments of triturated organoids were then resuspended in fresh matrigel as previously described.

2.2.2.2 Freeze-down of organoids

Frozen stocks of organoids were generated within early passages (p4-p10), depending on abundance of material. Organoids were passaged as previously described (2.2.2.1) and cultured for 3-4 days. Media was then lifted from each well in media and transferred to 1ml eppendorfs and centrifuged at 40g for 5 minutes. Organoids within matrigel were then resuspended in Cell Recovery Solution (life technologies) and transferred to cryovials (Nunc) at a final volume of 500 µl. 2-4 wells of a 24 well plate typically provided sufficient organoid numbers for a single cryovial. Cryovials were then placed in a freezing container at room temperature prior to storage within a -80°C freezer. For recovery, cryovials were quickly warmed in a water bath at 37°C and once thawed were resuspended in basal media, washed twice, and finally resuspended in matrigel and plated as described previously (2.2.2). Organoids used in this study showed successful recovery from frozen after 18 months of storage. Banks of frozen organoids facilitated experiments that could be carried out within approximately 10 passages of another.

2.3 General Organoid analysis techniques

2.3.1 Immunohistochemistry (IHC) techniques

Organoids embedded within matrigel were fixed in 10% formalin (Sigma) overnight at 4°C. Organoids were fixed after 5-14 days post isolation/passage. After overnight

fixation, organoids were washed with Phosphate Buffered Saline (PBS, Invitrogen) and stored in PBS until processing. For processing, pre-chilled PBS was added to wells to dissociate matrigel from wells. All material was then transferred into eppendorf tubes and gently washed in PBS to remove matrigel fragments from organoids. Organoids were then centrifuged at 1000X RPM for 1 minute. The remaining suspension was removed and replaced with 4% (w/v) low melting point agarose (Sigma). Fixed organoids were resuspended in low melting point agarose and set at room temperature. Agarose disks embedded with organoids were stored in 70% EtOH prior to sectioning. Organoid sections were then mounted onto slides prior to Hematoxylin & Eosin (H&E) staining.

2.3.2   Whole-mount Immunocytochemistry

This protocol was adapted from Lee at al (2007). Briefly, organoids were seeded within Matrigel in black, optical- bottomed, 96 well Nunc™MicroWell™ plates. 9μl of organoids embedded within matrigel was dispensed per well and incubated with Basal 7+ media containing 10μM ROCK inhibitor. Plates were then incubated for defined durations prior to fixation by 4% formalin at room temperature for 30 minutes. Wells were then washed with PBS containing 100mM glycine three times for 10 minutes at room temperature. Following washes, an overnight blocking step was performed by adding 10% horse serum in Immunofluorescence (IF) buffer (PBS containing 0.1% Bovine Serum albumin, 0.2% Triton X-100, 0.05% Tween 20) to chosen wells. Primary antibodies (Table 2.2)diluted in IF buffer were then applied overnight at 4°C prior to another overnight incubation in IF buffer. Secondary antibodies diluted in IF buffer (Table 2.3) were then exposed to wells overnight, prior to washes and an overnight incubation in IF buffer. Secondary antibodies used were Rabbit IgG AlexaFluor® 568 (Life Technologies) and Mouse AlexaFluor® 488 (Life Technologies), both at a dilution of 1:500. Hoechst was implemented as a counterstain and washed with PBS prior to imaging.

Table 2.2 Outline of primary antibodies used for Immunofluorescence (IF)

Primary Antibody	Marker type	Source	Catalogue Number	Dilution	IgG
Ki67	Proliferation	Millipore	AB9260	1/100	Rabbit
Caspase 3	Apoptosis	R&D	AF385	1/100	Rabbit
Beta-catenin	Wnt signaling	BD	610154	1/250	Mouse
Cyclin B1	Proliferation	Santa Cruz	SC-752	1/50	Rabbit
Lgr5	Intestinal stem cell	BD	562733	1/250	Rat
Cytokeratin 20	Differentiation	Abcam	AB76126	1/100	Rabbit

Table 2.3 Outline of secondary antibodies used for Immunofluorescence (IF)

Secondary antibody	Source	Catalogue Number	Dilution
Alexa Fluor 488 Phalloidin	Thermo Fisher	A12379	1:100
AlexaFluor® 488 Goat anti mouse	Life Technologies	A11029	1:500
AlexaFluor® 568 Goat anti rabbit	Life Technologies	A11011	1:500

2.3.3 Confocal Imaging and quantitative analysis

Images were acquired within 96 optical (clear bottomed) black plates using a Confocal Microscope, Leica TCS SP2 AOBS. A 20X objective was used to capture images, and were then subsequently processed using FIJI software, and IMARIS8 cell counting software, where appropriate. To quantitate proliferation levels in normal and treated conditions, the number of Ki67-positive stained cells per organoid was divided by the total number of cells within the corresponding organoid, to obtain a percentage value of cells undergoing active proliferation.

2.3.4 Lightsheet Microscopy

Organoids were seeded in usual culture conditions, either from triturated pieces or as single cells as specified previously. Following recovery and growth for a period of five days, organoids were fixed within matrigel by addition of a '5X Fix & Stain' solution (courtesy of OcellO) which facilitates a one-step stain of Phalloidin and Hoechst simultaneously. Fixation and staining took place overnight at room temperature, whilst organoids within the well were placed on a rocker. Following overnight incubation, structures within matrigel were lifted from wells and washed twice with PBS. For mounting, 10 µL of organoid suspension was added to approximately 10µL of low melting point agarose and placed in a glass capillary provided by Zeiss. Fluorescent images were taken on a Lightsheet Z.1 (Zeiss) microscope and images rendered within the Zeiss software package to generate maximum projection images.

2.3.5 Organoid genotyping

2.3.5.1 DNA extraction

Organoids in culture between 5 and 7 days were extracted for DNA, taken between passages 5 – 12. DNA was extracted from organoids using the Qiagen DNeasy blood and tissue kit as per the manufacturer's guidelines.

2.3.5.2 Next Generation Sequencing

Analysis of organoid genotypes was performed using the Next Generation Sequencing (NGS) SureSeq Solid Tumour 60-gene panel by Oxford Gene Technologies (OGT). Sequencing was performed on the Illumina MiSeq platform using TruSeq b3 chemistry in order to generate 2 X 150 base reads. Analysis was further carried out by Dr Kenneth Ewan (Dale Lab) to identify significant mutations per sample.

2.3.6   Measurements of organoid growth parameters

2.3.6.1   Assessing organoid growth

In order to assess organoid growth, organoid cultures plated in 24 well plates were imaged at different time points using GelCount™ scanner (Oxford Optronix). Images were then subject to data analysis using defined CHARM settings which recognised organoid structures within a well and provided various measurements (including organoid number, diameter average per well, organoid area). CHARM settings (Table 2.4) were established for an individual organoid line, dependent on their morphological features in culture (Figure 2.1). Data was acquired on a well-by-well basis and further analysed using Microsoft Excel and/or GraphPad Prism. In general, a minimum of three wells was used for analysis per biological repeat, unless otherwise stated. Where possible, data was collected from more than one biological repeat.

Table 2.4 Charm Settings for GelCount software

	Charm settings					
	Established cultures	Cultures from single cell suspensions				
	All isolations	Iso 50, Iso 72	Iso 48, Iso 49	Iso 34	Iso 75, Iso 78, Iso 73	All isolations/ general setting
Edge detection sensitivity	75.4	32.9	32.9	32.9	59.7	48.5
Center detection sensitivity	64.2	43.5	50.8	50.8	97.2	71.5
Soft colony lower diameter (µm)	40	60	35	55	25	30
Soft colony upper diameter (µm)	1000	600	600	600	70	600
Minimum center to center seperation	40	60	35	55	25	30
Smoothing	3	3	3	3	3	3
Circularity factor	62	80	62	62	52	82
Edge distance threshold	0.88	0.74	0.74	0.74	0.74	0.81
Number of spokes	32	32	32	32	32	32
Filter size	3	3	4	4	3	3
Shape processing	best fit circle	best fit circle	best fit circle	best fit circle	best fit circle	best fit circle
Colony diameter minimum (µm)	40um	70	55	55	10	30
Colony diameter maximum (µm)	1000um	375	375	375	70	375
Colony minimum intensity (optical density)	0.1	0.05	0.05	0.05	0.01	0.01
Colony maximum intensity (optical density)	0.32	10	10	10	10	10
Good edge factor	0.57	0.06	0.06	0.06	0.06	0.06
Borders from centeroids	yes	yes	yes	yes	yes	yes
Merge overlapping objects	yes	yes	yes	yes	yes	yes
Overlap threshold	0.67	0.75	0.75	0.75	0.75	0.75
overlap calculation	area	area	area	area	area	area
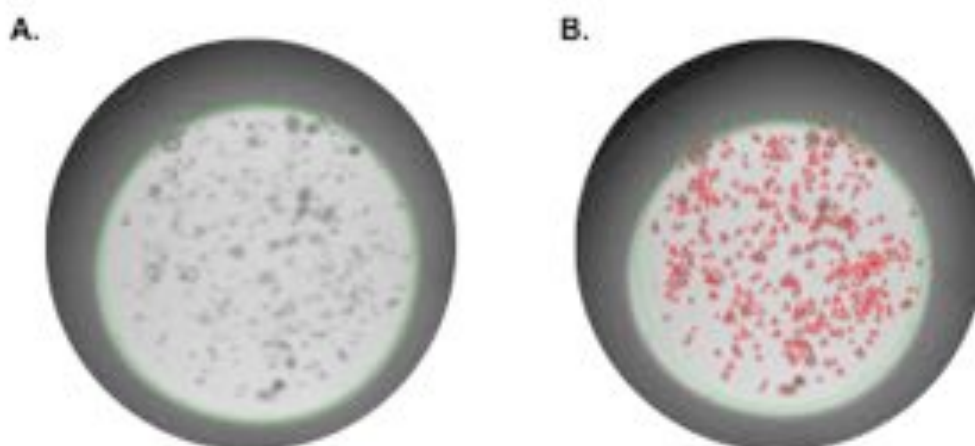
Figure 2.1Representative masks for individual organoids using GelCount Charm settings

A. Representative well of a 24 well plate containing organoids **B.** Mask settings applied to identify structures and generate basic morphometric readout.

2.3.6.2 Mitochondrial activity 'PrestoBlue' assay

Organoids were culture in clear, round bottomed 96 well plates at varying seeding densities. 10µl of Presto Blue reagent (Invitrogen) was added per 100µl of organoid growth media. 100µl of media and 10µl Presto Blue Reagent was also added to three wells of a 96 well plate to serve as a negative control. Following a three hour incubation at 37°C, 50µl was transferred from each well into a black, clear bottomed 96 well plate (Matrix). Fluorescent signal was read in a BMG Fluostar platereader with an excitation/emission spectra of 560nm/610nm. Relative fluorescence of samples was calculated by subtracting 'blank' value i.e negative controls from samples to compensate for background signal.

2.4 Quantitative Reverse Transcription Polymerase Chain Reaction (q-RTPCR)

qRT-PCR was used to quantify relative expression levels of genes within tumour organoids. For qRT-PCR experiments, organoids were plated to single cells as previously described (2.5.1) using a minimum of 8 wells of a 24 well plate per condition.

2.4.1 RNA extraction

RNA extraction was performed using a trizol (Life Technologies) based method, whereby organoids within matrigel were resuspended in trizol containing 125µg/ml glycogen (Life Technologies). The suspension was then transferred into 1ml microtubes prior to the addition of 160µl chloroform per 800µl trizol/glycogen mix. Samples were then vortexed and centrifuged for 15 minutes at 12000 g, at 4°C. The aqueous layer formed was collected from each sample and pipetted into fresh microtubes prior to the addition of an equal volume of isopropanol. Samples were centrifuged again for 10 minutes, and the supernatant discarded. The remaining pellets were washed three times with 70% EtOH, centrifuging at 500g for 5 minutes between each wash. The remaining pellets were left to air dry for 5 minutes and then resuspended in components of a TURBO DNA-free kit to remove any residual DNA. Samples were then incubated at 37°C for 30 minutes. Extracted RNA from each sample was quantified using the NanoDrop machine.

2.4.2 Reverse Transcription reaction

cDNA was synthesised from the RNA template of each sample using the Improm II Kit (Promega). The components required for the reverse transcription reaction mastermix are listed in Table 2.5. A mastermix containing no reverse transcriptase enzyme was also generated as an additional control for each sample. The mixtures were then incubated in a thermocycler at 70°C for a total of 5 minutes. Samples were then diluted in nuclease free water and stored at -20°C, or remained on ice prior to gene expression analysis.

2.4.3 Gene expression analysis

q-RTPCR was performed using the SensiFAST SYBR green Hi-ROX kit (Bioline) and was carried out in MicroAmp Fast optical 96 well reaction plates (Life Technologies). Primers were designed (Sigma) and listed below (Table 2.6). For qrt-pcr reactions, 10µl of 2X SensiFAST™SYBR® No-ROX , 3µl cDNA and 0.1µl of individual forward and reverse primers (10mM) and 6.8µl of Nuclease free water were added to each well. All samples were measured in triplicate, with gene expression normalized to a housekeeping gene, GAPDH. Plates were then sealed and reactions were measured on a Step One Plus real-time PCR instrument (Applied Biosystems). A fluorescent readout from the incorporation of SYBR product into the PCR product was used to determine the relative abundance of mRNA within each sample. The cycle times used were as follows:

1. 95°C for 2 minutes
2. 95°C for 5 seconds
3. 60°C for 10 seconds
4. 72°C for 20 seconds

Cycles 2-4 were repeated approximately 40 times.

Table 2.5 Mastermix for reverse transcription

	RT reaction (µl)	No RT control (µl)
Reverse Transcription Mix	1x	1x
Nuclease-Free Water (to a final volume of 15µl)	6.1	7.1
ImProm-II™ 5X Reaction Buffer	4	4
MgCl2 (6 uM final from 25 uM stock)	2.4	2.4
dNTP Mix (final concentration 0.5mM each dNTP)	1	1
Recombinant RNasin®Ribonuclease Inhibitor (optional)	0.5	0.5
ImProm-II™ Reverse Transcriptase	1	0

Table 2.6 Primers used for qRT-PCR by SYBR green.

Gene	Forward sequence	Reverse sequence
AXIN1	CTGGATACCTGCCGACCTTA	CCGGCATTGACATAATAGGG
AXIN2	GCGATCCTGTTAATCCTTATCAC	AATTCCATCTACACTGCTGTC
TNKS1	CCGCGTGTCTGTTGTAGAGT	ACAGAAGCCCCATGCCTTAC
TNKS2	TGGTGTGGGAGCCAAGTCTA	GTGGCAATTCACTCCTCTTCA
LGR5	GAGTTACGTCTTGCGGGAAAC	TGGGTACGTGTCTTAGCTGATTA
ASCL2	TGACCTGGGGGCGTAATAAAG	ACACAGGCTTCTCCCTAGCA
KRT20	ACGCCAGAACAACGAATACC	ACGACCTTGCCATCCACTAC
DKK1	CCCAGGCTCTGCAGTCAGCG	CGCACGGGTACGGCTGGTAG
GAPDH	TGAAGGTCGGAGTCAACGGA	CCATTGATGACAAGCTTCCCG

1.1.1 ΔΔCT method

Quantification of relative gene expression was calculated using the ΔΔCT method. Within each assay, the cycle threshold value (CT value) was determined by the number of thermocycles carried out by each well to reach a pre-assigned fluorescent threshold. CT values for each triplicate sample were then normalized to the housekeeping gene (GAPDH) to generate a ΔCT value. The ΔCT of the control cohort was then subtracted from the ΔCT of the test cohort to determine relative fold changes in gene expression. Triplicate wells from each reaction were then averaged

to generate a ΔΔCT value. To eliminate the possibility of primer contamination, melt curves were performed on samples following their end cycle times.

2.5   Endpoint Viability measurements for drug assays

2.5.1   Passaging to single cell

For single-cell passage, growth medium was removed from organoids in culture. Organoids were washed with PBS and incubated for approximately 5 minutes with TrypLE Express, a form of trypsin (Invitrogen). Following incubation, matrigel was suspended in TrypLE Express and placed in an eppendorf tube. If large fragments remained within tubes, Basal media was added with 10% FBS to inhibit Trypsin activity. The suspension was then filtered through a 40 µm filter and washed several times with 3+ media. The number of cells within the suspension were counted by staining cells using an Acridine Orange/Propidium Iodide Stain , and subsequently counting on an automated LUNA-FL™ fluorescence cell counter. Cells were then resuspended in Matrigel at a desired concentration /µl of matrigel. 9µl of Matrigel was then seeded in white, clear-bottomed 96 well plates (Matrix) and incubated at 37°C. Following incubation, 50µl of growth medium was then added to each well.

2.5.2   Addition of Drug Treatments

All compounds were prepared according to manufacturers' instructions (Table 2.7), typically dissolved in 100% DMSO (Sigma). A range of stock solutions at different concentrations were prepared, serially diluted in DMSO to make 100X stock solutions (1% DMSO). The intermediate stocks were then diluted ten-fold so that final concentrations of DMSO were 0.1% in 50µl growth media for any given sample. All experiments were performed in triplicate for each concentration.

Table 2.7 Table of compounds and concentrations used in organoid drug assays

Focus 4 ARM	Compound identifier	Name	Mechanism	Diluted in	Source	Dilution range (nM)		Fold change in dilution
						minimum	maximum	
BRAF mutation	GSK12118473	Dabrafenib	BRAF inhibitor	DMSO	Stratech Ltd	0.12	500	2
		Panitumumab	EGFR inhibitor	PBS	clinic	0.02	62.5	2
	GSK1120212	Trametinib	MEK inhibitor	DMSO	Stratech Ltd	0.06	250	2
PIK3CA mutation		Salicylic acid	unclear	DMSO	Sigma	19	5000	2
KRAS/p53 mutation	AZD1775	MK1775	Wee1 inhibitor	DMSO	Stratech Ltd	19	5000	2
WT with PTEN function	AZD8931	Sapitinib	HER 1,2,3 inhibitor	DMSO	Stratech Ltd	8	1250	2
ATM deficient	AZD6738	AZ20	ATR inhibitor	DMSO	R&D	19	5000	2
Non stratified		5FU	thymidylate synthase inhibitor	DMSO	Tocris	19	10000	2
	MSC2501490A		TNKS inhibitor	DMSO	Merck Serono	4	1250	2
	MSC2572070A		TNKS inhibitor	DMSO	Merck Serono	0.80	250	2
	MSC2524070A		TNKS inhibitor	DMSO	Merck Serono	0.39	100	2

Table 2.8 Concentrations of compounds used in single inhibitor, double inhibitor, and triple inhibitor combination assays

Single agent (nM)			Double agents (nM)			Triple agents (nM)
Dabrafenib	Trametinib	Panitumumab	Dabrafenib + Trametinib (2:1)	Trametinib + Panitumumab (4:1)	Panitumumab + Dabrafenib (1:8)	Dabrafenib, Trametinib + Panitumumab (8:4:1)
500.00	250.00	62.50	750.00	312.50	562.50	812.50
250.00	125.00	31.25	375.00	156.25	281.25	406.25
125.00	62.50	15.63	187.50	78.13	140.63	203.13
62.50	31.25	7.81	93.75	39.06	70.31	101.56
31.25	15.63	3.91	46.88	19.53	35.16	50.78
15.63	7.81	1.95	23.44	9.77	17.58	25.39
7.81	3.91	0.98	11.72	4.88	8.79	12.70
3.91	1.95	0.49	5.86	2.44	4.39	6.35
1.95	0.98	0.24	2.93	1.22	2.20	3.17
0.98	0.49	0.12	1.46	0.61	1.10	1.59
0.49	0.24	0.06	0.73	0.31	0.55	0.79
0.24	0.12	0.03	0.37	0.15	0.27	0.40
0.12	0.06	0.02	0.18	0.08	0.14	0.20

2.5.3 Endpoint Cell Titer Glo 3D ATP Measurements

For assay endpoint readout, 50µl of Cell Titre Glo 3D reagent was added per 50µl of growth media to each well of a 96 well plate. 50µl of media and reagent were also added to three wells of a 96 well plate to serve as a control (Blank values). Following an agitation step on a Rickman shaker for five minutes to initiate cell lysis for ATP extraction, the plate was incubated on the shaker for up to one hour at room temperature. Relative Luminescence values were obtained on a BMG Fluostar platereader. 'Blank' control values were subtracted from samples of interest to accomodate background signal.

2.5.4 Drug combination assays

2.5.4.1 Experimental design

For assessing the collective growth inhibition of EGFR, BRAF and MEK1/2 on BRAF-mutant organoids, methods developed by Chou and colleagues(Chou and Talalay 1984; Chou 2007) were implemented to determine whether compounds were additive, synergistic, or antagonistic using the Combination Index (CI) equation. Organoids were firstly treated with single agents to determine a suitable titration range, and potency of individual compounds. To investigate the effects of paired and triple drug combinations, ratios were selected according to the potency (IC_{50} values) of each agent alone, as determined by an ATP assay readout, and maintained within a fixed ratio from the other (8:4:1 for Dabrafenib:Trametinib:Panitumumab). Seven white, clear-bottomed 96 well plates were seeded as described in section 2.5.1. Individual plates used for each single agent, double agent combinations and triple agent combination. Cultures were overlaid with media, and following three days of recovery, were treated with each single agent, double agent in a fixed IC_{50} ratio, or triple agent in their established IC_{50} ratio. A 14 point titration of compounds was administered in single agent conditions, as well as in paired and three-drug mixtures, whereby titrations were in a constant ratio of IC_{50}., as detailed in Table 2.8. The constant ratio of IC_{50} values of each of the compounds allows the measurement

of outcome CI values across the whole dilution range in a series of experiments. In cases whereby a single drug demonstrated insufficient growth inhibition of BRAF-mutant organoids, relative potency levels were determined from cellular IC_{50} values within *the* literature (King *et al.* 2013; Yamaguchi *et al.* 2011; Freeman *et al.* 2009). A minimum of 4 replicate wells were established per treatment condition. Following 4 days of treatment, all plates were assayed simultaneously, using a Cell Titer Glo 3D kit.

2.5.4.2   Chou-Talalay data analysis for drug combinations

Interactions of two- or three- drug combinations were quantitatively analysed using Calcusyn™ software. Drug dose response curves generated from input raw data obtained from Cell Titer Glo 3D luminescent readouts, to calculate the average fraction affected (f_a) and fraction unaffected (f_u) per treatment condition. The dose response curves were then transformed by linear regression using the median-effect principle (Equation 2.1) to assess both potency (Dm) and shape (m) of the dose-effect curve for each dose of compound. Linear regression was performed by plotting the log[$(1/f_u)$-1] against the log(Dose), generating a line used to then calculate the log (IC_{50}) at the x intercept of the line. The median effect equation (Equation 2.1) then enabled a calculation of the inhibitor IC_{50} of each Dose (D) at the median effect (Dm).

Equation 2.1

$$\frac{fa}{fu} = \left(\frac{D}{Dm}\right)$$

whereby

D: Dose

Dm: Median-effect dose

fa: fraction affected

fu: fraction unbound

Following linearization of each respective drug dose response curve, drug combinations were analysed by the Combination Index (CI) equation (Equation 2.2).

By assigning multiple data points for constant-ratio combinations i.e. the IC50 value for each compound, the potency and shape of the curve can be determined across the entire spectrum which can then be used to equate the CI values for all doses. For the combination index equation, $(D)_1$ and $(D)_2$ were the concentrations of each drug in combination to inhibit x, whilst $(D_x)_1$ and $(D_x)_2$ were the dose of each drug as a single agent to generate the same x inhibition. CIs of <1, 1, and >1 are indicative of synergism, additive effect and antagonism, respectively. Upon treatments of organoids with two or three agents at a fixed ratio, the dose of the combination required to produce fractional survival could be separated into D1, D2, D3 of agents 1,2,3 respectively (equation shows two components only). For each level of cytotoxicity, or whereby the fraction affected, the combination index was thereby calculated.

The Dose Reduction Index (DRI) was then calculated to determine the degree to which a particular drug combination can achieve a given effect. The DRI measures a fold reduction in dose of each drug used in combination to reach an equivalent effect level (normally IC_{50}) comparative to the degree of effect observed as a single agent (Chou 2007)).

Equation 2.2

$$\mathrm{CI} = \frac{(D)_1}{(Dx)_1} + \frac{(D)_2}{(Dx)_2} = \frac{1}{(DRI)_1} + \frac{1}{(DRI)_2}$$

2.6   3D phenotypic profiling (OcellO analysis)

High-throughput image acquisition and data analysis were performed in collaboration with OcellO (Leiden) as described previously (Di, Klop, Rogkoti, Devedec, van de, *et al.* 2014; Sandercock *et al.* 2015; Herpers *et al.* 2014).

2.6.1   384 well plate set-up

Organoid lines in culture were detached to single cells as previously described in section 2.5.1. Cells were resuspended in growth factor-reduced Matrigel at 400 cells/ µl MT within black, clear-bottomed 384 well plates (Greiner). Following an

incubation of 15 minutes at 37°C to enable Matrigel polymerisation, 25µl of 7+ media containing ROCK inhibitor was added to each well. Compounds or control DMSO (0.1%) conditions were added upon seeding, or following 3 days in culture, dependent on experimental procedures. At day 7, plates were fixed using a 'fix and stain' solution, as described by Di *et al.,*2014, comprising of 3.7% formaldehyde in phosphate-buffered saline (PBS) containing 0.2% Triton X-100, 0.25 µM Tetramethylrhodamine (TRITC) phalloidin (Sigma) and 1 µg/mL Hoechst blue dye. Following overnight fixation at 4°C, wells were subsequently topped up with PBS and sealed with foil lids prior to shipping for imaging. Upon arrival, plates were washed twice with PBS and stored at 4°C.

2.6.2   High-throughput imaging

Imaging was performed on a high throughput XLS MetaXpress confocal imaging platform, courtesy of OcellO (Leiden). Image z-stacks were collected per well of a 384 well plate, with 25 image stacks taken at 10 micron steps per well. Images were taken at 4X magnification with image stacks captured from TRITC channel (f-actin stain, EX=548, EM= 645) and DAPI staining channel (nuclear stain, EX=380m EM =435).

2.6.3   Multi-parametric phenotypic analysis

2.6.3.1   OMiner™ phenotypic feature extraction software

Phenotypic analysis was performed within OMiner™ software (OcellO, Leiden), as described previously (Di, Klop, Rogkoti, Devedec, van de, *et al.* 2014; Sandercock *et al.* 2015). Briefly, upon acquisition of multiple images within the z-plane of each well, image segmentation was performed to define individual objects generated from each channel, resulting in the identification of distinct morphometries. A Gaussian filter radius was applied to enhance noise suppression. Overall, information gathered per individual channel, as well as combined channels, could be enhanced or deducted as appropriate. For segmentation of individual organoids within a well, information from both the nuclear and TRITC channels were used to enhance separation of individual organoids. To identify individual lumen within wells,

information gathered from the F-actin channel was used; this was of particular importance to distinguish multiple luminal structures within an organoid. Object filtering was then performed on all three of the segmentation parameters to remove irrelevant objects, such as fractions of loose cells and debris.

Masks were then generated from intensities of each channel; the outermost f-actin staining of an individual organoid was used to generate a 'whole organoid' mask, the internal f-actin staining used to generate a 'lumen' mask, and a nuclear staining used to generate 'nucleus' information per section within an organoid. Intensity information gathered from both channels simultaneously were also utilised to produce feature analysis per object. Objects within a single image that were out of focus were filtered and discarded from feature analysis.

Following the generation of relevant organoid masks, Ominer™ software was used to extract morphological features from projections of the F-actin and nuclei-derived image stacks to generate masks of individual organoids, internal lumen structures and nuclei. Individual measurements acquired per object were subsequently accumulated to represent collective objects within all sections imaged per well, generating a mean value for each feature. Approximately 600 quantified features were then extracted per well by assessing shape and fluorescence intensity of organoid, lumen, and nuclear masks, some of which are represented in Table 2.9. Data was pooled on a well by well basis, to define the average parameter with standard deviation. Any outliers were removed from analysis such as wells where the matrigel had been disrupted (as a result of plating or shipping conditions).

Table 2.9 Description of a subset of features extracted from intensity information of images gathered and corresponding outcomes of measurement

Feature	Measurement
Organoid count	Total organoid counts from a whole image stack
Organoid sum size	The total volume of organoids within a well
Organoid average size	The average organoid size per-section
Organoid roundness	Values assigned (0-1) to organoid roundness, with 1 depicting a spherical object
Nucleus count	Measurement of cell density per organoid
Organoid nucleus to organoid centre distance	Measurement of the average distance between the centre of an organoid, and centre of corresponding nuclei to represent nuclear spread within and organoid
Organoid nucleus to organoid boundary distance	Measurement of the average distance between the organoid edge, and centre of corresponding nuclei to represent nuclear spread within and organoid (to be used in conjunction with organoid nucleus to organoid centre distance)
Organoid branching	Identification of branching structures in the main architecture of an organoid
Lumen size	Average measurement of overall area of lumen/lumens within an organoid structure
Number of lumen	Total number of lumen within an organoid to identify complexity of structure
Lumen branching	Number of protrusions from lumen

2.6.3.2 Basic feature extraction

Over 600 variables were collected and analysed using OMiner software to generate a well by well profile of different organoid features. Basic analysis of dose dependent responses according to variable (e.g. organoid average size) was carried out on Microsoft Excel/ Graphpad Prism.

2.6.3.3 Principal Component Analysis (PCA) and Distance metric measurements

PCA was used to transform data from multiple quantified variables from phenotypic analysis, to a new coordinate system in order to identify components that attributed to the most variation in the data between control and negative control samples. The greatest variance in data (across variables within different conditions) therefore lies within the first coordinate, until all data points are assigned coordinates in descending order of variance in data. For each organoid line and treatment, a Mahalanobis distance metric was applied across the top 5 principle components, between negative controls and each sample observation (dose), in order to classify the degree of change in variables between control and treated samples. A distance metric would have the highest value in conditions whereby observations were distinctly different from negative controls, as reflected in the quantified data. Alternatively, no observed change between treatment and negative control would result in a small distance metric in multidimensional space. Further details of analysis methods implements can be found in Di et al 2014 and Caie et al 2010. PCA analysis was carried out using R studio software(http://cran.r-project.org). *Multi-dimensional analysis described in Chapter 5 was carried out by OcellO. The principles of this analysis were identical, with the exception that an Euclidean Distance metric was used to represent variance in parameter space.*

2.7 Experimental animals

NOD-SCID gamma irradiated mice were used to perform *in vivo* organoid engraftment experiments. All animals were obtained commercially from Charles River and housed under UK Home Office regulations.

2.7.1 Experimental procedures

Licensed individuals with appropriate training performed experimental procedures. All mouse experiments described in this thesis were carried out by Dr Kenneth Ewan (Dale lab).

2.7.2　Organoid transplantation

For organoid transplantation, organoids were taken to single cells and treated with DMSO or treatment for 24 hours prior to transplantation subcutaneously into one flank per mouse. Animals were checked every two days for tumour growth by palpation, according to protocol by Home office regulations.

2.8　Data and Statistical analysis

Raw data obtained was analysed using Microsoft Excel for Mac or GraphPad Prism software for Mac. Graphical representation of data included standard deviation or standard error of means. Statistical analysis was performed using GraphPad Prism sofrware for Mac. Statistical test used are dented in figure legends. Comparisons of means were performed using a T-test. Comparisons between experimental repeats were perfomed using analysis of variance analysis (ANOVA), with Dunnett's post-hoc analysis for comparison against one control. Statistically significant differences were determined when p values were less than or equal to ($\leq$) 0.05.

2.8.1　Generation of Drug dose response curves

Raw data obtained from relative luminescence of samples (2.5.3) was corrected for background absorption as determined from 'blank' wells containing the reagent/media mix. Drug dose response curves were generated using an 'XLFit' Microsoft Excel Plug-in. Within each experiment, curves were fitted for three technical replicates which then allowed the output of an IC_{50} value. For the analysis of experimental repeats, the mean of obtained IC_{50} were used as a representation, with experiments largely n=3 unless otherwise stated. For drug combination studies, data was plotted as a survival curve using GraphPad Prism software. For exploration of drug synergy, data was analysed using Calcusyn™ software (Biosoft) to generate Combination Index values as well as Dose reduction Indexes.

2.8.2 Kaplan Meier Survival analysis

A survival curve was generated using GraphPad Prism. Statistical analysis was conducted using the Log-rank (Mantel-Cox) test. Statistically significant differences were determined when p values were less than or equal to ($\leq$) 0.05. *Statistical analysis of survival was carried out by Dr Kenneth Ewan (Dale lab).*

3 Development and optimisation of high-throughput patient-derived colorectal cancer organoid assays

3.1 Introduction

The generation of 3D organoids from patient material could not only provide a valuable tool to gain insights into tumour and stem cell biology alike, but also hold potential as a relevant pre-clinical platform to validate oncological therapeutics. An experimental platform that more closely represents all characteristics of a tumour *in vivo* as well as response to therapeutic agents, whilst simultaneously retaining the usability of high throughput 2D cultures to facilitate the testing of a high number of compounds, is instrumental for drug discovery purposes. In order to establish organoids as a successful *in vitro* modelling system, their setup and use had to be optimised to ensure both relevance to patient tumours, as well as reproducibility within robust assay formats, compatible for the analysis of complex 3D structures. Here, we show the expansion of a cohort of patient-derived organoids cultures from primary CRC tumour material based on culture systems that have previously been described (Sato et al., 2011). As organoids are complex 3D structures, which show variability both within and across populations, we developed assay formats with the aim of generating quantitative data to assess the impact of small molecule inhibitors and drugs.

In summary, the key aims here were:

(i)   To generate and characterise colorectal tumour-derived organoids

(ii)   To optimise suitable growth conditions to facilitate maximal organoid expansion in culture which retain key characteristics of parental tumours

(iii)   To determine optimal assay formats and plating conditions, in terms of speed and output, which show high sensitivity as a readout for organoid responses to growth inhibition.

3.2 Results

3.2.1 Establishing epithelial organoids from patient derived colorectal cancer material

3.2.1.1 'Tumour, Node, Metastasis' (TNM) and Dukes' staging of colon tumour samples obtained from patient material

To generate a cohort of patient-derived organoids, a sample stream was established in collaboration with the Wales Cancer Bank, whereby surgically resected colorectal carcinoma tissue were retrieved with full patient consent. Collected material was examined and appropriately sectioned by histopathologists (University Hospital Wales); for each tumour sample, a section of live tissue was collected for our organoid establishment purposes, as described in Methods (2.1). Clinical samples were further characterised by histopathologists (University Hospital Wales) following sectioning of tumour material and fixation for histological assessments. This ensured that basic patient metrics were established from the same tumour region from which corresponding organoids were generated.

For routine diagnostic purposes, histopathologists obtained samples of each specimen as well as approximately 8 surrounding lymph nodes to determine the tumour grade, and to assess whether tumour cells had infiltrated into surrounding tissue. These samples were then cryosectioned prior to hematoxylin and eosin (H&E) staining for diagnostic analysis. Following both gross and microscopic analysis, tumour stage were set according to Dukes tumour grading, and the Tumour, Node, Metastasis criteria as noted in Table 3.1, respectively. All samples used within this study were isolated from different regions of the colon from both male and female patient within an age range of 43-83. 6 out of 11 samples were from patients with tumours that had spread into adjacent lymph nodes (N), with N1-2 indicative of increasing proportions of lymph nodes containing cancer cells. 1 of 11 samples ((Iso)48) was derived from a patient with a known history of metastasis of the primary tumour, as indicated by a 'metastasis' (M) score of 1. The 10 remaining

samples analysed were given a 'Mx' score to indicate unknown evidence of metastasis from patient data (Wales Cancer Bank).

Table 3.1 Patient tumour Staging.

Fragments of carcinoma isolated from surgically resected tissue have successfully generated organoids as indicated by 'Isolation number'. Patient ages range between 43-83 in this subset, and include mostly tissue derived from male patients (M denotes males, F denotes females). Dukes' tumour stages are denoted A-C2. Tumour, Node, Metastasis (TNM) staging is graded T1-4,N0-2,Mx-1. *Data collated by the Wales Cancer Bank.*

Isolation number	Age	Sex	Tumour Site	Tumour Differentiation	Dukes' Stage	TNM Stage
29	73	M	Upper Rectum	Well/ Moderate	C1	T1N1Mx
34	69	M	Transverse Colon	Well/Moderate	A	T2N0Mx
36	77	F	Rectum	Well/Moderate	B	T3N0Mx
38	64	M	Sigmoid Colon	Well/Moderate	C1	T3N1Mx
48	43	M	Rectum	Poor	C2	T4N2M1
49	75	M	Lower Sigmoid	Well/Moderate	C1	T3N1Mx
50	75	M	Rectum	Poor	C2	T3N1Mx
72	83	F	Caecum	Well/Moderate	B	T3N0Mx
73	60	M	Sigmoid Colon	Well/Moderate	B	T3N0Mx
75	76	F	Caecum	Poor	C1	T3N1Mx
78	66	F	Caecum	Well/Moderate	C1	T3N1Mx

3.2.1.2 Generation and establishment of growth conditions for epithelial organoids derived from primary tumour material

Previous and on-going work within the Dale lab (Dr Kenneth Ewan & Dr. Andrew Hollins) has demonstrated success in the processing of isolating epithelial cell fragments from colorectal tissue to generate organoids (denoted by Isolation number, 'Iso'), based on methods in the literature (Sato et al 2011) whereby patient material has successfully established in 3D culture. For the purposes of a wider study to generate a CRC organoid platform, the tissue isolation process and optimisation of organoid growth conditions was divided equally between Dale lab members (Iso 29-78 between Dr Andrew Hollins and Luned Badder, with previous samples having been generated between Dr Kenneth Ewan and Dr Andrew Hollins). Of the 78 samples processed to date, there has been an approximate 70% success rate in initial organoid establishment from tumour tissue, with improvements made over time following experience with culture requirements. For the purposes of this study, a subset of these were generated from fresh tumour tissue (with the exception of Iso 38, generated and characterised for optimal media conditions by Dr. Andrew Hollins), characterised, and further utilised for assay development. Fresh tissue was routinely collected and processed within 3-15 hours following surgical resection.

As depicted in Figure 3.1, following digestion and trituration of washed tissue pieces, cellular fragments derived from tumour tissue were filtered through a 70μm filter to ensure minimal aggregation, and resuspended in 10ml '3+' media, components of which are previously listed (Table 2.1). For counting purposes, 10μl samples were dispensed onto tissue culture plates, and clusters of cells were counted to seed 1000 per 50μl of growth factor-reduced Matrigel. Such protocols were established previously (Sato *et al.* 2011a) in the literature; by counting fragments as opposed to unsorted single cells, it prevented any other cell types that could be present (such as fibroblasts) from skewing the data. Preliminary work based on guidance within the literature (Sato *et al.* 2009; Sato *et al.* 2011b) was carried out on a subset of

organoids samples to establish optimal seeding densities. Following processing of tissue to epithelial cell fragments, organoids were plated at 1000 cell fragments or 2000 cell fragments per 50 µl Matrigel, in 'Full' or '7+' media conditions. The number of organoids generated were then counted on a well by well basis in each condition. As shown in Figure 3.2, it would suggest that 1000 cells per 50 µl Matrigel was sufficient to generate the highest yield of organoids. However, the number of organoids generated from primary material varied between patient samples due to nature of material, ranging from seeding a minimal 8 wells to a higher yield of 20 wells of a standard tissue culture 24-well plate. A limiting factor on the number of different growth and seeding conditions that could be implemented was thus due to the number of cell fragments isolated from tumour tissue, meaning that optimal seeding densities from fresh fragments could not always be calculated for each sample. All samples following Iso 29 were therefore seeded at a density of 1000 cell fragments / 50 µl matrigel. This difference is most likely due to a variety in necrotic regions within a primary tumour that reduce the number of viable cells that could potentially expand within culture. Once suspended and embedded within matrigel, fragments of cells formed multiple closed structures within 12 hours of seeding.
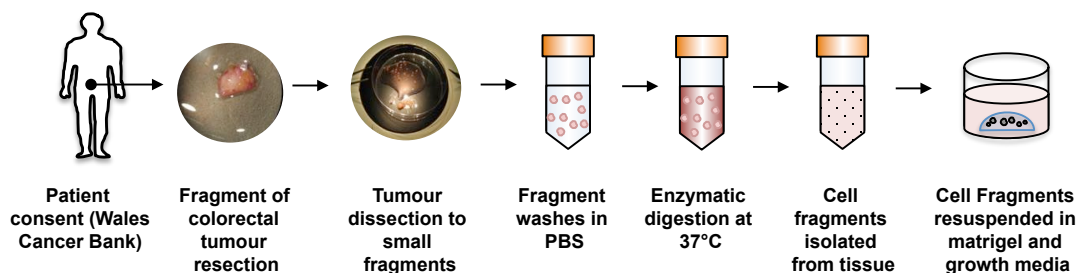
Figure 3.1 Depiction of organoid isolation process from human surgically resected colorectal tissue. Surgically resected colorectal material undergoes a process of dissection, digestion and trituration to release cellular fragments. Cells are then transferred to growth factor-reduced Matrigel and overlaid with growth media.
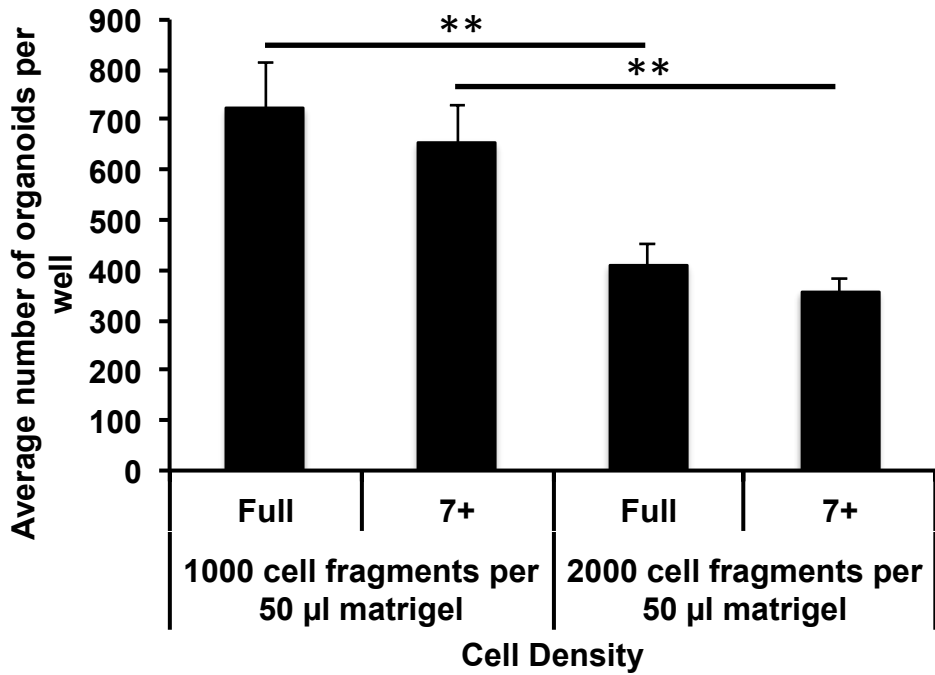
Figure 3.2 Establishment of optimal organoid seeding densities from isolation.

Following dissection, digestion and trituration of primary patient CRC material (Iso 29) from freshly resected specimens, cellular fragments were counted at a density of 1000 or 2000 cells per 50 µl of Matrigel, prior to plating . Cellular fragments embedded within matrigel were then overlaid in 'Full' or '7+' Media. The number of organoids per well were counted using GelCount charm settings. A minimum of n=3 wells were used per condition. Data shows mean ± standard deviation, paired student's t-test. For routine samples generated for this study, a density of 1000 cell fragments per 50 µl matrigel was deemed as a sufficient number to enable organoid formation.

3.2.1.3 Optimisation of culture conditions for CRC organoids

In order to maximise yield from patient material, basic growth requirements of structures derived from patient material were ascertained by treating fragments of tumour cells immediately following seeding (passage(P)0) with two different culture media compositions: '7+' basic media, and 'full' growth-factor rich media (Table 2.1). Both conditions were based on previous findings in the literature and were sought to enhance the growth of tumours with differential requirements of surrounding environmental factors. Many colon cancer cells require little addition of growth factors for culture as they typically harbour mutations which facilitate their own niche requirements (Sato *et al.* 2009). The niche dependency of other CRC organoids means that they require exogenous stimulation, such as those provided by 'full' media conditions, with additional Wnt and R-spondin conditioned media, as well as epidermal growth factor (EGF), Noggin, TGF-β inhibitor (A83-01) and a p38 inhibitor (SB202190). Recent studies have further highlighted the manipulation of niche dependencies of CRC required to support the growth of different tumour subtypes in culture (Fujii *et al.* 2016b) and will be considered further in the discussion section of this thesis.

In order to quantitatively analyse the most favourable growth parameters for each organoid line, organoid counts were generated using an automated colony counter, GelCount™ technology. To facilitate organoid detection and counts from structures present within each well, CHARM settings were established with threshold values for parameters such as optical density, size, circularity and quality of structure edges, as well as background detection to ensure minimal aggregates were detected as organoids. The software enabled automated morphometric readouts from organoid images taken from wells by generating a script, entitled CHARM settings. For CHARM settings generation, threshold values were firstly established to remove outliers of data. Parameters such as optical density, size, and definitive object outlines were used to determine objects that could be counted as organoids. Following one organoid line (Iso 75), it was shown that the number of organoids formed, as

counted using established CHARM settings of GelCount™ technology, were reliant on media conditions used. As shown in Figure 3.3, an average of 332(±94) organoids were generated in '7+' basal conditions, as opposed to 601±110 on average per well in 'full', growth factor-rich conditions. It is however worth noting that both counts and visual inspection were required to determine the best media conditions as masks generated using GelCount™ technology calculate the (unlikely) assumption that all structures are viable. As noted in previous assessments of organoid viability in mouse model systems (Grabinger *et al.* 2014), non-viable organoids are characterised by a loss of cellular organisation on the outermost edge of structures, surrounding cellular debris, and a lower optical density as structures overall contain a dark core . Collectively, such assessments enabled a determination of sufficient growth conditions for maximal expansion of each of organoid line, as listed in Table 3.2 . 9 out of 11 organoid lines established for this study demonstrated sufficient growth in basic '7'+ media conditions, whilst 2 lines were dependent on propagation in 'full' media conditions. Given that organoids were derived from a variety of tumour origins and stages, it was unsurprising that to reliance on particular niche factors for growth were variable.

Once media conditions for optimal growth had been established, the specified media was then utilised to grow continuing organoids throughout subsequent studies (Table 3.2)**.** By means of this selection process, it was possible to facilitate maximal survival for tumours with varying niche requirements for growth, despite being unable to fully interrogate individual niche factors required for each line.
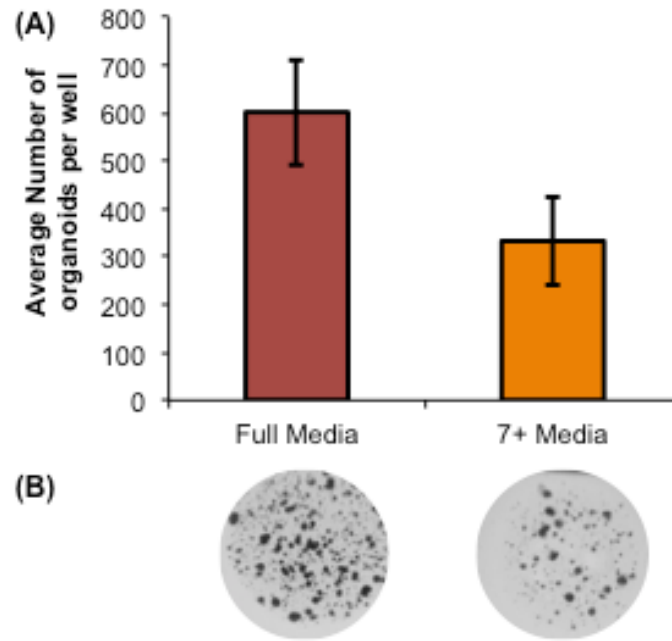
Figure 3.3 Analysis of media requirements for organoid growth

Following isolation of material from surgically resected colorectal tissue, Iso 75 organoids were

seeded as fragments of cells at a density of 1000 cells per 50µl of growth factor-reduced Matrigel.

Cultures were overlaid with two media conditions to determine optimal growth requirements; basal

'7+ Media' or Full Media containing growth factors, 10% R-spondin conditioned media and 40% Wnt

conditioned media. **(A)** Bar chart depicts the average number of organoids formed from seeding a

1000 fragments per well of a 24 well plate, using GelCount™ technology. Data are presented as

mean± standard deviation, whereby n=3 wells. **(B)** Representative images from each well per

condition were obtained using GelCount™ software, using standard settings as detailed in methods

(2.3.6.1)

Table 3.2 Established media requirements for organoid subset.

Following isolation of material from surgically resected colorectal tissue, two media conditions were used to determine optimal growth requirements. Optimal media requirements were assessed using basic growth parameters such as changes in gross morphometry as well as visual inspection of organoids to qualitatively assess the amount of potential dead cells present in culture. An accumulation of cellular debris as a result of cell death would often be visualised in sub-optimal conditions. *Media conditions for Iso 38 were determined by Dr.Andrew Hollins (Dale lab).*

Isolation number	Media conditions	Seeding density (number of wells of a 24 well plate)
29	7+	16
34	7+	12
36	7+	8
38	7+	16
48	7+	10
49	7+	14
50	7+	8
72	7+	14
73	7+	10
75	Full	20
78	Full	16

3.2.1.4 Patient-derived tumour organoids exhibit various morphologies and growth rates in tailored culture conditions

Based on early observations in organoid establishment, as well as findings from the literature, it was clear that a variety of tumour organoid morphologies were obtained, possibly reflective of mutational backgrounds or as a result of their surrounding environment (Sato et al. 2011a; Yin et al. 2013;Riemer *et al* 2017). Given that organoids could be generated from a range of CRC subtypes, it was therefore necessary to establish suitable methods to quantify changes in morphometry and organoid growth over time to ensure stability in culture. Using an automated colony counter, CHARM settings were optimised per organoid line to monitor growth in morphologically variable organoids to account for a variety of structure types. Organoids that formed generally more cystic structures for example required different density thresholds to be set compared with denser organoid structures. CHARM settings were then used to generate masks around individual objects within a well to detect basic morphometric features of the 2D image such as overall organoid size, (calculated) volume, density and number within a well.

Following initial selection of appropriate growth conditions, complex structures of colonic epithelial organoids grew typically for between seven- fourteen days prior to passage, with a split ratio between 1:2 – 1:8 (wells) implemented every 7-10 days, or as necessary. Epithelial organoids derived from different patients exhibited a variety of growth rates within the first few passages of culture, as depicted in Figure 3.4. As depicted, growth in basal 7+ media conditions was sufficient to yield an increase in overall organoid diameter over several days within these three organoid types. Defined culture conditions demonstrated that organoids were able to expand to sizes between 100µm- 500µm on average over two weeks, as calculated by GelCount™software from images over repeated measurements. Settings were

established for each organoid line and altered according to overall morphologies and cell densities per structure.

Distinct morphological variation was also seen across different patient-derived organoids, as shown in Figure 3.4 . Iso 29 was shown to yield a population of mainly cystic organoids, with occasional smaller, denser structures observed. Iso 36 demonstrated more complex morphologies, with budding structures protruding from the central 'lumen'-like structure. Differential morphology was further corroborated by images of various organoids fixed and stained (day 5) simultaneously with a Hoechst and Phalloidin (F-actin) stain, and captured using light sheet microscopy, as seen in Figure 3.5. These images showed a clear distinction between internal morphologies of organoids; Iso 75, for examples showed multiple lumen structures throughout the internal cellular composition whereas Iso 50 and 72 had a more basic internal morphology with occasional branching structures. Overall, organoid morphology and ratio of splitting remained stable over several passages, an important requirement of future drug screening studies, retaining morphologies observed in early culture, and was therefore suitable for expansion for subsequent assays.

As well as establishing optimal growth conditions, this work also aimed to maximise organoid yields to facilitate subsequent experimental repeats. A suitable organoid freeze- thaw protocol was therefore optimised to improve organoid recovery from freezing conditions. Organoids cultured for 4 days were lifted from matrigel and resuspended in cell recovery freezing medium (Invitrogen™). The suspension was then placed in cryovials and stored in -80°C conditions. For organoid recovery, cryovials were placed in the water bath at 37°C and thawed rapidly. Structures in suspension were then washed in 3+ media prior to embedding in growth factor-reduced matrigel, and then overlaid with media. To examine whether addition of ROCK inhibitor Y-27632, previously implicated in improving cell survival (Ashley *et al.* 2014), could enhance organoid formation efficiency, a subset of Iso 49 organoids were dissociated to single cells immediately after thawing, plated in matrigel and

overlaid with media ± ROCK inhibitor. As shown in Figure 3.6 ,single cell recovery and subsequent organoid formation for Iso 49 was enhanced when media contained 10 µM ROCK inhibitor Y-27632 for the first three days in culture. Recovery prior to passage was established between 5-10 days, dependent on organoid line.
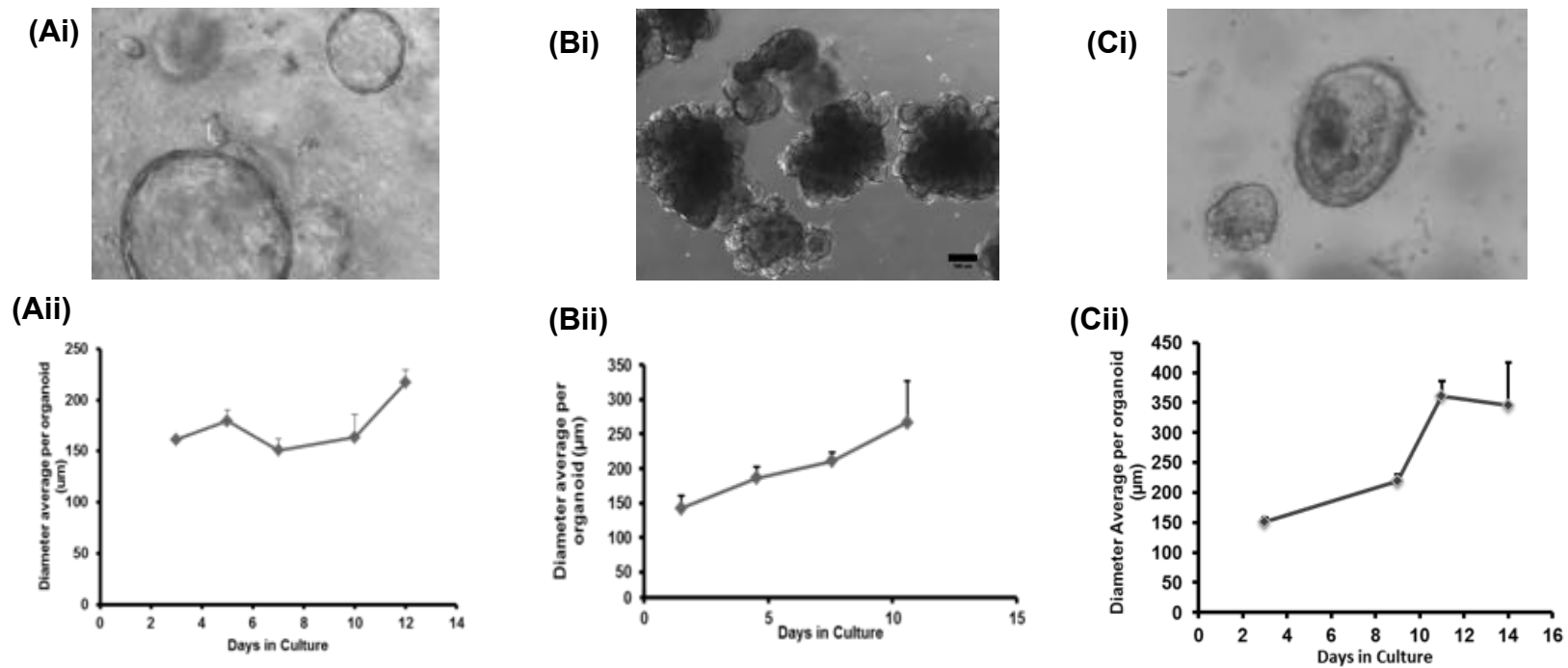
Figure 3.4 Intestinal organoids show a variety of morphologies and morphometries in defined culture conditions between different patient subsets.

Microscope images taken at day 7 in culture conditions (Scale bar= 100µm) and corresponding growth profiles from 3 different patient carcinoma samples (A) Iso29 (B) Iso36 (C) Iso34. Growth is indicated as diameter per organoid average per well (µm) ±Standard deviation measured by GelCount charm settings.
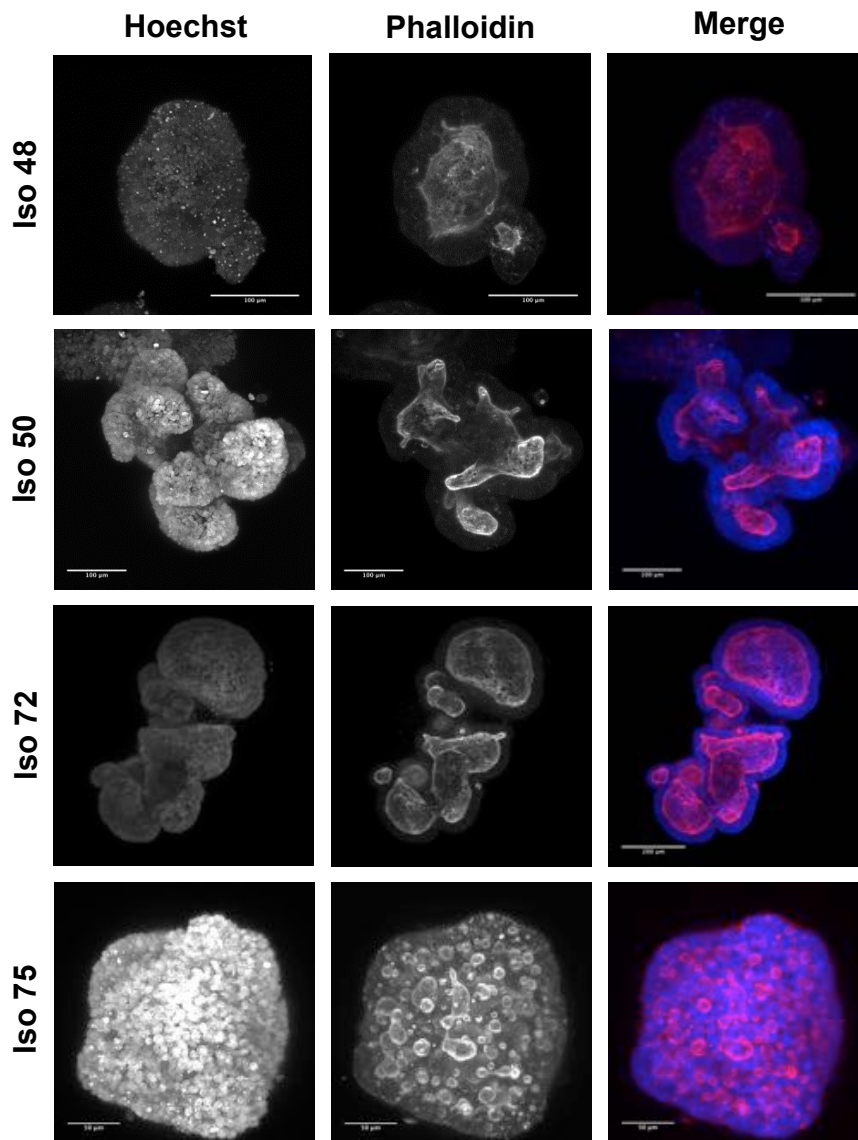
Figure 3.5 F-actin staining reveals internal complexity of organoid structures.

Organoids were passaged by trituration (p4-p10) prior to seeding within growth factor reduced matrigel in defined media conditions. Following 5-7 days of growth, cultures were fixed and stained simultaneously using a Fix& stain solution comprising of PFA (4%), Hoechst and TRITC-Phalloidin to stain F-actin. Organoids were then washed before transferred to agarose for imaging purposes. Scale bars depicted on each image are as follows; Iso 48, Iso 50= 100µm, Iso 72=200 µm, Iso 75= 50 µm.
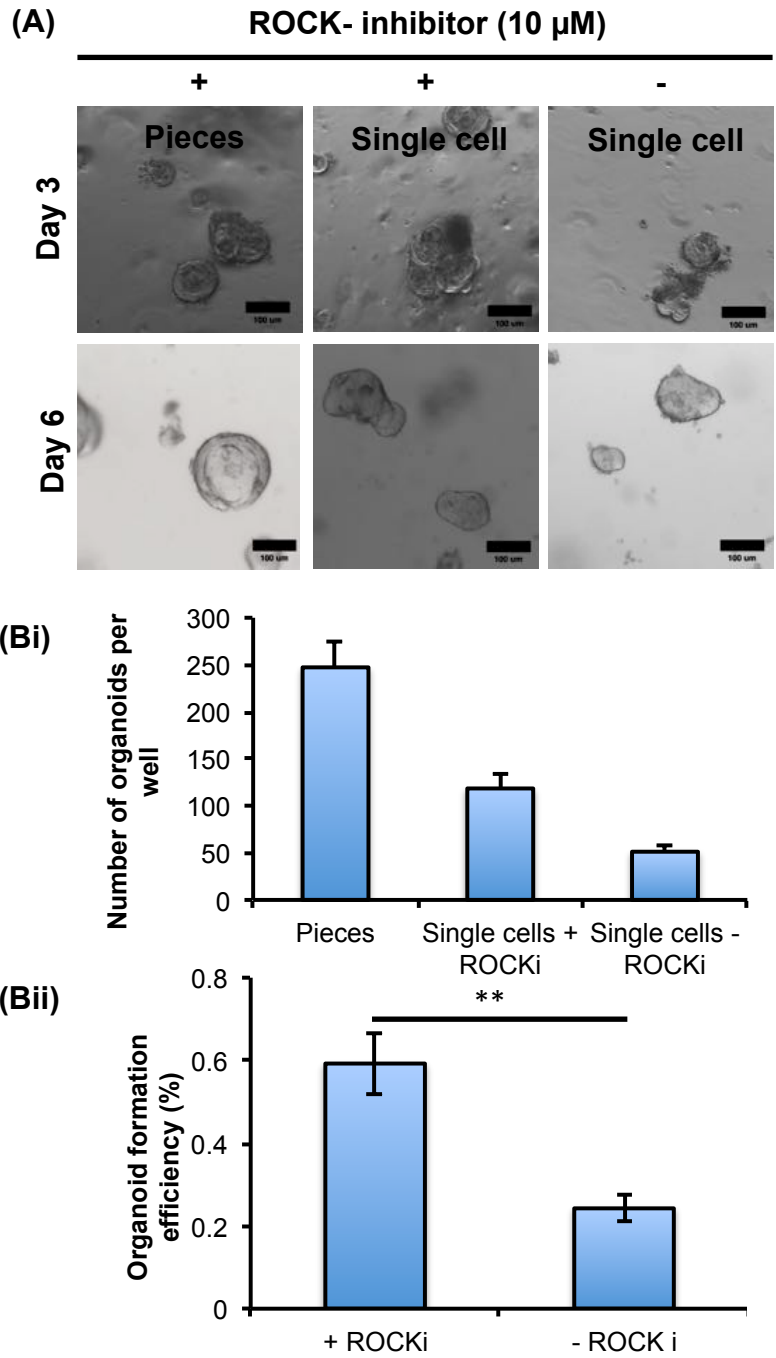
Figure 3.6 Organoid freeze-thaw recovery.

Iso 49 organoids were frozen in Cell Recovery freezing medium and stored at -80°C. For recovery, cryovials were thawed rapidly at 37°C, prior to organoid washes and embedding within matrigel. Organoids were plated as whole structures, or further trypsinised to calculate the number of cells present in culture after thawing, then overlaid with defined media conditions. **(A)** Representative images of organoids derived from whole frozen organoids('pieces'), or single cells, ± ROCK inhibitor. Scale bar = 100µm. **(Bi)** Bar chart to represent average number of organoids and **(Bii)** organoid formation efficiency (%) calculated by GelCount software. Data shows mean ± standard deviation (n=3 wells), unpaired t-test; ** $p < 0.01$.

3.2.2 Organoids retain overall histological architecture of matching primary tumours

In order to assess the capacity of organoids to recapitulate *in vivo* tumour biology, histological parameters were compared between clinical samples and counterpart organoids. Previous studies using such morphological parameters have enabled the identification and characterisation of clinical features in both patient colorectal tumours and the organoids from which they are derived (Fujii *et al.*, 2016).

Hematoxylin and eosin (H&E)-stained primary tumour sections were processed (Wales Cancer Bank) and analysed by the Histopathology team at University Hospital Wales (Dr. Delyth Badder). For comparative histology, organoids were freshly passaged into Matrigel and cultured for 4-7 days, prior to fixation (PFA, 4%) for 15 minutes at room temperature. Organoids were then washed following an incubation on ice to remove matrigel fragments, then resuspended in 4% low melting point agarose prior to cryo-sectioning, mounting and H&E staining.

Samples derived from the poorly differentiated samples (Iso) 48 (metastatic) and (Iso) 75 were defined as particularly aggressive tumours, as indicated by vascular invasion as well as a high level of lymphocyte infiltration as a result of an immune response, shown in Figure 3.7. Due to the epithelial nature of organoids such observations could not be captured in matching material. Iso 48 and Iso 75 samples were also found to contain high numbers of mitotic bodies reflective of multiple cell divisions. Overall, it was found that many epithelial characteristics found in parental tumours were also observed in counterpart organoids, with individual structures retaining similar features. Primary tumours containing high numbers of glandular structures, for example, were reflected by multiple lumen structures within organoid sections such as those observed in Figure 3.7 in which Iso 75 organoids are reflective of matching tumour tissue. An overall poorly differentiated tumour containing few small glands of differentiation (Iso 50) was shown to be capable of deriving a mixed morphology of organoids; some mono-cellular structures with a cystic phenotype

(Figure 3.7, black arrows) , as well as structures with a thick epithelial cell layer containing glandular structures within the organoid (Figure 3.7, purple arrows).

It was observed that Iso 72 was derived from a highly mucinous adenocarcinoma, as indicated by a significant component of extracellular mucin pools within the tumour section, as highlighted in Figure 3.7 Interestingly, features were retained in culture as identified by mucinous vacuoles within corresponding organoid sections. Previous studies have identified that such adenocarcinomas are characterised by a high proportion of Mucin 2-positive goblet cells within tumours, and have successfully linked patient histology with specific gene expression signatures, such as goblet-, stem cell-, transit-amplifying- and enterocyte-like tumours (Sadanandam *et al.* 2013).

For three CRC samples (Iso 50, Iso 72, Iso 75), organoids were additionally immunostained for Mucin 2 to evaluate the presence of goblet cells within samples and to further determine if primary cultures were able to retain differentiation characteristics observed in primary tumours. As shown in Figure 3.8, it was observed that Iso 72 organoids were heavily stained for Mucin 2, suggestive of a high goblet cell population, in concordance with observations from primary material. Iso 75 organoids demonstrated some mild staining, and no Mucin 2 positive staining was identified in Iso 50 cultures.

Due to limitations in retrieving organoid sections from paraffin blocks, a subset of only six patient and corresponding cultures were analysed from a variety of graded clinical samples. Observations collected from primary tumour samples were largely represented by counterpart organoids, with the exceptions of non-epithelial characteristics such as vascular invasion (Figure 3.7, yellow arrows), and filtration of neutrophils and lymphocytes (Figure 3.7, blue arrows) into tumour tissue. However, this data strongly indicates that histological grading and the cellular differentiation status is largely retained between patient and corresponding organoid culture within the samples analysed, in line with current knowledge of *in vivo* tumour histology.
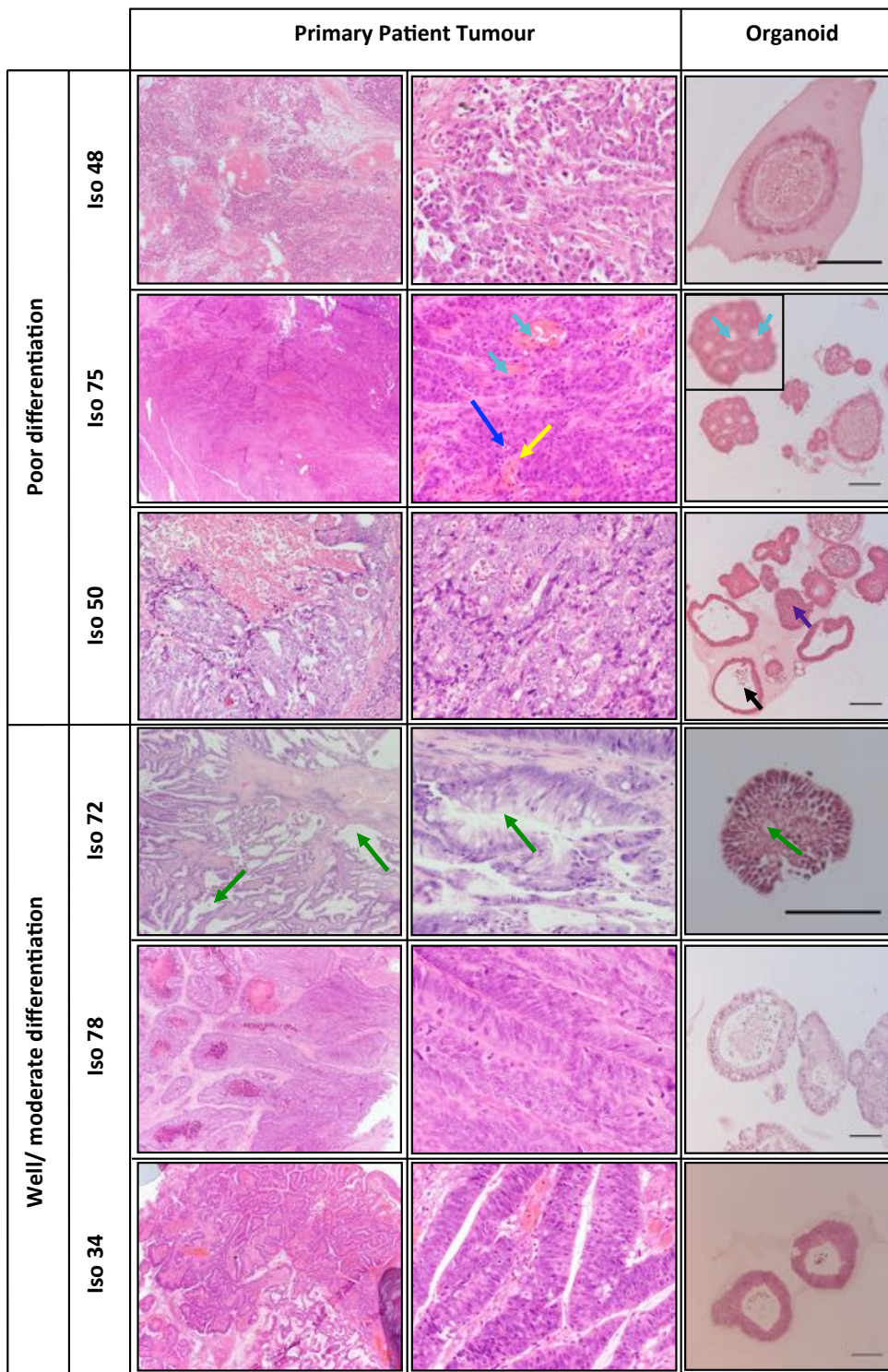
Figure 3.7 Representative images of immunohistochemical stains from surgically resected patient tumours.

Organoids were cultured in defined conditions, embedded in paraffin, sectioned, and stained to define cellular architecture. H&E stained patient tumours were kindly provided by the WCB, and analysed and imaged with the histopathology team (UHW) Scale bar=100μm. Arrows denote the following; (←)cystic structures; (←) dense epithelial structures (←)mucin pools; (←)neutrophil and lymphocyte invasion; (←) vascular invasion; (←) gland-like structures/ organoid lumen.
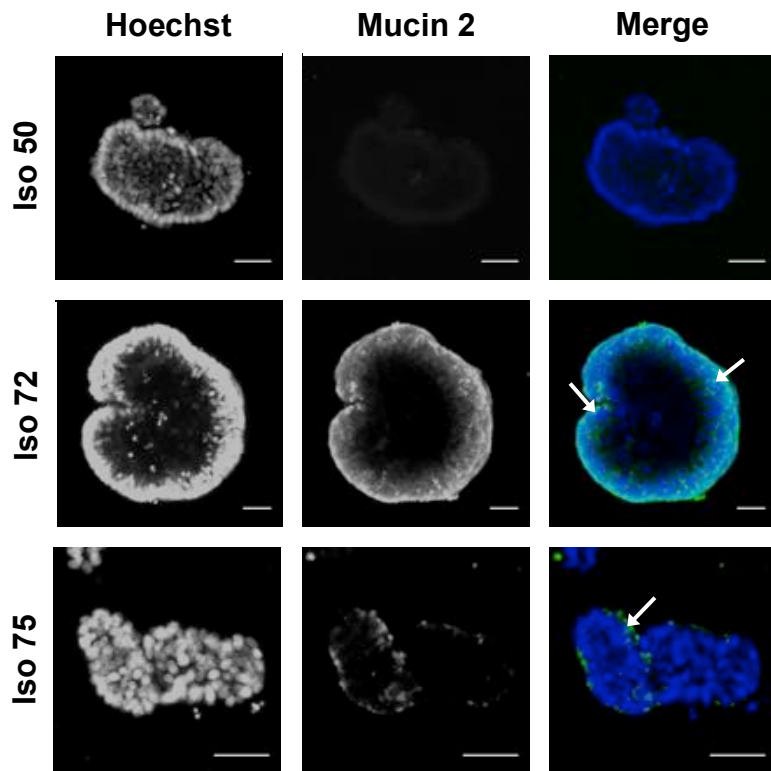
Figure 3.8 Organoids derived from primary material resemble differentiation profiles of primary tumours.

Organoids were cultured in defined growth conditions prior to fixation by PFA (4%) prior to immunostaining with anti-muc2 antibody to detected mucin positive cells as an indication of the presence of goblet cells. *Scale bar = 50 μm.*

3.2.3 Genotypic analysis of an organoid cohort reveals mutations in colorectal cancer-associated genes

In order to classify organoids according to their mutation status and investigate whether our cohort would encompass CRC relevant mutations, DNA was isolated from tumour organoids, using a Qiagen DNA extraction kit as per the manufacturer's protocol, and subject to analysis using the Next Generation Sequencing (NGS) SureSeq Solid Tumour panel carried out by Oxford Gene Technologies (OGT). This panel encompassed genomic regions of interest to characterise the status of 60 genes previously identified in cancer development and progression. A variant analysis report was carried out by OGT to generate the mutation status of each gene of interest from 8 organoid lines. Mutations were detected in both activating oncogenes and inactivating tumour suppressors frequently affected in colorectal tumours, including *APC*, *KRAS*, *BRAF*, *PIK3CA*, and *TP53*. The severity of detected mutations and subsequent impacts upon cellular functions were determined by integrating outputs of individual variants with the Sanger COSMIC database (Catalogue of somatic mutations in cancer), as shown in Table 3.3, which highlight relevant mutations within a particular tissue. Mutations that were identified in the sequencing data, but not previously noted in the COSMIC database were labelled as 'no COSMIC record'. It remains uncertain whether these mutated genes would significantly impact cellular function, as they have not been previously identified within colorectal tissue as frequent mutations. Given that sequencing was only carried out for tumour organoids and not matched normal DNA, it is difficult to fully distinguish between mutations as opposed to polymorphisms, and whether events were from germline or somatic variants. Analysis was therefore carried out in comparison to sources within the literature.

CRC is heavily associated with activating mutations within components of the Wnt signalling pathway, including APC and β-catenin encoded by *APC* and *CTBNN1*. Mutations in *APC* were observed in 8 organoid lines, with 5 out of 8 lines harbouring mutations that resulted in a truncated protein. Some lines possessed mutations previously unidentified within the COSMIC database therefore their relevance to APC

function is unknown. Previously identified *CTNNB1* mutations were present in 3 of the organoid lines, Iso 48, 75 and 78. Interestingly Iso75, and Iso 78 were reliant on full media conditions that contained exogenous Wnt and R-spondin conditioned media, demonstrating a complex niche requirement to be maintained within culture. In principle, ß-catenin mutations result in an overall activation of the Wnt signalling pathway, suggesting that such organoids would be capable of growth in absent Wnt or R-spondin. However without a complete dissection of required growth factors within the media, it is possible that growth within Iso 75 and Iso 78 are reliant on other exogenous components within Full media.

Mutations in genes involved in DNA Damage Response (DNA) were prevalent in most organoids sequenced. For the purposes of categorising organoids into clinically relevant biomarkers, the mutation status of *ATM* and *TP53* were assessed. Mutations within *ATM,* which has been previously associated with DNA replication stress, was identified in 3 out of 8 organoid lines. Whilst these had not been previously identified within the COSMIC database, these changes resulted in deleterious events and truncating mutations. The comparative analysis of germline DNA would therefore be useful for further studies of these organoid lines. It was also observed that *TP53* was frequently mutated among organoids, impacting 5 out of 8 lines sequenced.

Genetic alterations in the PI3K and RAS-MAPK pathway have previously been identified within CRC. The *PIK3CA* gene encodes the p110a catalytic subunit of phosphatidylinositol 3-kinase (PI3K), with mutations resulting in aberrant activation of the PI3K/ AKT pathway that promotes cell division. Within our organoid cohort, Iso 48 was found to harbour a missense mutation at codon 1625 (A>T), previously implicated in the large intestine according to the COSMIC database. Other mutations identified within Iso 49, 75 and 78 were not previously identified as having a high implication in other colorectal cancer tissue samples, however resulted in deleterious events. A comprehensive molecular characterisation of CRC has previously revealed that genomic amplifications or mutations of the gene *ERBB2,* is altered in approximately 6% of colorectal tumours (Cancer Genome Atlas Network

2012). In the organoids assessed, it was found that Iso 34, 48 and 78 contained alterations previously identified within the COSMIC database as pathogenic. It was found that most organoids also contained alterations within *EGFR,* that could lead to amplification of the EGFR receptor, however none of these could be identified as a mutation that could be classed as targetable within the clinic.

BRAF mutations occur in approximately 8-15% of patients with CRC, and are often associated with a poorer prognosis in patients. Based on previous findings within the literature, *BRAF* mutations within CRC are an activating missense mutation at amino acid position 600; whereby a glutamic acid amino acid is substituted for valine (V600E). Iso 75 was shown to harbour a mutation at this position, as well as a truncation at residue 40 (previously not identified within COSMIC). Iso 34 was also shown to carry a *BRAF* mutation at amino acid position 601, which has been lesser implemented in previous colorectal cancer tissues analysed. *KRAS* mutations, particularly G12V mutations resulting in a substitution at amino acid position 12 in KRAS are observed in approximately 40% of colorectal cancers, with 21% of these at the G12V position (Forbes *et al.* 2015). Iso 50, Iso 72, and Iso 73 were shown to have harboured these KRAS mutations from eight organoid lines sequenced. Another frequent mutation associated with CRC is a p.G12D mutation which results in the expression of constitutively active KRAS, and was identified within 2 of our organoid lines.

Table 3.3 Organoids harbour CRC-relevant mutations

Table depicting key gene mutations (by amino acid) in a cohort of organoids.

DNA extraction was carried out by Dr. Andrew Hollins (Dale lab). OGT (Oxford Gene Technologies) performed NGS and subsequent analysis of 8 organoid lines. COSMIC database comparison analysis was carried out by Dr. Kenneth Ewan (Dale lab).

Iso	APC	CTNNB1	BRAF	ATM	EGFR	ERBB2	KRAS	TP53	PIK3CA	PTEN
34	p.E1451	No COSMIC record	p.K601E	No COSMIC record		p.T862A,p.P1170A	No COSMIC record			
48	p.R259W	p.S33F		No COSMIC record		p.P1170A			p.E542V	
49	p.Q1447 p.R1450						p.G12D	p.R248Q	No COSMIC record	
50	p.E1286 p.R232						p.G12V	p.R248Q		
72	p.Q1291						p.G12V			
73	p.Q1228						p.G12V	p.R248R		
75	No COSMIC record	p.L46P	p.V600E p.D693N	No COSMIC record				No COSMIC record	No COSMIC record	No COSMIC record
78	p.R876 p.E1451	p.WC38C				p.P1170A	p.G12D	p.H193D	No COSMIC record	

3.2.4 Tumour organoids demonstrate highest metabolic activity within the first seven days of culture after seeding

To ascertain optimal conditions for maximal organoid viability to facilitate subsequent drug titration experiments, metabolic readouts were established from organoids in culture, as opposed to relying on basic parameters, such as organoid size, as an indication of growth.

Organoids (Iso 34) previously established in culture were split by trituration and embedded within growth factor-reduced matrigel. Media changes occurred every 3 days, or as necessary. To determine a live readout of metabolic activity, as a proportional measure to the number of viable cells Presto Blue (Sigma), a resazurin-based reagent that is reduced in the presence of metabolic activity in surrounding media of cells, was added to cells in culture at specific time points over a period of 14 days. As depicted in Figure 3.9, repeated fluorescent readouts of metabolic activity was shown to reach a peak within the first seven days of culture following routine organoid trituration. There was no significant increase in mitochondrial activity observed thereafter, indicating that exponential growth took place within the first seven days of culture.

Haematoxylin & Eosin (H&E) stained sections of Iso 34 cultured in parallel for 14 days demonstrated that organoids were composed of seemingly necrotic cores when cultured for a period of 14 days. This would suggest that a number of cells had been shed into the central lumen of the organoid and / or that the structures became too large for sufficient nutrient access to cells in the centre. Collectively, this data indicates a period of 7 days in culture is sufficient for optimal organoid growth, a prerequisite required for generating optimal output from patient material in terms of expansion in culture.
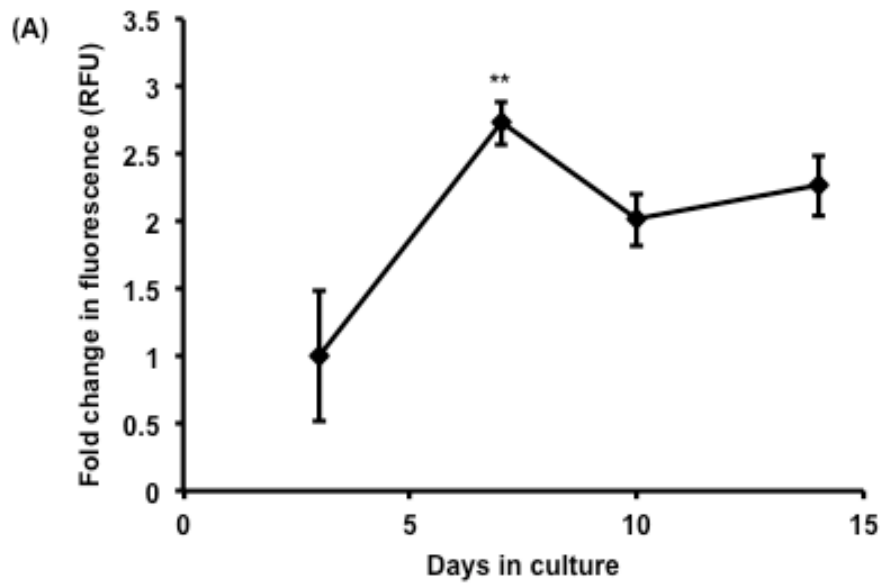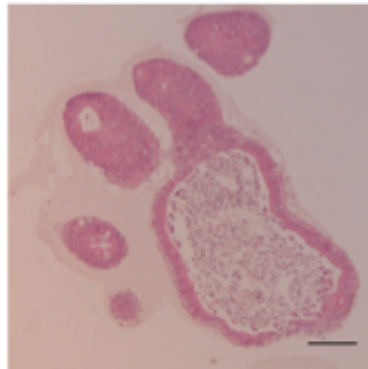
Figure 3.9 Metabolic activity of organoids increases within the first seven days of seeding.
Iso 34 organoids were split by trituration, embedded within growth factor-reduced matrigel and seeded within round, clear-bottomed 96 well plates in defined media conditions. **(A)** Presto Blue reagent was administered to organoids at day 3,7,10,14 following seeding, prior to collecting fluorescence measurements from supernatant on a Fluostar OPTIMA platereader (BMG Labtech) with an excitation of 570nm, emission 610nm as an indication of metabolic activity. Data is shown as fold change in fluorescence signal from first measurement (day 3) in culture ± standard deviation (n=4 wells). **p ≤ 0.01 using a paired student's t-test **(B)** Following 14 days in culture, Iso 34 organoids were fixed (4% PFA), embedded within paraffin, and sectioned prior to hematoxylin and eosin staining. Scale bar 50 μm.

3.2.5   Organoid formation from single cells

Given previous indications that organoid size is not necessarily correlated to the number of metabolically active cells within a structure, it was investigated whether further regulation of organoid size could be beneficial for generating organoids containing viable, proliferating cells. Here, the organoid line Iso 34, an organoid line generated within the first stages of this study, was used to explore whether organoids, enzymatically digested to near-single cell could recover appropriately to form elaborate, viable structures for subsequent assays.

Established cultures were dissociated using TrypLE (Life Technologies) and seeded at an approximate density of 2000 cells in 20μl of Matrigel in 96 well clear, round bottomed plates (Nunc), and incubated in Basal '7+' Media, containing 10μM ROCK inhibitor Y-27632 for three days. ROCK inhibitor Y-27632 has previously been implemented in promoting survival of intestinal epithelial cells which are likely to undergo anoikis following disruptive procedures such as trypsinisation (Ashley et al. 2014; Dr.Mairian Thomas - personal communication and PhD thesis). Iso 34 organoids were formed within less than 24 hours of culture, and further developed to form more lobular structures representative of previous structures identified from organoids cultured by trituration. It is worth noting that trypsinisation alone is unlikely to obtain definitive single cells, and that many doublets and cell aggregates would remain which could also influence growth rates. Over a period of 15 days in culture, organoids developed to form morphologically similar structures to those previously obtained by whole trituration.

To assess proliferation rates of single cell-derived organoids, quantitative analysis of mitochondrial activity was taken using Presto Blue. Multiple readouts were taken from the same wells (n=4 technical replicates) at different intervals over 14 days, with changes in media taking place at each time point. Fluorescent readouts were measured using a Fluostar OPTIMA (BMG Labtech™) platereader at excitation of 570nm and emission of 610nm. As depicted in Figure 3.10(B), the greatest increase

in mitochondrial activity was observed between days 2 and 7 in culture, with no significant increase in proliferation thereafter (p=<0.05, student's t-test). Morphologically, single cells formed whole structures capable of proliferation, as indicated by positive Ki67 immunostain in Iso 34 organoids at day 7 in culture.
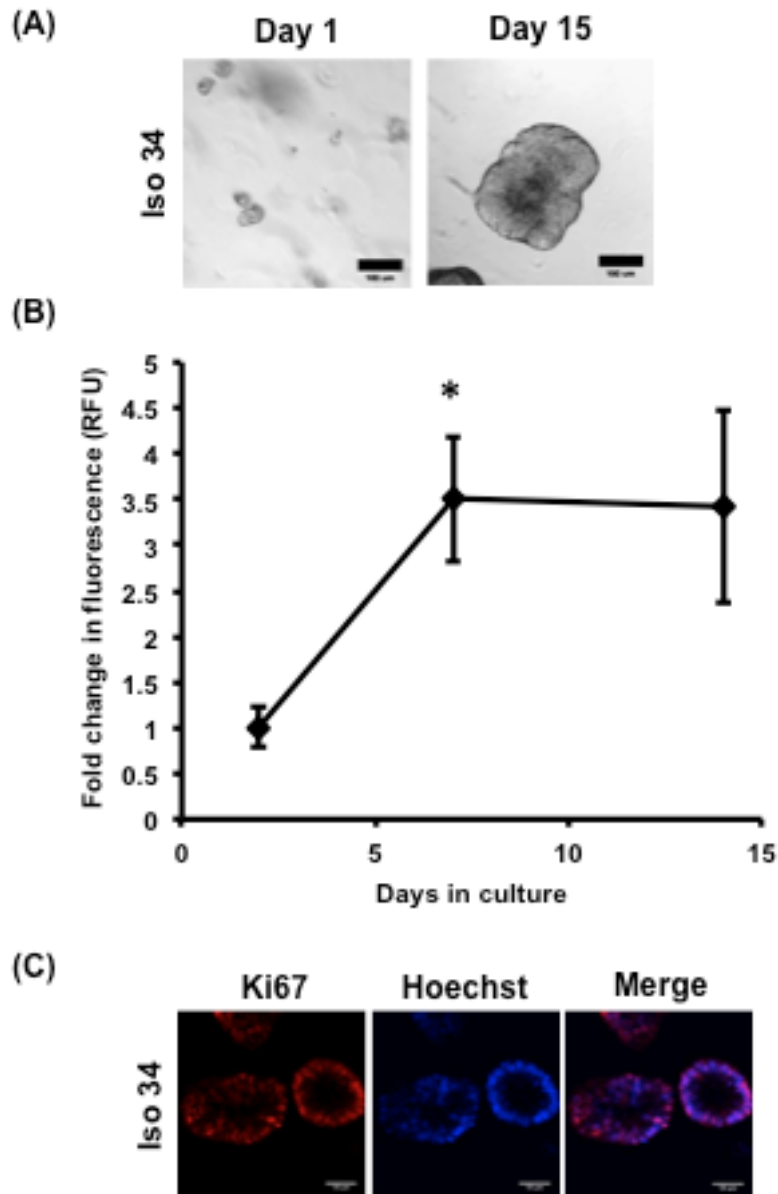
Figure 3.10 Iso 34 proliferation from near-single cells.

Iso 34 organoids were trypsinised to near-single cells and seeded at 2000 cells per 25 μl of matrigel in round, clear-bottomed 96 well plates. 7+ media conditions were applied, with ROCK inhibitor (Y-27632) included for 6 days to aid cell recovery from the trypsinisation process. **(A)** Representative images of organoids at 24 hours (day 1) and 15 days following seeding respectively. Scale = 100μm. **(B)** Proliferation was assessed at different time points in culture using a presto blue cell viability kit. Presto blue was added to media in wells and incubated for 3 hours, prior to fluorescent readings. Graph displays the fold change in fluorescent signal from spent media collected at each time point, normalized to first measurement. * $p ≤ 0.05$ (n=1, 4 technical repeats) from student's t-test **(C)** Confocal images of immunofluorescent staining of Iso 34 organoids derived from single cells, staining for Ki67. Nuclei were counterstained with Hoechst.

3.2.6 Optimal seeding densities are a necessity for maximal organoid viability

A plethora of factors have the potential to influence the rate of organoid growth and number of viable cells in culture. Previous studies in the literature have demonstrated the potential of influencing cell fates of intestinal stem cells by controlling self-renewal and differentiation (Yin *et al.* 2013). Furthermore, the niche environment that tumour organoids themselves generate has shown to be a deciding factor in dependency on exogenous growth factors within culture (Fujii *et al.* 2016a). It would therefore be a fair assumption that subsequent organoid formation and growth can be influenced by the number of cells seeded initially. To enhance organoid compatibility with a high throughput assay format, optimisation of appropriate seeding densities was performed using an organoid line, Iso 50.

Trypsinised cells of previously established organoids (Iso 50) were seeded at a range of densities within white clear-bottomed 96 well plates (n=6 wells). A range of seeding densities (100 - 1000 cells/ µl of Matrigel) within a total volume of 9 µl of matrigel were plated within each well. Cell seeding was based on calculations of viable cell counts, by counting trypan blue-negative stained cells only. Following a 7 day incubation in '7+'media, a Cell Titer Glo 3D endpoint assay (Figure 3.11) was implemented, in which the quantitation of ATP in relative luminescence, and thus quantity of metabolically active cells per well. If there were indeed an optimal seeding density for tumour organoids, it would be expected that under- and over-seeding could be detrimental to the balance of important secretory niche factors upon which organoids rely which could harbour growth.

Results demonstrated an overall increase in the relative luminescence signal obtained with increasing number of cells seeded . ATP readouts were however shown to plateau beyond an initial seeding density of of 500 cells/µl of Matrigel. A standard curve of Cell Titer Glo 3D measurements obtained from known ATP concentrations generated simultaneously indicated that the relative luminescence

values obtained from cultures were still within the range of the assay window, as shown in Figure 3.11 (**A**). This would therefore indicate that organoids, beyond a threshold seeding density of 500cells/µl of Matrigel, were perhaps restricted by limiting factors for growth such as physical space and nutrient access.

Organoid formation efficiency, as calculated by the percentage of organoids formed from viable single cells, was somewhat inversely correlated with seeding density as depicted by Figure 3.11 (**E**). Since trypsinisation of organoids are unlikely to form absolute single cells, the proportion of doublets or triplet cells could influence the rate of growth of organoids. However, it is more likely that a lack of physical space within a well would prevent such efficient organoid formation as they compete for nutrient access. Taken together, the optimal seeding density for plating was established at 400 cells/µl of matrigel. With the advantages of single-cell seeding formats clear, this density was incorporated as a standard across all organoid lines to incorporate sufficient number of organoids per well, maintaining maximal yields and viability.

Using established seeding densities, organoids formation efficiencies from three different isolations (Iso 34, Iso 49 and Iso 50, Figure 3.12) were calculated over three consecutive passages to ensure that growth characteristics remained stable for the purposes of experimental repeats. Despite some variation observed in formation efficiencies of Iso 50 organoids, overall it was deduced that organoid behaviour remained largely stable over passages with fluctuations more as a result of minor variations in seeding accuracy from manual counts.

Overall, these data demonstrate the establishment of optimal seeding densities required to facilitate future drug titration experiments. Although data were only collected on the basis of one organoid line, it is worth noting that the consistency from one assay to the next across organoid lines was also a factor to consider to facilitate further drug titration experiments.
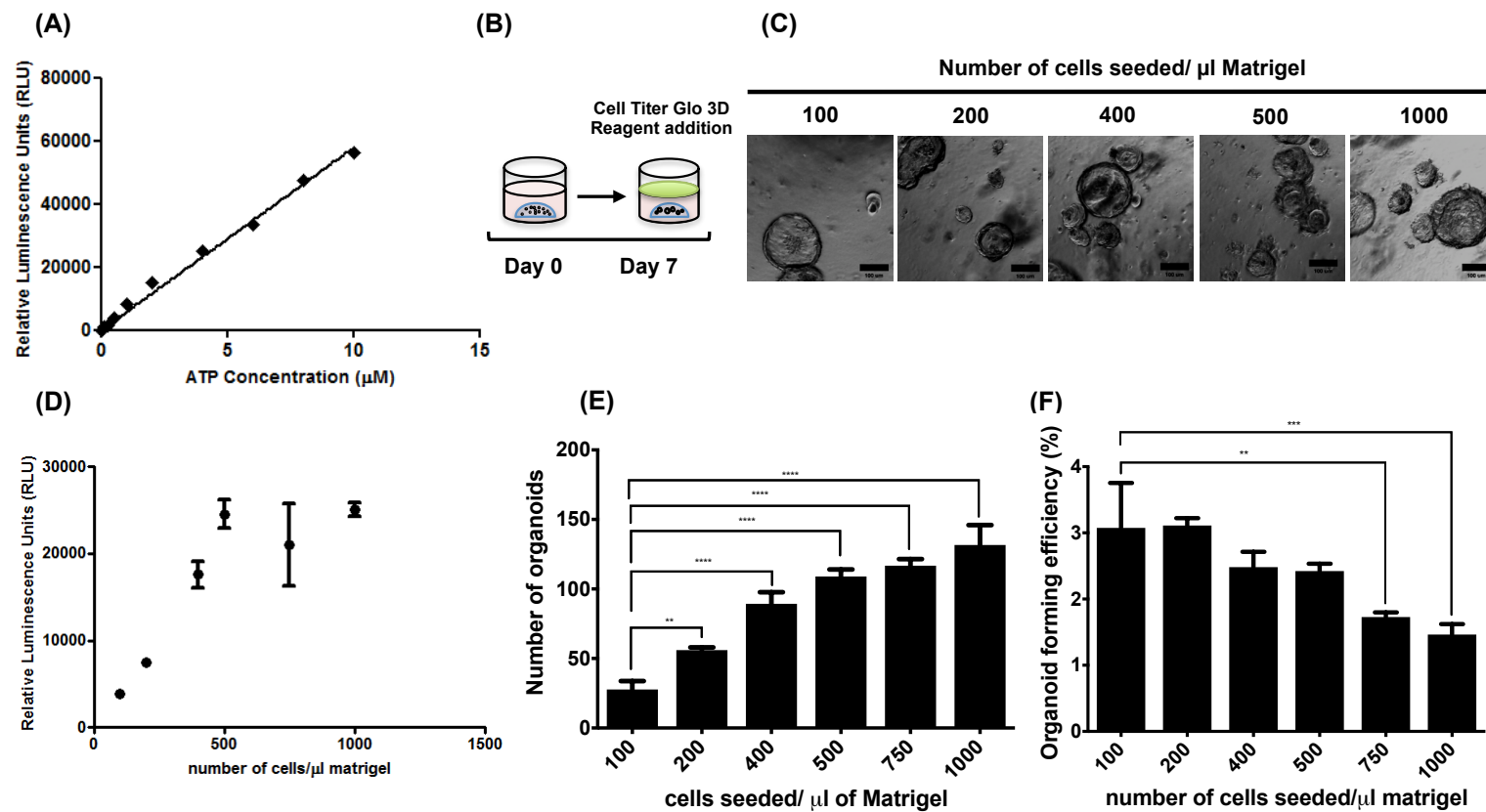
Figure 3.11 Assigning optimal cell seeding density for optimal organoid growth from single cell.

Iso 50 organoids were dissociated, seeded at a range of densities (100-1000 cells per µl of matrigel) and cultured in '7+' media before ATP measurements (**A**) Standard curve measured from known ATP concentrations within media measured using the Cell Titer Glo 3D reagent (n=3 technical replicates). (**B**) Representative images of organoids seeded from a range of densities (day 7), Scale bar = 100 µm. (**C**) Cell Titer Glo 3D readouts from organoids at day 7, (n=6 well). (**D**) Average number of organoids counted (n=6 wells) using GelCount software after 7 days in culture. (**E**) Average organoid formation efficiency generated per known viable cells seeded, per well. Data are presented as mean ±standard deviation, whereby (n=6) replicate wells. *$p<0.05$;**$p<0.01$;***$p<0.001$, ANOVA with Tukey's post hoc comparison.
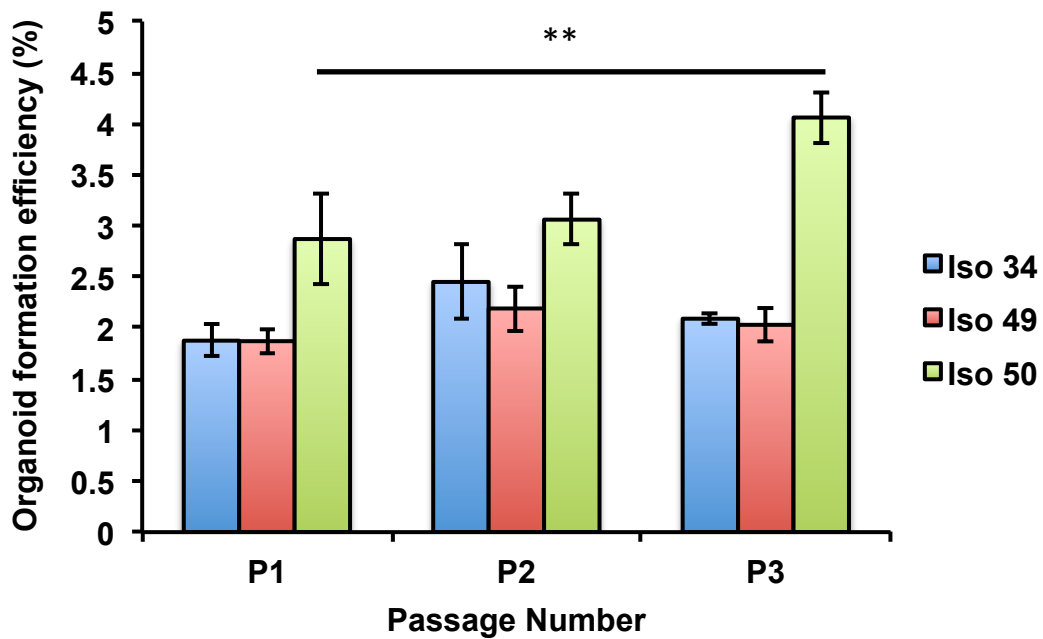
Figure 3.12 Organoid formation efficiency stability over three consecutive passages
The organoid lines (Iso 34, Iso 49, Iso 50) were digested with TrypLE, prior to plating at a density of 400 cells/ μl of growth factor-reduced matrigel within white, 96 well plates , and overlaid with defined media. Organoid formation efficiencies were calculated by the percentage of organoids formed from the known number of cells seeded per well. Data shown from n=3 technical replicates ± standard deviation. *$p < 0.05$;**$p < 0.01$;***$p < 0.001$, Two way ANOVA with Tukey's multiple comparison test.

3.2.7 Organoids seeded from single cells enhance assay quality in a 96 well plate format

To determine whether robust, reproducible treatment-dependent responses could be measured in tumour organoids in a high throughput setting, a proof-of-principle assay format was established, in which organoid viability was quantified following treatment with 5-Fluorouracil, a current standard of care (SOC) chemotherapeutic for CRC.

Iso 34 cultures were established from freshly dissociated cells and were incubated in basal '7+' media containing 10μM of ROCK inhibitor for the first three days in culture to enhance organoid recovery from single cells. Given that a log phase of growth was previously observed during the first seven days following seeding, treatment was administered during this period to ensure the inhibitor would exert maximal impact on overall organoid viability. Following three days of culture from dissociated cells, DMSO control conditions (0.1% in media) and a titration dose of 5FU, ranging from 9.76 nM to 2500 nM, were applied within media. Treatments were administered for a total of 4 days prior to an endpoint Cell Titer Glo 3D viability readout, whereby luminescence values were used to quantify ATP levels as an indication of the number of metabolically active cells present. Representative images of organoids acquired at day 5 and day 7 in culture (2 days, and 4 days following treatment, respectively) demonstrated that 5-FU exerted effects in a dose dependent manner within 2 days of treatment at highest concentrations; multiple structures demonstrated a lack of integrity, with smaller cells and an overall darker appearance, indicative of increased cell death.

The obtained results indicate that the number of viable cells were treatment-dependent, as demonstrated in Figure 3.13 (A). IC_{50} values, the concentration of compound required to induce a 50% inhibition of luminescence readouts compared to control conditions, were obtained from the dose response curve shown in Figure

3.13. Based on Cell Titer Glo 3D readouts, the IC_{50} values identified for Iso 34 organoids treated with 5FU for 4 days were 120 nM.

Taken together, these results demonstrated that a uniform population of organoid sizes during initial plating generated relatively robust assay readouts in terms of well-to-well variation, which could be quantified in response to treatments, further validating such assay formats for subsequent studies. Attempts to recapitulate this assay format in triturated organoids as opposed to those seeded from single cells (data not shown) further emphasised the importance of organoid size regulation in delivering more reproducible results.
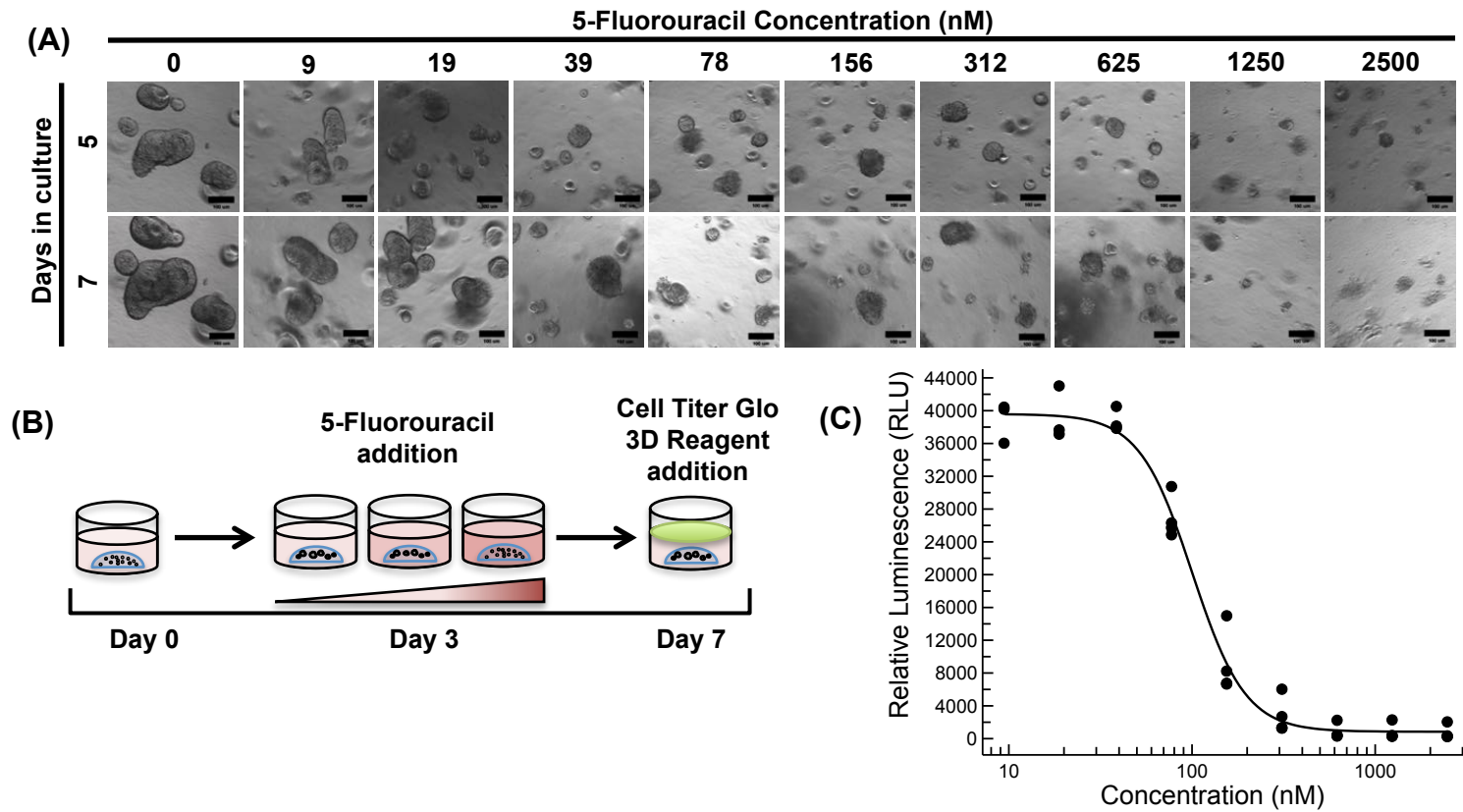
Figure 3.13 Effects of 5-FU treatment on Iso 34 organoids derived from dissociated cells.

Organoids were plated in 96 well plates at an optimal density of 400 cells/ μl of Matrigel, and treated with a two fold titration range (9 nM – 2500 nM) of 5-Fluorouracil, or 0.1% DMSO control within media, following three days in culture. (**A**) Representative organoid images at day 5 and 7 in culture. (**B**) Representative diagram of optimised assay format. (**C**) Drug-dose response curve generated from an endpoint Cell Titer Glo 3D viability assay (mean ±± standard deviation, n=3 wells) IC$_{50}$ values generated were of 120nM. (n=3 wells)

3.3 Summary

Here, the establishment and continuous culture of a cohort of patient-derived CRC organoids was explored to facilitate drug studies further discussed in chapters 4 and 5. Appropriate isolation protocols and media conditions propagated the generation of organoids that retained key histological characteristics from parental tumour sections generated from an array of TNM stages. A genotyped cohort were also shown to harbour CRC-relevant mutations, further highlighting their utility as a relevant model system for CRC therapeutics.

Work described here, using a subset of organoids to optimise suitable assay formats, demonstrated that organoids established from dissociated cells generate relevant, viable structures that could expand sufficiently from little material to yield maximal organoid outputs; facilitating the transition towards a high-throughput system. Reproducibility both within and across assays was also explored; plating conditions enabled sufficient assay sensitivity to highlight treatment-dependent responses, whilst the generation of sufficient organoid freezing protocols enables repeats to be performed within a few passages.

Furthermore, this preliminary work provides a strong foundation for subsequent analysis formats that can be further adapted to explore organoid-inhibitor relationships, demonstrated in Chapters 4 and 5, validating this amenable system for future compound testing.

4 Towards modelling a clinical trial *in vitro*: optimisation and utilisation of patient-derived colorectal organoid models

4.1 Introduction

The stratification and targeted treatment of patients according to the molecular profile of their tumour has shown some promise for the future of CRC therapeutics. Nevertheless, genomic profiling as a basis for therapy underestimates the complexity of signalling pathways in tumour cells, and therefore have limitations to accurately predict patient outcomes in the clinic (Pauli *et al.* 2017). Current methods to assess functional effects of therapies rely heavily on 2D clonal culture models as pre-clinical proxies for patient tumour drug sensitivity and responses. However, cell line models fail to represent some tumour subtypes and lack both phenotypic cellular and genotypic heterogeneity, limiting their relevance to tumours assessed within clinical trials.

The generation of a 3D colorectal organoid platform could thus serve as an alternative *in vitro* model system to provide a better representation of tumour biology in a more '*in vivo'* like context. Given the volume and complexity of pre-clinical data required to support clinical trials, further information is needed to support the utility of organoids in the context of live-cell biomarker readouts. The data presented here therefore aims to ensure whether sufficient data, through the use of organoids, can be generated to guide subsequent trial designs, complementary to genomic analyses. Within this study, the FOCUS 4 clinical trial was used as a basis to examine whether organoids could be utilised as suitable tools to capture beneficial *in vitro* data.

Employing methods described in chapter 3, the work presented in this chapter details advances made towards an organoid screen against a panel of biomarker-driven therapies relevant to the FOCUS 4 trial. To achieve this, a cohort of organoids

were treated with agents used in a number of arms of FOCUS 4, and assessed using viability and imaging analysis readouts. The outcome of this purely *in vitro* study should allow us to make a preliminary assessment of the value of specific tumour biomarkers as indicators of drug response in CRC organoids. Furthermore, this work should enable us to eventually cross-compare organoid responses with a population of independent patients who have been stratified with the same biomarkers within the FOCUS 4 trial. This will allow us to assess whether organoid responses, have the potential for independent power, from that of biomarkers, in the assessment of patient responses.

4.2   Results

As previously discussed (section 1.5.1), the MRC FOCUS 4 trial is a randomised multicentre clinical trial that aims to stratify patients according to the molecular profile of their tumour and treat them accordingly with hypothesis-driven therapies. As such, there are several potential drug candidates targeting several pathways within tumour development. Following genotyping of organoids, described in chapter 3, work described here aimed to characterise organoid responses to each relevant arm of the FOCUS4 trial, essentially enabling a small scale *in vitro* study. The main aim of this work is to establish whether organoid responses might be incorporated into future clinical trial designs.

4.2.1 Cell cycle inhibitors induce cell cycle arrest in CRC organoids.

As previously discussed in section 1.5.4, deficiencies in DDRs are contributing factors in tumour initiation and progression, and are therefore an attractive target for therapy. Several targets of the DDR pathway have been identified and subject to manipulation by many drug candidates, in order to induce synthetic lethality within tumour cells. Targets within the pathway, Wee1 and ATR, are currently under investigation within the FOCUS 4 clinical trial to assess whether selective compounds (Mk1775 and AZD6738) will result in improving progression free survival in patients harbouring *KRAS*/*TP53* and *ATM* mutations, respectively.

In order to validate whether organoids can be used within an *in vitro* trial setting, a selection of organoids that were well established in culture (as listed in Table 3.3) were administered with a Wee1 inhibitor (MK1775) and ATR inhibitor (AZ20, an analogue of AZD6738 suitable for *in vitro* use) to recapitulate two treatment arms of FOCUS 4, and assessed for readouts of viability as a representation of tumour growth inhibition. Preclinical *in vitro* and *in vivo* data have previously demonstrated the efficacy of AZD6738, particularly (but not exclusively) within ATM-deficient tumours, generating IC_{50} values of less than 1 µM in cell-based assays (Kim *et al.* 2017). MK1775 has also demonstrated promising pre-clinical results as a DNA-damaging agent (Kreahling *et al.* 2013).

A set of organoids previously seeded from single cells, at day 3 in culture, were administered with a titration of MK1775 (0 nM – 5000 nM), AZ20 (0nM- 5000 nM) as well as a DMSO control (0.1%), within the tailored media conditions as required for each organoid line (Table 3.2). Following 4 days of exposure to compounds, an ATP endpoint viability readout was generated from each condition and plotted to generate dose response curves per organoid line (data not shown for all lines). From each curve, EC_{50} (half maximal effective concentration) values were obtained from n=3 independent experiments, as listed in Table 4.1. All 8 organoids tested

demonstrated a range of sensitivities to both compounds with EC_{50} values in the range of 0.3 μM – 21 μM for AZ20, and 0.1 μM – 1 μM for MK1775, as indicated in Table 4.1. It was clear that Iso 48, Iso 50 and Iso 78 were the most sensitive organoid lines, mirroring EC_{50} values obtained in previous studies using LoVo colorectal adenocarcinoma cells (Foote *et al.* 2013). Iso 49 was shown to be the most resistant organoid line, generating EC_{50} values of approximately 21 μM, suggesting that any changes in organoid viability were only obtained at the highest doses. Whilst the degree of sensitivities varied, overall, all organoids were responsive to Wee1 inhibition, obtaining cellular EC_{50} values in a range identified previously in the literature, of approximately 0.08 – 0.3 μM (Hirai *et al.* 2009). Overall, given that many organoids harboured *TP53, KRAS* or *ATM* mutations, further studies using a larger sample cohort and appropriate controls such as wild type organoids would be beneficial to investigate whether ATR and Wee1 inhibition sensitivity is correlated with high levels of DNA damage.

Representative images from a sensitive organoid line, Iso 72, as illustrated in Figure 4.1, demonstrated the presence of extensive cellular debris following 4 days of treatment, indicative of cell death, following treatment with both AZ20 and MK1775. This in turn was concordant with data from ATP endpoint viability readouts at day 7 in culture. To further explore the impact of MK1775 and AZ20 treatment upon organoid growth, Iso 72 organoids were further scored according to number of Ki67 positive cells per organoid. Following 4 days of treatment, organoids were stained with a nuclear (Hoechst) and proliferation (Ki67) marker, prior to acquisition of z-stacks on a confocal microscope. Quantification was facilitated using IMARIS software (BITPLANE), as an automated counting tool to identify nuclei, as well as positively stained cells. The number of Ki67-positive cells were recorded as a percentage per organoid, with a minimum of 5 organoids counted per condition. Within control (DMSO, 0.1%) conditions, it was shown that 80%±13% of cells within organoids were positively immunostained for Ki67. Treatment with 150 nM MK1775 resulted in a significant reduction in proliferation, whereby an average of 57%±17% of cells per organoid were Ki67 positive (p ≤ 0.01, Welch two sample t-test). Following 4 days of treatment with AZ20, a similar trend was observed, as shown in

images acquired (Figure 4.2). However, given the overall diminished organoid size induced by drug addition, compared to control conditions, smaller organoid structures were more readily lost in wash steps required as a result of technical artefacts of methodology, limiting the number of organoids that could be counted.
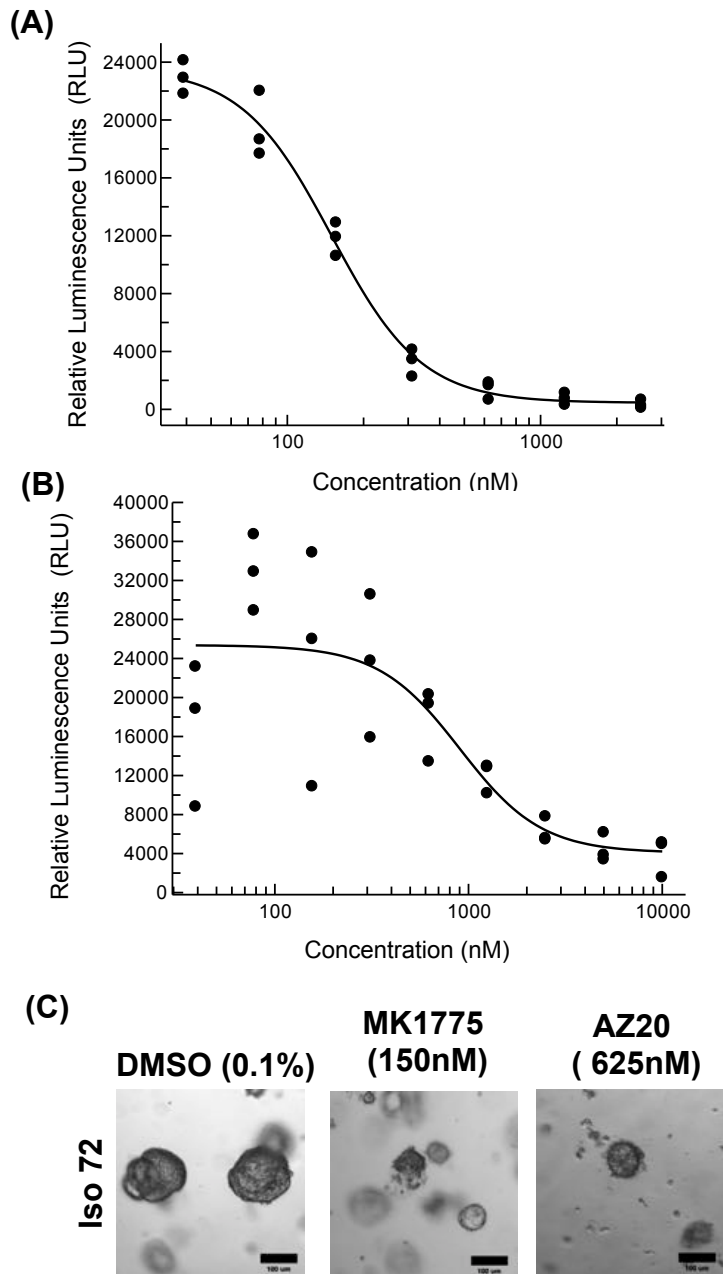
Figure 4.1 Iso 72 organoids respond to a Wee1 and ATR inhibitor

Freshly dissociated Iso 72 organoids were seeded in growth factor-reduced Matrigel at a density of 400 cells/ μl Matrigel and overlaid with media. Following three days of recovery, a titration of (**A**) MK1775 (19 nM – 5000 nM) or (**B**)AZ20 (39 nM – 10 μM) or DMSO (0.1%) negative control were supplemented within media. Following 4 days of treatment, a Cell Titer Glo 3D assay was performed to quantify relative ATP levels per well (Relative Luminescence Units, n=3). (**C**) Representative microscope images at day 7 following treatment with DMSO, MK1775 or AZ20. Data shows representative dose response from triplicate wells.
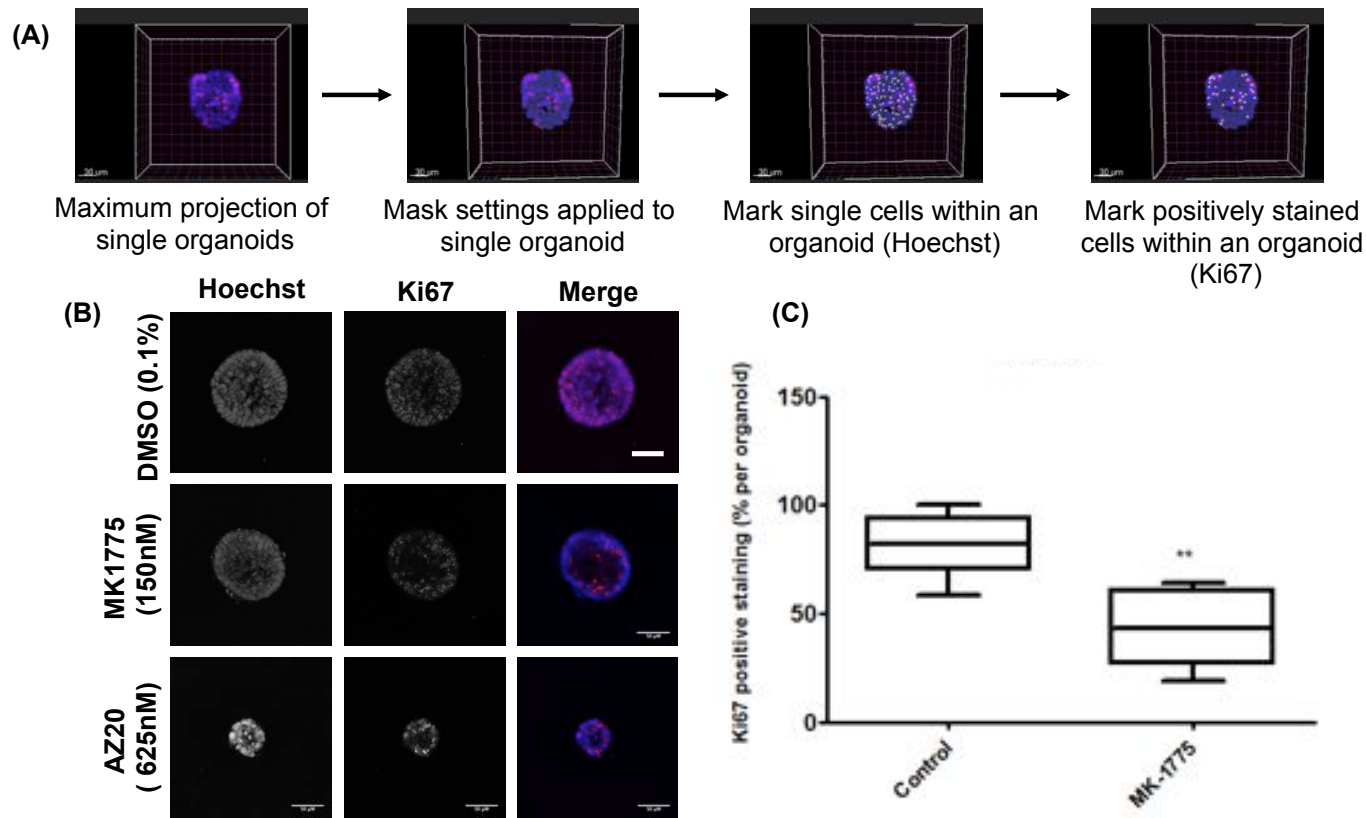
Figure 4.2 Scoring proliferation in CRC organoids following treatment with Wee1 inhibitor, ATR inhibitor.

Iso 72 Organoids were seeded as single cells prior to treatment with MK1775 (150 nM), AZ20 (625 nM) and DMSO (0.1%) within media for four days, then fixed with 4% PFA, prior to immunostaining with Hoechst and Ki67. Image z-stacks of organoids were captured on a confocal microscope and then quantified using IMARIS software **(A)** Flow chart depicting counting of whole 3D organoids using IMARIS software **(B)** Representative images of organoids treated and stained with Ki67 and Hoechst. Scale bar = 50 μm. **(C)** Quantification of the average number of Ki67 positive cells per organoid, n= 5-15 organoids. Significance of number of proliferating cells were calculated using Welch two sample t-test and Mann Whitney two-tailed test *p≤0.01, ** p≤0.05.*Images and IMARIS counts were collected and analysed by Kate Densley under my supervision.*

4.2.2 High-throughput phenotypic screening for robust quantification of responses to DDR inhibitors.

Despite the results obtained from proliferation counts of organoids exposed to AZ20, the extent to which measurements of cellular proliferation could be interpreted biologically was limited for several reasons. Firstly, the technical process involved limits the number of organoids counted as many smaller organoids, as a result of growth inhibition, are washed away during processing. This was particularly the case for Iso 75 organoids, as the structures were generally smaller in culture than organoid from other lines (data therefore not shown). This was also a relatively low-throughput readout to characterise drug effects. In order to further characterise the effects of cell cycle inhibitors upon organoids at greater detail to overcome limitations previously introduced, introducing stains that would be more compatible to fewer washes, a high throughput 3D image based screening process, in collaboration with OcellO (Leiden, Netherlands), was implemented. Such technology enabled the examination of morphological parameters from individual nuclei to whole organoid population levels that can be quantified.

All organoids were therefore prepared as single cells and cultured in 384 well plates in optimal media conditions (as previously outlined in Table 2.1) for 3 days, then treated with a titration of AZ20 and a DMSO (0.1%) control. Following 4 days of treatment, organoids were fixed and stained simultaneously with 4% PFA, Nuclear stain (Hoechst) and cytoskeletal stain (TRITC-Phalloidin), as described in (Di, Klop, Rogkoti, Devedec, Water van de, *et al.* 2014). Wells were then washed twice with PBS following fixation.

Individual z-stack images of whole 384 well plates were collated on a MetaXpress® high-content microscope at OcellO, then inputted into the novel OMiner analysis software developed by OcellO, as detailed previously in Chapter 2. Briefly, projections of F-actin and hoechst from individual z-stacks were used to extrapolate masks of individual organoids, internal lumen structures and nuclei from each well.

Image segmentation and filters were applied to distinguish individual objects per well, and enhance noise suppression to balance sensitivity of analysis. Relevant masks were then used to acquire approximately 650 quantifiable morphological features, as well as fluorescence intensities per channel (Di, Klop, Rogkoti, Devedec, Water van de, *et al.* 2014). Data from individual organoids were pooled on a well-by-well basis, with data from individual wells (minimum of 8 per condition) then gathered to yield average parameter readings per condition.

Following ATR treatment, several parameters were measured as an indication of organoid response. It was shown that ATR inhibition resulted in a slight decrease in overall organoid area, limiting complex internal features as shown in control conditions. Figure 4.3 depicts the effects on phenotypic profile of Iso 75 as an example. Assessing organoid mean area as a response to treatment, as previous data indicate, is somewhat limiting, as structures can appear larger as a result of accumulated cellular debris. Given that alterations in nuclear morphology have previously been associated within activation of cell death (Eidet *et al.* 2014; Edmondson *et al.* 2014), and the role of ATR inhibition within this response, the effects of AZ20 on nuclear morphology was studied. Several morphological hallmarks of apoptotic events upon the nucleus have previously been reported in the literature, such as chromatin condensation, visualized by Hoechst, overall nuclear shrinking as well as an increase in nuclear circularity (Ziegler and Groscurth 2004). Here, it was found that similar features were influenced in a dose-dependent manner by ATR treatment. Nuclei profiles of Iso 75 organoids revealed that an increasing concentration of AZ20 were correlated with an increase in average nuclear circularity, a decrease in the average number of nuclei per organoid structure, as quantified from individual masks nuclei per organoid. Taken together, it was found that there was a convincing correlation between hallmarks of apoptosis and reduction in overall organoid area.
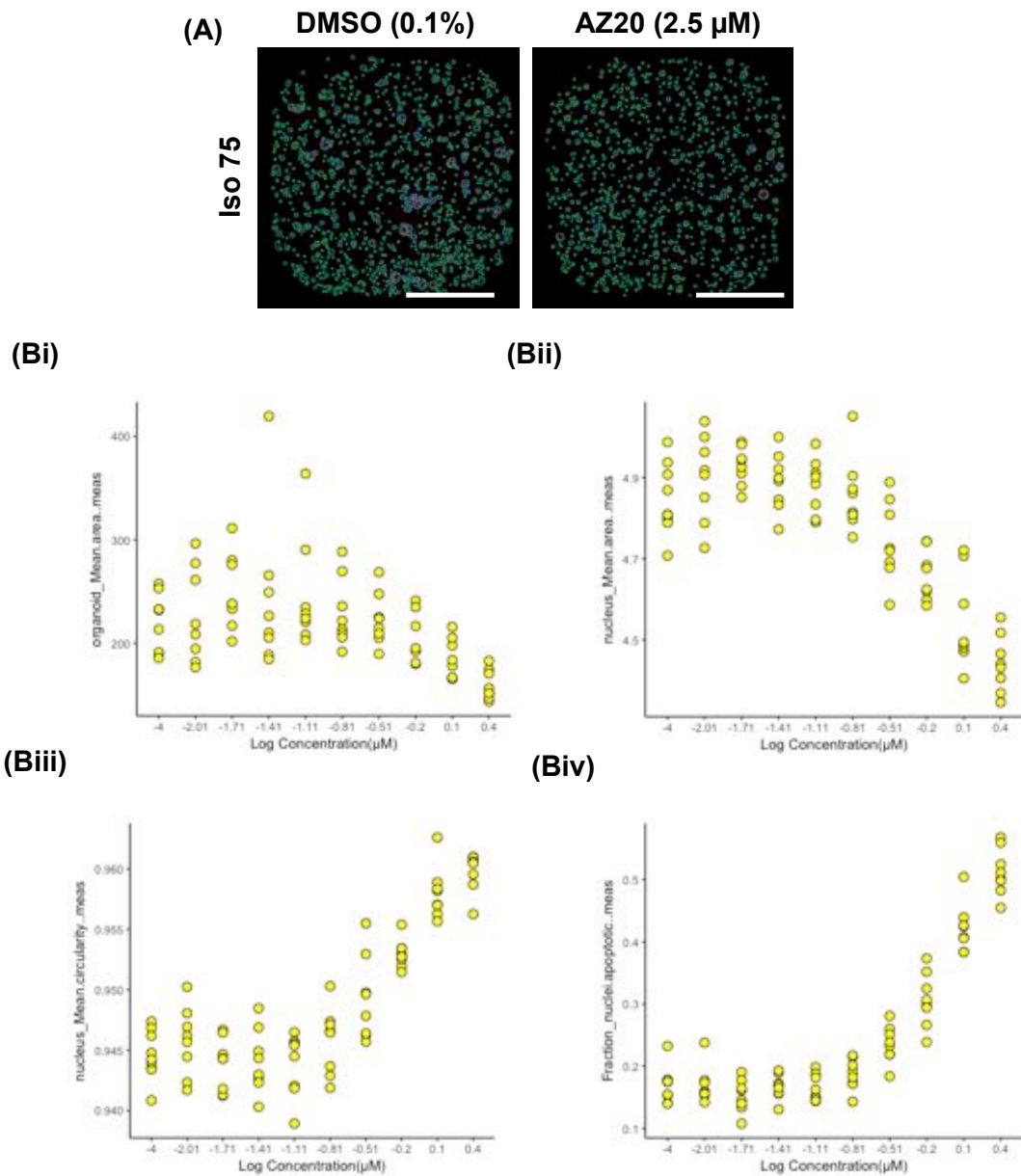
Figure 4.3 Phenotypic analysis reveals nuclear-dependent effects of ATR inhibitor treatment within CRC organoids.

Iso 75 Organoids were seeded as single cells within 384 well plates prior to treatment with a dose titration of AZ20 (0nM – 2500 nM) and DMSO control (0.1%) within media for four days, then fixation and staining with Hoechst and Phalloidin. Image z-stacks of organoids were captured, and parameters were quantified by OcellO. (A) Representative images of a well of organoids treated with AZ20 (2.5 µM) and DMSO control, and masked according to Hoechst and Phalloidin channels. Hoechst channel information was used to generate nuclear profile of organoids. (Bi-iv) Scatterplots of measurements acquired of (i) average organoid area(ii) average nucleus area and (iii) average nucleus circularity (iv)fraction of apoptotic cells per organoid, per dose titration within Iso 75 organoids. *Images captured at OcellO.* Scale bar = 1mm.

4.2.3 Organoids demonstrate differential sensitivities to an aspirin metabolite irrespective of *PIK3CA* mutation status

As discussed within Chapter 1 (1.5.3), retrospective studies within the literature have associated the reduction of tumour burden in CRC patients harbouring *PIK3CA* mutations when treated with aspirin compared to non-*PIK3CA* mutant tumours. The FOCUS 4 trial aims to identify whether *PIK3CA* can be used as a biomarker for aspirin responsiveness, and whether aspirin treatment will ultimately benefit patients harbouring *PIK3CA* mutations. *In vitro* studies have demonstrated a concurrent effect of many non-steroidal anti-inflammatory drugs (NSAIDs), including aspirin, upon colorectal cancer cells, suggesting that such compounds predispose tumour cells to apoptotic events. Here, organoids were administered with the active metabolite of aspirin, salicylic acid, and assessed for responses.

A set of organoids were digested to (near) single cells, counterstained with a dual Acridine Orange/Propidium Iodide live/dead cell stain and counted using an automated LUNA-FL™ fluorescence cell counter. 400 cells/ µl matrigel were then plated in 96 well plates, overlaid with optimum growth media per line, and incubated for 3 days. Orally-administered low dose aspirin can reach a peak plasma concentration of approximately 7µM (Alfonso *et al.* 2014). Organoids were therefore subject to treatment of a dose titration range of salicylic acid between 0.19 nM – 5 µM, as well as a volume matched DMSO control (0.1%) within triplicate wells for a further 4 days. An endpoint Cell Titer Glo 3D viability assay was implemented, in which the quantification of ATP and thus metabolically active cells per well demonstrated that treatment salicylic acid induced a clear dose-dependent response in some organoid lines. Each experiment was composed of a minimal of three technical replicates per condition. Growth curves generated from Cell Titer Glo 3D readouts of Relative Luminescence Units indicated that multiple organoid lines were responsive to treatment, generating average IC_{50} values 0.4 µM – 5 µM, as indicated in Table 4.1. Interestingly, organoids were more sensitive to effects of salicylic acid in comparison to CRC cell lines such as SW480, HT29 and HCT116, which have previously shown sensitivity at IC_{50} values ranging from 2.5 - 5mM (Pathi *et al.* 2012).

As shown in Figure 4.4, it was observed that Iso 73, was the most resistant organoid to salicylic acid effects (no EC_{50} value obtainable from a drug dose response curve). Conversely, Iso 72 organoids, as represented by Figure 4.4, demonstrated a degree of sensitivity to aspirin treatment, with EC_{50} values of approximately 2 μM (n=3 independent experiments) obtained. Having shown responses within ATP assays, Iso 72 was further counterstained with the proliferation antibody Ki67 following 4 days of treatment. Counts obtained demonstrated that 1.2 μM salicylic acid induced a reduction in the number of Ki67 positive cells (from 80% proliferation per average organoid to overall 40% proliferating cells per organoid) on an organoid-by-organoid basis compared to matched DMSO control.

As indicated in Chapter 3, Iso 48, Iso 49, Iso 75 and Iso 78 were shown to harbour *PIK3CA* mutations, and therefore were expected to respond to aspirin treatment under the assumption that *PIK3CA* mutations were a suitable biomarker for aspirin sensitivity. Corresponding EC_{50} values from viability assays demonstrated little correlation between aspirin sensitivity and *PIK3CA* mutation status, with the most sensitive organoid lines having demonstrated no evidence of harbouring *PIK3CA* mutations. However, given the multiple mechanisms of action and targets that are likely to be involved in aspirin-induced effects, it is somewhat challenging to delineate the exact correlation between aspirin and *PIK3CA* as a biomarker in this instance. This will further be considered in the discussion section of this thesis (Chapter 6).
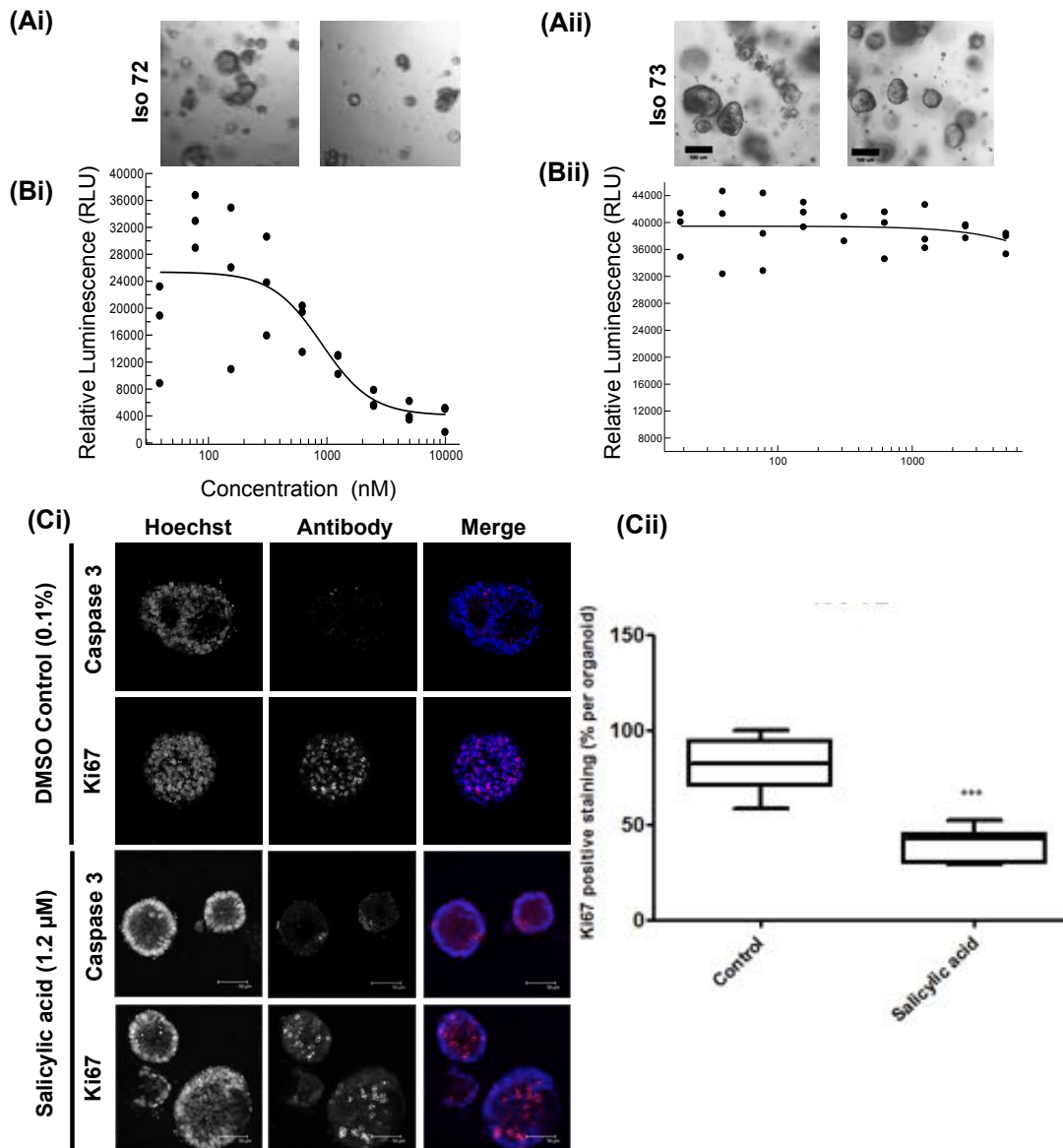
Figure 4.4 Analysis of aspirin metabolite on organoid growth.

Freshly digested organoids were seeded at densities of 400 cells/ µl Matrigel and overlaid with growth media. Following 3 days of culture, a titration range of salicylic acid (19nM- 5000 nM), or a volume matched DMSO control (0.1%)was administered. Representative images of (**Ai**) Iso 72 and (**Aii**) Iso 73 at day 7 in culture. Following 4 days of treatment, representative EC_{50} curves were generated from ATP quantification of (**Bi**) Iso 72 and (**Bii**) Iso 73 organoids expressed as Relative Luminescence Units versus concentration of salicylic acid administered, n=3 . (**Ci**) Representative images of Iso 72 Organoids fixed and stained for ki67(proliferation) and caspase 3 (apoptosis) markers following treatment with 1.2 µM salicylic acid (**Cii**) Ki67-positive cells were counted using IMARIS software. Scale bar indicates 50 µm, n=5-12 organoids per group. Levels of significance were determined using n unpaired t-test with Welch's correction , *P < 0.05, ** P < 0.01, *** P < 0.001. Representative images and subsequent data from (Ci) and (Cii) were collected by Kate Densley under my supervision.

Given the indications in the literature that metabolised aspirin induces apoptosis in a number of different tumour cell types *in vitro,* including breast, gastric and colorectal, we looked for markers of apoptosis in the organoid models. Following treatment with salicylic acid (1.2 µM) for 4 days, Iso 72 organoids were further counterstained with Caspase 3 as a marker for apoptosis, demonstrating some degree of staining. To further quantify this, and to ascertain whether apoptotic events were dose dependent, phenotypic profiling was implemented, as previously described. Briefly, organoids were plated in black, clear-bottomed 384 well plates as single cells and following 3 days of recovery, were treated with a 9—point dilution of salicylic acid, as well as a DMSO control. Following 4 days of treatment, wells were simultaneously stained with Hoechst (nuclei) and TRITC-phalloidin (F-actin), washed, and imaged on a high-content confocal microscope (images captured by OcellO). Z-stack images were then inputted through the OMiner platform to readily detect and quantify relevant features. For Iso 72 organoids, inspection of overall number and size of organoids demonstrated no dose-dependent effect of salicylic acid treatment. However, quantified measurements (Figure 4.5) were suggestive that aspirin treatment induced impacts upon individual nuclei. Whilst there was no direct evidence of involvement of apoptosis from phenotypic nuclei profiles, the overall presence of Caspase 3 within organoids could be indicative of apoptotic effects. It is most likely that inhibition of proliferation results in smaller organoids following treatment with salicylic acid. It is possible that further quantification of Caspase 3 in control and treatment conditions would enhance observations, as well as other assay improvements, further discussed in Chapter 6.
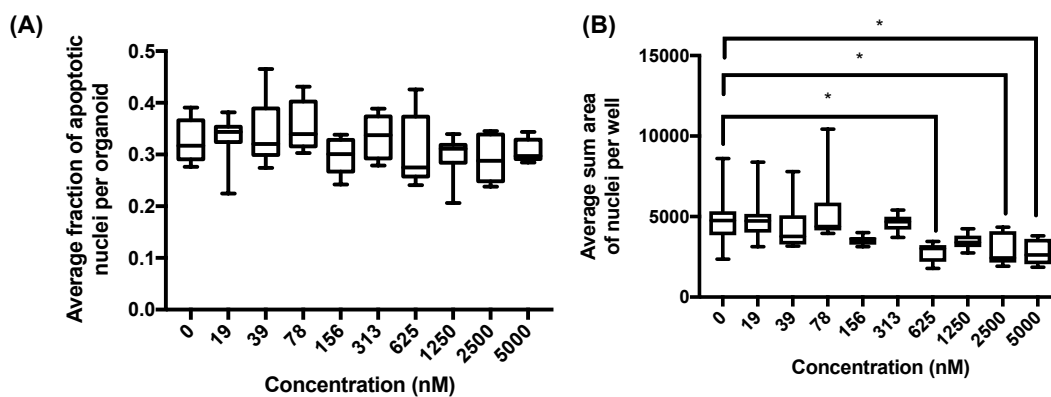
Figure 4.5 Analysis of aspirin metabolite on organoid phenotypes

Freshly digested organoids were seeded at optimal densities of 400 cells/ µl Matrigel and overlaid with growth media, prior to treatment of a titration range of salicylic acid (19nM- 5000 nM), or a volume matched DMSO control (0.1%)from day 4 to 7 in culture. Phenotypic profiling of Iso 72 organoids using OcellO readouts to identify changes in nuclei profiles in response to treatment with a dose range of salicylic acid. Significant changes in average number of apoptotic nuclei (**A**) and average area of nuclei per well (**B**)were calculated from a minimum of n=8 wells per treatment. Significant changes in nuclei profiles were calculated using a one way ANOVA with Dunnett's multiple comparison test, p<*=0.05.

4.2.4 Evaluating the impact of her1-3 inhibition upon organoids

AZD8931, clinically known as Sapitinib, is a potent ERBB2 and EGFR inhibitor, having previously shown capability of preventing EGF-driven cellular proliferation in multiple tumour cell lines. Within the FOCUS 4 clinical trial, Sapitinib is a proposed compound to treat patient carrying Erbb2 amplification and wild type for *BRAF, KRAS* and *PIK3CA*. As described in studies elsewhere, mammary tumour cell lines exhibiting Erbb2 amplification were inherently sensitive to Sapitinib treatment. A study by Mu *et* al., (2014) demonstrated that inhibition of EGFR dependent signalling resulted in a suppression of cell growth and induction of apoptotic events, findings which were then translated *in vivo,* when Sapitinib was administered in combination with a chemotherapeutic in a xenograft model (Mu *et al.* 2014).

To explore the impact of Sapitinib upon organoid viability, established organoids were digested to single cells and plated in 96 well plates, subjected to treatment with a titration of Sapitinib and administered with a Cell titer Glo 3D reagent to quantify relative ATP levels (Figure 4.5). Measurements indicated no clear dose dependent responses in a number of organoid lines (Table 4.1), with the exception of some responses from Iso 72 at the highest concentrations of Sapitinib administered (1μM – 5 μM). Recent studies have further demonstrated organoid sensitivity, reporting IC_{50} values of approximately 0.04 μM – 1 μM (Wetering, *et al.* 2015).

To further investigate the impact of Sapitinib upon proliferation within Iso 72, organoids were firstly treated with Sapitinib (40 nM) for four days and analysed for changes in Ki67 as an indicator of proliferation. It was found that Sapitinib treatment reduced the average number of proliferating cells per organoids from proliferation, from 81%±13% to 47%±16%, without fully inhibiting overall viability as indicated by ATP readouts. To further investigate the effects of Sapitinib upon organoids, phenotypic profiles of control (DMSO, 0.1%) versus a dose range of Sapitinib were analysed using OcellOs novel OMiner platform (conducted in collaboration with OcellO) , as previously described. Quantification of Iso 72 nuclei profiles revealed a

significant increase in the fraction of apoptotic nuclei per organoid with increasing doses of treatment (Figure 4.5 (C)). Taken together, this would support previous indications in the literature that Sapitinib exerts effects by suppressing proliferation and inducing apoptosis. However, given that EC_{50} values were within a high range compared to expected values in sensitive organoids, further work would need to further confirm downstream effects of Sapitinib treatment upon EGFR-mediated signalling.

As detailed in Chapter 3 (Table 3.3), many organoids exposed to Her1-3 inhibitor contained mutations within *BRAF, PIK3CA* and *KRAS*. It is therefore possible that such mutation profiles could interfere downstream from Sapitinib-mediated signalling inhibition, resulting in a lack of strong responses from most organoid lines.
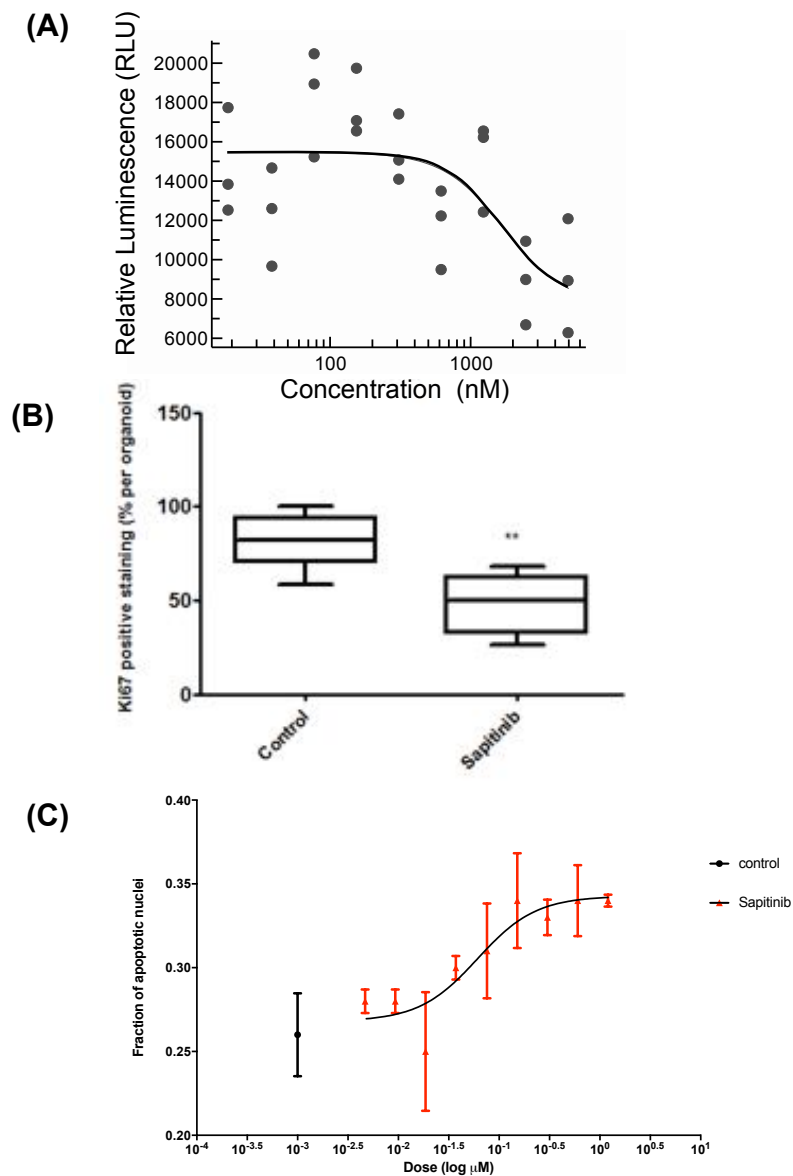
Figure 4.5 Assessing the effects of Sapitinib on organoid growth

Freshly digested organoids were seeded at 400 cells/ μl Matrigel and overlaid with growth media for 3 days, prior to treatment of a titration range of sapitinib (19nM- 5000 nM for viability assays, 5nM – 1250 nM for phenotypic screening), or a volume matched DMSO control (0.1%) for 4 days in culture. (**A**) Iso 72 Organoids fixed and stained for ki67(proliferation) marker following treatment with 39 nM Sapitinib, and counted using IMARIS software, n=5-12 organoids per group. Levels of significant were determined using n unpaired t-test with Welch's correction , * $P < 0.05$, ** $P < 0.01$, *** $P < 0.001$ (**B**) Representative EC_{50} best curves were generated following 4 days of Iso 72 organoid treatment and expressed as Relative Luminescence Units versus concentration of sapitinib administered, generating EC_{50} values of 868 nM (±1193 nM, n=3). (**C**)Phenotypic profiling of Iso 72 organoids using OcellO readouts to identify changes in nuclei profiles in response to treatment with a dose range of Sapitinib. *Data from (B) were collected by Kate Densley under my supervision.*

Table 4.1 Collective EC$_{50}$ values of inhibitors tested, generated from ATP assays.

Data acquired from ATP assay analysis of organoid lines tested with compounds within the FOCUS 4 trial. Data shown as mean ± standard deviation, n=3 independent biological replicates, unless otherwise indicated by symbols whereby * n=2. EC$_{50}$ curves were generated using XLFit plug-in for Excel; where no curve fit was possible this is indicated as such.

| | EC$_{50}$ (nM) | | | | | | | | |
	Iso 34	Iso 48	Iso 49	Iso 50	Iso 72	Iso 73	Iso 75	Iso 78
AZ20	65566(±1046)	416*	21638(±3537)	453(±136)	2136(±2646)	4272(±6269)	7011(±5263)	354(±254)
MK1775	1025(±187)	180(±9)	130*	3388(±78)	205(±119)	327(±150)	126(±28)	526(±673)
Salicylic acid	486(±108)	5309(±437)	732(±519)	740(±946)	2912(±3124)	No curve	1787(±1106)	1761(±24938)
Sapitinib	No curve	No curve	No curve	No curve	2912 (±3124)	No curve	No curve	No curve
5FU	80*		233±116	1770*			No curve	4198*

137

4.2.5 Assessing drug combination of BRAF, EGFR and MEK inhibitors within BRAF-mutant organoids

As discussed in chapter 1, *BRAF* mutations occur in approximately 8-12% of CRC patients and are associated with a poor prognosis (Corcoran *et al.* 2015; Corcoran 2015). Despite the development of BRAF-targeting agents, their use in the clinic for treating *BRAF*-mutant CRCs has thus far provided limited success. This is thought to be as a result of an upregulation of EGFR-mediated activation as a response to inhibition of MAPK pathway feedback inhibition, circumventing the effects of treatment (Corcoran *et al.* 2012). Based on this rationale, within the FOCUS 4 clinical trial, it has been postulated that combination therapy targeting BRAF and EGFR with/without MEK using Dabrafenib, Panitumumab ± Trametinib, respectively, will improve progression free survival in patients with *BRAF* mutant CRC, when used as a maintenance therapy following first line chemotherapy, compared to standard of care treatment. Here, having established the utility of viability readouts as a system to identify drug sensitivity, it was investigated whether combination therapy regimes could be administered to organoids. For the purposes of simplicity, the two BRAF-mutant organoids Iso 34 and Iso 75 (as opposed to the whole organoid cohort) only were used to investigate the effect of each compound as single agents, with Iso 34 utilised to measure the effects of compounds in double- and triple- combinations.

4.2.5.1 Trametinib is an effective growth inhibitor in organoids as a single agent

In order to assess whether combination treatments could impact the growth of organoids matched to FOCUS 4 patient biomarkers, the effects of each compounds as single agents were firstly established in a BRAF-mutant model. Iso 75 organoids were treated with Dabrafenib (250 nM), Panitumumab (200 nM), Trametinib (80 nM), respectively, as well as a DMSO control condition, for a total of 4 days. Following treatment, organoids were fixed and immunostained with phalloidin (F-actin) and Ki67 to obtain counts using IMARIS parameters as previously described. It was observed that 80 nM Trametinib significantly reduced the number of

proliferating cells on average per organoid, compared to Panitumumab and Dabrafenib, both of which showed no significant impact upon overall organoid proliferation, as shown in Figure 4.7. In order to further classify responses to Trametinib as a single agent, two BRAF mutant organoids , Iso 75 and Iso 34, were subject to phenotypic screening process, as described previously. Briefly, organoids were digested to single cell, and following three days of recovery, were treated with a dose titration range of Trametinib over 4 days. Organoids were then fixed and stained simultaneously with Hoechst and TRITC phalloidin to mark nuclear and f-actin structures. A total of 8 replicate wells were used per condition. Z-stack images of each well were captured, and images were further processed using OMiner™ software, in collaboration with OcellO. As shown in Figure 4.8, it was found that Trametinib had a dose dependent effect on overall organoid size indicative of inhibitory effects upon growth. Interestingly, Trametinib also induced impacts upon overall lumen size of both Iso 34 and Iso 75 as demonstrated in Figure 4.8. For Iso 75 in particular, this effect was observed at a much lower concentration than effects observed on overall organoid size, further emphasising the need to investigate particular organoid phenotypes as opposed to relying on organoid size as a measure of response, further discussed in Chapter 6.
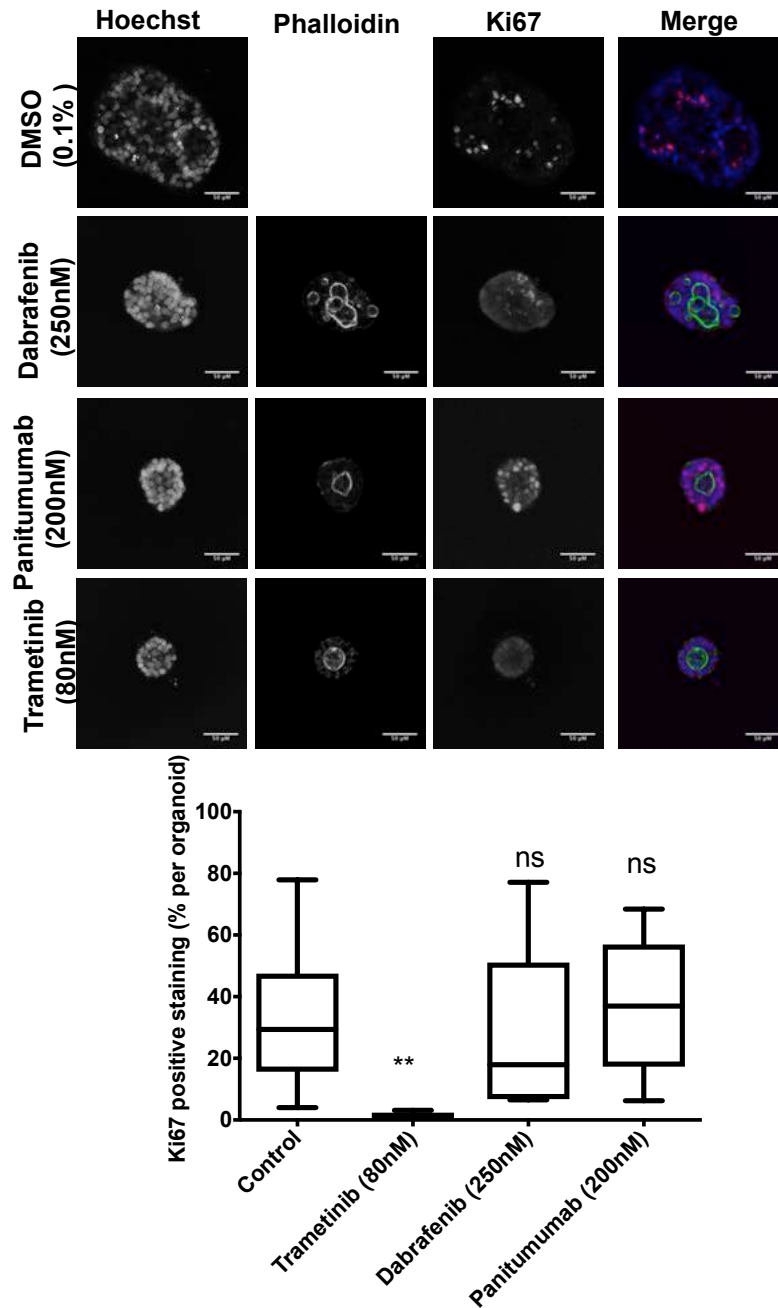
Figure 4.7 Assessing impact of single agents EGFR/BRAF and MEK inhibitors upon organoid growth
Iso 75 organoids were dissociated to single cells and cultured for three days. Organoids were then treated with 0.1% DMSO conditions and Trametinib (20 nM, 40 nM) for four days, prior to fixing and immunostaining for Ki67 proliferation marker and phalloidin for F-actin ,and imaging using confocal microscopy. Nuclei were counterstained with Hoechst (**Ai**) Representative images of organoids captured following treatment with each compound as single agents.(**Aii**) The number ki67% positive cells per organoid were counted using IMARIS software. The number of Ki67-postivie cells were counted as a percentage per organoid (n=5-15 organoid). Significance of number of proliferating cells were calculated using Welch two sample t-test and Mann Whitney two-tailed test *p≤0.01, ** p≤0.05. *Images and IMARIS counts were collected by Kate Densley under my supervision*
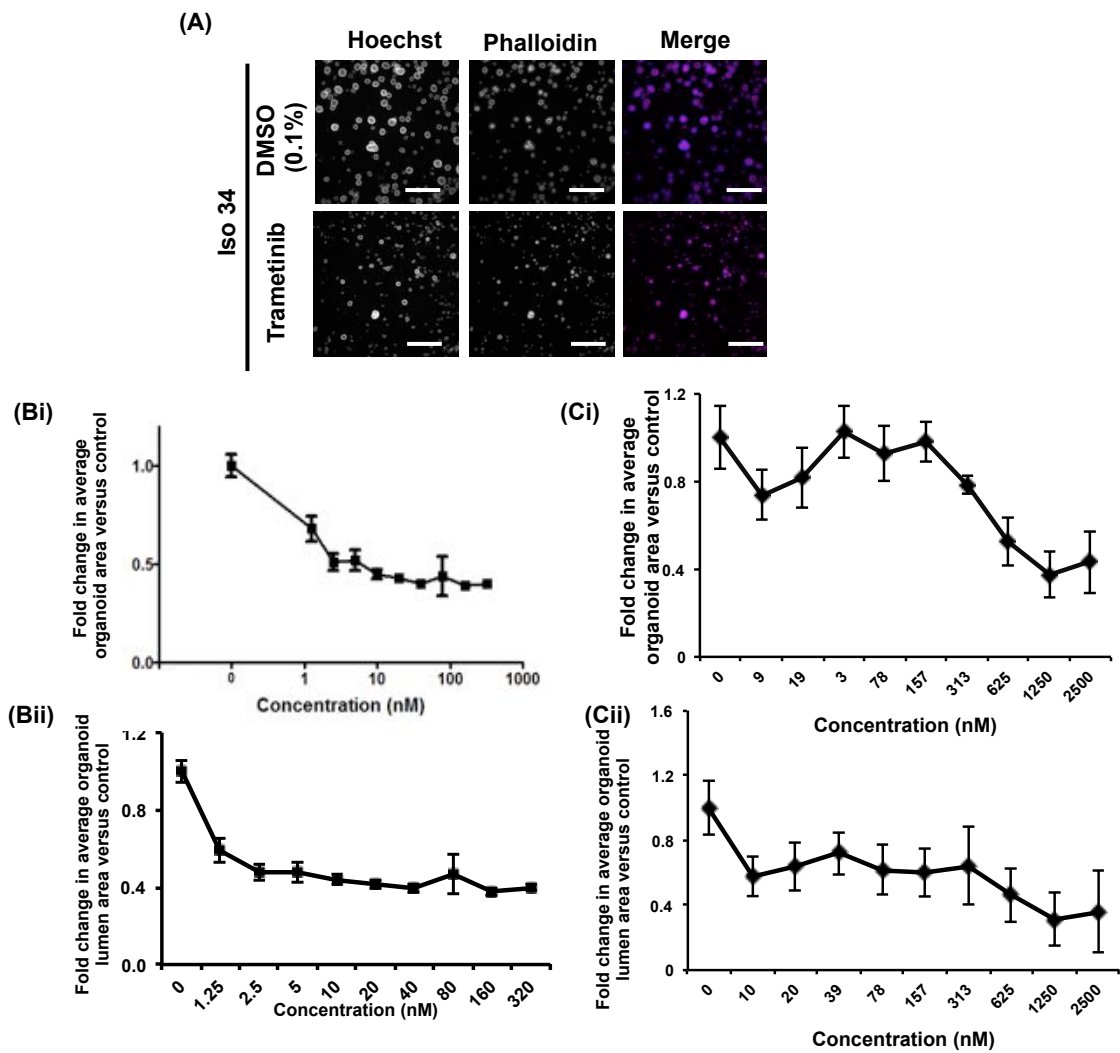
Figure 4.8 Phenotypic analysis reveals structural changes in response to Trametinib within organoids

Organoids were seeded as single cells within 384 well plates prior to treatment with a dose titration of Trametinib (320 nM) and DMSO control (0.1%) within media for four days, then fixed and stained with Hoechst and Phalloidin. Image z-stacks of organoids were captured, and parameters were quantified by OcellO. **(A)** Representative images of a well of Iso 34 organoids treated with trametinib and DMSO control, and masked according to Hoechst and Phalloidin channels. *Images captured at OcellO* **(B)** Scatterplots of measurements acquired of (i) average organoid area (ii)average lumen area in Iso 34 organoids. (**C**) Scatterplots of measurements acquired of (i) average organoid area (ii)average lumen area in Iso 75 organoids. Scale bar 0.5mm.

4.2.5.2 Dabrafenib and Panitumumab administration on BRAF mutant organoids potentiate growth inhibition

To assess the whether therapeutics exerted synergistic effects upon organoids, experiments were designed as previously described by Chou-Talalay (Chou and Talalay 1984; Chou 2010); detailed in Chapter 2). This methodology has been common practice in a number of studies in the literature to determine synergistic activity of compounds by quantitatively measuring dose-effect relationships of drugs, with some analyses having been performed on a combination of three or more compounds. A key principle of Chou-Talalay combination studies is based on maintaining the dose of each compound in a constant ratio to each other, most commonly their $IC_{50,}$ over a titration range. In theory, this can be applied to any given number of combinations; if multiple data points for constant- ratio combinations are collected, the entire spectrum of synergistic or antagonistic effects can be obtained at each concentration.

The *BRAF*-mutant Iso 34 organoid line was used to investigate synergistic effects of compounds upon organoid growth. Iso 34 organoids were treated with a 14-point dose titration of each respective compound to identify IC_{50} values in single inhibitor assay formats, as described. Following a Cell Titer Glo 3D ATP readout, it was observed that Trametinib had a clear inhibitory impact upon Iso 34 organoids, generating IC_{50} values of 3 nM (Figure 4.9, Bii) after 4 days of treatment. Both Dabrafenib and Panitumumab failed to generate such clear dose dependent responses, with Dabrafenib in particular appearing to impact Iso 34 only at the very highest concentrations administered (Figure 4.9, Bi and Biii). Given the fundamental requirement of Chou-Talalay analysis methods to maintain compounds at fixed ratios of their respective IC_{50} values spanning a suitable dose titration range to then assess combinatory effects, it was necessary to obtain IC_{50} values from *in vitro* systems within the literature under the assumption that this would be in the range of a cellular IC_{50} value.

In order to identify whether Dabrafenib and Panitumumab would potentiate the inhibitory effects, IC_{50} values of both compounds were set at 7.8 nM, 0.98 nM, respectively, thus generating a ratio of 8:1 between both compounds. In concordance with Chou-Talalay methodology, single inhibitor assays of Dabrafenib and Panitumumab were carried out in parallel with combination assays to ensure subsequent analysis was carried out in comparative systems. Following 4 days of treatment with Dabrafenib, Panitumumab or a combination of both inhibitors absolute ATP values were obtained using the Cell Titer Glo 3D reagent. It was observed that a combination of Dabrafenib and Panitumumab induced a stronger inhibitory effect upon overall organoid viability, as opposed to administration as single agents (Figure 4.9).

It would be expected a lack of interaction between compounds, otherwise referred to as an additive effect, would be in the range of 110nM from single agent dose response curves generated as shown in Figure 4.9. However, when administered as two compounds the IC_{50}s of Dabrafenib and Panitumumab combined were instead approximately 7nM, below expected values for an additive effect. Further calculations (using Equation 2.1) enabled a determination of the synergistic action of compounds. Combination index values calculated per dose of Dabrafenib and Panitumumab of 0.02±0.02 (n=3 independent experiments) confirmed that the compounds potentiated the effect of one another. Specifically, the dose reduction index, representative of the fold reduction in compound concentration that could be administered to reduce organoid growth by 50% demonstrated that in combination, Dabrafenib could be theoretically administered at a 133 fold reduction in dose, whereas Panitumumab could be administered at >1000 fold lower dose.

4.2.5.3   MEK inhibition potentiates inhibitory action of BRAF/EGFR inhibitors upon *BRAF*-mutant organoids

To establish whether Dabrafenib and Panitumumab activity could be further enhanced by administration of Trametinib, as tested in the FOCUS 4 clinical trial, Iso 34 was administered with the three compounds in combination. To determine the effects of three-agent combination, organoids were challenged with a dose titration range of compounds administered in a IC_{50}-constant-ratio dose (8:4:1 for Dabrafenib: Trametinib: Panitumumab) for 72 hours prior to quantification of cell viability. The ratio of IC_{50}s were previously determined by those generated from single-assay responses, where possible, or from IC_{50} values gathered from *in vitro* data within the literature.

Following exposure to compounds in double combination (Dabrafenib and Trametinib, Trametinib and Panitumumab and Panitumumab and Dabrafenib, respectively) or as triple agents, the effects upon overall viability of organoids were characterised by assessment of ATP levels using the Cell Titer Glo 3D assay, following 4 days of treatment. Given that Trametinib as a single agent induced a clear growth inhibitory response upon organoids it would be expected that it would perhaps potentiate the effects of both Dabrafenib and Panitumumab. Following establishment of dose response curves from each treatment as well as further linear regression analysis it was found that Trametinib treatment (MEK inhibition) potentiated the effects of BRAF inhibition by Dabrafenib upon Iso 34. This confirms observations from previous *in vitro* studies in the literature, whereby Dabrafenib and Trametinib together work favourably to reduce the growth of BRAF mutant lines (Corcoran *et al.* 2015). More specifically, as noted in Table 4.2, further calculations to determine dose reduction index revealed that by addition of Trametinib, Dabrafenib could be administered at >1000 fold lower dose to achieve a 50% inhibition in organoid growth. Similarly, it was demonstrated that addition of Trametinib to

Panitumumab-treated organoids worked favourable to enhance inhibitory effects on overall organoid viability in a dose dependent manner.

An overall reduction in growth was observed in Iso 34 organoids treated with Dabrafenib, Trametinib and Panitumumab in combination (n=3) compared to DMSO (0.1%) control conditions. Synergistic activity of the three compounds in combination was further confirmed by combination index value of 0.03±0.05, then by application of the dose reduction calculation, which demonstrated that when all three compounds were administered, both Dabrafenib and Panitumumab doses could be reduced by 1000 fold, whilst Trametinib doses could be reduced by 3 times, to achieve an inhibitory effect in 50% of Iso 34 organoids, as indicated in Table 4.2

Whilst this data is useful to demonstrate the application of organoids towards combination studies, it is based on multiple assumptions. Given the compounds examined exhibited complex modes of action, distinct IC_{50} values were hard to obtain for each compound using viability readouts and therefore subsequent analyses needed to consider this caveat. Overall, data indicated that agents were able to potentiate the effects of another to inhibit organoid growth.
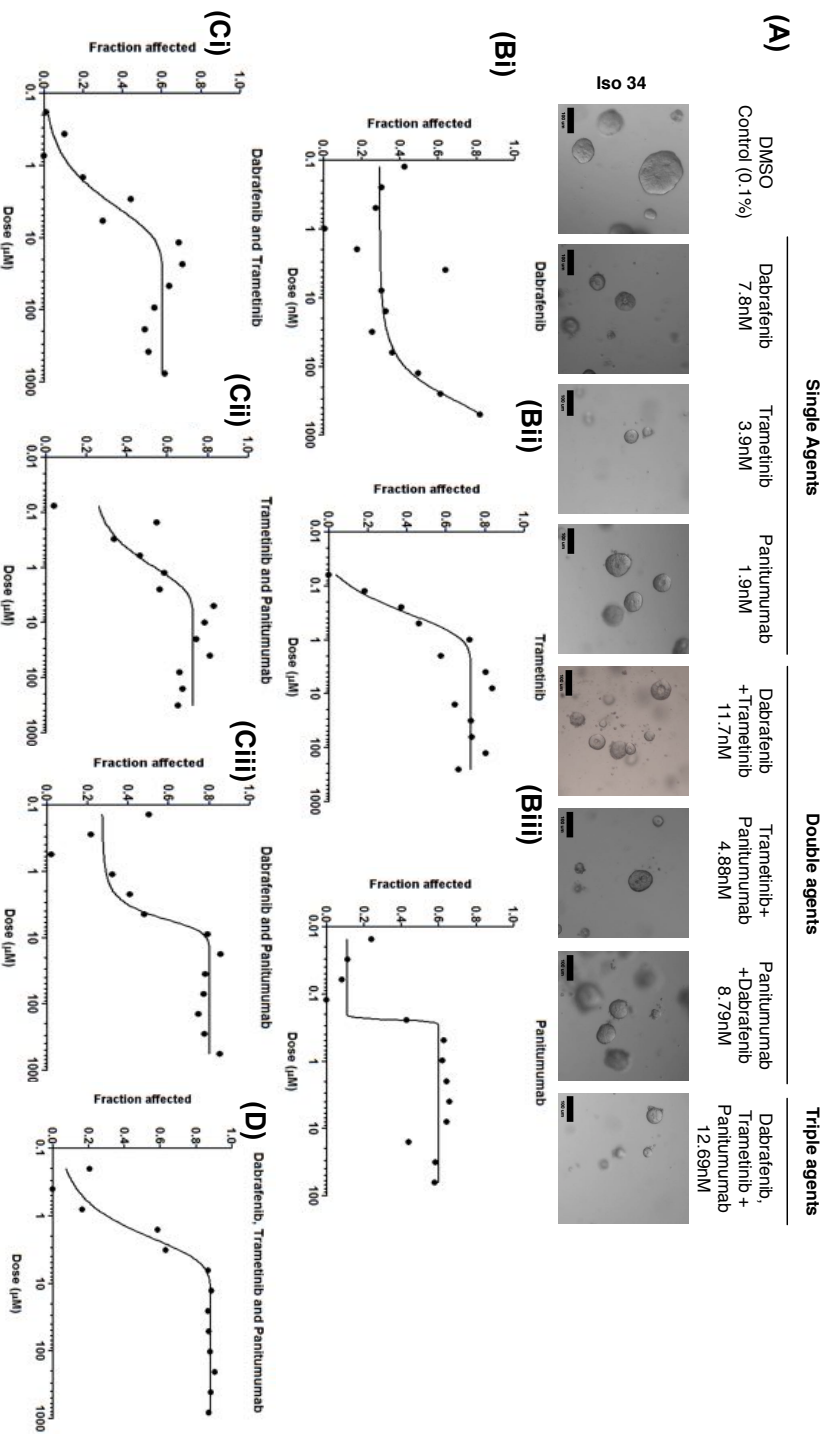
Figure 4.9 Compounds in combination potentiate the inhibitory effects upon BRAF-mutant organoid growth.

Iso 34 organoids at single cell were seeded at 400 cells/ μl of Matrigel and overlaid with media. Following 3 days of recovery in culture, media supplemented with a range of doses at a two fold dilution of compounds, for a total of 4 days in culture.(A) Representative images per condition at day 7 in culture. Following treatment, an endpoint Cell Titer Glo 3D readout of viability was used to measure a range of doses of (Bi) Dabrafenib (0.12 – 500 nM) (Bii) Trametinib (0.06 – 250 nM) (Biii) Panitumumab (0.02 – 62.5 nM), as well as a combination of (Ci) Dabrafenib and Trametinib (0.18 – 750 nM) at a ratio of (2:1), (Cii) Trametinib and Panitumumab at a ratio of (1:4) (Ciii) Dabrafenib and Panitumumab at a ratio of 8:1, or (Di) a combination of three compounds at a ratio of 8:4:1 (Dabrafenib, Trametinib, Panitumumab), to assess viability readouts. All titrations were graphed as 'fraction affected', normalised to DMSO (0.1%) control conditions. Dose response curves representative of one experiment.

Table 4.2 Combination index values (CI) and Dose reduction index (DRI) per treatment.

All data was inputted into Calcusyn software to generate combination index values (n=3 biological repeats) and Dose Reduction Index (DRI) at IC50 values of each combinations..

	DRI at IC50 (fold change in dose at combination)			CI Values (IC50)
	Dabrafenib	Trametinib	Panitumumab	
Dabrafenib+ Trametinib	>1000	59		0.92±1.28
Trametinib+ Panitumumab		>1000	>1000	0.02±0.03
Panitumumab + Dabrafenib	>1000		133	0.02±0.02
Dabrafenib, Panitumumab + Trametinib	>1000	3.21	>1000	0.03±0.05

4.2.6 Phenotypic screening variably aids discrimination between subtle dose dependent responses in cellular morphologies

Phenotypic profiling of pharmacologic responses is becoming an apparent approach to assess therapeutic effects upon distinct cellular morphologies and are beyond the scope of limited basic readouts. Using Principal Component Analysis (PCA), such platforms have condensed multiple phenotypic measurements to assess subtle changes in changes to nuclear, cellular and structural changes in cells in exposure to compounds (Caie *et al.* 2010; Reisen *et al.* 2013; Sandercock *et al.* 2015; Di, Klop, Rogkoti, Devedec, van de, *et al.* 2014). This has facilitated an enrichment of phenotypic data beyond basic metrics. Within this thesis, such analyses were found to be critical to identify organoid-specific signatures of response to Wnt inhibitors, as discussed within Chapter 5.

Relevant treatments from the FOCUS 4 clinical trial elicited a number of effects upon viability and basic phenotypic readouts in an organoid cohort. Further discrimination of drug-induced effects could therefore be beneficial to improve readouts of response to compounds. Here, it was investigated whether PCA of multiparametric data could capture drug-induced variance more successfully than a single parametric measurement (e.g. ATP viability readout). It was hypothesised that multiple phenotypic readouts would facilitate a more robust readout, facilitating the dissection of drug-dependent mechanisms. Ultimately, this would enable the identification of active compounds based upon subtle changes in organoid morphologies.

To investigate phenotypic profiles, a set of 6 organoids (Iso 34,49,50,72,75,78) were seeded as single cells and following a recovery for 3 days, were treated with a titration range of compounds administered within FOCUS 4 for a total of 4 days. Samples were then fixed and stained simultaneously for 24 hours at room temperature, as described in (Di, Klop, Rogkoti, Devedec, van de, *et al.* 2014) to visualise Hoechst (nuclear) and Phalloidin (F-actin). Following washes in PBS, 3D

structures were then imaged on a MetaXpress® high-content confocal microscope (carried out by OcellO, Leiden), which facilitated the acquisition of z-stacks from 384 well plates.

Individual images from each z-stack were then inputted within the bespoke OMiner™ analysis platform developed by OcellO, as depicted within Figure 4.10. Briefly, projections of the F-actin and nuclei-derived image stacks were used to extrapolate masks of individual organoids, internal lumen structures and nuclei. Image segmentation and filters were then applied to identify individual objects per well from each channel, and enhance noise suppression to balance sensitivity of analysis. Relevant masks were then used to acquire approximately 700 quantifiable morphological features per structure, including data relating to fluorescence intensities per channel. Measurements of individual features per organoid were pooled to generate measurements on a well-by-well basis. Data were then normalised to negative controls, per phenotypic measurement, to account for potential variability in plating conditions and staining procedures per experiment.

In order to condense phenotypic measurements to key principal components, PCA was performed upon the 700 morphological variables. PCA was carried out on each feature acquired from experimental drug conditions per organoid line, across a dose response. PCA enabled a reduction in the dimensionality of each dataset by facilitating the conversion of data from multiple variables (individual phenotypic features in this case) into a new coordinate. This conversion, whereby each coordinate is recognised as a principal component ,enables the greatest variances across data (between control and treatment conditions) to lie on one co-ordinate. The greatest variance in the principal components therefore lies on the first principal component, with the next greatest variance on the second principal component, and so forth.   Figure 4.11 demonstrates a typical scree plot of percentage (%) variation obtained in each component, as represented from Iso 72 treatment with aspirin. The variation within the first principal component in this instance was 28%.

To identify drug-induced effects from condensed data,a multidimensional Mahalanobis Distance metric was used to calculate the similarity of a data point to the negative control, based upon the correlation between variables contained within the first 5 principal components. The Mahalanobis distance metric facilitates the measurement of distances in 3D space. Here, this calculation was used to measure distances between each dose and control DMSO-treated samples per organoid line, per treatment. Theoretically, the Mahalanobis distance would enable a calculation of the similarity of a data vector to negative control conditions. Therefore, a larger Mahalanobis distance between DMSO control and treatment would equate to a greater difference in phenotype between both conditions. Alternatively, if the treatment induced a phenotype that was similar to DMSO control conditions, the distance would be small. This enabled extraction of the greatest variance between DMSO control and dose of compound from multiple features. Any outliers within the data analysis were confirmed by visual inspection of the image of the whole well (Appendix i-1) and were usually a result of either empty wells as a result of shipping conditions, or poor segmentation due to over-seeding in the well. Following identification and removal of this from data, a minimum of 6 wells were used per condition. Distances measured (Appendix I-2) from each treatment dose were then used to generate drug dose response curves, as represented in Figure 4.11, to determine EC_{50} values (dose response curves obtained from Mahalanobis distance measurements were plotted for each organoid line, as shown in Appendix I-2).

(A) Plate Set up

Organoid expansion → Single cell suspension and seeding → Treatment → Fix and stain

Day 0 — Day 4 — Day 7

(B) Image acquisition and analysis

Image acquisition of organoid z-stacks →

Image segmentation per channel, per z-stack →

Object filtering to remove enhanced morphological measurements →

DAPI and F-actin used to generate masks of whole organoid,lumen and nuclei area →

Ominer software used to extract multiple measurements acquired from masks

(C) Multiparametric phenotypic profiling analysis

Quantification of phenotypic features obtained from OMiner™ →

Normalisation of features by z-score →

PCA on the z-scores to extract variable features →

Mahalanobis distance metric applied based on the first 5 principle components →

Distance metric plotted per treatment dose compared to negative control

Figure 4.10 Multi-parameter phenotypic analysis workflow.

Organoids seeded from single cells were plated in 384 well plates within matrigel overlaid with growth media supplemented with a two-fold dilution of compounds over a a dose response range, or DMSO (0.1 %) for negative control conditions. Highest doses of each compound were used to select the most discriminating features that best sepearted treatments from negative controls. Euclidean distance between the treated and non-treated conditions was plotted for each treated organoid. *Flowchart adapted from Di et al.,(2014).*

(A)

(B)
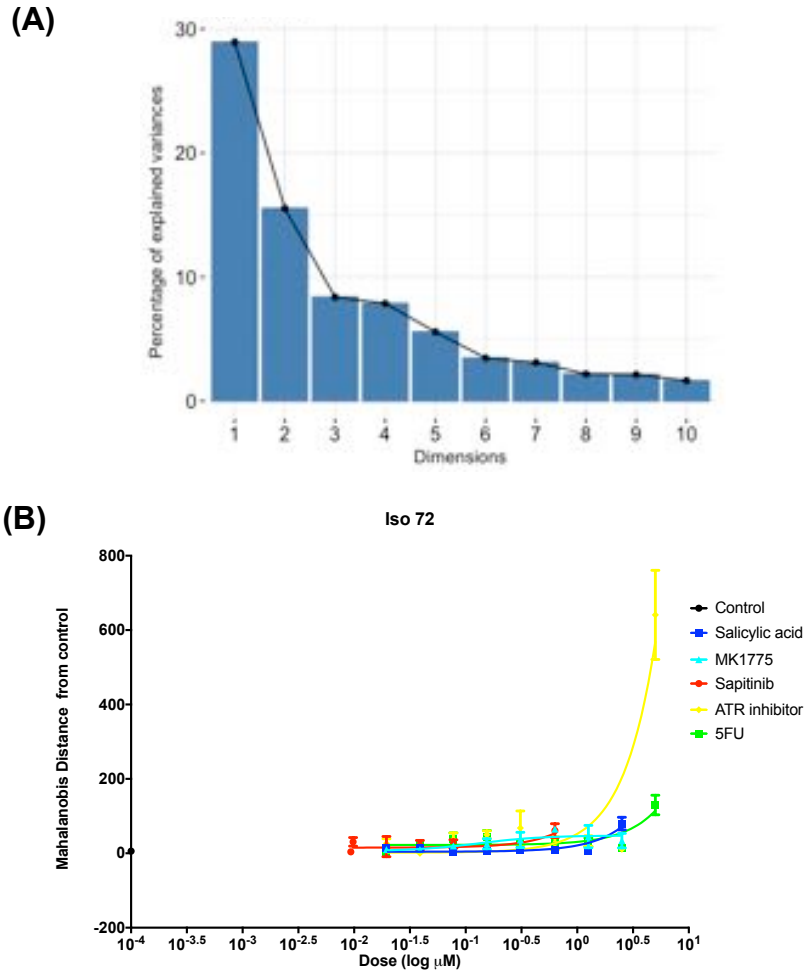
Iso 72

Figure 4.11 Multi-parametric analysis output from Iso 72 organoids

Freshly digested organoids were seeded within matrigel in 384 well plates and overlaid with optimal media for growth. Following 3 days of recovery, a dose titration of compounds within the FOCUS 4 trial were administered versus a DMSO negative control. Following 4 days of treatment, organoids were fixed and stained simultaneously for Hoechst and F-actin. Subsequent z-stack images were collected and inputted within OMiner™ software to generate multiple phenotypic measurements acquired from Hoechst and TRITC channel information. Data was inputted into R to generate Prinicipal Component Analysis (PCA) of features. (**A**) Screen plot from Principal component analysis demonstrates variables contributing to most variance within the data (**B**) Features within the first 5 components were used to measure Mahalanobis distance from treatment and control conditions. This measurement enabled a discrimination between each treatment dose compared to control, based on multiple measured features.

Overall, it was observed in some instances that clustering of multiple correlated phenotypic parameters identified drug-induced effects at lower concentrations of drug compared to preceding readouts of responses.

Multiparametric readouts identified Iso 34 and Iso 78 as aspirin-sensitive organoid lines, generating EC_{50} values of 5 µM and 1 µM (Figure 4.12). Whilst this data corresponded to previous observations from ATP readouts, the overall sensitivity of the multiparametric assay did not necessarily further discriminate aspirin-dependent responses within the organoid cohort. It is possible that a number of factors could contribute to this. Firstly, the magnitude of difference between the experimental groups was not large enough for distances to be varied within increasing doses. It is also possible that only a few features, such as nuclear morphologies, were altered in response to aspirin. In this case, it is possible that a large number of readouts that are not perturbed as a result of treatment represent assay noise and could therefore interfere with the accuracy obtained by a smaller collection of parameters (Hutz *et al.* 2012).An optimized set of key morphological signatures could more accurately identify the separation between treatment and control conditions, enabling fewer variables to capture more biological variation.

Multi-parametric analysis of compounds that targeted DDRs were also shown to corroborate previous findings from ATP assays. EC_{50} values of Iso 50 exposed to AZ20 treatment were found to be closer to an expected IC_{50} value when multiple variables were measured (1 nM). Analysis of phenotypes also demonstrated that MK1775 induced a number of alterations on phenotypes in all organoids assessed, further corroborating ATP readouts of dose range response. Collectively, organoid responses to 5-FU were varied in sensitivity following assessment of collective phenotypic responses. Iso 78 was shown to be the most resistant organoid line to 5-FU treatment.

Administration of the Her1-3 inhibitor, Sapitinib, also demonstrated that organoids overall showed limited sensitivity to compound inhibition. Iso 72, similarly to CTG measurements, generated a high EC_{50} value, further confirming that observations

were likely due to off target effects. Interestingly, Iso 75, having shown no response to Sapitinib in ATP readouts, showed sensitivity to Sapitinib treatment based on multi-parametric data, yielding EC_{50} values of approximately 30 nM. It is possible that morphological readouts were able to detect subtle changes in Iso 75 in response to Sapitinib that could not be measured by ATP viability readouts.

(A)
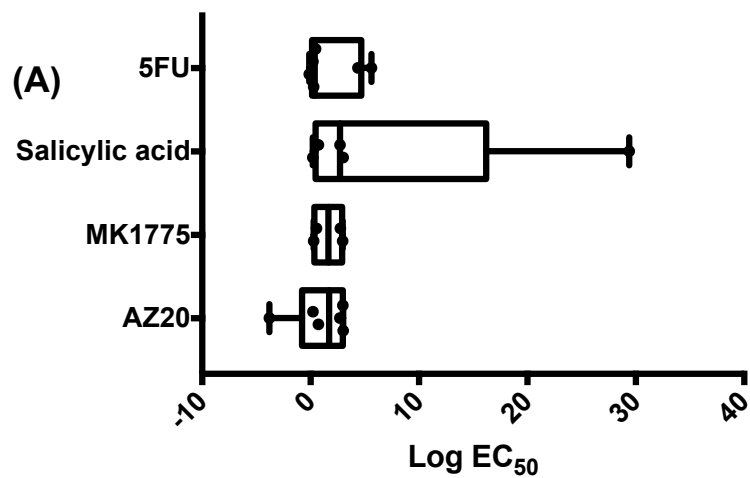
Figure 4.12 Organoids revea[...]

A cohort of 8 Organoids wer[...] [...]ubject to
a dose titration range of con[...] [...]g, PCA
was performed in order to p[...] [...]ent
principle component space. [...] [...] of data
variation were then subject [...] [...]data
point to the negative contro[...] [...]lotted as
dose response curves (Appe[...] [...]og EC$_{50}$ of
each compound administere[...] [...]anoid
line.

4.3   Summary

The work described here has shown a possible utility of patient colorectal tumour organoids towards mirroring a clinical trial *in vitro.* Using assay formats previously described in Chapter 2, in combination with specific optimised culture conditions per line, enables the investigation of multiple pathways relevant to clinical trials. This format has facilitated the measurement and assessments of effects of many different groups of inhibitors.

Using such systems, this work has particularly highlighted the utility of organoids to investigate the combination therapies of 3 compounds, which have yet to be studied *in vivo.* As combination therapies become increasingly popular within the clinic, this shows a direct future application of organoids to study complex interactions between multiple targeted therapies.

This work further demonstrates the need for relevant pre-clinical models to accompany biomarker driven strategies for CRC. Through this system, the differential responses of organoids to hypothesis-driven therapies regardless of mutational status was apparent. Overall, whilst the use of phenotypic screening to identify more subtle responses could also be used to guide effects that would otherwise be ignored for lack of cytotoxic effects, it was found that monitoring viability of organoids was a useful readout for treatment versus phenotype. This affirms that such assay set-ups could be suitably incorporated within the design of parallel patient-organoid clinical trials.

5 Characterisation of the effects of novel Wnt inhibitors on human CRC organoids using 3D image-based multi-parametric phenotypic profiling

5.1 Introduction

Aberrant Wnt signalling, as a result of activating mutations within the pathway, has a prominent role in tumour cell proliferation and survival in CRCs. As such, an array of components within the Wnt signalling pathway have been postulated as viable molecular targets to limit the enrichment of CSCs and thus improve clinical outcomes. Attenuation of Wnt signalling through the use of Tankyrase inhibitors (TNKSi) have been characterised within the literature, and have previously been linked to prevent the growth of Apc-deficient tumours within mice (Waaler, Machon, Tumova, Dinh, Korinek, Wilson, Paulsen, Pedersen, Tor J Eide, *et al.* 2012; Lau *et al.* 2013; Wu *et al.* 2016). However, overall, pre-clinical drug discovery for Wnt pathway modulators have thus far proven difficult, with few small molecule inhibitors having entered clinical trial and thus remaining within the drug discovery pipeline (Novellasdemunt *et al.* 2015; Waaler, Machon, Tumova, Dinh, Korinek, Wilson, Paulsen, Pedersen, Tor J Eide, *et al.* 2012) despite encouraging evaluations *in vitro* and *in vivo*. This may be a result of a number of factors; firstly *in vivo* studies often administer treatments at maximum tolerated doses of compounds to test for efficacy based on *in vitro* studies within 2D cell lines, resulting in potentially unnecessary toxicity. Secondly, given the variation of Wnt dependency from one tumour to the next, and the complexity of targeting cancer stem cell dynamics, it is unsurprising that 2D cell lines fail to reflect results *in vivo,* and raises questions as to their capacity as sufficient surrogate tumour models. The need for translatable model systems within drug discovery pipeline, capable of demonstrating on-target effects of a compound, whilst retaining patho-physiological tumour dynamics could prove invaluable to show the effects of such novel therapeutics.

Given the capacity of 3D primary organoids to retain stem/differentiated cells it is possible that they could become useful model systems to study stem cell dynamics. However, complex 3D models provide a challenging platform to quantify reproducible drug sensitivity, particularly to compounds possessing equally complex effects upon cell dynamics. Analysis platforms therefore need to be compatible with counterpart models to yield quantitative data.

Whilst previous chapters have described the utility of organoids as a medium-throughput system to assess clinically relevant compounds, this thesis also aims to establish organoids as a useful tool in a drug discovery setting. In order to explore this, multi-parametric phenotypic screening (OcellO) of organoids were used to assess the impact of novel cancer stem cell-targeting tankyrase inhibitors (Merck Serono).

Some data analysis presented in this chapter was performed by Bram Herpers, Kuan Yan, and Leo Price (OcellO), as specified within figure legends. *In vivo* data was carried out by Kenneth Ewan (Dale lab). Data presented within this chapter is currently being formatted for submission as a literature article.

5.2 Results

To fully investigate the capacity of organoids to demonstrate on-target effects of novel compounds, three compounds in development with Merck Serono with log fold changes in EC_{50} values (i.e effective concentration to limit growth of 50% of cells) were tested within the established organoid cohort previously described. EC_{50} values of each compound (MSC2501490A, MSC2572070A, MSC2524070) were provided by Merck Serono, as detected by a luminex assay against AXIN2, indicating EC_{50} values of 300 nM, 36nM and 3nM, respectively. This 2D cell-based assay utilises AXIN2 stabilisation as a readout, as AXIN2 is a target of TNKS1/2. Upon administration of the compound, the TNKS-dependent degradation of AXIN2 is inhibited, promoting the stabilisation of the protein, as detected by an immunobead assay.

5.2.1 Tankyrase inhibitors induce a dose dependent response within sensitive organoids in a functional ATP readout

Given that TNKSi have previously been implicated in the literature as potential compounds to target stem cell niches within tumour populations (Zhong *et al.* 2015; Arqués *et al.* 2016) , it was investigated here whether organoid formation and subsequent growth in culture would be affected by treatment. 3 organoid lines were therefore administered with a dose titration range (0.19 nM – 50nM) of a tool TNKSi developed by Merck Serono (MSC2524070), which will be made available to the wider research community for testing.

Organoids previously established in culture were suspended to single cells within matrigel and treated with a nine-point, two-fold dilution of compound or DMSO control (0.1%) in triplicate wells per condition, for a total of six days. Morphologically, both Iso 72 and Iso 75 organoids displayed sensitivity to TNKS inhibition, as indicated in Figure 5.1. Iso 72 structures treated with TNKSi were shown to be overall reduced in size compared to control conditions, whereas Iso 75 organoids were also arranged more sparsely indicating a lower density of organoids

formed. It appeared however, that TNKSi did not appear to induce typical cytotoxic effects, frequently characterised by an increased level of cellular debris and dense structures.

Following 6 days of treatment, Cell Titer Glo 3D reagent was administered to wells and luminescent readouts, as a representation of ATP levels were acquired. A dose-dependent response was generated in both Iso 72 and Iso 75, as shown in Figure 5.1, eliciting mean EC_{50} values of 2 ± 0.7nM and 14 ± 8 nM, respectively from three independent experiments. Iso 50 appeared to have a less prominent response to increasing concentrations of TNKSi according to ATP readouts, with EC_{50} values of 1043.9 ± 621.2nM obtained. An overall reduction in ATP levels (Relative Luminescence Units) were observed at the highest concentrations of TNKSi administered (50 nM), indicative of off-target effects in comparison with sensitive lines.

To further corroborate qualitative findings as well as ATP quantification, images of wells of organoids were acquired and quantified for basic morphometric measurements using GelCount™ CHARM settings, at day 3 and day 6 in culture, whilst exposed to a dilution of treatment conditions. Measurements of total organoid volume, as shown in Figure 5.2 were shown to be consistent between control and treatment conditions within all organoid lines at day 3. Following 6 days of treatment, a reduction in overall volume was observed in Iso 72 organoids in particular between control and MSC2524070 treatment (1.56 nM – 50 nM), indicating that overall growth was minimized following treatment. Iso 75, despite showing some reduction in an endpoint ATP assay readout at day 6, showed little variation between average organoid volumes in control and treatment conditions. This could be the result of partial TNKS inhibition, stimulating organoid growth to reach similar volumes as observed by control organoids, highlighting the complexity of signaling events when using such compounds. However, it is more likely that this is a result of a lack of sensitivity from basic morphometric readouts obtained using GelCount charm settings; data acquired from inherently small structures,

such as Iso 75 in routine culture, could harbor sensitivity of detection in differences in overall sizes.

A count of average number of organoids formed per well (n=3 wells) by day 6 in culture were generated from established CHARM settings and used to calculate organoid formation efficiency from a known number of single cells seeded (Figure 5.3). Organoid formation efficiency (%) was significantly reduced in 50 nM of TNKSi treatment conditions compared to control DMSO (0.1%) conditions in Iso 75 organoids (n=3, one way ANOVA with Dunnett's post hoc test). Interestingly, Iso 72, showed no treatment dependent effect on organoid formation efficiencies (%) despite overall changes in growth. This could be as a result of TNKS inhibition eliciting affects upon this line at a later point in treatment compared with Iso 75. Iso 50, a non responder line, as expected, showed no overall alteration in organoid formation efficiency (%) in treatment conditions.

Taken together, this data indicates that TNKSi induces marked effects on overall organoids formation or subsequent growth in culture. It was notable that even at highest concentrations of treatment, TNKSi did not appear to induce obvious signs of cell death, such as an increased number of debris in wells.
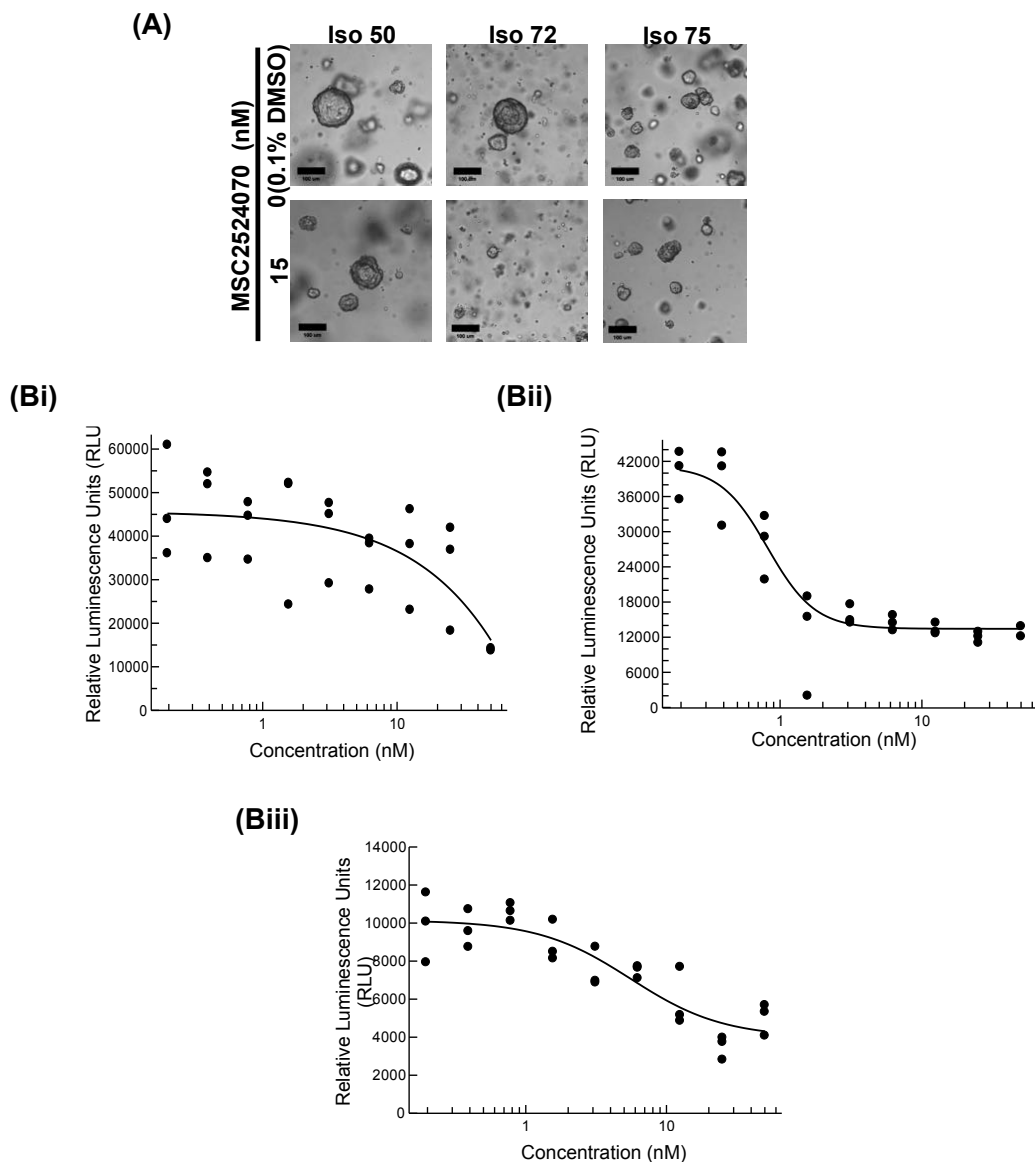
Figure 5.1: Analysis of the effects of the Tankyrase inhibitor MSC2524070 on the viability of three tumour organoids.

Iso 50, Iso 72 and Iso 75 organoids were seeded at 400 cells/µl Matrigel and overlaid with previously specified growth media, supplemented with MSC2524070 at a two-fold dilution (0.195 nM – 50 nM), and a matched DMSO control (0.1% in media). (**A**) Representative images at day 6 in culture. (**B**)ATP endpoint assay readouts across a dilution of drug doses in Iso 50 (i), Iso 72 (ii), Iso 75 (iii) were performed following 6 days of exposure to TNKS inhibitor. EC_{50} best fit curve were plotted using XLFit plug-in for Microsoft Excel, and are shown from one representative experiment. Each plot represents data obtained from a single well within an assay. **(C)** Organoid volumes calculated on day 6 of culture with each treatment of compound, measured using GelCountTM analysis software for Iso 50 (i), Iso 72 (ii) and Iso 75 (iii). Data generated by Jennifer Shone under my supervision. *Dose response curves generated by Jennifer Shone, referenced in report 'Maniuplating the Wnt signaling pathway', PTY report (2015-2016)*

(Ai)

(Aii)

(Aiii)
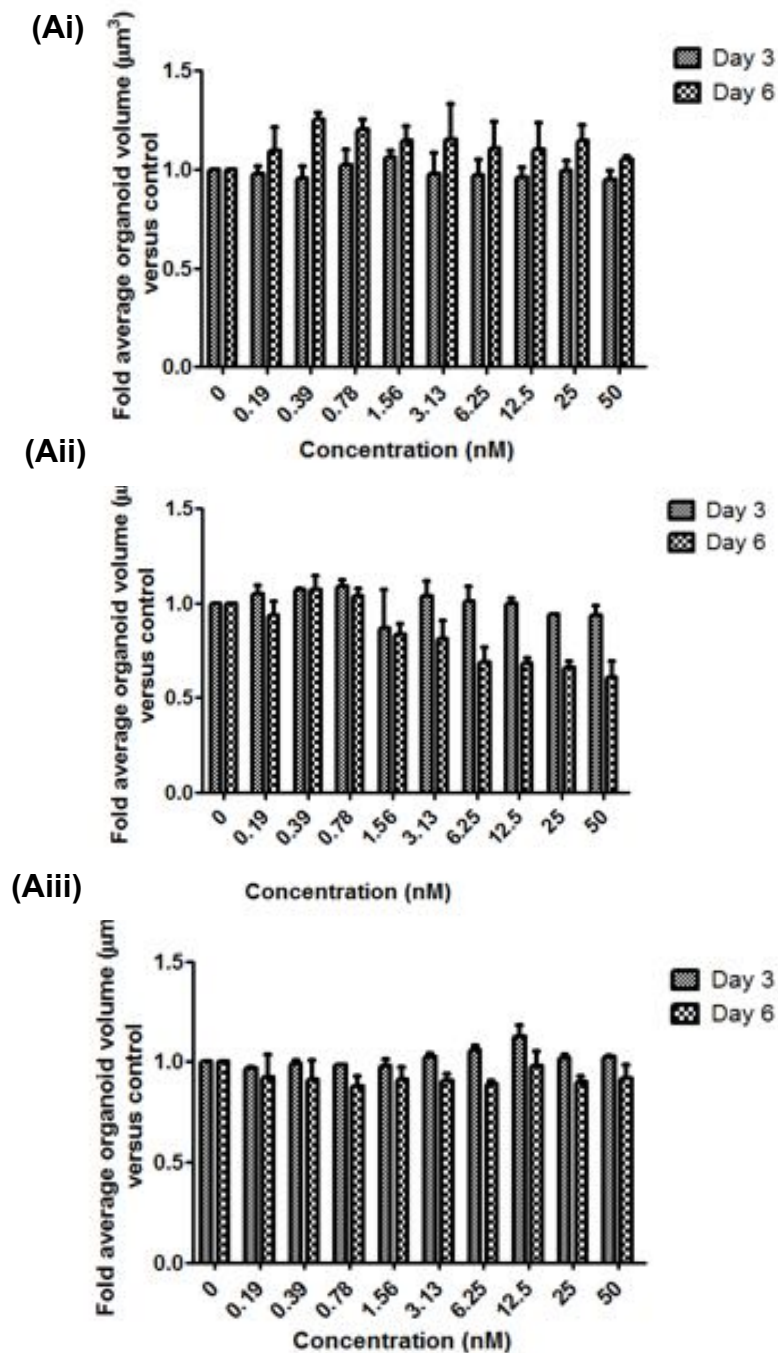
Figure 5.2 Analysis of the effects of the Tankyrase inhibitor MSC2524070 on overall organoid volume

Iso 50, Iso 72 and Iso 75 organoids were seeded at 400 cells/µl Matrigel and overlaid with previously specified growth media, supplemented with MSC2524070 at a two fold dilution (0.195 nM – 50 nM), and a matched DMSO control (0.1% in media). (A)Organoid volumes of (i) Iso 50, (ii) Iso 72, (iii) Iso 75 calculated on day 6 of culture with each treatment of compound, measured using GelCountTM analysis software. *Data generated by Jennifer Shone under my supervision.*

(Ai)

(Aii)

(Aiii)
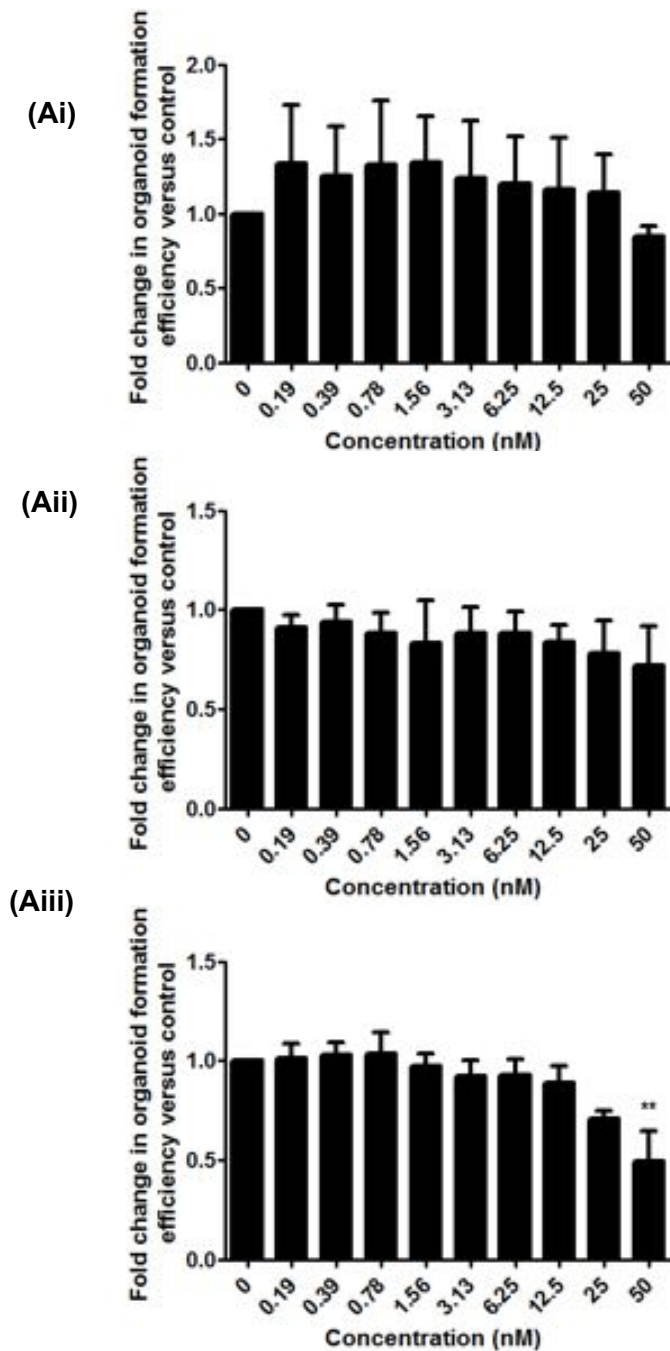
Figure 5.3 Analysis of the effects of the Tankyrase inhibitor MSC2524070 on organoid formation efficiency.

Freshly trypsinised organoids were seeded at 400 cells/μl Matrigel and overlaid with previously specified growth media supplemented with concentrations of each of the MSC2524070 at a two fold dilution (0.195 nM – 50 nM), and a matched DMSO control (0.1% in media) for 6 days in culture. (**A**) Bar charts depicting organoid formations efficiencies calculated following 3 days in culture for (i) Iso 50; (ii) Iso 72;(iii) Iso 75. Data are shown as mean±s.e.m, whereby n=3. Statistical significance as compared to control as indicated by * (p≤0.05) ** (p≤0.01), calculated by a one way ANOVA, followed by Dunnett's multiple comparison post-hoc testing. *Data generated by Jennifer Shone under my supervision.*

5.2.2 Tankyrase inhibition significantly reduces proliferation

Prompted by indications that TNKSi induced differential levels of growth responses in a subset of organoids, it was further explored whether treatment with MSC2524070 impacted cell proliferation.

Following 6 days of treatment with 25nM MSC2524070A or 0.1% DMSO untreated control, Iso 50 and Iso 72 structures (a non-responder and responder organoid line, respectively) were fixed by addition of 4% PFA to each well at room temperature for 15 minutes. Organoids were washed and stained within black, clear-bottomed 96 well plates and stained with a nuclear stain (Hoechst) and proliferation marker (Ki67), prior to acquisition of z-stack images on a confocal microscope. To detect and quantify positively stained cells within organoids, an automated counting tool was established using IMARIS software (BITPLANE). A number of thresholds were generated to assess staining intensity and morphology to ensure that counted objects were not duplicated. For counting purposes, a mask was generated to quantify the number of Hoechst-stained nuclei present, and Ki67 positive cells on an organoid-by-organoid basis. The number of ki67-positive cells were then calculated as a percentage per whole organoid (%).

Using the established settings for automated cell counts, it was possible to score the number of cells per organoid structure from Hoechst stained nuclei as a further measurement of organoid growth. As shown in Figure 5.4, Iso 72 organoids contained an average of 108±12 cells per organoid in untreated control conditions, as opposed to 47±11 in the presence of TNKSi MSC2524070. On the contrary, Iso 50 showed no significant alteration in the number of nuclei per organoid following a six-day exposure to compound, with no significant difference in number of nuclei in control and treated conditions.

Quantification of ki67 positive cells revealed a significant reduction in the percentage of proliferating cells per organoid following 6 days of TNKSi treatment compared to control conditions in Iso 72 organoids (0.33% ± 0.2562% versus 34.38%

± 8.510%, p=0.005, unpaired t-test with Welch's correction). In contrast, a non-TNKSi-sensitive organoid line, Iso 50, showed no significant difference in the overall ratio of ki67 positive cells per organoid in both conditions, indicating that proliferation was unaffected despite treatment.

Despite organoids assessed showing a TNKSi-dependent decrease upon proliferation in sensitive organoids (Iso 72), it is worth noting that such counts have technical limitations upon what can be interpreted biologically; such a low-throughput system restricts the number of organoids which can be quantified, and in this case were limited to a maximum of 12 organoids per condition.
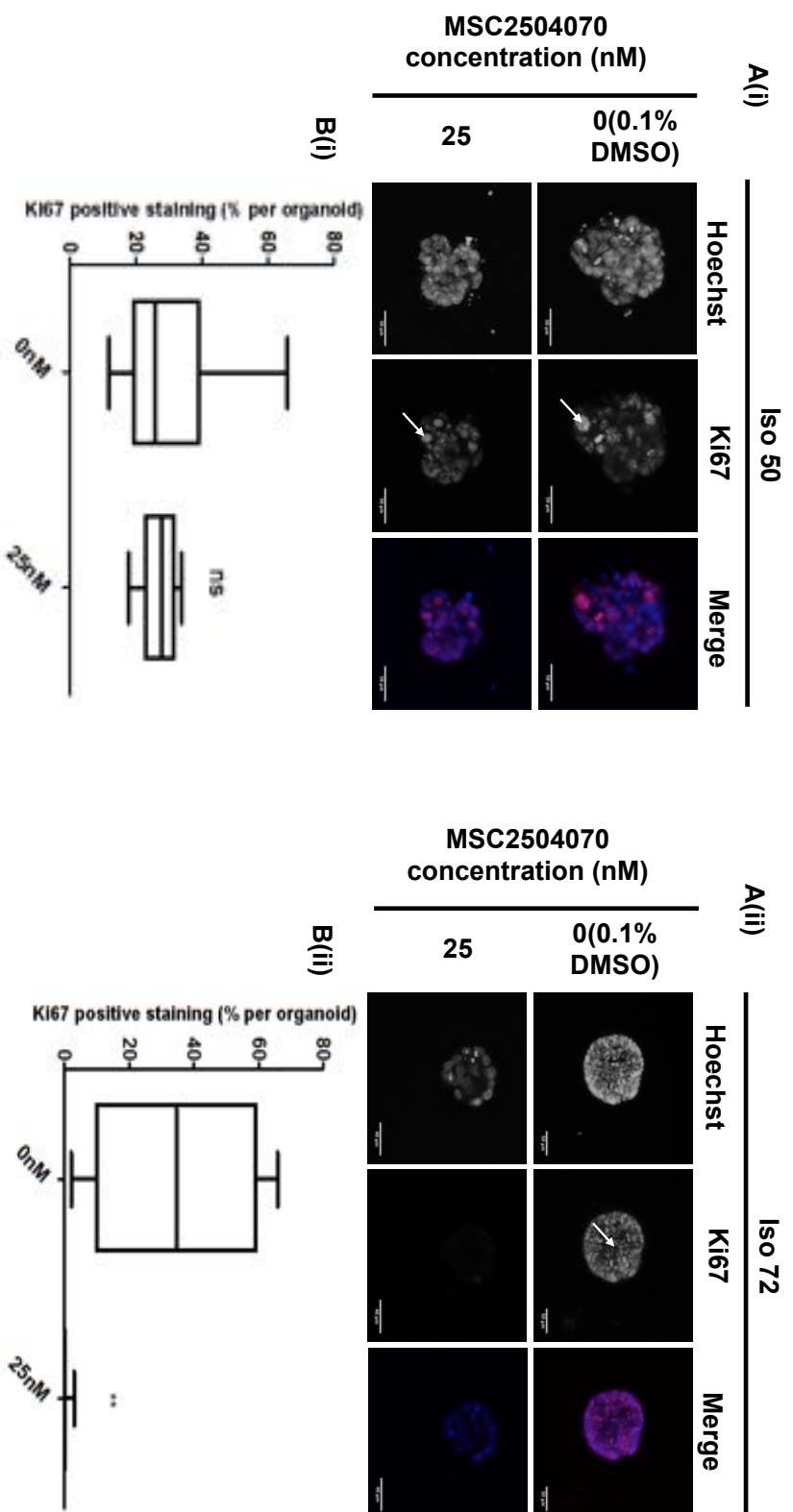
Figure 5.4 Assessing the effects of the Tankyrase inhibitor MSC2524070 on organoid proliferation

Freshly trypsinised organoids were seeded at 400 cells/μl Matrigel and overlaid with media supplemented with 15mM of MSC2524070 or DMSO (0.1 %). Organoids were fixed with 4% PFA following 6 days in culture, and subsequently stained with Ki67 (proliferation) marker and Hoechst (nuclear) within matrigel. A(i-iii) Z-stack images of stained organoids. Scale bars = 50 μm, 40 μm (Ai, Aii)B(i-ii) Following image acquisition, the number of Ki67 positive cells were calculated per whole organoid within each condition using IMARIS software. (n=8-14) organoids were counted per condition. unpaired t-test with Welch's correction p ≤0.005). *Images and raw data counts were generated by Jennifer Shone under my supervision.*

167

5.2.3 Phenotypic screening of TNKSi-treated organoids

Given the limitations of quantifiable readouts used thus far, it was necessary to further interrogate the functional effects of TNKSi upon organoids beyond such basic measures, to facilitate a clearer discrimination between dose-dependent effects of treatment. As such, a high-throughput multi-parametric phenotypic analysis screen was performed, in collaboration with OcellO (Leiden University). Phenotypic screening has been implicated as a successful way to identify drug responses relying on functional effects of cell behaviour as opposed to focusing purely on molecular targets (Moffat *et al.* 2014; Sandercock *et al.* 2015). Within the literature, OcellO have established a refined system whereby images z-stacks can be interrogated to identify certain treatment-dependent feature responses which can take place (Sandercock *et al.* 2015; Di, Klop, Rogkoti, Devedec, Water van de, *et al.* 2014). Here, the high-throughput format of such an assay system was used to investigate the impact of three novel TNKSi with log-fold changes in known EC_{50} values (previously established by Merck Serono) upon 8 organoid lines.

5.2.3.1 Multi-parametric quantification of morphological and fluorescence intensity reveals TNKSi-dependent effects within an organoid cohort

8 organoid lines (Iso 34, 38, 48, 49, 50 , 72, 75, 78) were seeded as single cells at a density of 400 cells/µl matrigel per well of a 384 plate, to a total volume of 12µl within a matrigel meniscus. Upon matrigel polymerisation, tailored media, as previously established per line (Chapter 3) was added to each well with a titration of compounds (MSC2524070A 0.39 nM -100nM; MSC2572070A 0.8 nM – 250 nM; MSC2521490A 4nM – 1250 nM) at a ten-point, two-fold dilution, with DMSO (0.1%) as a negative control. A total of 8 replicate wells were used per condition. Organoids were subject to treatment for a total of 6 days prior to simultaneous fixation and staining with F-actin (TRITC phalloidin) and nuclear stains (Hoechst 3568) (as described by Di et al 2014).

Individual z-stack images of whole 384 well plates were collected on a MetaXpress® high-content microscope at OcellO. Images were then inputted into the OMiner analysis software developed by OcellO, as detailed previously in Chapter 2 (section 2.6.3). Briefly, projections of the F-actin and nuclei-derived image stacks were used to extrapolate masks of individual organoids, internal lumen structures and nuclei. Image segmentation and filters were applied to distinguish individual objects per well, and enhance noise suppression to balance sensitivity of analysis. Relevant masks were then used to acquire approximately 700 quantifiable morphological features, including data relating to fluorescence intensities acquired per channel.

Data from individual organoids were then pooled on a well-by-well basis, with data from individual wells then gathered to yield average parameter readings per treatment condition. Variation in specific measured parameters across a plate were assessed by heat mapping, as shown in Figure 5.5, to ensure that technical replicates were valid for analysis; any outliers were removed from analysis, resulting in a minimum of 6 replicate wells used for subsequent data accumulation. Any outliers from analysis were usually a result of matrigel disruption within the well (as a consequence of plating or shipping conditions).

Images and corresponding masks obtained from nuclei and F-actin channels demonstrated that within control conditions, organoids formed distinct structures with intense f-actin staining within organoid lumens. F-actin integrity has previously been implicated as a critical factor for overall cell viability and structural support, as well as nuclear division (Caie *et al.* 2010). Measurement of individual parameters, such as overall organoid size, showed clear TNKSi-induced effects in Iso 72, as indicated by heat mapping across the plate , as depicted in Figure 5.5, further corroborating previous data. Consistent with previous findings using GelCount measurements, morphometric analysis highlighted a dose-dependent difference in overall organoid sizes of Iso 72 treated MSC2524070 compared to negative control conditions (DMSO, 0.1%). In concordance with this, using measurements generated from masks of Hoechst channel information, it was also observed that there was an

overall decrease in the number of nuclei per organoid compared to control conditions.

Morphometric analysis also revealed that iso 72 demonstrated a change in overall lumen size as a result of tankyrase inhibition. Interestingly, in the lowest concentrations of compound administered, it was found that an overall increase in lumen size occurred, which did not seem to equate to overall increase in organoid size. In a recent study by Lau *et al* (2013), it was also found that TNKSI G007-LK and G244-LM, mediated a similar effects in organoids cultured from Apc^{min} small intestine adenomas. A similar effect could be taking place in organoids cultured here, whereby an increase in size with tankyrase inhibitor could be coupled with the induction of differentiation whereby cells are shed into the central lumen. This might also occur if epithelial cell to cell junction integrity were disrupted, whereby polarised lumens are no longer formed in response to TNKS inhibition.
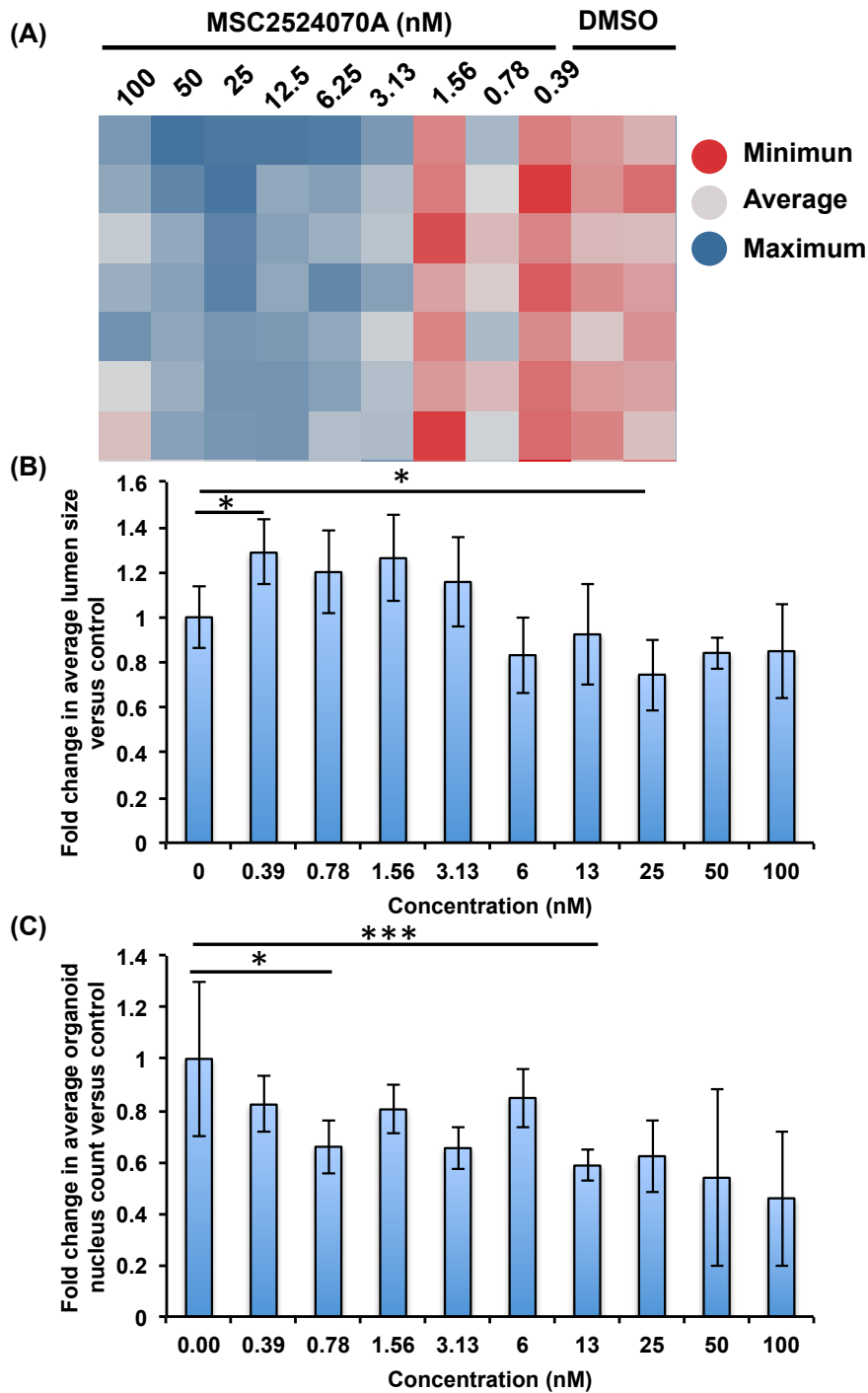
Figure 5.5 TNKSi mediate morphological changes in Iso 72 organoids.
Iso 72 organoids were seeded in 384 well format within growth factor-reduced matrigel and administered with a titration of MSC2524070A compound at a range of concentrations (19nM – 50nM). Organoids were subject to treatment for 6 days prior to simultaneous fix and stain, then analysed by OcellO Ominer software. (**A**) Heat map based on total organoid area within a 384 well plate between DMSO (0.1 %) and MSC2522070A conditions (Heat map generated by OcellO readout, raw data obtained by Ominer software, OcellO). (**B**) Fold change in average lumen size in response to tankyrase inhibition (**C**) Counts of changes in average number of nuclei per organoid in response to treatment; p<0.05*;p<0.01**; p<0/001***, ANOVA with Dunnett's multiple comparison test.

5.2.3.2 Feature-space training of phenotypic screening reveals targeted effects of TNKSi treatments within organoids

To assess whether on-target effects of compounds could be measured by phenotypic screening, multi-parametric feature space training analysis was implemented to facilitate further discrimination of phenotypes observed between administered doses and negative control conditions. Previous studies within the literature have utilised such methods of analysis to enable a selection of optimum features to classify responses to a particular compound (Sandercock *et al.* 2015; Di, Klop, Rogkoti, Devedec, Water van de, *et al.* 2014; Caie *et al.* 2010).

Firstly, following morphometric and fluorescent measurements of individual organoid components, all data were normalised per feature by robust z-score (Described in (Di, Klop, Rogkoti, Devedec, Water van de, *et al.* 2014), supplementary information), to account for variability between plates (such as potential differences in staining intensities). The highest doses of each compound were then used to select features that maximally separated high dose treatment from negative controls, based on robust z-scores. Principal component analysis (PCA) was then performed on each data set for compound and control DMSO-treated samples, per organoid line, to reduce phenotypic measurements to key principal components (PC) only, as opposed to assessing individual parameters. By reducing data into key components of variation, it was possible to visualise responses across a titration range of doses, to clearly discriminate between the highest doses and negative control (DMSO, 0.1%) conditions. The distances between the primary principal components (PC0) in phenotypic space were then measured using an Euclidean distance metric (equivalent to Mahalanobis distance metric utilised in chapter 4) between control and treatment conditions of organoids. It would be expected that a maximal separation of Euclidean distances would be observed in wells whereby phenotypes are most dissimilar. Based on this assumption, TNKSi sensitivity would therefore result in larger segregation of Euclidean distances in measured principal

components between DMSO conditions and increasing concentrations of an inhibitor.

Euclidean distance analyses of three compounds measured against DMSO control conditions in a cohort of 8 organoids were plotted with a log EC_{50} (μM). As shown in Figure 5.6 (B) the organoid lines Iso 72, Iso 75 and Iso 78 were shown to have a clear dose-dependent response upon phenotypic parameters induced by compounds. Figure 5.6 (A) further highlights the morphometric output of sensitive organoid line Iso 75 treated with the highest concentration of each compound, compared to Iso 50, showing visually little alteration in the presence of compounds administered. Interestingly, both Iso 75 and Iso 78 were dependent on Full media containing Wnt and R-spondin to facilitate normal growth in culture, indicative of high levels of Wnt dependency. However, Iso 72 was shown to sustain growth independent of Wnt in the media, suggesting that response if not necessarily correlated of external growth factor dependence. Iso 38 and 34 appeared to have a strong response to two of the inhibitors; MSC2501490A and MSC2572070A, but we were unable to detect such a clear EC_{50} for the most potent tested TNKSi, MSC2524070A. It was observed that TNKSi appeared to have a minimal effect across the range of phenotypes measured in the remaining lines, with little changes in Euclidean distance measurements between DMSO control conditions and an increasing dose range of TNKSi . Iso 50 responses corroborated previous data collected on a lack of impact upon overall organoid size as an indication of growth, as well as no impact upon overall proliferation.

Plotting principal components of a number of phenotypes in a multidimensional plot enabled a higher level of discrimination between highest and lowest dose of treatment, enabling the measurement of a clear dose-response curves whose aggregate quality far exceeded that of individual parameters. Importantly, such responses correlated with expected EC_{50}s over 3 log fold changes, indicating that collective data obtained from multiple phenotypic profiles were able to represent targeted effects of compounds.
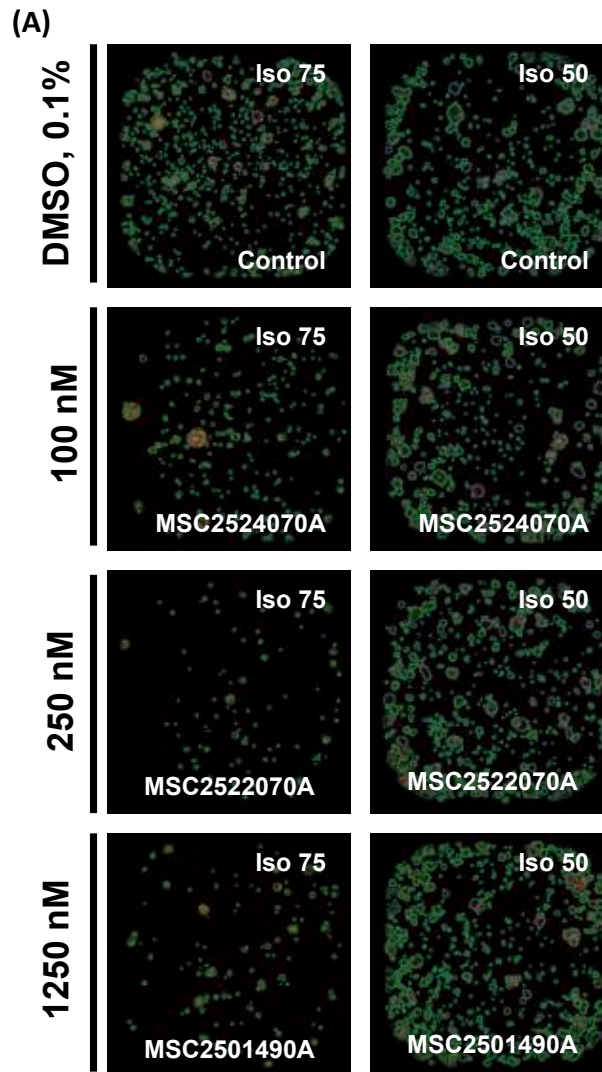
Figure 5.6 3D image analysis demonstrates on-target effects of TNKSi within organoid cultures

Tumor organoids were seeded within 384 well plates and overlaid with optimal growth media supplemented with MSC2501490A,MSC2524070A, MSC2572070A in a nine-point, two-fold drug titration, or a DMSO (0.1%) negative control. Cultures were treated for six days, prior to fixing and staining simultaneously with DAPI (nuclei; blue) and phalloidin (F-actin; red). (**A**) Representative images of individual wells of a 384 well plate, demonstrating slight morphological effects of highest tankyrase inhibitor doses in a sensitive and non-sensitive organoid line (Iso 72, Iso 50) (**B**) Principal component analysis was used to select the top 10 most discriminating features to separate compound-induced phenotypes between high and low doses of tankyrase inhibitors. Selected parameters were used for feature space training, whereby Euclidean distance metrics were calculated between high and low doses of each compound for each organoid line. Highest doses of each compound were used to select the most discriminating features that best separated treatments from negative controls. Euclidean distance between the treated and non-treated conditions was plotted for each treated organoid. Data are presented as mean Euclidean distance from 8 replicate wells ± standard deviation. *Images captured and analysed by OcellO.*

(B)

Iso 72 — Euclidian Distance from neg. ctrl — Dose (log μM)
Legend: DMSO, MSC2501490A, MSC2524070A, MSC2572070A

Iso 48 — Euclidian Distance from neg. ctrl — Dose (log μM)
Legend: DMSO, MSC2501490A, MSC2524070A, MSC2572070A

Iso 75 — Euclidian Distance from neg. ctrl — Dose (log μM)
Legend: DMSO, MSC2501490A, MSC2524070A, MSC2572070A

Iso 34 — Euclidian Distance from neg. ctrl — Dose (log μM)
Legend: DMSO, MSC2501490A, MSC2524070A, MSC2572070A

Iso 38 — Euclidian Distance from neg. ctrl — Dose (log μM)
Legend: DMSO, MSC2501490A, MSC2524070A, MSC2572070A

Iso 49 — Euclidian Distance from neg. ctrl — Dose (log μM)
Legend: DMSO, MSC2501490A, MSC2524070A, MSC2572070A

Iso 50 — Euclidian Distance from neg. ctrl — Dose (log μM)
Legend: DMSO, MSC2501490A, MSC2524070A, MSC2572070A

Iso 78 — Euclidian Distance from neg. ctrl — Dose (log μM)
Legend: DMSO, MSC2501490A, MSC2524070A, MSC2572070A

Table 5.1 EC_{50} values obtained from multi-parametric analysis.

	EC_{50} (nM)							
	Iso 34	Iso 38	Iso 48	Iso 49	Iso 50	Iso 72	Iso 75	Iso 78
MSC2501490A	300	2000	no curve	no curve	300	1200	400	400
MSC2524070A	3	9	no curve	no curve	2.6	3	3	2
MSC2572070A	70	40	no curve	no curve	30	400	30	30

5.2.4 Assessing changes in organoid gene expression as a result of TNKSi treatment

5.2.4.1 TNKSi treatment simultaneously attenuates stem-cell marker expression and increases expression of differentiated intestinal cell markers in TNKSi-sensitive organoid lines

As previously discussed, activation of Wnt signalling specifically induces the expansion of stem cell populations in the intestine, as well as an active role in the maintenance of cancer stem cells. To determine whether inhibition of Wnt dependent growth by TNKSi induced an overall change in the stem cell signature of tumour organoids, quantitative RT-PCR analysis was used to examine the relative expression levels of a range of epithelial markers of stem and differentiated cell activity relevant to the large intestine. It was hypothesised that TNKSi would induce a downregulation of stem cell markers in sensitive organoid lines, impacting differentiation and subsequent organoid growth. Previous studies have highlighted the impact of gene expression as a response to TNKS inhibitors in culture (Lau *et al.* 2013).To determine whether TNKSi treatment impact the overall stem cell signature of organoids, quantitative RT-PCR analysis examining the expression of published ISC markers *Lgr5*, *Ascl2* as well as the differentiation markers *KRT20* and *DKK1*.

Organoids previously established in culture were dissociated to single cells by administration of TrypLE, washed, then embedded at a density of 400 cells/ µl within growth factor-reduced matrigel. Iso 72 and Iso 50 were overlaid with 7+ media conditions, whilst that Iso 75 required exogenously supplied Wnt, R-spondin and other growth factors within 'Full' media, as indicated by previous experiments. Treatment was administered within media upon seeding (0.1% DMSO control, 15nM MSC22524070A). Following 6 days of treatment, organoids were dissociated to extract RNA to be utilised for subsequent gene expression analysis. Overall, as shown in Figure 5.7, a significant reduction was found in the expression of both Lgr5

and Ascl2 following 6 days of treatment, with the most enhanced effects on Lgr5 and Ascl2 gene expression observed in sensitive lines Iso 72 and Iso 75. Interestingly, Ascl2 expression was also diminished in a resistant organoid line, Iso 50 whereas Lgr5 expression was unaffected. This could potentially suggest that Iso 50 is inherently reliant on different stem cell populations that were not assessed here, such as Olfm4, or that TNKSi treatment induces an effect to up-regulate different stem cell populations to compensate and facilitate organoid growth.

To further corroborate this data, TNKSi-treated organoids were immunostained with an Lgr5 antibody. Following treatment with MSC2524070A or DMSO (control conditions, 0.1 %) for 6 days, organoid lines were stained phalloidin to mark F-actin to highlight overall cellular architecture. Lgr5 staining was found prominently on the basal edges of all organoids in control conditions, with some variability in degree of Lgr5 positive cells. Lgr5 expression of TNKSi-sensitive lines was abrogated in both Iso 72 and Iso 75, as shown in Figure 5.8 with no staining visible in organoids per well (n=3 technical replicates) as depicted by representative images. Morphologically, the number of nuclei per organoid was generally diminished per structure, within sensitive organoid lines. Iso 72 structures in particular were composed of few cells, as indicated by Hoechst staining and a generally poor cellular organisation. Interestingly, F-actin staining intensity was also somewhat diminished. Overall, these observations support qRT-PCR data; however, given that counts could not be obtained from Lgr5 positive cells due to the nature of the immunostain, the corroborating conclusions are purely qualitative.

An enhanced expression of an intestinal differentiation marker cytokeratin 20, *KRT20*, was also observed in two TNKSi-sensitive organoid lines (Iso 72, Iso 75) following treatment with MSC2524070 (8.9±1.8 and 13.3±4.58 fold change compared to DMSO control, respectively). Iso 50, a previously identified non-responder line was however was shown to have a non-significant increase in *KRT20* expression (1.7±0.67 fold increase in *KRT20* gene expression normalised to control conditions) indicative that differentiation was not substantially enhanced. However,

it is worth noting that KRT20 is not the only possible marker that could have been used as an indication of differentiation within intestinal stem cells.

Consistent with these findings, immunostaining three organoid lines for *KRT20* expression also revealed an increased expression of cytokeratin 20 upon treatment, compared to control conditions (Appendix II-1, Figure 7.3), in TNKSi sensitive lines, particularly in the lumen compartments of each organoid. However, given that TNKSi-sensitive organoids lines (Iso 72, Iso 75) were generally smaller structures as a result of treatment, this could be a staining artefact whereby antibody penetration is vastly improved. As this method is not quantifiable it is not possible to comment on levels of significance these results at present. This is particularly important to note for Iso 72 treated with MSC2504070A as the organoids were more readily washed away in the preparation for staining as they were so small, which lowers confidence in numbers.
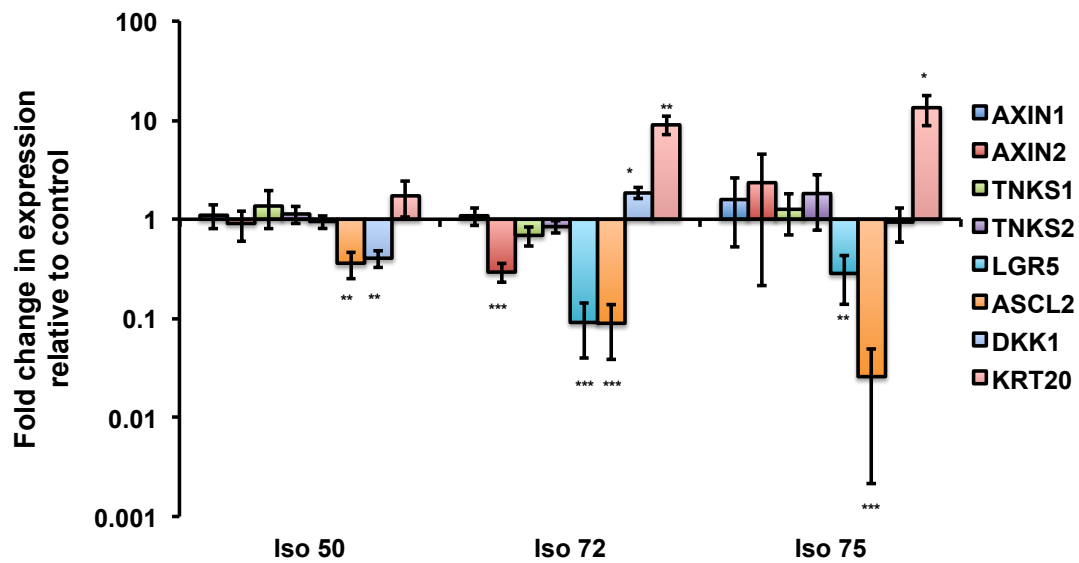
Figure 5.7 Organoid gene expression in response to tankyrase inhibitor.

Organoids were dissociated to near single cells using TrypLE, and seeded at a density of 400 cells/ µl of Matrigel. Cells were administered with appropriate media conditions supplemented with control (DMSO, 0.1%) or treatment conditions (MSC2524070) for a total of six days in culture. Following treatment or control conditions, gene expression was evaluated by quantitative RT-PCR. Data are expressed as fold change (vs. untreated DMSO control, means ± standard error of the mean, n=3 independent experiments). Statistical analysis was performed using paired Student T Test whereby *indicates p≤0.05, ** indicates p≤0.01, *** indicates p ≤0.001.
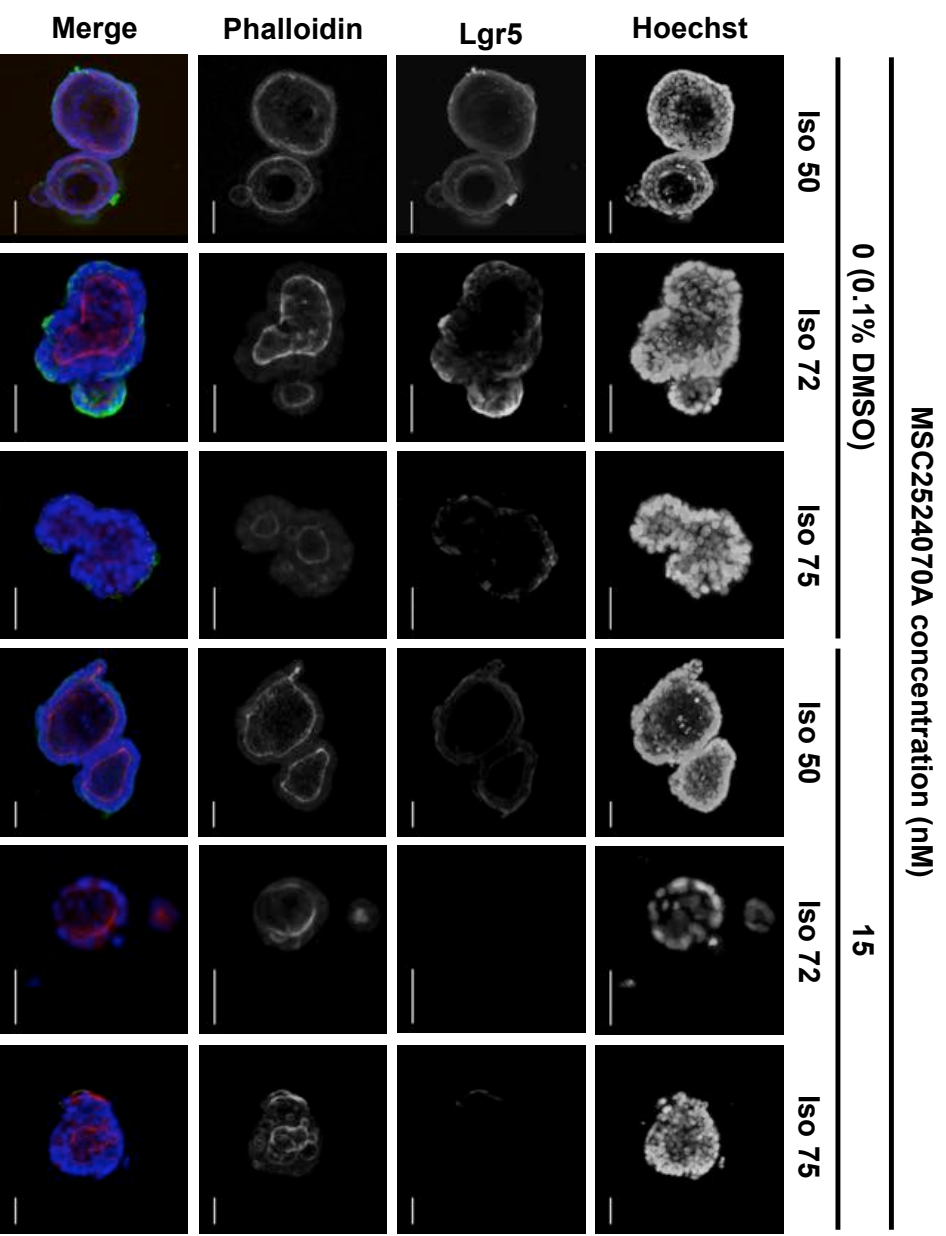
Figure 5.8 Analysis of the effects of the Tankyrase inhibitor MSC2524070A on Lgr5 expression.

Freshly trypsinised organoids (Iso 50, Iso 72, Iso 75) were seeded at 400 cells/µl Matrigel and overlaid with previously specified growth media supplemented with MSC2524070A (15nM, 6 days), and a matched DMSO control (0.1% in media). Organoids were then fixed and immunostained for Lgr5 and TRITC-phalloidin within treatment and control conditions. Scale bar = 50µm.

5.2.4.2 TNKSi impact on Wnt/ ß-catenin targets

In order to further investigate the downstream impacts of tankyrase inhibitors, gene expression profiles of Wnt target genes, including *AXIN 2, TNKS 1/2,* were obtained in 3 organoid lines (Iso 50, Iso 72, and Iso 75). Iso 72, a TNKSi sensitive line, exhibited stabilisation of *AXIN 2* as a result of treatment. *AXIN1* was unaffected in all lines measured, as shown in Figure 5.7.

DKK1, a direct Wnt/ß-catenin signalling antagonist (Lau *et al.* 2013) demonstrated a marked reduction in expression of Iso50 organoids treated with MSC2424070 normalised to control, but a significant increase in a sensitive organoid line Iso 72. This difference could be essential in their converse responses to TNKS inhibition as DKK1 may increase Wnt negative regulation, leading to an overall reduction in Wnt/ß-catenin signalling and a reduction in proliferation. Increase gene expression of DKK1, observed in the TNKSi sensitive line Iso 72, may further increase Wnt negative regulation, resulting in an overall reduction of Wnt/ ß-catenin signalling. It is clear that responses and feedback outcomes are therefore highly dynamic, further highlighting the complexity of Wnt signalling.

In order to further investigate the downstream impacts of tankyrase inhibitors, the cellular distribution of ß-catenin was also assessed by immunofluorescence in organoids treated with MSC2524070 (15nM, 6 days) as depicted in Figure 5.9. In a population of DMSO (0.1%) – treated organoids, all three lines expressed ß-catenin in both cytoplasmic and nuclear compartments. However, MSC2524070 treatment induced a general reduction in total ß-catenin levels in both sensitive and non-sensitive lines. Iso 72, in particular demonstrated no levels of ß-catenin stain within structures.

Overall, this data would suggest that TNKS inhibition elicits a downstream effect upon Wnt signalling gene targets in both sensitive and non-sensitive organoid lines, which may or may not subsequently impact growth and proliferation in the different

cellular contexts in each line. Given that the stem cell markers were somewhat downregulated, and differentiated markers upregulated compared to control and treatment conditions, this would suggest that the stem cell signature becomes reduced in organoids. However, given that the stem and differentiated markers explored here were by no means exhaustive, further work would need to be in place to identify whether some organoids lines were better adapted to compensate for loss of stem cell activity, potential that compensatory mechanisms could be induced in some lines to overcome effects of TNKS inhibition.
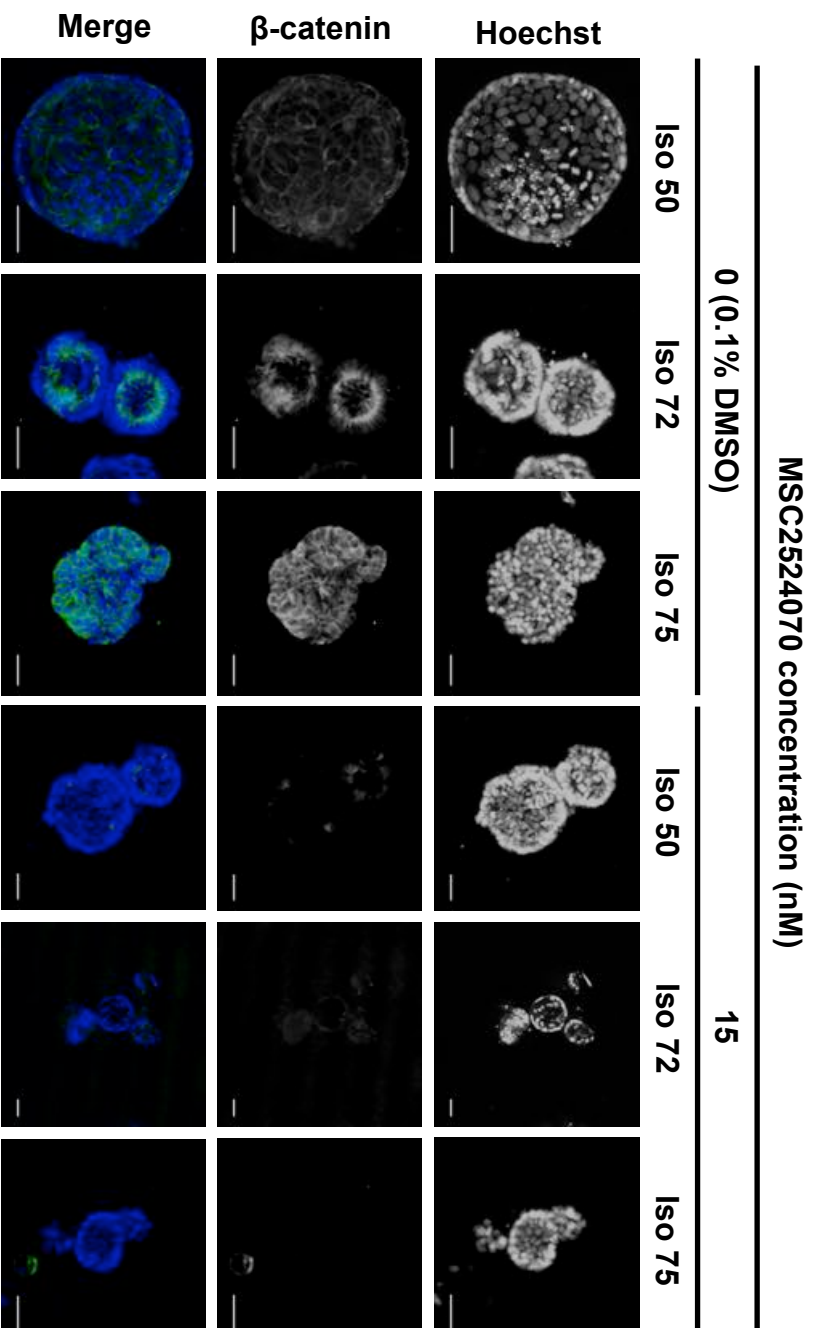
Figure 5.9 Analysis of β-catenin expression following tankyrase inhibitor MSC2524070 treatment.
Organoids (Iso 50, Iso 72, Iso 75) were seeded at 400 cells/µl Matrigel and overlaid with previously specified growth media supplemented with MSC2524070 (15 nM, 6 days), and a matched DMSO control (0.1% in media). Organoids were fixed and immunostained with B-catenin in both treatment and control conditions prior to confocal imaging. Scale 50 µm.

5.2.5 TNKS inhibition significantly delays tumour growth in an organoid-derived xenograft model

To assess whether functional and phenotypic effects of TNKSi-sensitive organoids would translate to tumour growth inhibition *in vivo*, a novel organoid-derived xenograft model was generated within the Dale Lab.

To investigate the therapeutic potential of TNKSi to target stem cell capacity of CRC, organoids pre-treated with TNKSi were transplanted into mice to assess whether this would alter the capacity of tumours to form, as well as an indication of proliferative status of cells. Given that Iso 75 had shown reliance upon Wnt and R-spondin within media, as well as other growth factors, and was shown to be sensitive to TNKSi within *in vitro* assays, experiments were performed with this line since it was expected to show maximal effects. Freshly trypsinised Iso 75 organoids were embedded in Matrigel and overlaid with Full media containing MSC2524070A at a concentration of 30 nM (EC$_{50}$, 10 X concentration) or DMSO (0.1%) as a negative control. Following growth for 24 hours, which was estimated to be long enough to induce biochemical changes without being long enough to alter the total number of cells in the organoids, samples from each condition were injected into the flanks of of 16 γ-irradiated Non- Obese Diabetic (NOD/SCID) mice, using one injection site per mouse, per condition.

It was observed that tumour formation occurred in 100% of sites injected, showing promise for this method to generate organoid-derived xenograft models. Furthermore, it was noted that organoids pre-treated with MSC2524070A resulted in a significant delay in tumour formation compared to control organoids, resulting in an increase in overall median survival of mice (Figure 5.10). This would suggest that MSC2524070A was sufficient to limit proliferative capacity of injected organoids. Given the complexity of stem cell dynamics within tumours, further experiments, including analysis of tumours formed, would need to take place to determine the mechanisms in place. It is possible that whilst tankyrase inhibition depleted Lgr5+

stem cells, that Lgr5- cells could have maintained proliferation formed enabling tumours to eventually form. This is in line with previous studies that have demonstrated pharmacological inhibition of Lgr5+ cells result in tumour regrowth after cessation of treatment (Junttila *et al.* 2015). Furthermore, a recent study has demonstrated that in the absence of Lgr5+ CSCs, Lgr5- cells are capable of maintaining proliferation, to a lesser degree of function (Shimokawa *et al.* 2017). In this context, it would appear that pre-treatment of organoids with TNKSi limited initial CSCs population within the tumour, that was able to recover following lack of treatment.

Despite this, the data give initial promise for potential therapies, which could possibly be used in combination with agents to treat bulk tumour cells following ablation of a pool of certain cancer stem cells. Furthermore, our observations confirm that *in vitro* work described here is translatable to *in vivo* studies, highlighting the possibilities of further work for the organoid model system.
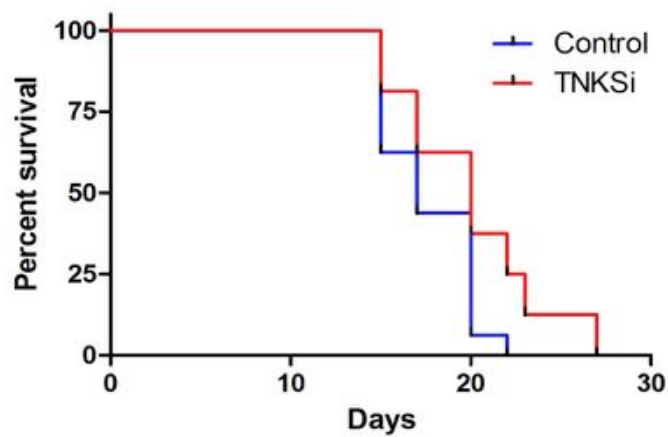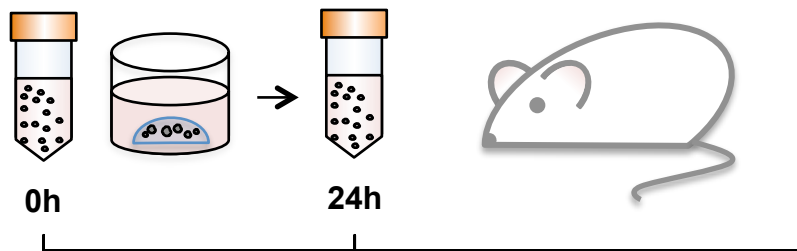
Figure 5.10 Kaplan-Meier survival analysis of NOD/SCID/ γ-irradiated mice injected with control or TNKSi treated organoids.

Mice were randomised to be injected with organoid treated for 24 hours. Organoids were exposed to either DMSO (0.1%) or 4070 (15nM). TNKSi treatment was found to delay the formation of tumours compared to control conditions (p value=0.032*, n=16 mice per cohort, Log-rank Mantel-cox test). *Experimental procedures and Kaplan-Meier survival analysis carried out by Dr. Kenneth Ewan (Dale lab)*

5.3   Summary

The work described in this chapter has shown a potential utility of colorectal organoids within drug discovery. Here, a cohort of primary CRC organoids were used to investigate novel inhibitors of the Wnt signalling pathway.

Through the use of phenotypic screening in collaboration with OcellO, it was shown that clear organoid responses could be obtained from readouts of overall organoid morphology in response to compounds. Given the complexity of Wnt signalling inhibitors and their potential subtle effects upon cells, demonstrating clear efficacy over 3 log EC_{50} values has emphasised organoids as a valuable asset for future drug discovery programmes. The results also indicated that TNKSi successfully limited the number of Lgr5+ cells within organoids, as well as limiting ß-catenin levels, suggesting an overall inhibitory effect upon Wnt signalling. Functionally, this was shown to have differential effects dependent on the organoid line, further highlighting the complexity of Wnt responses and the need for a range of phenotypic readouts.

Encouragingly, this work also demonstrated a concordance between effects of Wnt signalling inhibitors observed *in vitro* and in a comparative *in vivo* model. Whilst this was performed on a select cohort with limited follow-up analysis on *in vivo* effects, this was a particularly encouraging result to form the basis of future studies to assess whether organoids be used as an initial readout for compounds in drug discovery, thus limiting the overall number of mouse models required.

6 Discussion

The prospective modelling of CRC mutations in a patient-derived organoid system to generate functional predictive readouts for stratified medicine and the drug discovery pipeline is a promising avenue for cancer precision medicine. Despite the increasing evidence in the literature to support the notion that organoids provide a more sufficient model system than preceding 2D *in vitro* cell lines, their overall validation in terms of providing a robust screening tool in the context of biomarker-driven therapeutics in the clinic requires further proof-of-concept studies. In order to ultimately measure concordance between organoids and respective patient counterparts, a number of challenges associated with complex 3D culture need to be addressed, enabling the employment of organoids as a pre-clinical model system.

The overarching aim of this thesis was thus to validate the utility of organoids derived from CRC patient material as a relevant pre-clinical platform, in order to ascertain their application within stratified medicine and drug discovery. To address this, this thesis aimed to:

1. Develop suitable methodologies to transfer patient-derived organoids towards functional readouts.
2. Establish the capacity of organoids to provide functional readouts for biomarker-driven therapies by mirroring the FOCUS 4 clinical trial, towards assessing their predictive power.
3. Validate the potential utility of organoids in the drug discovery pipeline using novel Wnt-signalling inhibitors.

As a result, many interesting findings were raised and will be discussed in turn in this chapter, to explore the extent to which the aims have been addressed, and the overall contribution of this thesis.

6.1 Niche requirements facilitate organoid culture from patient derived samples

The isolation of human crypts and consecutive culture conditions to propagate organoid development, previously published by Sato *et al* (2011) and further adapted for our primary human samples, were shown to support robust long-term culture of patient derived organoids that can be adapted towards more high-throughput screenings.

Here, it was shown that parallel processing of samples within two media conditions was sufficient to generate tumour organoids in the first instance from approximately 80% of all samples processed. The generation of an organoid biobank from CRC material has previously been established (Wetering, Francies, Garnett, Wetering, *et al.* 2015) to generate 22 primary organoid lines, however failed to encompass rectal cancers. Within our collection stream at the Dale lab, a total of 78 samples have been isolated thus far, with 8 of these extensively characterised for the purpose of this study, inclusive of rectal cancer. From our processed samples, a clear divide was found in terms of reliance of some of our subset on 'Full' growth-factor and Wnt/R-spondin- containing media, as opposed to Basal '7+' media conditions. Both Iso 75 and Iso 78 were dependent on Full media to sustain growth; Iso 75 harboured no truncating APC mutations, therefore it is possible that the exogenous Wnt and R-spondin were essential to maintain cells in culture. CRISPR-mediated engineering of intestinal organoids have previously shown that *APC* wild type cells require the presence of Wnt and R-spondin within the media to continue in culture (Matano *et al.* 2015). However, without fully characterising the effects of titrating various components within the media, these observations are purely speculative. It is possible that the tumour grades may have a role in determining reliance upon multiple growth factors; previous studies have demonstrated the importance of the organoid niche as maintained by Wnt, Notch and Bone-morphogenetic protein (BMP), to determine differentiation of epithelial cell lineages (Sato *et al.* 2009; Yin *et al.* 2013). It is plausible that advanced tumours are so far adapted to this environment they have a requirement for multiple growth factors (Sachs et al 2013), or even hypoxic conditions (Fujii *et al.* 2016b).

The importance of the niche environment for optimal tumour organoid growth as noted here has been further explored by Fujii *et al.,* (2016), where they describe the formation of a tumour organoid biobank, established from eight various growth conditions containing different combinations of EGF, Noggin Wnt and R-spondin within the base medium. Within this study, the authors established niche factor dependencies by withdrawing each factor from the media and investigating the impact upon colony formation, until the minimal essential niche factor combinations for growth were deduced. However, a limiting factor of adopting this approach to establish conditions to favour organoid growth for a range of clinical subtypes is the quality of the surgically resected tissue in the first instance; if samples were necrotic, few viable cells were capable of survival. This would limit the number of growth conditions that could be tested in the crucial first hours-days of culture.

A key consideration for evaluating the potential of organoids as an effective pre-clinical model is reliant upon their capacity to represent molecular and biological components of parental tumours. Collaborative efforts with the WCB have enabled us to mostly integrate our data with patient data to generate a full cohort of degree stages corresponding to development of organoids. Organoids grown under optimal conditions were shown to recapitulate histologically relevant architectures to corresponding parent tumours (Figure 3.7), as well as functional differentiation, matching those from mirrored patient histology (Figure 3.8). Further exploration of specific markers to characterise tumours suggested that not only were organoids representative of particular tumours subtypes but, to a degree, were able to recapitulate expression of differentiated cell markers such as Mucin, as marked by Muc2, indicating that tumour characteristics were retained in culture.

A subset of organoids that were characterised by next generation sequencing were further shown to harbour a diverse pattern of genetic mutations, consistent with those reported within the Cancer Genome Atlas study (Cancer Genome Atlas Network 2012) whereby a collection of clinical CRC samples demonstrated the most commonly mutated genes in CRC. Similarly, the most frequent mutations within our

organoid cohort were genes such as *APC, PIK3CA* and *TP53*. As well as showing clinical relevance, our cohort were shown to have successfully established in culture, irrespective of mutational background. The organoid cohort here further demonstrates a similar distribution of specific genotypes as described in a recent generation of a CRC tumour organoid biobank (Wetering, Francies, Garnett, Wetering, *et al.* 2015). The comparative genomic profiles between CRC organoids and parental tumours are yet to be determined due to limited access to patient genotype data during the timeline of this study. Previous studies have demonstrated that overall, organoids capture the overall genetic landscape of their parental tumour, which translates through to organoid-xenograft models, and further maintaining stability over subsequent passage (Schütte *et al.* 2017) with some discrepancies arising as a result of intratumour heterogeneity. It is plausible that different tumour regions may have variable responses to targeted therapies. Tumour heterogeneity can occur on a regional basis within a tumour (Weeber *et al.* 2015) and thus organoid culture from multiple tumour sites could potentially give a more rounded overview of heterogeneity and therefore overall drug responses. However, broadly speaking, biomarkers such those relevant to the FOCUS 4 clinical trial, were shown to be retained across tumour sites (Weeber *et al.* 2015), which was sufficient for our particular studies.

6.2   Functional testing in a relevant model system is necessary to support genetic data; biomarkers do not always predict drug responses.

Despite the understanding of critical components that form the basis of tumour progression and malignancy, the ability to effectively treat tumours based on their biomarker profile has proved challenging. Stratification of patients based on the genomic imprint of their tumour ideally requires functional readouts to assess therapeutic effects of compounds. Chapter 4 described the application of organoids as a predictive model for biomarker-driven therapies, by mimicking compounds utilised within the FOCUS 4 clinical trial. The findings gathered from this thesis therefore hold some clinical implications, in particular to the molecularly stratified phase II MRC FOCUS 4 clinical trial for metastatic CRC patients. The design of an *in*

vitro clinical trial discussed here was sought to establish the potential efficacy of biomarker driven therapeutics in a relevant pre-clinical system, which could ultimately be compared with patient responses harbouring similar mutations. Unlike the FOCUS 4 clinical trial, it was possible to test all treatments upon organoids to establish optimal treatments. Interestingly, it was noted that the overall genotypic profile of organoids did not necessarily equate to growth inhibition by the treatment assigned to each arm, further highlighting the requirement of functionally relevant models. The most relevant findings will be discussed in turn here.

6.2.1 Aspirin metabolite induces growth inhibition within a subgroup of organoids, irrespective of PIK3CA mutation status.

An apparent observation within this work was the varied level of responses of organoids to aspirin metabolite treatment in order to mirror treatments that will be administered to patients within *PIK3CA* mutant arm of FOCUS 4. Within responsive organoids it was found that aspirin induced partial growth inhibition, and ultimately increased the number of apoptotic cells per organoid, in agreement with studies in aspirin-sensitive CRC cell lines (Goel *et al.* 2003). In a retrospective study by (Liao *et al.* 2012), it was shown that regular aspirin use following a diagnosis of colon cancer has been associated with an improved clinical outcome in patients with mutated *PIK3CA* as opposed to wild type, further corroborated in studies by (Domingo *et al.* 2013). However, no such correlation was observed in this organoid cohort treated with aspirin; organoids responsive to aspirin metabolite were not necessarily *PIK3CA* mutant, and not all *PIK3CA* mutant organoids were responsive to aspirin.

The lack of response in *PIK3CA* mutant organoids could be as a result of the assay format itself; previous studies have indicated that Aspirin has also been shown to be more effective in rapidly dividing cells only; as cell doubling rates in were not deduced for all organoid lines in this assay format, it is possible that the assay window to detect responses could vary (Zumwalt *et al.* 2017). The discordance in our findings is arguably, most likely, a result of the plethora of different mechanisms that could be induced by aspirin treatment, regardless of *PIK3CA* mutation status in cells,

and the few sample numbers of organoids tested. PIK3CA mutations leads to an upregulation of PI3K-AKT activation, which have an array of interactions upon the cell and can also be activated by receptor tyrosine kinases or activated RAS (Engelman 2009b). Despite the overall survival benefit for regular aspirin administration in *PIK3CA*-mutated CRC, the mechanistic understanding of this association is yet to be established. The molecular mechanisms of aspirin are strongly debated as to their effect upon tumour formation and/or growth; aside from their effects upon the immune system, studies have investigated the role of aspirin metabolites upon glycolytic metabolism in tumour cells, disruption of multiple signalling pathways, and inhibition on the basis of DNA MMR proficiency. Studies have also proposed that the use of NSAIDs such as aspirin mediates a reduction in Lgr5 expression within carcinoma cell lines (DLD1 cells) in a PGE2-dependent manner (Al-kharusi *et al.* 2013). Theoretically, a reduced Lgr5+ cell population would thus result in a reduced clonogenic growth of CSCs, thus preventing tumour formation. Given that organoids are capable of retaining a stem cell population, this mechanism could be further investigated in future studies. Aspirin has multiple targets and thus PI3KCA is not necessarily the best as a predisposed biomarker and may have numerous influences that determine overall tumour responses. The variable responses to aspirin from organoid could indicate a major mechanism is on the immune cells and/or stroma, which are absent in organoids.

The major caveat of this work described in chapter 4 is that the organoids described were not necessarily obtained from patients recruited to the FOCUS 4 clinical trial. However, the organoids described were representative of relevant biomarkers and thus hold some basis to mirror biomarker-targeted drug responses administered within the trial. Given that a subset of 8 organoids were used for this study also, further analysis would be required to assess the true predictive power of organoids. Taken together, the data presented herein would suggest that *PIK3CA* mutations were not the only apparent biomarker to indicate aspirin response, which could have important clinical implications within the FOCUS 4 clinical trial.

6.2.2 Compounds targeting DNA damage responses impose anti-proliferative and pro-apoptotic effects within organoids harbouring TP53 mutations.

The therapeutic potential of compounds targeting Wee1 and ATR, both crucial components within the DNA damage responses was assessed in our organoid cohort to ultimately assess whether similar treatment outputs would be observed in patients. Ultimately, this data may hold some clinical value on the overall efficacy of reducing tumour growth. It would be hypothesised that synthetic lethality by administration of Wee1 and ATR inhibitor, would prevent cell cycle progression, and thus inhibit growth in the organoid model.

Administration of MK1775 (Wee1 inhibitor) and AZ20 (ATR inhibitor) resulted in an inhibition of overall organoid growth, as indicated by measurements of viability and basic morphometric measurements following 4 days of exposure with the compound. As described previously, Wee1 has a major role in mediating the G2/M checkpoint in the cell cycle, enabling time to repair any remaining double strand breaks before cell division (Weisberg *et al.* 2015). Administration of Wee1 inhibitor upon organoids was also shown to potentiate apoptotic effects, as evident by phenotypic readouts. This is in accordance with previous studies that have elucidated the cytotoxic effects of this compound in an array of cell lines, and further shown to be effective in mouse models (Guertin *et al.* 2013). Mechanistically, studies have shown that p53 loss in cells result in mitotic catastrophe in cell lines and thus the main cause of synthetic lethality (Aarts *et al.* 2012). However, recent studies have identified further epigenetic biomarkers such as trimethylation of histone H3K36me3 (Pfister *et al.* 2015) and shown that Wee1 can also induce synthetic lethality in p53 wild-type cells. This further highlights the need for functional systems which can encompass potentially multiple biomarkers for identification of therapeutic responses. Studies have also demonstrated that gastric cell lines lacking ATM, or contain TP53 defects, are vulnerable to inhibition of ATR by AZD6738

(analogue of AZ20), inducing replication initiation and fork stalling, ultimately resulting in DNA damage and an overall cytotoxic effects upon cells (Min *et al.* 2017). The data presented here suggests that targets of the DNA damage response may provide a suitable target for CRC therapy in ATM or Tp53 mutant patients. However, the overall relevance of the model system must be considered. Whilst readouts of toxicity upon organoids derived from patients provides encouraging support for the relevance of such compounds, the lack of readout on toxicity upon normal cells restricts the utility of organoids to confidently predict patient responses to therapy. Whilst the culture of healthy colorectal material was attempted during this study, growth was restricted to a month in culture, preventing the possibility of generating sufficient material as a control for subsequent drug readouts. A biobank of CRC organoids have recently presented the comparison of CRC-relevant compounds upon both normal and tumour tissue to achieve a basic readout of toxicity (Wetering, Francies, Garnett, Wetering, *et al.* 2015). Such systems could be employed for future studies whereby organoids are generated and treated in parallel with such clinical trials. An important consideration for this work is also the lack of suitable organoid based controls that were available for this study; given that all organoids generated were both ATM and tP53 mutant a clear distinction of the effects between ATM wild type and tp53 wild type were not able to take place. This would be hugely important to collect population-based data that is required for stratification studies.

6.2.3 Combination therapy targeting RAF-ERK signalling potentiates organoid growth inhibition

Despite the initial promise of BRAF and EGFR targeting therapies, clinical studies have demonstrated an overall limited success for treatment of CRC due to a lack of therapeutic effect. Both *in vitro* and *in vivo* studies support the notion that this lack of effect is mediated by the up-regulation of mechanisms to compensate for pathway inhibition (Corcoran *et al.* 2015; Corcoran 2015), as well as pre-existing mutations that predict non-response. Whole-exome sequencing of paired pretreatment and post-progression biopsies from BRAF mutant CRC samples from

patients have identified significant alteration in MAPK pathway such as BRAF and MEK amplifications. (Ahronian *et al.* 2015). As such, drug development strategies and pre-clinical investigations have justifiably focused efforts to target components of BRAF-mediated signalling. Within the MRC FOCUS 4 clinical trial it is hypothesised that targeting three components of BRAF-mediated signaling will improve tumour free progression within CRC patients (Figure 6.1). Here, to address whether such hypotheses could be tested in a relevant preclinical model, organoids propagated from BRAF mutant patients were assessed for their sensitivity to BRAF, EGFR and MEK inhibition, mirroring treatments administered to patients within the FOCUS 4 trial.
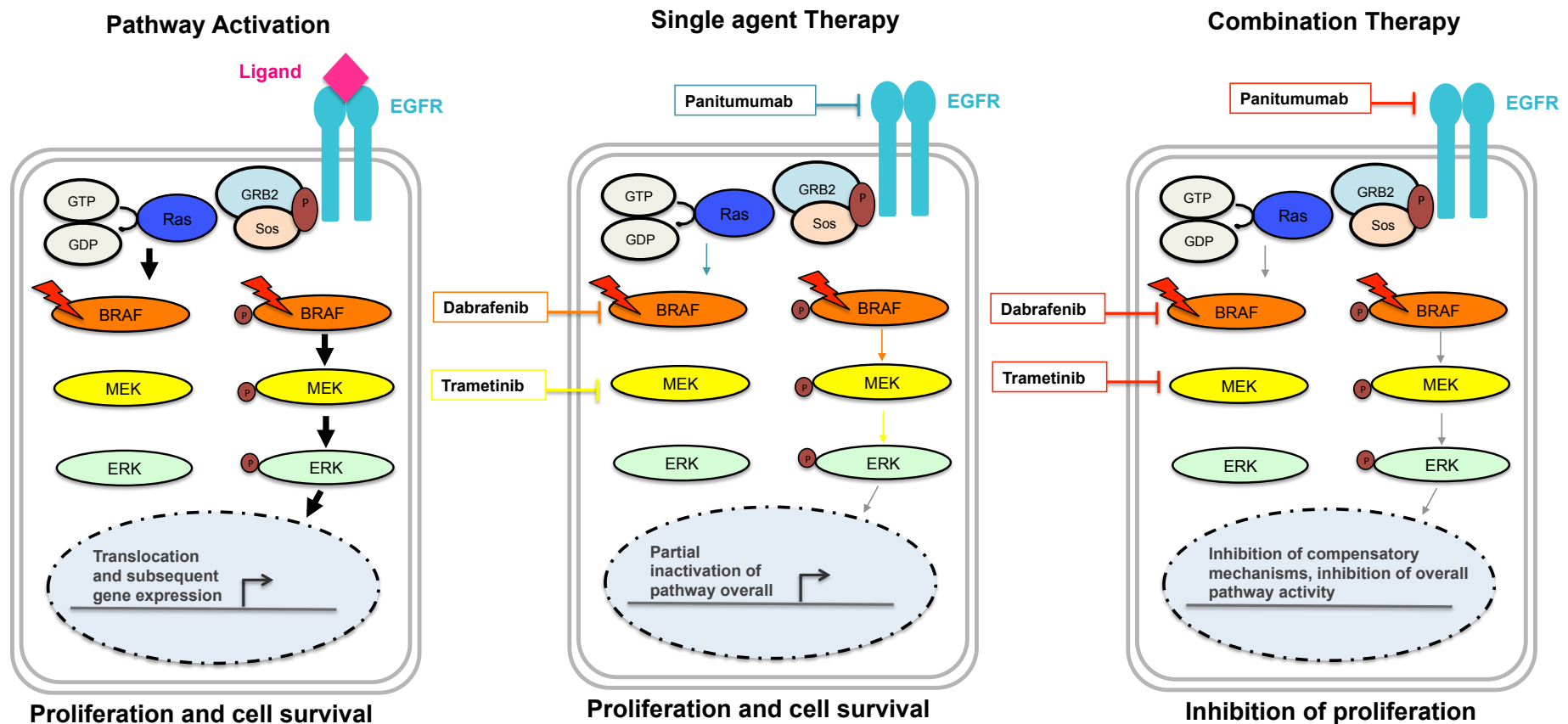
Figure 6.1 Inhibition of RAS-ERK signaling ; targeting adaptive feedback mechanisms

EGFR activates RAS-ERK signalling pathway to induce gene expression of components involved in cell proliferation and growth. Combination therapies, targeting multiple components within the pathway is theorized to overcome adaptive feedback reactivation induced by single agent therapies.

The therapeutic effects of each compound in turn were assessed to determine whether as hypothesised, BRAF mutations would incur sensitivity. Trametinib (MEK inhibitor) administration upon organoids resulted in a pro-apoptotic effect within cells, as opposed to Dabrafenib (BRAF inhibitor) and Panitumumab (EGFR inhibitor), compounds that showed little effect as single agents. Trametinib was further shown to potentiate the growth inhibition potential of both Dabrafenib and Panitumumab within combination drug screens. Previously, assessment of Trametinib and Dabrafenib in combination has shown favourable effects in BRAF mutant PDX models, as well as within CRC patients setting, improving overall prognosis (Corcoran *et al.* 2015). Some data has also shown the improvement of dual BRAF and MEK inhibition to treat metastatic colorectal adenocarcinomas (Williams *et al.* 2015). Importantly, sub-optimal inhibition of MAPK pathway has been shown to play a role in limited efficacy in patients, further highlighting the need for relevant model systems to test target affinity. Our studies also demonstrated a dose reduction index could be applied to both compounds, further corroborating findings that co-administration of BRAF and MEK inhibitor Dabrafenib and Trametinib improve overall safety profiles of compounds (King *et al.* 2013). In a recent study administration of Trametinib and an ERK inhibitor within organoids were able to induce cell cycle arrest, further affirming the application of Trametinib as an effective compound (Verissimo and et al. 2016). However, as well as demonstrating the effects of given compounds, the dose reduction effects were not established in this study, and are of equal importance to consider to ensure full tumour regression.

A BRAF-mutant organoid was further exposed to 3 compounds in combination and were found to impact growth, and limit the dosage of drug required of each compound to induce an IC_{50} effect. These findings suggest that targeting multiple components of EGFR-RAS-RAF signalling may succeed in preventing compensatory mechanisms to induce proliferation. Given the increasing number of combination strategies that require multiple targets for tumour growth inhibition, the capacity of organoids to be used within such a pre-clinical setting could be invaluable to generate data on the most appropriate combinations. A recent study demonstrated

the use of basic readouts of toxicity upon normal organoids to establish the effects of combination therapies upon the stem cell capacity in the colon (Verissimo and et al. 2016). It was found that EGFR inhibition induced similar effects in normal colonic organoids as to RAS Wild type organoids. Here, by utilising Chou-Talalay methods of analysis it was further possible to determine a fold change in compound treatment that could be effective in organoids at a much lower dose comparative to single agent administration.

In order to increase confidence in this analysis and drug regime, further studies upon multiple organoid lines would be required to fully establish the effects of BRAF inhibition. Ideally, findings would require some corroboration to determine the effects *in vivo*. A recent study within our group aiming to establish the *in vivo* activity of MEK and PI3K inhibitors within GEMMs as a pre-clinical evaluation for FOCUS4 (a preceding FOCUS 4 outline) found that not only were favourable compound combinations essential for anti-tumour effects, but also the dosage regime and order of treatment (Raja *et al*., 2015). As such studies can be time consuming, the promise of carrying out preliminary dose scheduling combination in organoids, prior to translating within *in vivo* systems could be invaluable for acquisition of preclinical data. Organoid-derived xenografts based on the lines used here may be useful in this respect.

Taken together, this work would suggest that biomarkers do not necessarily predispose effective responses in an organoid-based system, supporting observations in the literature that biomarker-led analyses alone are not sufficient to predict patient responses to therapies (Voest and Bernards 2016). Despite the promise of genetic biomarkers alone to guide precision medicine, it is becoming increasingly apparent that multiple factors influence and somewhat obscure genotype-phenotype drug response outcomes. A number of reasons would account for this, some, some of which are noted herein.

Firstly, preclinical biomarker-driven therapeutic studies have classically relied upon *in vitro* studies within a uniform cellular context. The representation of tumour heterogeneity to explore genotype-phenotype interactions has therefore been limited due to clonal nature of 2D cell lines, resulting in some failures between the translations of targeted therapy to patients (Weeber *et al.* 2017; Barretina *et al.* 2012). Whilst pharmacogenomics interactions between genotypes and cellular phenotypes with the intention of targeting select tumour cell subpopulations have therefore improved clinical outcomes for a number of patients (Iorio *et al.* 2016), it is widely accepted that such studies do not necessarily capture the biology of the whole tumour (Pauli *et al.* 2017) .Furthermore, biomarkers alone do not sufficiently account for gene expression profiles in CRC; recent transcriptomic analyses of CRC have further emphasized the complexity of predicting drug responses based solely on genetic biomarkers (Guinney *et al.* 2015; Sadanandam *et al.* 2013) and the need for further subclassification of CRC types. A lack of biomarker-dependent responses in the clinic could also by accounted for by the use of pharmacological agents with uncharacterized mechanisms of action that do not necessarily correspond to a single pathway biomarker thus making it more complex to elucidate outcomes.

Most notably, the lack of translation between targeted genotypes and phenotypic outcomes are likely to be obscured by the cross-talk between a complex network of signalling pathways, which can ultimately overcome therapeutic efficacy (Voest and Bernards 2016). Pathway activation or inactivation within the tumour is therefore

entirely context dependent, relying on multiple feedback loops, therefore cannot necessarily be defined on the basis of static genomic and transcriptomic profiling.

Organoids, having shown the capacity to reflect overall tumour phenotypic heterogeneity, could provide further information as a context dependent model to assess therapeutic efficacies of targeted therapies, as well as explore further mechanisms of action to elicit responses to readily available compounds.

6.3 Sophisticated phenotypic assays measure drug-induced effects of complex 3D models

In order to establish organoids as a model suitable to the drug discovery pipeline, assay validation is of fundamental importance; robustness, sensitivity and reproducibility are critical to determine the suitable application of organoids. Furthermore, the successful incorporation of 3D *ex vivo* organoids into drug discovery requires the confirmation that increased physiological relevance and complexity is not compromised by a lack of ability to extract accurate measurements of drug sensitivity. Part of this thesis has aimed to overcome such challenges by addressing the need to expand organoids from relatively low yield of starting material and adaption to suitable assay formats, as well as investigating whether sophisticated phenotypic readouts are sufficient to encompass complexity of 3D structures.

Experiments conducted demonstrated the application of organoids towards higher-throughput assay formats, in 96- or 384-well plates, having expanded successfully from relatively small amounts of viable patient material, as described in Chapter 3. Organoids were able to proliferate functionally following digestion to single cells, consistent with previous findings showing that single cells derived from CRC material, when suspended into a matrix and appropriate growth conditions, self-organise into individual organoid structures (Sato *et al.* 2009; Boehnke *et al.* 2016). It was shown that regulation of organoid size using enzymatic digestion was critical to obtain relatively consistent numbers of structures within replicate wells and across replicate plates for drug screening studies. The adaptation of organoids to such formats was shown to improve overall assay noise. Supporting data in the literature has further emphasised the importance of organoid uniformity in terms of sizes per structure to obtain statistically data (Boehnke *et al.* 2016), a crucial requirement of the drug discovery pipeline in order to obtain robust and reproducible data .

Further to the above observations, this work also highlighted the importance of suitable assay readouts to generate quantifiable data from 3D structures for drug screening purposes. Overall, optimisation of ATP readouts within 96 well assay formats were sufficient to determine IC_{50} values of compounds that induced clear cytotoxic effects within organoids, such as those shown in Figure 3.13. However, in instances whereby effects of compounds were limited on the overall organoid population, sensitivity of detection of responses was also limited . In the studies of Wnt inhibition using TNKSi, whilst a reduction in overall ATP in a dose response titration of doses was considered as a positive outcome on reduction of overall growth, such assay formats suffered from small assay windows that prevented the production of definite cellular EC_{50} values that are required to drive compound development pipelines during drug development. By providing readouts that are relevant to the effect of compounds on prospective populations of CSCs, the organoid assays, when combined with appropriate morphometric readouts constitute a suitable system for next-generation drug discovery efforts.

 A recent proof-of-concept study incorporated ATP assay readouts to assess the effects of a multiple compounds relevant for CRC therapies upon a biobank of 20 patient-derived CRC organoids (Wetering, Francies, Garnett, Francis, *et al.* 2015). In some instances, a clear correlation was observed between mutations in organoids and sensitivity to compounds. However, it was also noted that IC_{50} values obtained from treated organoids were variable between experiments, potentially as a result of the organoid suitability within assays, or, most likely, a relatively limited dose response range of compounds administered, resulting in a poorer assay sensitivity, potentially resulting in observation of off-target effects of compounds. Given the complexity of pathways targeted for therapeutic intervention, targeted pathways in these culture systems, capturing exact mechanism of compounds is important if organoids are going to become clinically-relevant models.

As described in both Chapters 4 and 5, it was found that phenotypic assays were able to successfully quantify organoid responses to compounds on the basis of multiple morphometric parameters. Importantly, such sophisticated assay formats

had the capacity to detect effects of compounds otherwise missed by basic metabolic readouts, classifying organoid responses to both clinically relevant, and novel cancer-stem-cell targeting compounds. The data acquired using novel software by OcellO (Leiden, Netherlands) selected over 500 features for organoid characterisation in responses to treatment, including intensity information gathered from nuclear and F-actin staining, as well as morphological measurements of whole organoid structures and nuclei. Whilst the number of features investigated may seem redundant for each system, it enabled the analysis of multiple features that contributed most to separation between negative control and treatment data to assess multiple biological effects of organoids. Testing a novel TNKSi within organoids over a three-log fold changes in IC_{50}, increased confidence that this is a result of on target effects. Such analysis methods has previously been used in the literature to facilitate an unbiased method to relate the effects of particular groups of compounds upon biological function of immortal cell lines cultured in 3D (Di, Klop, Rogkoti, Devedec, van de, *et al.* 2014; Sandercock *et al.* 2015).

 Given the biological complexity of 3D organoids, it is likely that a number of organoid-specific characteristics contribute to treatment-induced changes in phenotypic responses. An alteration that could be detected by phenotypic screening is overall organoid structure; one of the main advantages of organoid culture compared to preceding *in vitro* culture systems is their overall capacity to retain a hierarchy of cell lineages within a self-directed spatial organisation. Both histological and basic morphometric analysis of patient derived organoids demonstrated a variety of overall structures dependent upon tumour subtypes, as demonstrated in Figure 3.5. This is in line with preceding studies of organoid heterogeneity across CRC tumour samples (Fujii *et al.* 2016b). Iso 75, in particular was shown to retain glandular structures found in matching patient material (Figure 3.7) as multiple lumen structures within an organoid.

Analysis of F-actin, a critical factor for overall cell viability and structural support, as well as nuclear division (Caie *et al.* 2010), facilitated a detailed analytical approach to organoid response to treatment. Interestingly, TNKS inhibition resulted in an overall

diminished F-actin staining intensity within structures, suggesting a compromised integrity of cell-to-cell connections. Furthermore, F-actin staining also facilitated the detection of lumen structures, which were altered by low concentrations of TNKS inhibitors, with cystic structures morphologies induced as a result in Iso 72 organoids. This was further observed by a study published by Lau, using the TNKSi GL007-LK, they found induced cystic morphologies at low concentrations of compound (Lau *et al.* 2013). Such a change induced by overall cell organisation would be lacking in 2D structures, further supporting the notion that organoid models have the potential to reveal more complex characteristics of tumours of origin, making them a more suitable model for drug discovery purposes.

A unique characteristic of organoids is their ability to retain different cell types within individual structures, likely to be composed of cells at various stages of the cell cycle such as proliferating, quiescent, apoptotic and necrotic. As a result, changes in cell signalling as a result of environmental or mutational background could alter organoid responses to treatment that would translate through to multi-parametric screening. Organoids described in this study were shown to harbour APC and ß-catenin mutations, which have been previously associated with increased Wnt signalling activation in the intestine, resulting in a loss of polarity and cellular organisation (Barker 2014b; Sansom *et al.* 2004). Iso 75, a multi-lumen structure could be resultant of such a loss of cellular polarity. The importance of phenotype as a representation of potential cell signalling has been somewhat identified in other organoid model systems. Organoids generated from a mouse model of APC inactivation demonstrated that a loss of APC resulted in a loss of epithelial cell organisation, as confirmed further *in vivo* (Fatehullah *et al.* 2013) A recent study by Riemer *et al* (2017) further demonstrated the relationship between cancer phenotypes and signalling in organoids, whereby the authors generated transgenic mice to create stabilized ß-catenin and PIK3CA-mutant organoids. ß-catenin upregulation was found to induce cystic organoids in culture, enriched for Lgr5 and myc dependent stem-cell activity (Riemer *et al.* 2017). It was found that changes in cell signalling initiated by compound activity resulted in changes in overall

phenotypes, further highlighting the possibility of phenotypic screening as a drug discovery approach for organoids.

6.4   Organoids provide a platform to assess stem and differentiation of cell populations

The role of Wnt signalling at tumour initiation and progression in the intestine has been well documented in the literature, with many studies indicating that a continued dependency on ß-catenin mediated Wnt signalling is required for tumour growth, which varies from one tumour to the next. Studies have emphasised the reliance of tumour progression on a 'just-right' level of Wnt signalling; according to this hypothesis, there is a gradient of Wnt signalling which is sufficient for tumour formation, whereby impairment of APC function is within a finite window to enable sufficient accumulation of nuclear ß-catenin. Conversely, over accumulation of nuclear ß-catenin also results in cell death leading to inhibition of tumour development (Albuquerque *et al.* 2002) , further highlighting the need for precise levels of Wnt signalling in the intestine. Reliable *in vitro* models, capable of encompassing the complexity of the Wnt signalling pathway, relatable to tumours, have proved challenging so far, most likely due to a lack of all tumour cell types within 2D cell lines which fail to encompass all relevant cell types and signalling networks.

The investigation of Wnt signalling inhibition was therefore of interest here in a relevant model; predominantly, the effect of Wnt inhibition upon stem-cell containing organoid phenotypes, as described in the previous section, as well as further assessment of effects upon CSC compartments. It would be hypothesised that Wnt inhibition would prevent the CSC activity and thus reduce the likelihood of tumour growth, or in this case organoid growth. Assay formats were designed to simulate similar conditions, by assessing the effects of TNKSi inhibition upon overall organoid formation and downstream signalling, in an attempt to manipulate the CSC population.

Phenotypic screening of three novel TNKS inhibitors against a panel of 8 organoids highlighted TNKSi-sensitive organoids, representing known, on -target EC_{50} values. Iso 75 and Iso 78 (*APC* and *CTNNB1* mutant) were two lines of the cohort that relied on a growth-factor rich media, including exogenous Wnt and R-spondin and both showed responses to TNKS inhibition. However, Iso 72 (*APC* mutant), having showed sufficient growth in 7+ media was also responsive, suggesting that this is not only a readout for the growth factor conditions in which organoids are maintained. Previous work in the literature has shown that the inhibition of Wnt/ß-catenin signalling by TNKSi is complete within cell lines harbouring wild-type *APC*, simulated with exogenous Wnt. Similarly, complete inhibition of ß-catenin-driven Wnt signalling has previously been implicated in cell lines containing wild-type APC and are stimulated with exogenous Wnt (Huang *et al.* 2009; Waaler, Machon, Tumova, Dinh, Korinek, Wilson, Paulsen, Pedersen, Tor J Eide, *et al.* 2012).

 Further gene expression analysis of two responders, Iso 72 and Iso 75, showed a downregulation in stem cell markers *Ascl2* and *Lgr5* following TNKSi treatment, coupled with an upregulation in the differentiation markers *Krt20* and *Dkk1* and corresponding diminished ß-catenin levels. Both *Ascl2* and *Lgr5* have been previously implicated as identifiers of ISCs with functional roles in the intestine. Several studies have reported that LGR5 functions as a receptor of R-spondins within SCs, and thus is an activator of Wnt signalling (de Lau *et al.* 2011b). *Ascl2* has also been implicated as a marker of stem cells, is a Wnt target gene, and has been reported to govern the identity of Lgr5+ stem cells in the normal intestine (van der Flier *et al.* 2009) and can be upregulated as a result of a feedback loop dependent on Wnt signalling (Schuijers *et al.* 2015). Taken together, this would indicate that TNKS inhibition mediates diminished Wnt signalling within organoids, and as a result reduces the overall stem cell population, inducing differentiation and mediating phenotypic changes in organoids.

Interestingly, Iso 50, having shown little change in overall proliferation in response to TNKSi treatment, was shown to retain a baseline level of Lgr5+ expression, and a decreased expression of another stem cell marker *Ascl2*. Furthermore,

immunohistochemical staining demonstrated a complete loss of ß-catenin markers, indicating diminished Wnt signalling activity. On one hand, results may suggest that Iso 50 organoids harbour a TNKSi-resistant population, or partial inhibition by Wnt signalling, so that CSCs continue to divide, producing more CSCs. Given that an exhaustive list of stem cell markers were not assessed here it is possible that Iso50 is either inherently reliant on different stem cell populations, or becomes reliant as a result of TNKS inhibition. Furthermore, it is possible that co-operating mutations may result in an alternative driver of growth, leading to independence from Wnt signalling for overall proliferation. An alternative assay system would be required to pinpoint specific mechanisms highlighted from this organoid cohort in response to TNKS inhibition.

Importantly, this work demonstrated a concordance between *in vitro* and a respective organoid-derived xenograft model. The gold standard method for the identification of cancer stem cells is often obtained by transplantation of tumour cells within immune deficient animal models and assessing subsequent formation of structures. There is some controversy as to the accuracy of this statement, as xenotransplantation does not necessarily model an environment of relevance to tumour growth and could thus be measuring an overall selective pressure for cell survival as opposed to CSC activity. However, for the purposes of this study it was deemed a sufficient assay format to assess the capacity of organoids to form tumours, and to secondly assess the effects of Wnt signalling inhibition upon tumour formation. It was hypothesised that the pre-treatment of organoid cells with TNKSi would result in a transcriptional effect following diminished Wnt signalling, thus affecting the capacity of stem cell -directed formation of a tumour.

A 100% take rate was observed from mice implanted with control and TNKSi pre-treated Iso 75 organoids. However, organoids pre-treated with TNKSi were found to significantly delay tumour formation in mice compared to control conditions. Taken together with gene expression data it would seem that a reduced Wnt signalling signature following TNKSi administration resulted in a decreased number of stem

cells, resulting in a reduction in the capacity to form tumours compared to control conditions, as illustrated by Figure 6.2.

Given that treatment did not entirely prevent tumour outgrowth in the mouse, further detailed assessments would be required to identify mechanisms involved. It is possible that whilst transcriptional events were able to occur within 24 hours of treatment, that some stem cells remained active and were not completely ablated by exposure to TNKSi. Alternatively, a lack of continual TNKSi treatment within the mouse resulted in eventual recovery of cells; studies within organoids had demonstrated that the effects of TNKSi were not completely cytotoxic, resulting in a lower tumour formation capacity. It is also possible that alternative stem cell pools, not necessarily marked by *Lgr5* or *Ascl2*, were also able to compensate for effects of Wnt signalling inhibition. Studies have identified that Wnt inhibitors have the capacity to convers stem cells to a transit amplifying fate in a mouse model expressing oncogenic ß-catenin (Clarke *et al.* 2016) .An alternative explanation could be inferred by recent studies that have investigated plasticity of CSCs in the mouse intestine. Increasing data in the literature supports the notion that Lgr5+ cell populations are not strict lineages and are in fact heterogeneous, capable of expressing a distinct subset of Wnt target genes (Shiokawa *et al.* 2017). In the instance of Lgr5+ cell ablation, Lgr5- cells are able to compensate these effects by replenishing the Lgr5+ cell population (Shimokawa *et al.* 2017; Cortina *et al.* 2017). Further lineage tracing experiments have also shown that differentiated cells marked by Krt20 can reverse into Lgr5 cells following Lgr5+ cell ablation, thus driving tumour re-growth. It is possible herein that stem cell plasticity enabled the upregulation of Lgr5+ cells from a differentiated cell population stem cell pools as described in previous studies following ablation of some, or all CSCs (Shimokawa *et al.* 2017) to eventually re-populate the tumour. Further studies would be required to elucidate this in context to work carried out here.

The validation of an organoid-derived xenograft model that demonstrates concordance between comparative organoid line studies is encouraging for the drug discovery pipeline. To further explore this, histological analysis of mouse tumours

would be beneficial, as well as studies in a larger organoid-xenograft cohort. From a clinical perspective, further detailed investigation of a Wnt signalling inhibitor as a potential therapeutic would be required. Given that treatment did not entirely ablate tumour organoids, or subsequent tumours developed *in vivo* it is difficult to estimate the clinical benefit TNKSi would hold, particularly with increasing evidence that CSC trans -differentiation can facilitate tumour growth. Furthermore, the assay formats used here were in relation to looking at the cancer stem cell signature as opposed to a therapeutic effect, and would thus require care in their interpretation given that established tumours would potentially hold completely different cell dynamics. Nevertheless, cancer stem cell-targeting therapies are not currently in clinical trial and would therefore benefit study in a relevant model system that can represent true on-target doses.
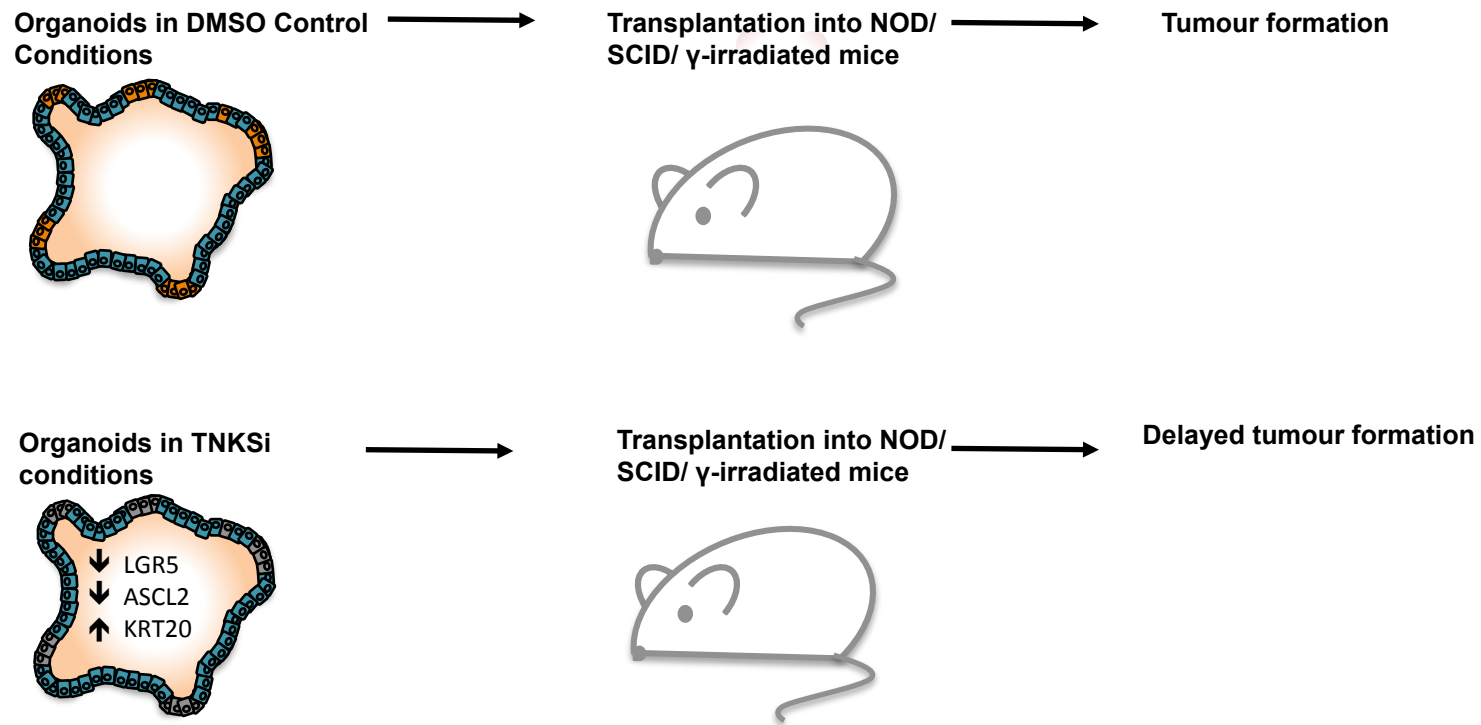
Figure 6.1 Schematic representation of a potential mechanism for the effects of TNKS inhibition upon tumour forming capacity of organoids

This hypothesis would propose that TNKS inhibition reduces levels of Wnt-signalling within organoids , thus reducing the number of active cycling cancer stem cells, as cells are promoted to undergo differentiation, as suggested by increased levels of Krt20. The remaining cells have the capacity to form tumours, with a significant delay compared to DMSO-treated organoids.

6.5   Further work in the organoid model

Whilst data generated here supports the expansion of patient-derived CRC organoids from relatively little material, with relevant histological representation of patient subtypes, the concordance of organoids between patient counterparts would need to be ascertained to successfully recapitulate human tumours, and thus responses to therapy.

6.5.1   Towards a clinical trial *in vitro*

The work presented in this thesis forms the basis towards suitable assay formats to enable organoids to be transitioned to be run in parallel alongside clinical trials to provide "live cell biomarkers" as a functional readout of patient responses. Collection of patient-derived material and their expansion in culture could provide a mirrored response between organoid treatment and patient responses to therapies. Early work in the Dale lab has established the successful culture of CRC tumour organoids from punctured tumour resections to recapitulate a thin needle biopsy collection. This would therefore be amenable to collection from patients recruited for the FOCUS 4 clinical trial, as well as other future clinical trials. By comparing organoid responses directly to those of patients this would enable us to answer whether organoids recapitulate tumour biology. Given the take rate and successful protocols for relatively rapid expansion in culture, organoids could even be used to test multiple compounds in combination to direct improved therapeutic options. Ideally, with patient consent, biopsies collected prior and after treatment would help delineate any mechanisms of resistance to therapy.

Collection of normal colorectal tissue could also improve drug response readouts by generating an additional control for responses to therapy. This would be of particular importance for compounds such as MK1775 and AZ20, both of which demonstrated substantial effects to inhibit overall organoid growth from the cohort

tested. By generating organoids from normal corresponding tissue as previously published (Wetering, Francies, Garnett, Wetering, *et al.* 2015; Sato *et al.* 2011a), this would provide an opportunity to test standard of care chemotherapeutics against biomarker-driven therapies. If an improved level of toxicity was obtained from normal organoids, it would provide some premise that compounds were more selective for tumour cells than current chemotherapeutics used for the treatment of CRC.

An important future direction for work described in this thesis is the optimisation of assay methods that would enable the co-culture of an immune component alongside organoids to facilitate the study of immune-based therapies. Immune based therapies have shown promising pre-clinical data for CRC treatment and would thus require a representative model system for testing. The understanding between tumour and immune system has important implications for the design and development of novel cancer immunotherapies (Weeber *et al.* 2017). The role of the tumour environment should not be ignored in establishing such methods.

Whilst work described here provides some evidence as to the utility of organoids as a model system, the ultimate comparison between concordance between organoids and patients will come from large-scale clinical trials whereby organoids can be used as a functional test alongside acquisition of patient data. The aggregation of both genomic, patient-derived organoid responses and clinical responses could then be used to provide justification of the suitability of organoids as a predictive clinical model (Picco and Garnett 2017).

6.6   Future directions for organoid technology

Whilst data generated here has shown the amenability of organoids towards higher throughput assay formats for supporting clinical data, as well as the discovery pipeline, there are some limitations to consider, as with any other model system. Broadly speaking, organoid culture is still in infancy as a successful tumour model; a relatively reductionist approach has thus far been employed to select for epithelial

cells, deprived of a surrounding stroma, vasculature and immune component. This has some restrictive effects upon studies that wish to explore the interaction between organoids and their surrounding niche. It is certain that the field is moving towards including some of these components in co-culture systems to further utilise this model, with some systems having included fibroblasts in co-culture with murine organoids (Pastula *et al.* 2016). Furthermore, whilst PDO models have the capacity to move towards high throughput screening, the use of Matrigel can provide issues in terms of batch-to-batch inconsistency, which can result in discrepancies between experiments (Gjorevski *et al.* 2016). The influence of the micro-environment of organoids should not be underestimated in terms of their effects upon organoid growth.

A promising avenue that is becoming increasingly prominent in the organoid-based literature is the implementation of genetic modifications *in vitro* using CRISPR/Cas9 systems to assess the effects of particular disease-causing genes and their downstream effects (Fujii *et al.* 2016b; Matano *et al.* 2015). This technology could facilitate the assessment of tumourigenesis at early stages, for indications as to consequences of mutations prior to tumour development. Further to this, genetic manipulation could generate organoids that carry tailored mutations as a model to test relevant biomarker-driven therapies.

The generation of 3D stem cell-containing organoid culture systems has enabled the long-term expansion of an array of adult tissue types, and has resulted in a paradigm shift in their application towards accurately modelling tumours for precision oncology and drug discovery. The findings in this thesis, collectively, have shown the potential of organoids within both stratified medicine and drug discovery alike, whilst raising potential enquiries for furthering the understanding of tumour dynamics in a relevant model system.

Bibliography

Cancer Research UK [Online]. Available: http://www.cancerresearchuk.org/health-professional/cancer-statistics/statistics-by-cancer-type/bowel-cancer/mortality

FOCUS4-C (2017). FOCUS4-C Protocol [Online]. ; available at http://www.focus4trial.org.

Aarts, M., Sharpe, R., Garcia-Murillas, I., Gevensleben, H., Hurd, M.S., Shumway, S.D., Toniatti, C., *et al.* (2012). Forced mitotic entry of S-phase cells as a therapeutic strategy induced by inhibition of WEE1. *Cancer Discovery* **2**:524–539.

Adams, R.A., Meade, A.M., Seymour, M.T., Wilson, R.H., Madi, A., Fisher, D., Kenny, S.L., *et al.* (2011). Intermittent versus continuous oxaliplatin and fl uoropyrimidine combination chemotherapy for fi rst-line treatment of advanced colorectal cancer : results of the randomised phase 3 MRC COIN trial. *Lancet Oncology*

Ahronian, L.G., Sennott, E.M., Van Allen, E.M., Wagle, N., Kwak, E.L., Faris, J.E., Godfrey, J.T., *et al.* (2015). Clinical acquired resistance to RAF inhibitor combinations in BRAF-mutant colorectal cancer through MAPK pathway alterations. *Cancer Discovery* **5**:358–367.

Al-kharusi, M.R.A., Smartt, H.J.M., Greenhough, A., Collard, T.J., Emery, D., Williams, A.C. and Paraskeva, C. (2013). LGR5 promotes survival in human colorectal adenoma cells and is upregulated by PGE 2 : implications for targeting adenoma stem cells with NSAIDs. **34**:1150–1157.

Albuquerque, C., Breukel, C., van der Luijt, R., Fidalgo, P., Lage, P., Slors, F.J.M., Leitão, C.N., *et al.* (2002). The 'just-right' signaling model: APC somatic mutations are selected based on a specific level of activation of the beta-catenin signaling cascade. *Human molecular genetics* **11**:1549–1560.

Alfonso, L., Ai, G., Spitale, R.C. and Bhat, G.J. (2014). Molecular targets of aspirin and cancer prevention. *British Journal of Cancer* **111**:61–67.

Alizadeh AA, Aranda V, Bardelli A, Blanpain C, Bock C, BorowskiC, Caldas C, Califano A, Doherty M, Elsner M, Esteller M,Fitzgerald R, Korbel JO, Lichter P, Mason CE, Navin N, Pe'er D, Polyak K, Roberts CW, Siu L, Snyder A, Stower H,Swanton C, Verhaak RG, Zenklusen JC, Zuber J, Zucman-Rossi J. (2015) *Nature Medicine* .**21**:846-53.

Andre, T., Louvet, C., Raymond, E., Tournigand, C. and Gramont, A. De (1998). Bimonthly high-dose leucovorin , 5-fluorouracil infusion and oxaliplatin leucovorin and 5-fluorouracil regimen. :1251–1253.

Arqués, O., Chicote, I., Puig, I., Tenbaum, S.P., Argilés, G., Dienstmann, R., Fernández, N., *et al.* (2016). Tankyrase Inhibition Blocks Wnt/b-Catenin Pathway and Reverts Resistance to PI3K and AKT Inhibitors in the Treatment of Colorectal Cancer. *Clinical Cancer Research* **22**:644–656.

Ashley, N. (2013). Regulation of intestinal cancer stem cells. *Cancer letters* [Online] **338**:120–126..

Ashley, N., Jones, M., Ouaret, D., Wilding, J. and Bodmer, W.F. (2014). Rapidly Derived Colorectal Cancer Cultures Recapitulate Parental Cancer Characteristics and Enable Personalised Therapeutic Assays. *The Journal of pathology* **234**:34–45.

Ashley, N., Yeung, T.M. and Bodmer, W.F. (2013). Stem cell differentiation and lumen formation in colorectal cancer cell lines and primary tumors. *Cancer research* **73**:5798–5809.

Auclair, B.A., Benoit, Y.D., Rivard, N., Mishina, Y. and Perreault, N. (2007). Bone Morphogenetic Protein Signaling Is Essential for Terminal Differentiation of the Intestinal Secretory Cell Lineage.

Gastroenterology **133**:887–896.

Badalà, F., Nouri-mahdavi, K. and Raoof, D.A. (2011). The Role of Notch Signaling in Colon Homeostasis and Carcinogenesis. *Cancer Science* **144**:724–732.

Barker, N. (2014a). Adult intestinal stem cells: critical drivers of epithelial homeostasis and regeneration. *Nature reviews. Molecular cell biology* **15**:19–33.

Barker, N., van Es, J.H., Kuipers, J., Kujala, P., van den Born, M., Cozijnsen, M., Haegebarth, A., *et al.* (2007). Identification of stem cells in small intestine and colon by marker gene Lgr5. *Nature* **449**:1003–7.

Barker, N., Ridgway, R.A., Es, J.H. Van, Wetering, M. Van De, Begthel, H., Den, M. Van, Danenberg, E., *et al.* (2009). Crypt stem cells as the cells-of-origin of intestinal cancer. *Nature* **457**:608–612.
Barker, N., Tan, S. and Clevers, H. (2013). Lgr proteins in epithelial stem cell biology. *Development (Cambridge, England)* **140**:2484–94.

Barlaam, B., Anderton, J., Ballard, P., Bradbury, R.H., Hennequin, L.F.A., Hickinson, D.M., Kettle, J.G., *et al.* (2013). Discovery of AZD8931, an Equipotent, Reversible Inhibitor of Signaling by EGFR, HER2, and HER3 Receptors. **4**:742–746.

Barretina, J., Caponigro, G., Stransky, N., Venkatesan, K., Margolin, A. a, Kim, S., Wilson, C.J., *et al.* (2012). The Cancer Cell Line Encyclopedia enables predictive modelling of anticancer drug sensitivity. *Nature* **483**:603–7.

Batts, L.E., Brent Polk, D., Dubois, R.N., Kulessa, H. and Hogan, B. (2006). Bmp signaling is required for intestinal growth and morphogenesis. *Developmental Dynamics* **235**:1563–1570.

Bertotti, A., Papp, E., Jones, S., Adleff, V., Anagnostou, V., Lupo, B., Sausen, M., *et al.* (2016). The Genomic Landscape of Response to EGFR blockade in Colorectal Cancer. **526**:263–267.

Binefa, G., Rodriguez-Moranta, F., Teule, A., Medina-Hayas, M. (2014). Colorectal cancer: From prevention to personalized medicine. *World Journal of Gastroenterology* **20**:6786–6808.

Blanpain, C., Mohrin,M.,Panagioat,A.,Sotiropoulou,E., (2011) DNA-Damage Response in Tissue-Specific and Cancer Stem Cells. *Cell Stem Cell* **8**(1);16-29

Bodmer, W., Bailey, C., Bodmer, J., Bussey, H., Ellis, A., Gorman, P., Lucibello, F., *et al.* (1987). Localization of the gene for familial adenomatous polyposis on chromosome 5. *Nature* **328**:614–6.

Boehnke, K., Iversen, P.W., Schumacher, D., Lallena, M.J., Haro, R., Amat, J., Haybaeck, J., *et al.* (2016). Assay Establishment and Validation of a High-Throughput Screening Platform for Three-Dimensional Patient-Derived Colon Cancer Organoid Cultures. *Journal of Biomolecular Screening* **21**:931-41.

Breslin, S. and O'Driscoll, L. (2013). Three-dimensional cell culture: The missing link in drug discovery. *Drug Discovery Today* **18**:240–249.

Burotto, M., Chiou, V., Lee, J.-M. and Kohn, E.C. (2015). The MAPK pathway across different malignancies; A new perspective. *Cancer* **120**:3446–3456.

Byrne, A.T., Alférez, D.G., Amant, F., Annibali, D., Arribas, J., Biankin, A. V., Bruna, A., *et al.* (2017). Interrogating open issues in cancer precision medicine with patient-derived xenografts. *Nature Reviews Cancer* **17**:254-268.

Caie, P.D., Walls, R.E., Ingleston-Orme, A., Daya, S., Houslay, T., Eagle, R., Roberts, M.E., *et al.* (2010). High-content phenotypic profiling of drug response signatures across distinct cancer cells. *Molecular cancer therapeutics* **9**:1913–1926.

Cancer Genome Atlas Network (2012). Comprehensive molecular characterization of human colon and rectal cancer. *Nature* **487**:330–7.

Centenera, M.M., Gillis, J.L., Hanson, A.R., Jindal, S., Taylor, R.A., Risbridger, G.P., Sutherland, P.D., *et al.* (2012). Evidence for Efficacy of New Hsp90 Inhibitors Revealed by Ex Vivo Culture of Human Prostate Tumors. *Clinical Cancer Research* **18**:3562–3571.

Chou, T. (2007). Theoretical Basis , Experimental Design , and Computerized Simulation of Synergism and Antagonism in Drug Combination Studies □. *Pharmacological reviews*.**58**:621-81

Chou, T. and Talalay, P. (1984). Quantitative Dose-effect relationships : the combined effects of multiple drug or enzyme inhibitors. *advanceds in enzyme regulation* **22**.
Chou, T.C. (2010). Drug combination studies and their synergy quantification using the chou-talalay method. *Cancer Research* **70**:440–446.

Clarke, P.A., Ortiz-Ruiz, M.J., Tepoele, R., Adeniji-Popoola, O., Box, G., Court, W., Czasch, S., *et al.* (2016). Assessing the mechanism and therapeutic potential of modulators of the human mediator complex-associated protein kinases. *eLife* **5**:1–25.

Clevers, H. (2016). Modeling Development and Disease with Organoids. *Cell* [Online] **165**:1586–1597.

Clevers, H. (2011). The cancer stem cell : premises , promises and challenges. *Nature Medicine* **17**:313–319.

Colussi, D., Brandi, G., Bazzoli, F. and Ricciardiello, L. (2013). Molecular pathways involved in colorectal cancer: implications for disease behavior and prevention. *International journal of molecular sciences* **14**:16365–16385.

Corcoran, R.B. (2015). New therapeutic strategies for BRAF mutant colorectal cancers. *Journal of Gastrointestinal Oncology* **6**:650–659.

Corcoran, R.B., Atreya, C.E., Falchook, G.S., Kwak, E.L., Ryan, D.P., Bendell, J.C., Hamid, O., *et al.* (2015). Combined BRAF and MEK inhibition with dabrafenib and trametinib in BRAF V600-Mutant colorectal cancer. *Journal of Clinical Oncology* **33**:4023–4031.

Corcoran, R.B., Ebi, H., Turke, A.B., Coffee, E.M., Cogdill, A.P., Brown, R.D., Pelle, P. Della, *et al.* (2012). EGFR-mediated re-activation of MAPK signaling contributes to insensitivity of BRAF mutant colorectal cancer to RAF inhibition with vemurafenib. *Cancer Discovery* **2**:227–235.

Cortina, C., Turon, G., Stork, D., Hernando-Momblona, X., Sevillano, M., Aguilera, M., Tosi, S., *et al.* (2017). A genome editing approach to study cancer stem cells in human tumors. *EMBO Molecular Medicine* **9**:869-79.

Crockford, A., Jamal-Hanjani, M., Hicks, J. and Swanton, C. (2013). Implications of Intratumour Heterogeneity for Treatment Stratification. *The Journal of pathology* **2**:264-73.

Daniela,S., Leiserson,M.,Ruppin,E., Ronai,Z. (2017). Precision Oncology: The Road Ahead. *Trends in Molecular Medicine.*

Davies, B.R., Logie, A., McKay, J.S., Martin, P., Steele, S., Jenkins, R., Cockerill, M., *et al.* (2007). AZD6244 (ARRY-142886), a potent inhibitor of mitogen-activated protein kinase/extracellular signal-regulated kinase kinase 1/2 kinases: mechanism of action in vivo, pharmacokinetic/pharmacodynamic relationship, and potential for combination in preclinical. *Mol Cancer Ther* **6**:2209–2219.

Dhillon, A.S., Hagan, S., Rath, O. and Kolch, W. (2007). MAP kinase signalling pathways in cancer. *Oncogene* [Online] **26**:3279–90.

Di, Z., Klop, M., Rogkoti, V.-M., Devedec, S., van de, B., Verbeek, F.J., Price, L.S., *et al.* (2014). Ultra High Content Image Analysis and Phenotype Profiling of 3D Cultured Micro-Tissues. *PloS one* **9**:1–10.

Domingo, E., Church, D.N., Sieber, O., Ramamoorthy, R., Yanagisawa, Y., Johnstone, E., Davidson, B., *et al.* (2013). Evaluation of PIK3CA Mutation As a Predictor of Benefit From Nonsteroidal Anti-Inflammatory Drug Therapy in Colorectal Cancer. *Journal of Clinical Oncology* **31**:14–17.

Douillard, J.Y., Cunningham, D., Roth, A.D., Navarro, M., James, R.D., Karasek, P., Jandik, P., *et al.* (2000). Irinotecan combined with fluorouracil compared with fluorouracil alone as first-line treatment for metastatic colorectal cancer : a multicentre randomised trial. *The Lancet* **355**:1041–1047.

Dow, L.E., O'Rourke, K.P., Simon, J., Tschaharganeh, D.F., van Es, J.H., Clevers, H. and Lowe, S.W. (2015). Apc Restoration Promotes Cellular Differentiation and Reestablishes Crypt Homeostasis in Colorectal Cancer. *Cell* **161**:1539–1552.

Drewes, J.L., Housseau, F. and Sears, C.L. (2016). Sporadic colorectal cancer: microbial contributors to disease prevention, development and therapy. *British Journal of Cancer* [Online] **115**:273–280.

Edmondson, R., Broglie, J.J., Adcock, A.F. and Yang, L. (2014). Three-dimensional cell culture systems and their applications in drug discovery and cell-based biosensors. *Assay and drug development technologies* [Online] **12**:207–18. A

Egeland, E.V., Flatmark, K., Nesland, J.M., Flørenes, V.A., Mælandsmo, G.M. and Boye, K. (2016). Expression and clinical significance of Wee1 in colorectal cancer. *Tumour biology : the journal of the International Society for Oncodevelopmental Biology and Medicine* **37**:12133–12140.

Eidet, J.R., Pasovic, L., Maria, R., Jackson, C.J. and Utheim, T.P. (2014). Objective assessment of changes in nuclear morphology and cell distribution following induction of apoptosis. *Diagnostic pathology* **9**:92.

Engelman, J.A. (2009). Targeting PI3K signalling in cancer : opportunities , challenges and limitations. **9**:550–562

van Es, J.H., de Geest, N., van de Born, M., Clevers, H. and Hassan, B. a (2010). Intestinal stem cells lacking the Math1 tumour suppressor are refractory to Notch inhibitors. *Nature communications* **1**:18.

Evans, G.S., Flint, N., Somers, a S., Eyden, B. and Potten, C.S. (1992). The development of a method for the preparation of rat intestinal epithelial cell primary cultures. *Journal of cell science* **101**:219–231.

Fatehullah, A., Appleton, P.L., Näthke, I.S. and B, P.T.R.S. (2013). Cell and tissue polarity in the intestinal tract during tumourigenesis : cells still know the right way up , but tissue organization is lost

Fearon, E.F. and Vogelstein, B. (1990). A genetic model for Colorectal Tumorigenesis. *Cell* **61**:759–767.
Fevr, T., Robine, S., Louvard, D. and Huelsken, J. (2007). Wnt / β -Catenin Is Essential for Intestinal Homeostasis and Maintenance of Intestinal Stem Cells. *Mol Cell Biol* **27**:7551–7559.

van der Flier, L.G., van Gijn, M.E., Hatzis, P., Kujala, P., Haegebarth, A., Stange, D.E., Begthel, H., *et al.* (2009). Transcription Factor Achaete Scute-Like 2 Controls Intestinal Stem Cell Fate. *Cell* **136**:903–912.

Foote, K.M., Blades, K., Cronin, A., Fillery, S., Guichard, S.S., Hassall, L., Hickson, I., *et al.* (2013). Discovery of 4-{4-[(3R)-3-Methylmorpholin-4-yl]-6-[1-(methylsulfonyl)cyclopropyl]pyrimidin-2-yl}-1H-indole (AZ20): a potent and selective inhibitor of ATR protein kinase with monotherapy in vivo antitumor activity. *Journal of Medicinal Chemistry* **56**.

Forbes, S.A., Beare, D., Gunasekaran, P., Leung, K., Bindal, N., Boutselakis, H., Ding, M., *et al.* (2015). COSMIC: Exploring the world's knowledge of somatic mutations in human cancer. *Nucleic Acids Research* **43**:D805–D811.

Fre, S., Huyghe, M., Mourikis, P., Robine, S., Louvard, D. and Artavanis-Tsakonas, S. (2005). Notch signals control the fate of immature progenitor cells in the intestine. *Nature* **435**:964–8.

Freeman, D.J., Bush, T., Ogbagabriel, S., Belmontes, B., Juan, T., Plewa, C., Van, G., *et al.* (2009). Activity of panitumumab alone or with chemotherapy in non-small cell lung carcinoma cell lines expressing mutant epidermal growth factor receptor. *Molecular cancer therapeutics* **8**:1536–1546.

Fujii, M., Shimokawa, M., Date, S., Takano, A., Matano, M., Nanki, K., Ohta, Y., *et al.* (2016a). A Colorectal Tumor Organoid Library Demonstrates Progressive Loss of Niche Factor Requirements during Tumorigenesis. *Cell Stem Cell* **18**:827–838.

Fujii, M., Shimokawa, M., Date, S., Takano, A., Matano, M., Nanki, K., Ohta, Y., *et al.* (2016b). A Colorectal Tumor Organoid Library Demonstrates Progressive Loss of Niche Factor Requirements during Tumorigenesis. *Cell Stem Cell*:1–12.

Gao, H., Korn, J.M., Ferretti, S., Monahan, J.E., Wang, Y., Singh, M., Zhang, C., *et al.* (2015). High-throughput screening using patient-derived tumor xenografts to predict clinical trial drug response. *Nature Medicine* **21**:1318–1325.

Garnett, M.J. and Mcdermott, U. (2014). The evolving role of cancer cell line-based screens to define the impact of cancer genomes on drug response. *Current Opinion in Genetics & Development* [Online] **24**:114–119.

Gervaz, P., Bucher, P. and Morel, P. (2004). Two colons-two cancers: paradigm shift and clinical implications. *Journal of surgical oncology* **88**:261–6.

Gibson, T.B., Ranganathan, A. and Grothey, A. (2006). Randomized Phase III Trial Results of Panitumumab, a Fully Human Anti—Epidermal Growth Factor Receptor Monoclonal Antibody, in Metastatic Colorectal Cancer. *Clinical Colorectal Cancer* **6**:29–31.

Gill, S., Thomas, R.R. and Goldberg, R.M. (2003). Review article: colorectal cancer chemotherapy. *Aliment. Pharmacol. Ther.* **18**:683–692.

Gjorevski, N., Sachs, N., Manfrin, A., Giger, S., Bragina, M.E., Ordóñez-Morán, P., Clevers, H., *et al.* (2016). Designer matrices for intestinal stem cell and organoid culture. *Nature Publishing Group* **539**:560–564.

Goel, A., Chang, D.K., Ricciardiello, L., Gasche, C. and Boland, C.R. (2003). A Novel Mechanism for Aspirin-mediated Growth Inhibition of. **9**:383–390.

Goldberg, R.M., Carolina, N., Hill, C. and Carolina, N. (2005). Advances in the Treatment of Metastatic Colorectal Cancer. *The Oncologist* **10**:40–48.

Grabinger, T., Luks, L., Kostadinova, F., Zimberlin, C., Medema, J.P., Leist, M. and Brunner, T. (2014). Ex vivo culture of intestinal crypt organoids as a model system for assessing cell death induction in intestinal epithelial cells and enteropathy. *Cell death & disease* **5**:e1228.

Greene, F.L. (2004). The Staging of Colorectal Cancer : 2004 and Beyond. *Cancer journal for clinicians* **54**:295–308.

Guertin, A.D., Li, J., Liu, Y., Hurd, M.S., Schuller, A.G., Long, B., Hirsch, H.A., *et al.* (2013). Preclinical Evaluation of the WEE1 Inhibitor MK-1775 as Single-Agent Anticancer Therapy. *Molecular cancer therapeutics* **12**:1442–1453.

Guinney, J., Dienstmann, R., Wang, X., de Reyniès, A., Schlicker, A., Soneson, C., Marisa, L., *et al.* (2015). The consensus molecular subtypes of colorectal cancer. *Nature Medicine* **21**:1350–1356.

Hanahan, D. and Weinberg, R. a (2011). Hallmarks of cancer: the next generation. *Cell* **144**:646–674.

Haramis, A.-P.G., Begthel, H., van den Born, M., van Es, J., Jonkheer, S., Offerhaus, G.J.A. and Clevers, H. (2004). De Novo Crypt Formation and Juvenile Polyposis on BMP Inhibition in Mouse Intestine. *Science* **303**:1684 LP-1686.

He, X.C., Zhang, J., Tong, W.-G., Tawfik, O., Ross, J., Scoville, D.H., Tian, Q., *et al.* (2004). BMP signaling inhibits intestinal stem cell self-renewal through suppression of Wnt-beta-catenin signaling. *Nature genetics* **36**:1117–21.

Herpers, B., Terpstra, V., Commandeur, J.N.M., Water, B. Van De and Price, L.S. (2014). A 3D in vitro model of differentiated HepG2 cell spheroids with improved liver   like properties for repeated dose high   throughput toxicity studies. *Archives of Toxicology* **88**:1083–1095.

Hidalgo, M., Bruckheimer, E., Rajeshkumar, N. V, Garrido-Laguna, I., De Oliveira, E., Rubio-Viqueira, B., Strawn, S., *et al.* (2011). A pilot clinical study of treatment guided by personalized tumorgrafts in patients with advanced cancer. *Molecular cancer therapeutics* **10**:1311–1316.

Hirai, H., Iwasawa, Y., Okada, M., Arai, T., Nishibata, T., Kobayashi, M., Kimura, T., *et al.* (2009). Small-molecule inhibition of Wee1 kinase by MK-1775 selectively sensitizes p53-deficient tumor cells to DNA-damaging agents. :2992–3001.

Hofmann, C., Obermeier, F., Artinger, M., Hausmann, M., Falk, W., Schoelmerich, J., Rogler, G., *et al.* (2007). Cell-Cell Contacts Prevent Anoikis in Primary Human Colonic Epithelial Cells. *Gastroenterology* **132**:587–600.

Hongisto, V., Jernström, S., Fey, V., Mpindi, J.-P., Kleivi Sahlberg, K., Kallioniemi, O. and Perälä, M. (2013). High-throughput 3D screening reveals differences in drug sensitivies between culture models of JIMT1 breast cancer cells. *PloS one* **8**:e77232.

Huang, S.-M. a, Mishina, Y.M., Liu, S., Cheung, A., Stegmeier, F., Michaud, G. a, Charlat, O., *et al.* (2009). Tankyrase inhibition stabilizes axin and antagonizes Wnt signalling. *Nature* [Online] **461**:614–620.

Hutz, J.E., Nelson, T., Wu, H., Mcallister, G., Moutsatsos, I., Jaeger, S.A., Bandyopadhyay, S., *et al.* (2012). The Multidimensional Perturbation Value : A Single Metric to Measure Similarity and Activity of Treatments in High-Throughput Multidimensional Screens. *Journal of Biomolecular Screening* **18**:367-77.

Iorio, F., Knijnenburg, T.A., Vis, D.J., Bignell, G.R., Menden, M.P., Schubert, M., Aben, N., *et al.* (2016). A Landscape of Pharmacogenomic Interactions in Cancer. *Cell* **166**:740–754.

Ireland, H., Kemp, R., Houghton, C., Howard, L., Clarke, A.R., Sansom, O.J. and Winton, D.J. (2004). Inducible Cre-Mediated Control of Gene Expression in the Murine Gastrointestinal Tract: Effect of Loss of ß-Catenin. *Gastroenterology* **126**:1236–1246.

Julien, S., Merino-Trigo, A., Lacroix, L., Pocard, M., Goéré, D., Mariani, P., Landron, S., *et al.* (2012a). Characterization of a large panel of patient-derived tumor xenografts representing the clinical heterogeneity of human colorectal cancer. *Clinical cancer research : an official journal of the American Association for Cancer Research* **18**:5314–5328.

Julien, S., Merino-Trigo, A., Lacroix, L., Pocard, M., Goéré, D., Mariani, P., Landron, S., *et al.* (2012b). Characterization of a large panel of patient-derived tumor xenografts representing the clinical

heterogeneity of human colorectal cancer. *Clinical cancer research : an official journal of the American Association for Cancer Research* [Online] **18**:5314–28.

Junttila, M.R., Mao, W., Wang, X., Wang, B.-E., Pham, T., Flygare, J., Yu, S.-F., *et al.* (2015). Targeting LGR5+ cells with an antibody-drug conjugate for the treatment of colon cancer. *Science translational medicine* **7**:314-186.

Karlsson, H., Fryknäs, M., Larsson, R. and Nygren, P. (2012). Loss of cancer drug activity in colon cancer HCT-116 cells during spheroid formation in a new 3-D spheroid cell culture system. *Experimental Cell Research* **318**:1577–1585.

Khalil, H.S., Tummala, H., Chakarov, S., Zhelev, N. and Lane, D.P. (2012). Targeting ATM pathway for therapeutic intervention in cancer. *BIodiscovery*:1–13.

Kim, H.-J., Min, A., Im, S.-A., Jang, H., Lee, K.H., Lau, A., Lee, M., *et al.* (2017). Anti-tumor activity of the ATR inhibitor AZD6738 in HER2 positive breast cancer cells. *International journal of cancer* **140**:109–119.

Kim, K.-A., Kakitani, M., Zhao, J., Oshima, T., Tang, T., Binnerts, M., Liu, Y., *et al.* (2005). Mitogenic Influence of Human R-Spondin1 on the Intestinal Epithelium. *Science* [Online] **309**:1256 -1259.

Kim, K., Wagle, M., Tran, K., Zhan, X., Dixon, M.A., Liu, S., Gros, D., *et al.* (2008). R-Spondin Family Members Regulate the Wnt Pathway by a Common Mechanism. **19**:2588–2596.

King, A.J., Arnone, M.R., Bleam, M.R., Moss, K.G., Yang, J., Fedorowicz, K.E., Smitheman, K.N., *et al.* (2013). Dabrafenib ; Preclinical Characterization , Increased Efficacy when Combined with Trametinib , while BRAF / MEK Tool Combination Reduced Skin Lesions. *PloS one* **8**.

Koo, B.-K., Spit, M., Jordens, I., Low, T.Y., Stange, D.E., van de Wetering, M., van Es, J.H., *et al.* (2012). Tumour suppressor RNF43 is a stem-cell E3 ligase that induces endocytosis of Wnt receptors. *Nature* **488**:665–9.

Krausova, M. and Korinek, V. (2014). Wnt signaling in adult intestinal stem cells and cancer. *Cellular signalling* [Online] **26**:570–579.

Kreahling, J.M., Foroutan, P., Reed, D., Martinez, G., Razabdouski, T., Bui, M.M., Raghavan, M., *et al.* (2013). Wee1 Inhibition by MK-1775 Leads to Tumor Inhibition and Enhances Efficacy of Gemcitabine in Human Sarcomas. **8**.

Kuhnert, F., Davis, C.R., Wang, H.-T., Chu, P., Lee, M., Yuan, J., Nusse, R., *et al.* (2004). Essential requirement for Wnt signaling in proliferation of adult small intestine and colon revealed by adenoviral expression of Dickkopf-1. *Proceedings of the National Academy of Sciences of the United States of America* **101**:266–71.

Lau, T., Chan, E., Callow, M., Waaler, J., Boggs, J., Blake, R.A., Magnuson, S., *et al.* (2013). A novel tankyrase small-molecule inhibitor suppresses APC mutation-driven colorectal tumor growth. *Cancer Research* **73**:3132–3144.

de Lau, W., Barker, N., Low, T.Y., Koo, B.-K., Li, V.S.W., Teunissen, H., Kujala, P., *et al.* (2011a). Lgr5 homologues associate with Wnt receptors and mediate R-spondin signalling. *Nature* **476**:293–7.

de Lau, W., Peng, W.C., Gros, P. and Clevers, H. (2014). The R-spondin/Lgr5/Rnf43 module: regulator of Wnt signal strength. *Genes & development* **28**:305–16.

Lee, G. Y., Kenny, P. A., Lee, E. H., & Bissell, M. J. (2007). Three-dimensional culture models of normal and malignant breast epithelial cells. *Nature Methods*, *4*(4), 359–365

Li, L., Zhou, Q., Voss, T.C., Quick, K.L. and LaBarbera, D. V. (2016). High-throughput imaging: Focusing in on drug discovery in 3D. *Methods* **96**:97–102.

Liao, X., Lochhead, P., Nishihara, R., Morikawa, T., Kuchiba, A., Yamauchi, M., Imamura, Y., *et al.* (2012). Aspirin Use, Tumor PIK3CA Mutation, and Colorectal Cancer Survival. *New England Journal of Medicine* **367**:1596–1606.

Linardou, H., Dahabreh, I.J., Kanaloupiti, D., Siannis, F., Bafaloukos, D., Kosmidis, P., Papadimitriou, C. a, *et al.* (2008). Assessment of somatic k-RAS mutations as a mechanism associated with resistance to EGFR-targeted agents: a systematic review and meta-analysis of studies in advanced non-small-cell lung cancer and metastatic colorectal cancer. *The Lancet. Oncology* **9**:962–72.

Little, A.S., Balmanno, K., Sale, M.J., Dry, J.R., Hampson, M., Edwards, P.A.W., Smith, P.D., *et al.* (2014). Amplification of the Driving Oncogene , KRAS or BRAF , Underpins Acquired Resistance to MEK1 / 2 Inhibitors in Colorectal Cancer Cells. *Science* **4**.

Liu, P., Cheng, H., Roberts, Th. and Zhao, J.. (2009). Targetting the phosphinositide 3-kinase (PI3K) pathway in cancer. *Nature reviews. Drug discovery* **8**:627–644.

Longley, D.B., Harkin, D.P. and Johnston, P.G. (2003). 5-Fluorouracil : Mechanisms of action and clinical strategies. *Nature reviews* **3**:330–338.

Luca, A.C., Mersch, S., Deenen, R., Schmidt, S., Messner, I., Schäfer, K.L., Baldus, S.E., *et al.* (2013). Impact of the 3D Microenvironment on Phenotype, Gene Expression, and EGFR Inhibition of Colorectal Cancer Cell Lines. *PLoS ONE* **8**.

Lugli, A., Iezzi, G., Hostettler, I., Muraro, M.G., Mele, V., Tornillo, L., Carafa, V., *et al.* (2010). Prognostic impact of the expression of putative cancer stem cell markers CD133, CD166, CD44s, EpCAM, and ALDH1 in colorectal cancer. *British journal of cancer* **103**:382–90.

Luo, J., Emanuele, M.J., Li, D., Creighton, C.J., Schlabach, M.R., Westbrook, T.F., Wong, K.K., *et al.* (2009). A Genome-wide RNAi Screen Identifies Multiple Synthetic Lethal Interactions with the Ras Oncogene. *Cell* **137**:835–848.

Maira, S., Stauffer, F., Brueggen, J., Maira, S., Brueggen, J., Furet, P., Schnell, C., *et al.* (2008). Identification and characterization of NVP-BEZ235 , a new orally available dual phosphatidylinositol 3-kinase / mammalian target of rapamycin inhibitor with potent in vivo antitumor activity Identification and characterization of NVP-BEZ235 , a new orally. *Molecular cancer therapeutics* **7**.

Matano, M., Date, S., Shimokawa, M., Takano, A., Fujii, M., Ohta, Y., Watanabe, T., *et al.* (2015). Modeling colorectal cancer using CRISPR-Cas9–mediated engineering of human intestinal organoids. *Nature Medicine* **21**.

Matheson, C.J., Backos, D.S. and Reigan, P. (2016). Targeting WEE1 Kinase in Cancer. *Trends in Pharmacological Sciences* [Online] **37**:872–881.

Mebratu, Y. and Tesfaigzi, Y. (2009). How ERK1/2 Activation Controls Cell Proliferation and Cell Death Is Subcellular Localization the Answer? *Cell cycle (Georgetown, Tex.)* **8**:1168–1175.

Merlos-Suárez, A., Barriga, F.M., Jung, P., Iglesias, M., Céspedes, M.V., Rossell, D., Sevillano, M., *et al.* (2011). The intestinal stem cell signature identifies colorectal cancer stem cells and predicts disease relapse. *Cell stem cell* **8**:511–524.

Min, A., Im, S.-A., Jang, H., Kim, S., Lee, M., Kim, D.K., Yang, Y., *et al.* (2017). AZD6738, a novel oral inhibitor of ATR, induces synthetic lethality with ATM-deficiency in gastric cancer cells. *Molecular Cancer Therapeutics*.

Moffat, J.G., Rudolph, J. and Bailey, D. (2014). Phenotypic screening in cancer drug discovery - past, present and future. *Nature reviews. Drug discovery* **13**:588–602.

Mouradov, D., Sloggett, C., Jorissen, R.N., Love, C.G., Li, S., Burgess, A.W., Arango, D., *et al.* (2014). Colorectal cancer cell lines are representative models of the main molecular subtypes of primary cancer. *Cancer research*.**15**:3238-47.

Mu, Z., Klinowska, T., Dong, X., Foster, E., Womack, C., Fernandez, S. V and Cristofanilli, M. (2014). AZD8931, an equipotent, reversible inhibitor of signaling by epidermal growth factor receptor (EGFR), HER2, and HER3: preclinical activity in HER2 non-amplified inflammatory breast cancer models. *Journal of experimental & clinical cancer research* **33**:47.

Novellasdemunt, L., Antas, P. and Li, V.S.W. (2015). Targeting Wnt signaling in colorectal cancer. *American Journal of Physiology - Cell Physiology* **309.**

Nunes M, Vrignaud P, Vacher, Richon, Lièvre, Cacheux W,Weiswald LB, Massonnet G, Chateau-Joubert S, Nicolas A, Dib C,Zhang W, Watters J, Bergstrom D,Roman-Roman S, Bièche I,Dangles-Marie V (2015). Evaluating patient-derived colorectal cancer xenografts as preclinical models by comparison with patient clinical data. *Cancer Research* **75**:1560–1566.

O'Brien, C.A., Pollett, A., Gallinger, S., Gallinger, S. and Dick, J.E. (2007). A human colon cancer cell capable of initiating tumour growth in immunodeficient mice. *Nature* **445**:111–115.

Ootani A(1), Li X, Sangiorgi E, Ho QT, Ueno H, Toda S, Sugihara H, Fujimoto K, Weissman IL, Capecchi MR, Kuo CJ. (2009). Sustained in vitro intestinal epithelial culture within a Wnt-dependent stem cell niche. *Nature medicine* **15**:701–706.

Pastula, A., Middelhoff, M., Brandtner, A., Tobiasch, M., Höhl, B., Nuber, A.H., Demir, I.E., *et al.* (2016). Three-Dimensional Gastrointestinal Organoid Culture in Combination with Nerves or Fibroblasts : A Method to Characterize the Gastrointestinal Stem Cell Niche. **2016**.

Pathi, S., Jutooru, I., Chadalapaka, G., Nair, V., Lee, S. and Safe, S. (2012). Aspirin Inhibits Colon Cancer Cell and Tumor Growth and Downregulates Specificity Protein (Sp) Transcription Factors. *PloS one* **7**.

Pauli, C., Hopkins, B.D., Prandi, D., Shaw, R., Fedrizzi, T., Sboner, A., Sailer, V., *et al.* (2017). Personalized *In Vitro* and *In Vivo* Cancer Models to Guide Precision Medicine. *Cancer Discovery* **7**:462-477.

Pfister, S.X., Markkanen, E., Jiang, Y., Sarkar, S., Woodcock, M., Orlando, G., Mavrommati, I., *et al.* (2015). Inhibiting WEE1 Selectively Kills Histone H3K36me3-Deficient Cancers by dNTP Starvation. *Cancer Cell* **28**:557–568.

Picco, G. and Garnett, M.J. (2017). In the Spotlight A Road Map for Precision Cancer Medicine Using Personalized Models Personalized Cancer Medicine. *Cancer Discovery*. **7**:456–459.

Pinto, D. and Clevers, H. (2005). Wnt, stem cells and cancer in the intestine. *Biology of the cell* **97**:185–96

Pinto, D., Gregorieff, A., Begthel, H. and Clevers, H. (2003). Canonical Wnt signals are essential for homeostasis of the intestinal epithelium.*Genes & Development* **17**:1709–1713.

Poon, M.A., O'Connell, M.J., Wieand, H.S., Krook, J.E., Gerstner, J.B., Tschetter, L.K., Levitt, R., *et al.* (1991). Biochemical modulation of fluorouracil with leucovorin: Confirmatory evidence of improved therapeutic efficacy in advanced colorectal cancer. *Journal of Clinical Oncology* **9**:1967–1972.

Prahallad, A., Sun, C., Huang, S., Nicolantonio, F. Di, Salazar, R., Zecchin, D., Beijersbergen, R.L., *et al.*

(2012). Unresponsiveness of colon cancer to BRAF(V600E) inhibition through feedback activation of EGFR. *Nature* **483**:100–103.

Puig, I., Chicote, I., Tenbaum, S.P., Arques, O., Herance, J.R., Gispert, J.D., Jimenez, J., *et al.* (2013). A Personalized Pre-clinical Model to Evaluate the Metastatic Potential of Patient-derived Colon Cancer Initiating Cells. *Clinical cancer research : an official journal of the American Association for Cancer Research*.

Qi Z, Li Y, Zhao B, Xu C, Liu Y, Li H, Zhang B, Wang X, Yang X, Xie W, Li B, Han JJ, Chen YG. (2017). BMP restricts stemness of intestinal Lgr5+ stem cells by directly suppressing their signature genes. *Nature Communications* **8**:13824.

Qiao, L. and Wong, B.C.Y. (2009). Role of Notch signaling in colorectal cancer. *Carcinogenesis* **30**:1979–1986.

Raja, M., Zverev, M., Seipel, K., Williams, G.T., Clarke, A.R., Shaw, P.H.S., (2015). Assessment of the In Vivo Activity of PI3K and MEK Inhibitors in Genetically Defined Models of Colorectal Cancer. *Molecular cancer therapeutics* **14**:2175–86.

Reisen, F., Zhang, X., Gabriel, D. and Selzer, P. (2013). Benchmarking of multivariate similarity measures for high-content screening fingerprints in phenotypic drug discovery. *Journal of biomolecular screening* **18**:1284–97.

Resnick, M.B., Routhier, J., Konkin, T., Sabo, E. and Pricolo, V.E. (2004). Epidermal Growth Factor Receptor , c-MET , NL -Catenin , and p53 Expression as Prognostic Indicators in Stage II Colon Cancer : A Tissue Microarray Study. **10**:3069–3075.

Riccio, O., van Gijn, M.E., Bezdek, A.C., Pellegrinet, L., van Es, J.H., Zimber-Strobl, U., Strobl, L.J., *et al.* (2008). Loss of intestinal crypt progenitor cells owing to inactivation of both Notch1 and Notch2 is accompanied by derepression of CDK inhibitors p27Kip1 and p57Kip2. *EMBO reports* **9**:377–83.

Richman, S.D., Adams, R., Quirke, P., Butler, R., Hemmings, G., Chambers, P., Roberts, H., *et al.* (2015). Pre-trial inter-laboratory analytical validation of the FOCUS4 personalised therapy trial. *Journal of Clinical Pathology* **69**: 35-41.

Riemer P, Rydenfelt M, Marks M, van Eunen K, Thedieck K, Herrmann BG, Blüthgen N, Sers C, Morke M.(2017). Oncogenic β-catenin and PIK3CA instruct network states and cancer phenotypes in intestinal organoids. *The Journal of Cell Biology* **216**: 1567-77.

Roberts, P.J. and Der, C.J. (2007). Targeting the Raf-MEK-ERK mitogen-activated protein kinase cascade for the treatment of cancer. *Oncogene* **26**:3291–3310.

De Roock W, Claes B, Bernasconi D, De Schutter J, Biesmans B, Fountzilas G, Kalogeras KT, Kotoula V, Papamichael D, Laurent-Puig P, Penault-Llorca F, Rougier P, Vincenzi B, Santini D, Tonini G, Cappuzzo F, Frattini M, Molinari F, Saletti P, De Dosso S, Martini M, Bardelli A, Siena S, Sartore-Bianchi A, Tabernero J, Macarulla T, Di Fiore F, Gangloff AO, Ciardiello F, Pfeiffer P, Qvortrup C, Hansen TP, Van Cutsem E, Piessevaux H, Lambrechts D, Delorenzi M, Tejpar S. (2010). Effects of KRAS, BRAF, NRAS, and PIK3CA mutations on the efficacy of cetuximab plus chemotherapy in chemotherapy-refractory metastatic colorectal cancer : a retrospective consortium analysis. **11**:753–762.

Sachs, N. and Clevers, H. (2014). ScienceDirect Organoid cultures for the analysis of cancer phenotypes. :68–73.

Sadanandam A, Lyssiotis CA, Homicsko K, Collisson EA, Gibb WJ, Wullschleger S, Ostos LC, Lannon WA, Grotzinger C, Del Rio M, Lhermitte B, Olshen AB, Wiedenmann B, Cantley LC, Gray JW, Hanahan D. (2013). A colorectal cancer classification system that associates

cellular phenotype and responses to therapy. *Nature medicine* **19**:619–25.

Samuels, Y., Diaz, L.A., Schmidt-kittler, O., Cummins, J.M., Delong, L., Cheong, I., Rago, C. Huso,D. Lengauer,C. Kinzler, KW. Vogelstein,B. Velculescu, VE. (2005). Mutant PIK3CA promotes cell growth and invasion of human cancer cells. *Cancer Cell* **7**:561–573.

Samuels, Y. and Velculescu, V. (2004). Oncogenic mutations of PIK3CA in human cancers. *Cell Cycle* **3**.

Samuels Y(1), Wang Z, Bardelli A, Silliman N, Ptak J, Szabo S, Yan H, Gazdar A, Powell SM, Riggins GJ, Willson JK, Markowitz S, Kinzler KW, Vogelstein B, Velculescu VE. (2004). High Frequency of Mutations of the PIK3CA Gene in Human Cancers. *Science* **304**:554.

Sandercock, A.M., Rust, S., Guillard, S., Sachsenmeier, K.F., Holoweckyj, N., Hay, C., Flynn, M. Huang,Q. Yan,K. Herpers,B. Price,LS. Soden,J.Freeth,J. Jermutus,L. Hollingsworth, R. Minter, R. (2015). Identification of anti-tumour biologics using primary tumour models , 3-D phenotypic screening and image-based multi-parametric profiling. *Molecular Cancer* [Online] **14**:1–18.

Sansom, O.J., Reed, K.R., Hayes, A.J., Ireland, H., Brinkmann, H., Newton, I.P., Batlle, E., *et al.* (2004). Loss of Apc in vivo immediately perturbs Wnt signaling, differentiation, and migration. *Genes and Development* **18**:1385–1390.

Santarpia, L.L., Lippman, S. and El-Naggar, A. (2012). Targeting the Mitogen-Activated Protein Kinase RAS-RAF Signaling Pathway in Cancer Therapy. *Expert Opin Ther Targets* **16**:103–119.

Sato, T., Stange, D.E., Ferrante, M., Vries, R.G.J., Van Es, J.H., Van den Brink, S., Van Houdt, W.J.Pronk,A. Van Gorp, J. Siersema, PD. Clevers,H. (2011). Long-term expansion of epithelial organoids from human colon, adenoma, adenocarcinoma, and Barrett's epithelium. *Gastroenterology* **141**:1762–1772.

Sato, T., Vries, R.G., Snippert, H.J., van de Wetering, M., Barker, N., Stange, D.E., van Es, J.H.Abo,A. Kujala, P. Peters,PJ. Clevers,H. (2009). Single Lgr5 stem cells build crypt-villus structures in vitro without a mesenchymal niche. *Nature***459**:262–5.

Schuijers, J. and Clevers, H. (2012). Adult mammalian stem cells: the role of Wnt, Lgr5 and R-spondins. *The EMBO journal* **31**:2685–96.

Schuijers, J., Junker, J.P., Mokry, M., Hatzis, P., Koo, B.K., Sasselli, V., Van Der Flier, L.G. Cuppen,E. van Oudenaarden,A. Clevers, H. (2015). Ascl2 acts as an R-spondin/wnt-responsive switch to control stemness in intestinal crypts. *Cell Stem Cell* **16**:158–170.

Schütte M, Risch T, Abdavi-Azar N, Boehnke K, Schumacher D,Keil M, Yildiriman R, Jandrasits C, Borodina T, Amstislavskiy V,Worth CL, Schweiger C, Liebs S, Lange M, Warnatz HJ, ButcherLM, Barrett JE, Sultan M, Wierling C, Golob-Schwarzl N, Lax S,Uranitsch S, Becker M, Welte Y, Regan JL, Silvestrov M, Kehler I, Fusi A, Kessler T, Herwig R, Landegren U,Wienke D, Nilsson M, Velasco JA, Garin-Chesa P, Reinhard C, Beck S, Schäfer R, Regenbrecht CR, Henderson D, LangeB, Haybaeck J, Keilholz U, Hoffmann J, Lehrach H, Yaspo ML. (2017). Molecular dissection of colorectal cancer in pre-clinical models identifies biomarkers predicting sensitivity to EGFR inhibitors. *Nature Communications* **8**:14262.

Shimokawa, M., Ohta, Y., Nishikori, S., Matano, M., Takano, A., Fujii, M., Date, S. Sugimoto, S. Kanal, T. Sato, T. (2017). Visualization and targeting of LGR5+ human colon cancer stem cells. *Nature* [Online] **545**:187–192.

Shiokawa, D., Sato, A., Ohata, H., Mutoh, M., Sekine, S., Kato, M., Shibata, T.Nakagama, H. Okamoto, K. (2017). The Induction of Selected Wnt Target Genes by Tcf1 Mediates Generation of Tumorigenic Colon Stem Cells. *Cell Reports* **19**:981–994.

Simian, M. and Bissell, M.J. (2016). Organoids : A historical perspective of thinking in three dimensions. *The Journal of Cell Biology*:1–10.

Siolas, D. and Hannon, G.J. (2013). Patient-derived tumor xenografts: transforming clinical samples into mouse models. *Cancer research* **73**:5315–9.

Smith, G., Carey, F., Beattie, J., Wilkie, M., Lightfoot, T., Coxhead, J., Garner, R. Steels, RJ. Wolf, CR. (2002). Mutations in APC, Kirsten-ras, and p53—alternative genetic pathways to colorectal cancer. *Proceedings of the National Academy of Sciences* **9**:9433–8.

Snippert, H.J., Schepers, A.G., van Es, J.H., Simons, B.D. and Clevers, H. (2014). Biased competition between Lgr5 intestinal stem cells driven by oncogenic mutation induces clonal expansion. *EMBO reports* **15**:62–9.

Sottoriva, A., Kang, H., Ma, Z., Graham, T.A., Salomon, M.P., Zhao, J., Marjoram, P., *et al.* (2015). A Big Bang model of human colorectal tumor growth. *Nature Publishing Group* **47**:209–216.

de Sousa, E.M.F., Vermeulen, L., Richel, D. and Medema, J.P. (2011). Targeting Wnt signaling in colon cancer stem cells. *Clinical cancer research : an official journal of the American Association for Cancer Research* **17**:647–53.

de Sousa, F. and Vermeulen, L. (2016). Wnt signaling in cancer stem cell biology. *Cancers* **8**.

Spano, J.P., Lagorce, C., Atlan, D., Milano, G., Domont, J., Benamouzig, R., Attar, A., Benichou,J., Martin,A.,Morere,JF., Raphael,M., Penault-Llorca,F., Breau, JL., Fagard,R., Khayat,D.,Wind,P (2005). Impact of EGFR expression on colorectal cancer patient prognosis and survival. *Annals of Oncology* **16**:102–108.

Tian, H., Biehs, B., Chiu, C., Siebel, C.W., Wu, Y., Costa, M., De Sauvage, F.J.,Klein,OD., (2015). Opposing activities of notch and wnt signaling regulate intestinal stem cells and gut homeostasis. *Cell Reports* **11**:33–42.

Verissimo CS, Overmeer RM, Ponsioen B, Drost J, MertensS, Verlaan-Klink I, Gerwen BV, van der Ven M, WeteringMV, Egan DA, Bernards R, Clevers H, Bos JL, SnippertHJ. (2016) Targeting mutant RAS in patient-derived colorectal cancer organoids by combinatorial drug screening. *eLife* **5***.

Vermeulen, L., De Sousa E Melo, F., van der Heijden, M., Cameron, K., de Jong, J.H., Borovski, T., Tuynman, J.B., *et al.* (2010). Wnt activity defines colon cancer stem cells and is regulated by the microenvironment. *Nature cell biology* **12**:468–476.

Vermeulen, Todaro, L., Sousa, M. de, Mello, F., Sprick, M.., Kemper, K., Perez Alea, M., Richel, DJ.,Stassi,G.,Medema,JP. (2008). Single-cell cloning of colon cancer stem cells reveals a multi-lineage differentiation capacity. *Proceedings of the National Academy of Sciences***105**:13427–13432.

Visvader, J.E. and Lindeman, G.J. (2008). Cancer stem cells in solid tumours : accumulating evidence and unresolved questions. *Nature Reviews Cancer* **8**:755–768.

Voest, E.E. and Bernards, R. (2016). DNA-guided precision medicine for cancer: A case of irrational exuberance? *Cancer Discovery* **6**:130–132.

Vogelstein, B., Fearon, E.R., Hamilton, S.R., Kern, S.E., Preisinger, A.C., Leppert, M., Smits, A.M.M., *et al.* (1988). Genetic Alterations during Colorectal-Tumor Development. *New England Journal of Medicine* **319**:525–532.

Voskoglou-Nomikos T, Pater JL, Seymour L.(2003) Clinical predictive value of the *in vitro* cell line, human xenograft, and mouse allograft preclinical cancer models. *Clinical Cancer Research* **9**:4227-39.

Waaler, J., Machon, O., Tumova, L., Dinh, H., Korinek, V., Wilson, S.R., Paulsen, J.E., Pedersen, N.M., Eide, T.J., Machonova O, Gradl D, Voronkov A, von Kries JP, Krauss S. (2012). A novel tankyrase inhibitor decreases canonical Wnt signaling in colon carcinoma cells and reduces tumor growth in conditional APC mutant mice. *Cancer Research* **72**:2822–2832.

Waaler, J., Machon, O., Tumova, L., Dinh, H., Korinek, V., Wilson, S.R., Paulsen, J.E., Pedersen, N.M., Eide, T.J., *et al.* (2012). A Novel Tankyrase Inhibitor Decreases Canonical Wnt Signaling in Colon Carcinoma Cells and Reduces Tumor Growth in Conditional APC Mutant Mice. **72**:2822–2833.

Watson, C.L., Mahe, M.M., Múnera, J., Howell, J.C., Sundaram, N., Poling, H.M., Schweitzer, J.I., Vallance JE, Mayhew CN, Sun Y, Grabowski G, Finkbeiner SR, Spence JR, Shroyer NF, Wells JM, Helmrath MA. *et al.* (2014). An in vivo model of human small intestine using pluripotent stem cells.*Nature Medicine* .**20**:1310-4.

Weber, A.M. and Ryan, A.J. (2015a). ATM and ATR as therapeutic targets in cancer. *Pharmacology and Therapeutics* **149**:124–138.

Weeber, F., Ooft, S.N., Dijkstra, K.K. and Voest, E.E. (2017). Tumor Organoids as a Pre-clinical Cancer Model for Drug Discovery. *Cell Chemical Biology*:1–9.

Weeber, F., Wetering, M. Van De, Hoogstraat, M., Dijkstra, K.K., Krijgsman, O. and Kuilman, T. (2015). Preserved genetic diversity in organoids cultured from biopsies of human colorectal cancer metastases. **112**:13308–13311.

Weisberg, E., Nonami, A., Chen, Z., Liu, F., Zhang, J., Sattler, M., Nelson, E., Cowens K, Christie AL, Mitsiades C, Wong KK, Liu Q, Gray N, Griffin JD. (2015). Identification of Wee1 as a novel therapeutic target for mutant RAS-driven acute leukemia and other malignancies. *Leukemia* . **29**:27–37.

van der Flier LG, van Gijn ME, Hatzis P, Kujala P, Haegebarth A, Stange DE,Begthel H, van den Born M, Guryev V, Oving I, van Es JH, Barker N, Peters PJ, vande Wetering M, Clevers H.(2009). Transcription factor achaete scute-like 2 controls intestinal stem cell fate. *Cell.* 136:903-12.

van de Wetering M, Francies HE, Francis JM, Bounova G, Iorio F,Pronk A, van Houdt W, van Gorp J, Taylor-Weiner A, Kester L,McLaren-Douglas A, Blokker J, Jaksani S, Bartfeld S, Volckman R, van Sluis P, Li VS, Seepo S, Sekhar Pedamallu C, Cibulskis K,Carter SL, McKenna A, Lawrence MS, Lichtenstein L, Stewart C,Koster J, Versteeg R, van Oudenaarden A, Saez-Rodriguez J, VriesRG, Getz G, Wessels L, Stratton MR,McDermott U, Meyerson M,Garnett MJ, Clevers H. (2015). Prospective Derivation of a Living Organoid Biobank of Colorectal Cancer Patients Resource Prospective Derivation of a Living Organoid Biobank of Colorectal Cancer Patients. *Cell* **161**:933–945.

Williams, C., Mcmahon, C., Klein, J. and Mckean, H. (2015). A metastatic colon adenocarcinoma harboring BRAF V600e has a durable major response to dabrafenib / trametinib and chemotherapy. *OncoTargets and Therapy*:3561–3564.

Wood LD, Parsons DW, Jones S, Lin J, Sjöblom T, Leary RJ, Shen D, Boca SM, Barber T, Ptak J, Silliman N, Szabo S, Dezso Z, Ustyanksky V, Nikolskaya T, Nikolsky Y, Karchin R, Wilson PA, Kaminker JS, Zhang Z, Croshaw R, Willis J, Dawson D, Shipitsin M, Willson JK, Sukumar S, Polyak K, Park BH, Pethiyagoda CL, Pant PV, Ballinger DG, Sparks AB, Hartigan J, Smith DR, Suh E, Papadopoulos N, Buckhaults P, Markowitz SD, Parmigiani G, Kinzler KW, Velculescu VE, Vogelstein B. (2007). The genomic landscapes of human breast and colorectal cancers. *Science (New York, N.Y.)* [Online] **318**:1108–13.

Wu, X., Luo, F., Li, J., Zhong, X. and Liu, K. (2016). Tankyrase 1 inhibitor XAV939 increases chemosensitivity in colon cancer cell lines via inhibition of the Wnt signaling pathway. *International Journal of Oncology* :1333–1340.

Yamaguchi, T., Kakefuda, R., Tajima, N., Sowa, Y. and Sakai, T. (2011). Antitumor activities of JTP-74057 (GSK1120212), a novel MEK1 / 2 inhibitor , on colorectal cancer cell lines in vitro and in vivo.

Internatintional Journal of Oncololgy **39**:23–31.

Yeung, T.M., Chia, L. a, Kosinski, C.M. and Kuo, C.J. (2011). Regulation of self-renewal and differentiation by the intestinal stem cell niche. *Cellular and molecular life sciences : CMLS* [Online] **68**:2513–23.

Yeung, T.M., Gandhi, S.C., Wilding, J.L., Muschel, R. and Bodmer, W.F. (2010). Cancer stem cells from colorectal cancer-derived cell lines. *Proceedings of the National Academy of Sciences of the United States of America* [Online] **107**:3722–7. A

Yin, X., Farin, H.F., van Es, J.H., Clevers, H., Langer, R. and Karp, J.M. (2013). Niche-independent high-purity cultures of Lgr5(+) intestinal stem cells and their progeny. *Nature methods* **11**:106-12.

Young, M. and Reed, K.R. (2016). Organoids as a Model for Colorectal Cancer. *Current Colorectal Cancer Reports***12**:281–287.

Yui S, Nakamura T, Sato T, Nemoto Y, Mizutani T, Zheng X, Ichinose S, Nagaishi T, Okamoto R, Tsuchiya K, Clevers H, Watanabe M. (2012). Functional engraftment of colon epithelium expanded in vitro from a single adult Lgr5$^+$ stem cell. *Nature medicine* **18**:618–23.

Zeilstra, J., Joosten, S.P.J., Dokter, M., Spaargaren, M. and Pals, S.T. (2008). Deletion of the WNT Target and Cancer Stem Cell Marker CD44 in Apc (Min / +) Mice Attenuates Intestinal Tumorigenesis.*Cancer Research* :3655–3662.

Zhao, L. and Vogt, P.K. (2008). Class I PI3K in oncogenic cellular transformation. *Oncogene* **27**:5486–5496.

Zhong, Y., Katavolos, P., Nguyen, T., Lau, T., Boggs, J., Sambrone, A., Kan, D., *et al.* (2015). Tankyrase Inhibition Causes Reversible Intestinal Toxicity in Mice with a Therapeutic Index < 1. *Toxicologic Pathology* **44**:267–278.

Ziegler, U. and Groscurth, P. (2004). Morphological features of cell death. *News in physiological sciences***19**:124–8.

Zumwalt TJ, Wodarz D, Komarova NL, Toden S, Turner J, Cardenas J, Burn J, Chan AT, Boland CR, Goel A. (2017). Aspirin-Induced Chemoprevention and Response Kinetics Are Enhanced by PIK3CA Mutations in Colorectal Cancer Cells. *Cancer Prevention Research* **10**:208 LP-218.
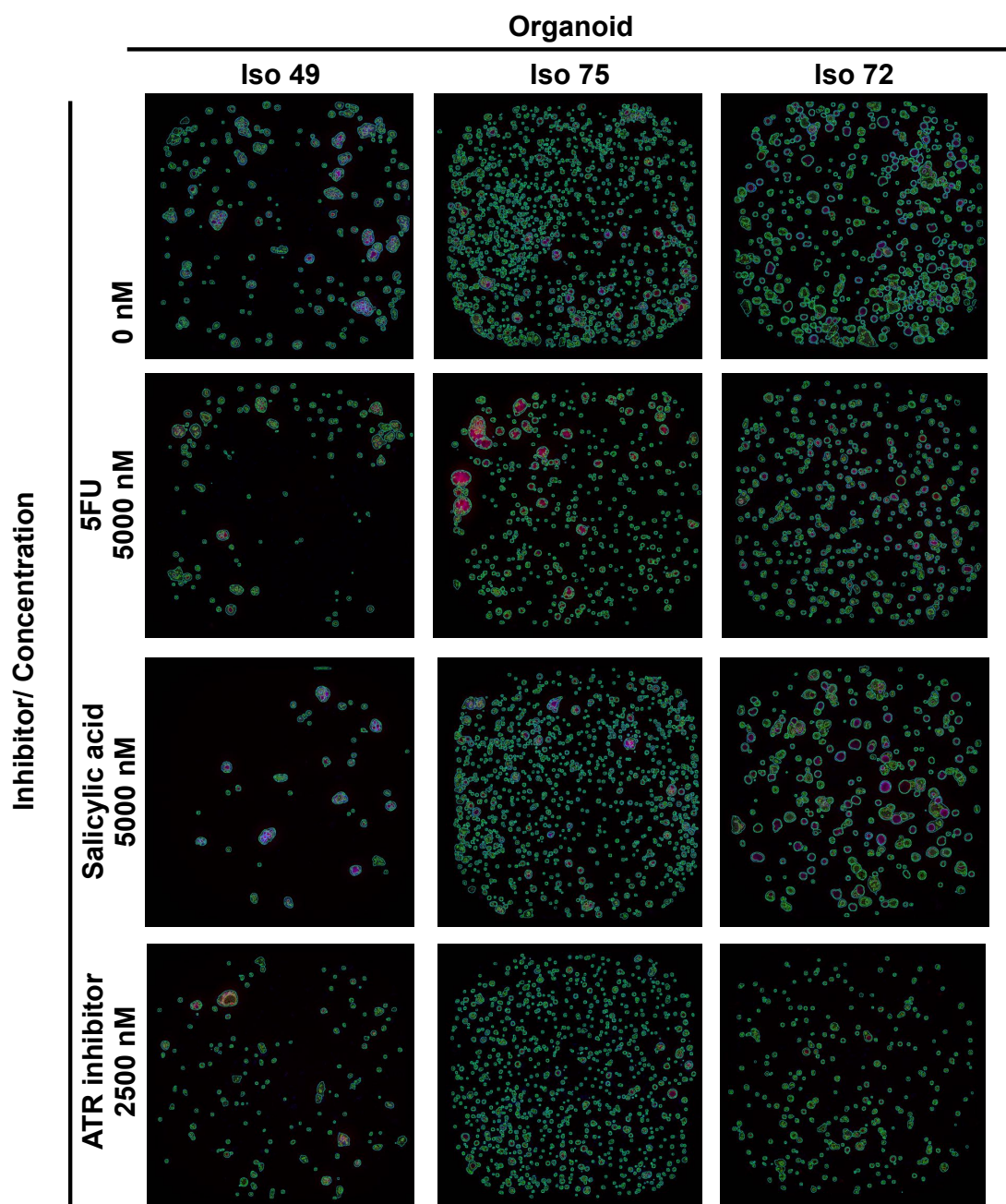
7 Appendices

Appendix I Image analysis output images and FOCUS 4 compound titration studies

Appendix II Analysis of Tankyrase inhibition effects upon Lgr5 and Cytokeratin 20 expression.

Appendix III Media components

# 7.1 Appendix I : Image analysis output images and FOCUS 4 compound titration studies

Appendix I-1 Representative image masks of compound-treated organoid lines for phenotypic screening.

Organoid lines Iso 49, Iso 75, and Iso 72 were cultured in 384 well plates and treated with a dose response range of 5FU, Salicylic acid and ATR inhibitor, following 3 days of recovery. After 4 days of treatment, organoids were fixed with Hoechst and TRITC-phalloidin. Images were captured on a high content confocal microscope and subject to analysis. Masks of organoids were generated for subsequent downstream image analysis applications (OcellO).
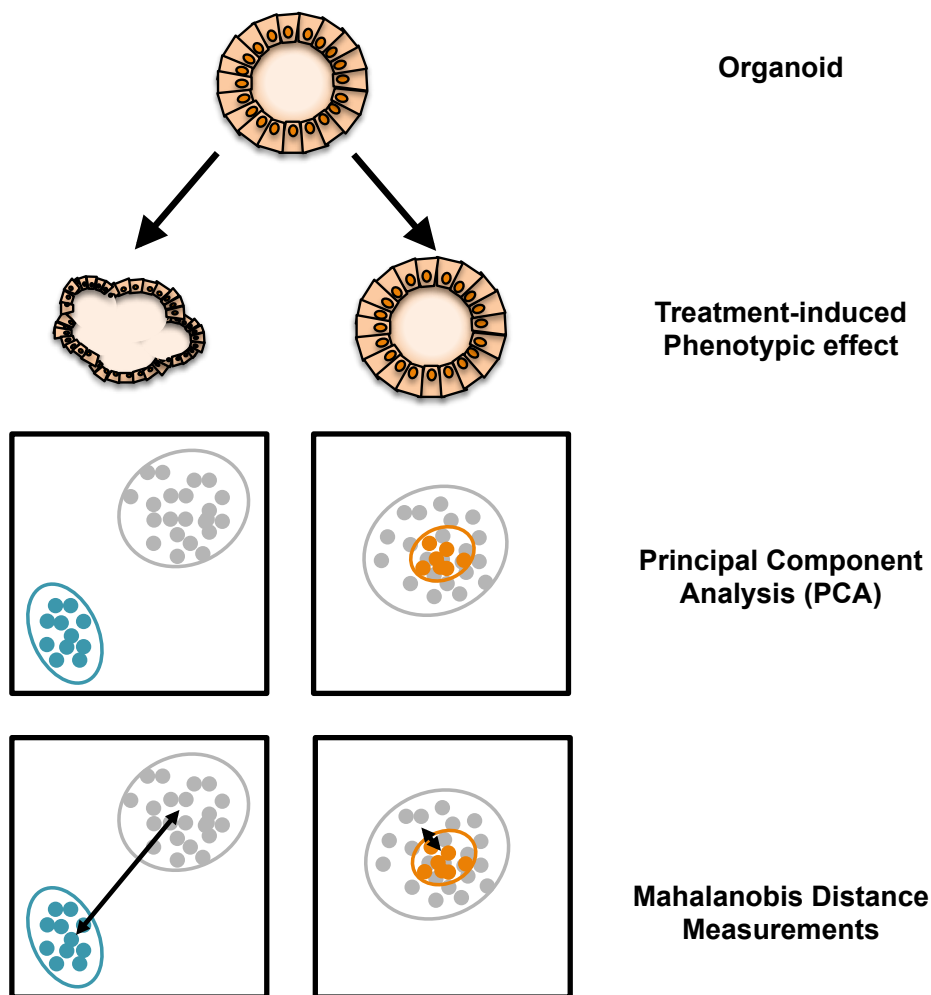
**Appendix I-2 Schematic of Mahalanobis Distance Calculation**

Data output from OMiner software was inputted to generate Principal Component Analysis (PCA) of extracted features. After performing normalisation, multidimensional data subsets were created for each organoid, per treatment, containing technical replicates for each treatment and control (DMSO, 0.1 %). PCA was performed , and components are scaled by the proportion of variance that they explain. Features within the first 5 components were then used to measure Mahalanobis distance between each dose and control condition. This measurement facilitates a quantifiable separation between the principal components. A larger degree of separation correlates with an increasing phenotypic effect between treatment and control conditions. *Image adapted from Hutz* et al*., (2012).*
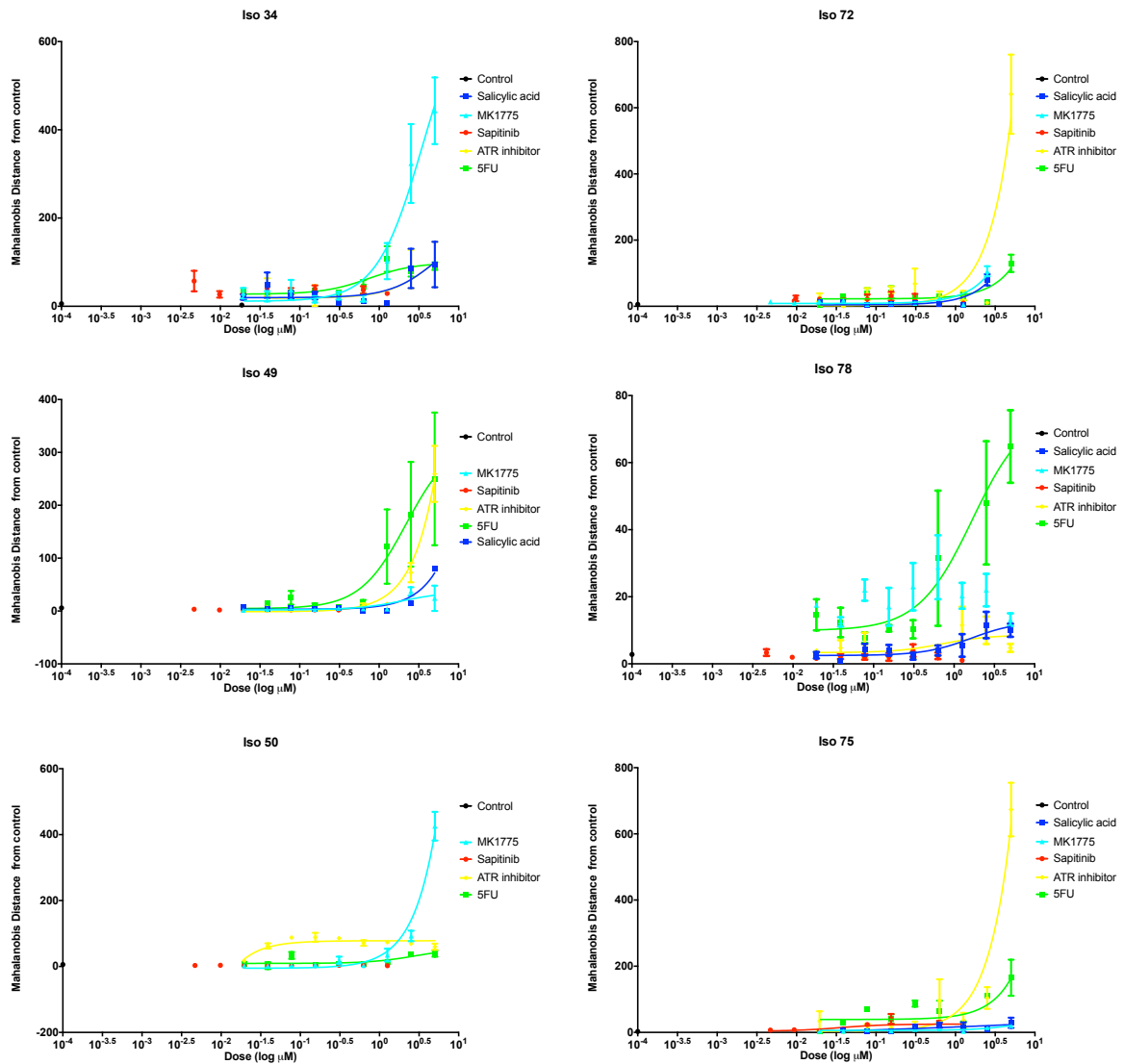
Appendix I-3 Mahalanobis distance analysis from phenotypic screening of each organoid line with compounds relevant to the FOCUS 4 clinical trial.

Freshly digested organoids were seeded within matrigel in 384 well plates and overlaid with optimal media for growth. Following 3 days of recovery, a dose titration of compounds within the FOCUS 4 trial were administered versus a DMSO negative control. Following 4 days of treatment, organoids were fixed and stained simultaneously for Hoechst and F-actin. Subsequent z-stack images were collected and inputted within OMiner™ software to generate multiple phenotypic measurements acquired from Hoechst and TRITC channel information. Data was inputted into R to generate Prinicipal Component Analysis (PCA) of features. Features within the first 5 components were used to measure Mahalanobis distance from treatment and control conditions. This measurement enabled a discrimination between each treatment dose compared to control, based on multiple measured features.

7.2 Appendix II: Analysis of Tankyrase inhibition effects upon Lgr5 and Cytokeratin 20 expression.
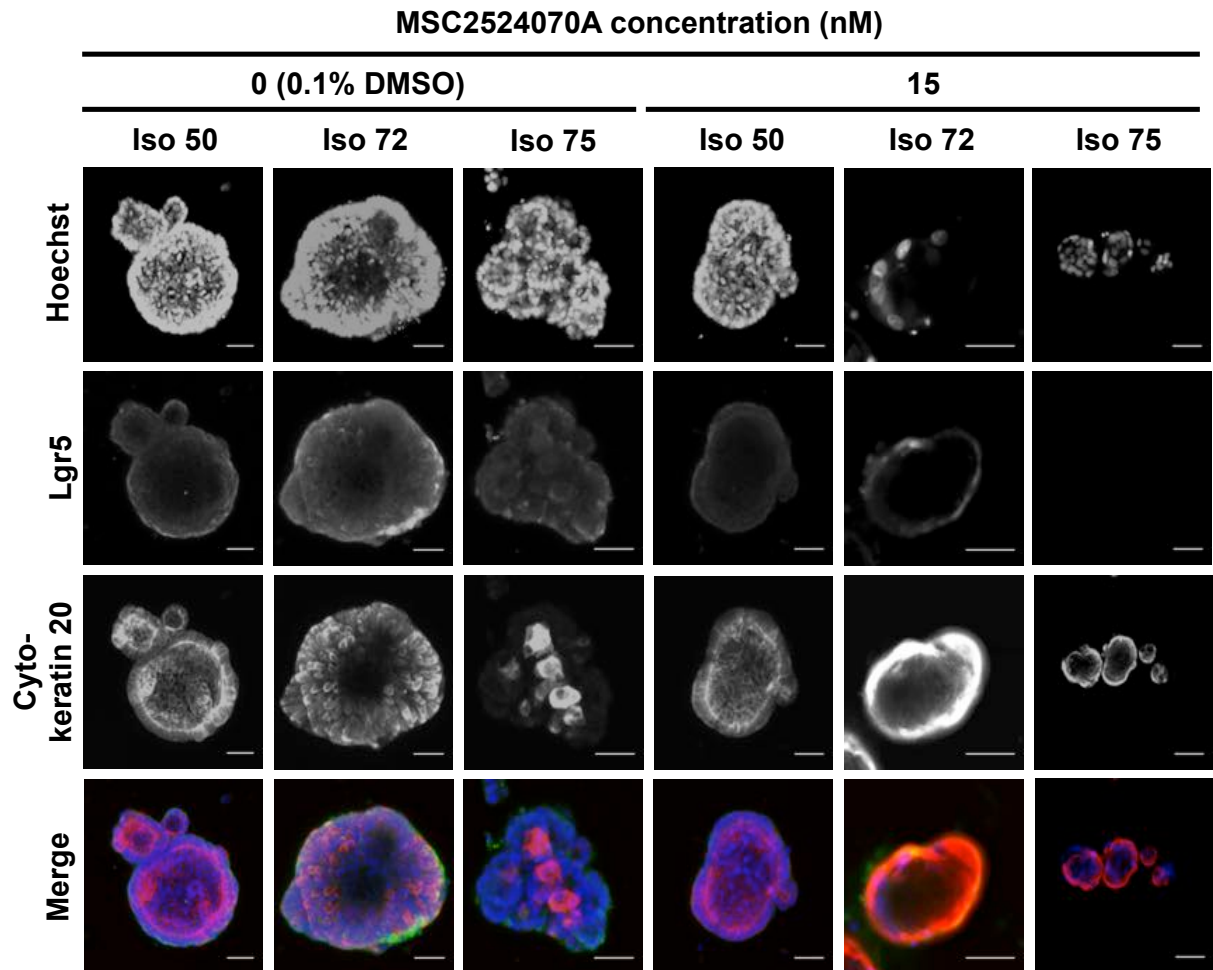
Appendix II-1 Analysis of the effects of the Tankyrase inhibitor MSC2524070 on Lgr5 and cytokeratin 20 expression.

Freshly trypsinised organoids (Iso 50, Iso 72, Iso 75) were seeded at 400 cells/µl Matrigel and overlaid with previously specified growth media supplemented with MSC2524070 (15nM, 6 days), and a matched DMSO control (0.1% in media). Organoids were then fixed and immunostained for Lgr5 and cytokeratin 20 within treatment and control conditions. Scale bar = 50µm.

7.3 Appendix III: Media Components

Appendix III-1 Table of media components and sources.

Component	Target/ purpose	Source	Catalogue Number	7+ Media	Full Media
ADV-DMEM/F12		Invitrogen	12634-028	1X	1X
Penicillin/ Streptocymcin		Invitrogen	15140-122	100 U/ml	100 U/ml
HEPES (1M)		Invitrogen	15630-056	10mM	10mM
GlutaMAX (100X)		Invitrogen	35050-079	2mM	2mM
N2 (100X)		Invitrogen	17502-048	1X	1X
B27 (50X)		Invitrogen	17504-044	1X	1X
N-acetylcysteine	Anti-oxidant	Sigma-Aldrich	A9165-5G	1mM	1mM
Epidermal Growth Factor (EGF)		Sigma-Aldrich	E4127		50ng/ml
Mouse recombinant Noggin		Peprotech	250-38		100ng/ml
A-83-01	Alk4/5/7 inhibitor	Tocris	2939		500µM
SB202190	P38 MAP kinase inhibitor	Sigma-Aldrich	57067		10µM
Wnt3A conditioned medium					40% (v/v)
R-spondin conditioned medium					10% (v/v)
Fungizone*		Invitrogen		2µl/ml	2µl/ml
Y-27632*	ROCK inhibitor	R&D	129830-38-2	10µM	10µM